The University of Nottingham
UNITED KINGDOM · CHINA · MALAYSIA

Roberts, Gethin Wyn (1997) Real time on-the-fly kinematic GPS. PhD thesis, University of Nottingham.

Access from the University of Nottingham repository:
http://eprints.nottingham.ac.uk/13395/1/362918.pdf

Copyright and reuse:

The Nottingham ePrints service makes this work by researchers of the University of Nottingham available open access under the following conditions.

- Copyright and all moral rights to the version of the paper presented here belong to the individual author(s) and/or other copyright owners.
- To the extent reasonable and practicable the material made available in Nottingham ePrints has been checked for eligibility before being made available.
- Copies of full items can be used for personal research or study, educational, or not-for-profit purposes without prior permission or charge provided that the authors, title and full bibliographic details are credited, a hyperlink and/or URL is given for the original metadata page and the content is not changed in any way.
- Quotations or similar reproductions must be sufficiently acknowledged.

Please see our full end user licence at:
http://eprints.nottingham.ac.uk/end_user_agreement.pdf

A note on versions:

The version presented here may differ from the published version or from the version of record. If you wish to cite this item you are advised to consult the publisher's version. Please see the repository url above for details on accessing the published version and note that access may require a subscription.

For more information, please contact eprints@nottingham.ac.uk

Real Time On-The-Fly Kinematic GPS

by

Gethin Wyn Roberts, B.Eng.(Hons)

Thesis submitted to The University of Nottingham for the degree of Doctor of Philosophy, April 1997

Abstract

Considerable interest has been show in the development and application of real time On-The-Fly (OTF) kinematic GPS. A major error source and limitation of such a positioning technique is that caused by cycle slips. When these occur, the integer ambiguities must be resolved for, which can take hundreds of epochs to complete depending on satellite availability and geometry.

This research has focused on investigating the applications of real time OTF GPS, as well as its limitations and precision, which has been shown in the thesis to be precise to a few millimetres. The limitations of such a system at present include the use of UHF telemetry links, which at best have a line of sight range of ~10 km. The research has shown that alternatives are required, and the use of a relay station can prove invaluable.

Cycle slips are another major limiting factor when using OTF GPS, as once a cycle slip occurs, it can either be corrected for or the integer ambiguities resolved for. The second option can take hundreds of seconds, depending on the algorithms used and the satellite number and geometry. This research has partly focused on the development of software which will instantaneously detect and correct for cycle slips in high rate GPS data.

The applications of real time OTF GPS are numerous. Research has been carried out to investigate its use to monitor and control construction plant as well as monitoring the movement of large structures. As OTF positioning is precise to a few millimetres, it is ideal for the control of construction plant, and has been compared to laser levelling and precise digital levelling. Such a GPS system gives the user a 3-dimensional position for the bulldozer blade, for example. Such information can prove invaluable for quality control as well as developing an automated system, which would be controlled by real time OTF

GPS. In addition, real time OTF GPS has been shown in the research to provide instantaneous positioning of large structures in the form of bridges. Such information could provide future systems which would monitor the structure for dangerous movements, resulting in a failure alarm.

Carrier phase kinematic GPS has previously been shown to work over baseline lengths of < 20 km. The use of Multiple Reference Stations (MRS) has been shown in this research to enable OTF GPS to be applied over longer baseline lengths, with a precision in the order of 12 cm over 132 km.

Acknowledgements

This thesis is a result of research at the Institute of Engineering Surveying and Space Geodesy (IESSG) within the Department of Civil Engineering at the University of Nottingham. The research has been conducted with the support of the Director of the IESSG, Professor V. Ashkenazi and the head of the Department of Civil Engineering, Professor D. A. Nethercott.

The author would like to thank Professor V. Ashkenazi and Professor A. H. Dodson for their supervision, help and advice during the research and for providing the opportunity and the resources required to carry out the research.

The author would like to give special thanks to all members of the IESSG, past and present, who have helped with the thesis. Special thanks are due to Dr. R. Bingley for his advice throughout the research, as well as Dr. G. Ffoulkes-Jones, Dr. P. Shardlow and Dr. W. Chen, and the help and advice obtained from Dr. P. Hansen about his NOTF software. The author is very grateful to Dr. R. Bingley, Dr. G. A. Beamson, Dr. M. Dumville, Miss H. Baker and Mr N. T. Penna for proof reading the thesis, and providing useful advice. Special thanks is due to the late Pete Clarke for his enthusiastic help during the field trials.

The author would like to thank Ashtech Europe Ltd for setting up the reference receivers at Oxford during the trials carried out for Chapter 7, as is indebted to the staff at RAF Cranwell for their invitation on the ARIES'96 Polar Flight.

The trials conducted in Chapter 9 were made possible through Stephen Simmons of Sinbad Plant Hire, Nottingham, through providing his plant and laser equipment for trials.

The trials conducted in Chapter 10 were made possible through numerous people and organisations, namely Roger Evans at The Humber Bridge Board, Flintshire County Council and Steve Jones of Gifford Graham and Partners for allowing the author to access to the Dee Bridge. Thanks is also due to Nottingham County Council for allowing access to the Clifton Bridge.

Finally, I would like to thank my wife Sarah for being so patient and supportive.

Table of Contents

1 Introduction

1.1 Satellite Navigation 1
1.2 Real Time Kinematic GPS 2
1.3 Engineering Applications of Real Time OTF GPS 3
1.4 Thesis Overview 3
1.5 References 4

2 The Concepts of GPS

2.1 Introduction 5
2.2 Motives Behind the GPS System 5
2.3 The System 6
2.3.1 The Control Segment 7
2.3.1.1 Satellite Ephemerides 7
2.3.2 The Space Segment 9
2.3.3 The User Segment 9
2.3.3.1 The Standard Positioning Service 10
2.3.3.2 The Precise Positioning Service 10
2.4 References 11

3 GPS Measurements and Observables

3.1 Introduction 12
3.2 GPS Signal Structure 13
3.2.1 The Carrier 14
3.2.2 Pseudo Random Noise Codes 14
3.2.2.1 Coarse Aquisition Code 15
3.2.2.2 Precise Code 15
3.2.3 The Navigation Message 16
3.2.4 Degradation of the GPS Signal 17
3.2.4.1 Anti Spoofing 17
3.2.4.2 Selective Avalability 18
3.3 GPS Receiver Technology 18
3.3.1 Code Correlation 18
3.3.2 Signal Squaring 19
3.3.3 Cross Correlation 19
3.3.4 P-W Tracking 20
3.4 Dilution of Precision Parameters 20
3.5 References 21

4 GPS Positioning Techniques

4.1 Introduction 22
4.2 Pseudorange Positioning 23
4.2.1 Absolute GPS Positioning 23

4.2.2 Differential GPS 26
4.2.3 Pseudorange Differencing 27
4.2.4 Phase Smoothed Pseudoranges 27
4.2.5 Wide Area Differential DGPS 27
4.3 Carrier Phase Positioning 28
4.3.1 The Pure Phase Observable 29
4.3.2 The Single Difference Observable 30
4.3.3 The Double Difference Observable 32
4.3.4 The Triple Difference Observable 33
4.4 Carrier Phase Positioning Techniques 34
4.4.1 Static Surveying 35
4.4.2 Fiducial GPS 36
4.4.3 Rapid Static Surveying 37
4.4.4 Stop and Go Kinematic GPS (Semi Kinematic) 38
4.4.5 Pseudo-Kinematic (Nottingham Technique) 39
4.4.6 Kinematic 'On The Fly' Ambiguity Resolution 39
4.5 Conclusions and Recommendations 40
4.6 References 41

5 OTF Integer Ambiguity Resolution

5.1 Introduction 43
5.2 Integer Ambiguity Search Technique 44
5.3 The 'Four Observables' Equation 50
5.4 Multiple Reference Stations 51
5.5 Further Ambiguity Resolution Techniques 51
5.6 References 52

6 The Accurate Recovery of Cycle Slips

6.1 Introduction 56
6.2 Code Minus Carrier (Range Residual) Comparison 58
6.3 Cycle Slip Detection Through the Use of the 'Four Observables' Equation 62
6.4 Cycle Slip Detection Through the Use of Doppler Data 64
6.5 Cycle Slip Detection Through the Use of the Ionospheric Residual 68
6.6 Solution Constraints 73
6.6.1 Pseudorange Constraints 73
6.6.1.1 Measurement Noise 74
6.6.1.2 Multipath 81
6.6.2 Doppler Constraints 85
6.6.2.1 Measurement Noise 86
6.6.2.2 Velocity Changes 88
6.6.2.3 Spurious Doppler Values 89
6.6.3 Ionospheric Residual Constraints 89
6.6.3.1 Measurement Noise 89
6.6.3.2 Ambiguous Cycle Slip Combinations 90
6.7 Implementation and Testing of the Cycle Slip Detection Techniques 93

6.8 Conclusions and Recommendations 97
6.9 References 98

7 Long Range OTF Kinematic GPS

7.1 Introduction 102
7.2 134 km Baseline Tests 103
7.2.1 Test Set-up 103
7.2.2 Short baseline results 104
7.2.3 Long Baseline Results 105
7.3 ARIES 96 Polar Flight Results 111
7.3.1 Cycle Slip Analysis 114
7.3.2 Positioning Through OTF GPS 115
7.4 Conclusions and Recommendations 116
7.5 References 117

8 Real Time OTF System Description

8.1 Introduction 118
8.2 Real Time OTF GPS Hardware 120
8.2.1 Telemetry Links 121
8.2.2 Real Time Processing Using a Laptop PC 123
8.2.3 Real Time Processing Within the GPS Receiver 128
8.3 Alternative Telemetry Links 130
8.4 Resolution of the Real Time System Through the use of a Zero Baseline 132
8.5 Short Baseline Results 136
8.6 Real Time OTF Precision Using a Bipole 142
8.7 Required Accuracy of the Reference GPS Receiver Coordinates for Successful OTF Initialisation 144
8.8 Other Error Sources 148
8.9 Conclusions and Recommendations 149
8.10 References 150

9 Construction Plant Control and Monitoring by GPS

9.1 Introduction 152
9.2 The Use of Laser Levels and Ultra Sonic Devices for Plant Control 153
9.3 The Use of Real Time OTF for Plant Control 158
9.4 The Use of a Single GPS Antenna on a Bulldozer Blade 160
9.5 The Use of Three GPS Antennas on a Bulldozer 162
9.6 OTF GPS Positioning Results 163
9.6.1 Height Precision of the Fixed Integer OTF GPS Solution 165
9.6.2 Comparison of OTF GPS Height With a Digital Level 169
9.6.2.1 Tilt Correction Calculation 171
9.6.3 Positional Precision of the Fixed Integer OTF GPS Solution 175
9.6.4 System Noise 176
9.6.5 The Use of Real Time OTF to Measure the Tilt of the 181

Bulldozer Blade
9.7 Conclusions and Recommendations 188
9.8 References 189

10 Monitoring Large Structures by Real Time OTF GPS

10.1 Introduction 192
10.2 Real time On-The-Fly GPS monitoring of the Humber Bridge 193
10.2.1 Bridge Deck Real Time Deformation Results - Trial 1 195
10.2.2 Bridge Deck Real Time Deformation Results - Trial 2 198
10.2.3 Bridge Support Tower Real Time Deformation Results - Trial 1 201
10.2.4 Bridge Deck Real Time Deformation Results - Test 3 204
10.3 Real Time Positioning of the Dee Estuary Bridge Deck 210
During its Construction
10.3.1 Dee Bridge - Trial 1 213
10.3.2 Dee Bridge - Trial 2 216
10.4 Real Time Monitoring of the Clifton Bridge 222
10.5 Conclusions and Recommendations 227
10.6 References 229

Chapter 11
Conclusions and Recommendations 232

Appendix A
Appendix B
Appendix C
Appendix D
Appendix E
Appendix F

List of Figures

2 The Concepts of GPS

Figure 2.1 Location of the Control Segment's Tracking Network 8

3 GPS Measurements and Observables

Figure 3.1 GPS Signal Structure (Reproduced from [MOORE. T , 1994]) 15

Figure 3.2 Illustration of the pseudo range concept. 16

4 GPS Positioning Techniques

Figure 4.1 The Concept of the Integer Ambiguity 29

Figure 4.2 The Single Difference Observables 31

Figure 4.3 The Double Difference Observable 33

Figure 4.4 The Triple Difference Observable 34

5 OTF Integer Ambiguity Resolution

Figure 5.1 Setting up a Search Window Using DGPS for the Initial Position 46

Figure 5.2 Determination of Redundant Satellite Ambiguity and Pre-Adjustment Residual (Adapted from [HANSEN, 1996]) 47

Figure 5.3 Illustration of the Ambiguity Search Technique in 2-D 49

6 The Accurate Recovery of Cycle Slips

Figure 6.1 A plot showing the Ashtech Z-XII L1 Y-code Minus L1 Carrier Phase (L1 Range Residuals) for satellite 20, during the presence of AS. A scatter of about ± 2 cycles is seen for data recorded at a 1 second epoch interval 59

Figure 6.2 A plot showing the Ashtech Z-XII L2 Y-code Minus L2 Carrier Phase (L2 Range Residuals) for satellite 20, during the presence 60

	of AS. A scatter of about ±2 cycles is seen for data recorded at a 1 second epoch interval	
Figure 6.3	A plot showing the Ashtech Z-XII L1 C/A-code Minus L1 Carrier Phase (L1 Range Residuals) for satellite 20, during the presence of AS. A scatter of about ±6 cycles is seen for data recorded at a 1 second epoch interval	60
Figure 6.4	A plot showing Trimble 4000 SSE L1 C/A-code Minus L1 Carrier Phase (L1 Range Residuals) for satellite 22, during the presence of AS. A scatter of about ±4 cycles is seen for data recorded at a 1 second epoch interval	61
Figure 6.5	A plot of a Trimble 4000 SSE Wide Lane Residuals for satellite 22 during the presence of AS. Data recorded at a 1 second epoch interval	63
Figure 6.6	A plot of an Ashtech Z-XII Wide Lane Residuals for satellite 20 during the presence of AS. Data recorded at a 1 second epoch interval.	63
Figure 6.7	The Effect of a Cycle Slip Upon Carrier Phase and Doppler Data for a Trimble 4000 SSE receiver. Data recorded at a 1 second epoch interval.	65
Figure 6.8	A plot of an Ashtech Z-XII L1 Doppler Residuals for satellite 26 during the presence of AS. Data recorded at a 1 second epoch interval.	66
Figure 6.9	A plot of an Ashtech Z-XII L2 Doppler Residuals for satellite 26 during the presence of AS. Data recorded at a 1 second epoch interval.	67
Figure 6.10	A plot of a Trimble 4000 SSE L1 Doppler Residuals for satellite 22 during the presence of AS. Data recorded at a 1 second epoch interval.	67
Figure 6.11	A plot of a Trimble 4000 SSE L2 Doppler Residuals for satellite 22 during the presence of AS. Data recorded at a 1 second epoch interval.	68
Figure 6.12	The effect on the Ionospheric Residual of the Introduction of One	72

	L1 Cycle Slip on Trimble 4000 SSE data. Data recorded at a 1 second epoch interval.	
Figure 6.13	A plot of an Ashtech Z-XII Ionospheric Residuals for satellite 26 during the presence of AS. Data recorded at a 1 second epoch interval.	72
Figure 6.14	A plot of a Trimble 4000 SSE Ionospheric Residuals for satellite 22 during the presence of AS. Data recorded at a 1 second epoch interval.	73
Figure 6.15	Typical Noise Value Obtained from a Zero Baseline for an Ashtech Z-XII L1 Y-Code for Satellite Combination 22, 6. AS was on during the Experiment.	75
Figure 6.16	Typical Noise Value Obtained from a Zero Baseline for an Ashtech Z-XII L1 C/A-Code for Satellite Combination 22, 6. AS was on during the Experiment.	75
Figure 6.17	Typical Noise Value Obtained from a Zero Baseline for an Ashtech Z-XII L2 Y-Code for Satellite Combination 22, 6. AS was on during the Experiment.	76
Figure 6.18	Typical Noise Value Obtained from a Zero Baseline for a Trimble 4000 SSE L1 C/A-Code for Satellite Combination 26, 23. AS was on during the Experiment.	76
Figure 6.19	Typical Noise Value Obtained from a Zero Baseline for a Trimble 4000 SSE L2 P-Code for Satellite Combination 26, 12. AS was off for Satellite 12 during the Experiment.	77
Figure 6.20	Typical Noise Value Obtained from a Zero Baseline for a Trimble 4000 SSE L2 Y-Code for Satellite Combination 26, 23. AS was on during the Experiment.	77
Figure 6.21	Typical Noise Value Obtained from a Zero Baseline for a Trimble 4000 SST L1 C/A-Code for Satellite Combination 26, 5. AS was on during the Experiment.	78
Figure 6.22	Typical Noise Value Obtained from a Zero Baseline for a Trimble 4000 SST L1 Carrier Phase for Satellite Combination 26, 5. AS was on during the Experiment.	79

Figure 6.23	Typical Noise Value Obtained from a Zero Baseline for an Ashtech Z-XII L1 Carrier Phase for Satellite Combination 26, 6. AS was on during the Experiment.	79
Figure 6.24	Typical Noise Value Obtained from a Zero Baseline for a Trimble 4000 SSE L1 Carrier Phase for Satellite Combination 26, 23. AS was on during the Experiment.	80
Figure 6.25	Typical Noise Value Obtained from a Zero Baseline for a Trimble 4000 SSE L2 Carrier Phase for Satellite Combination 26, 23. AS was on during the Experiment.	80
Figure 6.26	SNR and L1 C/A-code Range Residuals for Areas of Varying Multipath.	82
Figure 6.27	SNR and L1 Y-code Range Residuals for Areas of Varying Multipath.	82
Figure 6.28	SNR and L1 C/A-code Range Residuals for an Area of Low Multipath.	84
Figure 6.29	SNR and L1 Y-code Range Residuals for an Area of Low Multipath.	84
Figure 6.30	SNR and L1 C/A-code Range Residuals, Having Been Corrected for Multipath, for Areas of Varying Multipath.	85
Figure 6.31	A Plot of an Ashtech Z-XII Doppler Residuals for Satellite 6 During the Presence of AS. Data Recorded at a 1 Second Epoch Interval.	86
Figure 6.32	A Plot of an Ashtech Z-XII Doppler Residuals for Satellite 6 During the Presence of AS. Data Recorded at a 5 Second Epoch Interval.	87
Figure 6.33	A Plot of an Ashtech Z-XII Doppler Residuals for Satellite 6 During the Presence of AS. Data Recorded at a 30 Second Epoch Interval.	87
Figure 6.34	A Plot of an Ashtech Z-XII Doppler Residual Values for Satellite 4 During the Presence of AS. Data Recorded at a 2.5 Second Epoch Interval.	88
Figure 6.35	Monthly mean sunspot numbers. January 1953 - December 1996.	92

Figure 6.36 A Flow Diagram Showing the Principles Behind the Cycle Slip Correction Program. 95

7 Long Range OTF Kinematic GPS

Figure 7.1 Satellite 07 L1 Range Residual Showing Spikes at High Multipath. 106

Figure 7.2 Satellite 07 L2 Range Residual Showing Spikes at High Multipath. 106

Figure 7.3 Satellite 07 L1 Doppler Residual, Showing Higher Resolution at Constant Velocities. 107

Figure 7.4 Satellite 07 L2 Doppler Residual, Showing Increased Accuracies at Constant Velocities. 107

Figure 7.5 Satellite 07 Ionospheric Residual for the Considered Data. 108

Figure 7.6 Short Baseline L1 minus Long Baseline L1 Radial Error for the Kinematic Trial. 109

Figure 7.7 Short Baseline L1 minus Long Baseline Lw Radial Error for the Kinematic Trial. 109

Figure 7.8 Total Trpopspheric Zenith Delay for Kinematic Trial. 111

Figure 7.9 The Comet Plane. 112

Figure 7.10 The GPS Receivers Located at Thule, Greenland. 113

Figure 7.11 A View of the North Pole. 114

Figure 7.12 The Resulting L1 Integer Fixed Position. 115

Figure 7.13 The L1 Integer Fixed Solution at the North Pole. 116

8 Real Time OTF System Description

Figure 8.1 The Stena Line HSS 1500 Catamaran docking at Holyhead. The use of real time OTF GPS allows this procedure to be accelerated. 120

Figure 8.2 The Real Time System's Telemetry Links. Shown, from left to right, are the receiving telemetry link antenna, the receiving datalink, the GPS receiver, the transmitting telemetry link antenna, the transmitting datalink and a 12 V power 122

	supply for the transmitting datalink.	
Figure 8.3	The Real Time OTF system used by the Author. The GPS antenna is situated upon the bipole. The GPS receiver is housed inside the rucksack, as is the telemetry link unit. The telemetry link antenna is situated on top of the rucksack, where it receives the GPS data from the reference GPS receiver. The data from the two GPS receivers is processed within the laptop computer in a real time manner.	124
Figure 8.4	The Real Time System Using a Laptop Computer for Processing and OTF Positioning.	125
Figure 8.5	The PNAV Processing Screen.	126
Figure 8.6	The PNAV Graphical Processing Screen.	127
Figure 8.7	A Real Time OTF System, Using one of the GPS Receivers to Process the Data.	130
Figure 8.8	A Schematic of the Principles Behind the Relay Station. This Allows the Transmission of Data to be Carried Out Even Without Line of Sight.	132
Figure 8.9	Zero Baseline GPS OTF Test Results (Northings).	134
Figure 8.10	Zero Baseline GPS OTF Test Results (Eastings).	135
Figure 8.11	Zero Baseline GPS OTF Test Results (Height).	135
Figure 8.12	The GPS Receivers' Set-up Used for the Short Baseline Trial.	136
Figure 8.13	The Eastings Component of the OTF Position for the Short Baseline Trial.	138
Figure 8.14	The Northings Component of the OTF Position for the Short Baseline Trial.	138
Figure 8.15	The Height Component of the OTF Position for the Short Baseline Trial.	139
Figure 8.16	The Eastings Component of the OTF Vector for the Short Baseline Trial.	140
Figure 8.17	The Northings Component of the OTF Vector for the Short Baseline Trial.	141
Figure 8.18	The Height Component of the OTF Vector for the Short	141

	Baseline Trial.	
Figure 8.19	The Eastings Component of the OTF Positions for the Bipole Trial.	143
Figure 8.20	The Northings Component of the OTF Positions for the Bipole Trial.	143
Figure 8.21	The Height Component of the OTF Positions for the Bipole Trial.	144
Figure 8.22	Radial Error for an OTF Position Resulting from Entering the True Reference Receiver's Coordinates.	145
Figure 8.23	Integer Fix Flag for an OTF Position Resulting from Entering the True Reference Receiver's Coordinates.	146
Figure 8.24	Radial Error for an OTF Position Resulting from Entering Inaccurate Reference Receiver's Coordinates.	147
Figure 8.25	Integer Fix Flag for an OTF Position Resulting from Entering Inaccurate Reference Receiver's Coordinates.	148

9 Construction Plant Control and Monitoring by GPS

Figure 9.1	A Schematic Showing the Dimensions of the Blade Used for the Trials. The Diagram Shows the Laser Level Receptors Situated on top of the Extendible Masts, as well as the GPS Antenna Situated on One of the masts.	154
Figure 9.2	A grader using a laser level for the control of height and tilt of the blade. The laser itself is seen on the left side of the photo, whilst the two laser level receptors are seen on each side of the blade.	155
Figure 9.3	A laser level being used to control height and tilt on a bulldozer. The wheel at the back of the bulldozer is used to measure distance.	156
Figure 9.4	A Laser Level being used to control an Asphalt Paver.	157
Figure 9.5	The laser level System being used in conjunction with the 'Curve Control' System to measure anomalies in the road's surface [KELLY, 1995(ii)].	158
Figure 9.6	Diagram showing the GPS Antenna and a Leica NA2000	161

	Digital Levelling Staff Located on the Laser Level Receptor's Mast on the Bulldozer's Blade.	
Figure 9.7	Diagram showing the Bulldozer with three Ashtech GPS Antennas Attached at Key Locations.	163
Figure 9.8	Illustration showing the conversion from Eastings and Northings to Along Track (x') and Across Track (y').	165
Figure 9.9	GPS Height of the Antenna Located over the Driver's Cab During Trial 3.	166
Figure 9.10	The GPS Height Component of all Three Antennas Located on the Bulldozer During Trial 3.	167
Figure 9.11	Graph Showing the Noise Level for the GPS Height of the Antenna Located on the Bulldozer's Cab During Trial 3.	168
Figure 9.12	Along Track Plot During Trial 1, During which the Blade was Moved Down Twice by 100 mm at a Time, then up Twice by 100 mm at a Time.	171
Figure 9.13	Across Track Plot During Trial 1, During which the Blade was Moved Down Twice by 100 mm at a Time, then up Twice by 100 mm at a Time.	172
Figure 9.14	GPS Height Plot During Trial 1, During which the Blade was Moved Down Twice by 100 mm at a Time, then up Twice by 100 mm at a Time.	172
Figure 9.15	Along Track Against Across Track Results, During Trial 1, Showing the Antenna's Position During Blade Movement, and Repeatability of the GPS.	173
Figure 9.16	Illustration of the Dimensions and Angles Involved During Blade Movement.	174
Figure 9.17	Across Track Plot for S1 During Trial 3 Illustrating the Precision of the System.	176
Figure 9.18	Across Track Plot for S2 During Trial 3 Illustrating the Precision of the System.	176
Figure 9.19	Across Track Plot for S3 During Trial 3 Illustrating the Precision of the System.	177

Figure 9.20	Vector S1 to S2 Showing Increased Vibration During Bulldozer Movement.	178
Figure 9.21	Vector S1 to S3 Showing Increased Vibration During Bulldozer Movement.	178
Figure 9.22	Graph Showing GPS Height Against Time During Trial 1. The Red Boxed Portions of the Graph Represent Times when the Bulldozer was Standing Still, Showing a Smaller Vibration Noise.	180
Figure 9.23	Illustration of the Blade's Movement During Tilting.	182
Figure 9.24	Along Track Against Across Track Plot.	183
Figure 9.25	The Bulldozer Travelling with a Tilted Blade During Trial 3.	185
Figure 9.26	The GPS Height Component During a to and fro Tilting Manoeuvre, where the Blade was Moved from Left Hand Tilt to a Right Hand Tilt and Back Again.	186
Figure 9.27	Distance Along the Track During a to and fro Tilting Manoeuvre, where the Blade was Moved from Left Hand Tilt to a Right Hand Tilt and Back Again.	186
Figure 9.28	Distance Across the Track During a to and fro Tilting Manoeuvre, where the Blade was Moved from Left Hand Tilt to a Right Hand Tilt and Back Again.	187

10 Monitoring Large Structures by Real Time OTF GPS

Figure 10.1	The equipment located at the mid span of the Humber Bridge. The GPS antenna is attached to the bridge via a bipole, firmly attached to the barrier. The Ashtech Z-XII GPS receiver was located inside the orange rucksack, which also houses the UHF telemetry link. The real time OTF processing was carried out on a Pentium-90 laptop PC, loaded with Ashtech's Real Time PNAV software.	195
Figure 10.2	Longitudinal Movement of the Bridge Deck During Trial 1.	196
Figure 10.3	Vertical Displacement of the Bridge Deck During Trial 1.	197

Figure 10.4	Lateral Movement of the Bridge Deck During Trial 1.	198
Figure 10.5	Longitudinal Movement of the Humber Bridge During the Second Trial.	199
Figure 10.6	Height Deflection of the Humber Bridge During the Second Trial.	200
Figure 10.7	Lateral movement of the Humber Bridge During the Second Trial.	200
Figure 10.8	The GPS antenna located on the top of the bridge's northern tower.	202
Figure 10.9	North-South Movement of the Northern Support Tower.	202
Figure 10.10	East-West Movement of the Northern Support Tower.	203
Figure 10.11	Vertical Movement of the Northern Support Tower.	204
Figure 10.12	Two GPS Antennas Clamped onto the Side Rail of the Humber Bridge.	205
Figure 10.13	Lateral movement of the Humber Bridge During the Third Trial.	206
Figure 10.14	Longitudinal movement of the Humber Bridge During the third Trial.	207
Figure 10.15	Vertical movement of the Humber Bridge During the Third Trial.	207
Figure 10.16	Lateral Vector Between the Two GPS Antennas Situated Upon the Humber Bridge During the Third Trial.	208
Figure 10.17	Longitudinal Vector Between the Two GPS Antennas Situated Upon the Humber Bridge During the Third Trial.	209
Figure 10.18	Height Vector Between the Two GPS Antennas Situated Upon the Humber Bridge During the Third Trial.	209
Figure 10.19	The Dee Estuary Bridge under Construction.	211
Figure 10.20	Dee Bridge Eastings During Trial 1.	213
Figure 10.21	Dee Bridge Northings During Trial 1.	214
Figure 10.22	Dee Bridge Heights During Trial 1.	215
Figure 10.23	An Ashtech Z12 GPS Receiver and Geodetic Choke Ring Antenna Situated upon the Dee Estuary Bridge During Construction.	217
Figure 10.24	Movement of the Dee Bridge in the Eastings (longitudinal) Direction.	218
Figure 10.25	Movement of the Dee Bridge in the Northings (lateral) Direction.	218
Figure 10.26	Movement of the Dee Bridge in the Vertical Direction.	219

Figure 10.27	Vector between the two Antennas Situated upon the Dee Bridge in the Eastings Component.	220
Figure 10.28	Vector between the two Antennas Situated upon the Dee Bridge in the Northings Component.	220
Figure 10.29	Vector between the two Antennas Situated upon the Dee Bridge in the Height Component.	221
Figure 10.30	Movement of the Clifton Bridge in the Eastings Component (lateral).	223
Figure 10.31	Movement of the Clifton Bridge in the Northings Component (longitudinal).	223
Figure 10.32	Movement of the Clifton Bridge in the Height Component.	224
Figure 10.33	Vector between the two Antennas Situated upon the Clifton Bridge in the Eastings Component.	225
Figure 10.34	Vector between the two Antennas Situated upon the Clifton Bridge in the Northings Component.	226
Figure 10.35	Vector between the two Antennas Situated upon the Clifton Bridge in the Height Component.	226

List of Tables

4 GPS Positioning Techniques

Table 4.1 Rapid Static Observation Times 38
[TRIMBLE NAVIGATION, 1992]

6 The Accurate Recovery of Cycle Slips

Table 6.1 Computed Ionospheric Residuals Using L1 and Lw 70
Table 6.2 $\delta\phi$ Resulting from Various Multiples of 9L1 and 7L2 Integers. 91
Table 6.3 Times and Magnitudes of the Synthetic Cycle Slips for Satellite 16. 96
Table 6.4 The Synthetic Cycle Slips as Detected by the Various Techniques, and the Programs Overall Estimate of their Values. 96

7 Long Range OTF Kinematic GPS

Table 7.1 Vehicle speeds during the trial. 104
Table 7.2 Baseline differences due to ionospheric activity. 110

9 Construction Plant Control and Monitoring by GPS

Table 9.1 Digital Level Readings Compared to the GPS Height. 170
Table 9.2 Table Showing the Manoeuvres Corresponding to Figures 9.20 and 9.21. 179
Table 9.3 Along Track and Across Track Values Before and After the Manoeuvre. 183

Chapter 1

Introduction

Kinematic GPS has been the focus of research for many years, [SUMMERFIELD, 1990], [WESTROP, 1990], [WALSH, 1994], [HANSEN, 1996]. All the research has focused on the development of OTF software and algorithms to enable efficient kinematic carrier phase positioning to be achieved. The more recent research has been focused upon the development of On The Fly (OTF) algorithms, whereby carrier phase integer ambiguity resolution is achieved whilst on the move. The applications to which OTF GPS can be used on are numerous, especially when the OTF algorithms are used in a real time system.

1.1 Satellite Navigation

Ever since the first sputnik satellite was placed into orbit, it was realised that data transmitted suffered from the effect of Doppler shift. Scientists at the Applied Physics Laboratory (APL) of Johns Hopkins University found that the position of the satellite could be determined by measuring the Doppler shift at ground points of known coordinates. The idea was developed by APL to form the basis of the US Navy's Navigation Satellite System (NNSS), commonly known as the Transit Doppler System. This began operating in 1964, and was used by Geodesists as well as navigators to enable precise positioning. The main reason for the system's development, however, was for Polaris submarines

to be able to coordinate themselves anywhere in the world. The system, however, was very tedious to use, as there were only a few satellites, and the user had to wait for hours to be able to position.

The US Department of Defense (DoD) decided to develop a new system, which would enable instantaneous positioning anywhere in the world, day or night during any weather. The use of microprocessors and accurate atomic clocks meant that satellites could be developed which could transmit precise signals at accurate times, the time taken by the signal to travel to the user, scaled by the speed of light gives the range. Four ranges are required to correct for the user's three dimensional position, as well as the clock errors between the accurate satellite clocks and the digital clocks within the receiver.

The system is the DoD's NAVSTAR (NAVigation Satellite, Timing and Ranging) GPS (Global Positioning System), which is detailed in Chapter 2 and 3. GPS is an all weather, 24 hour system, which allows positioning anywhere in the world. Authorised users can position themselves to an accuracy of ~20 m, whilst civilian users can position themselves to ~ 100 m. Research, however, has seen the development of techniques which can increase the accuracies obtained, from a few metres using DGPS, to millimetres by using carrier phase techniques.

1.2 Real Time Kinematic GPS

An accuracy of 100 m is good enough for many navigation applications, but is nowhere near accurate enough for surveying. Carrier phase techniques have been developed which allow millimetre level precision, but require the GPS receiver to remain stationary. OTF GPS allows the user to move whilst positioning, and when the OTF system incorporates a telemetry link it is possible to achieve real time millimetre level positioning. The applications for such a real time positioning technique are numerous, ranging from precise

navigation, real time setting out, construction plant control and the monitoring of large structures.

1.3 Engineering Applications of Real Time OTF GPS

Real Time OTF kinematic GPS has the advantages over other GPS positioning techniques that it can be used in a dynamic situation. Many engineering applications, such as setting out, may take advantage of using this type of kinematic GPS. In addition, the integration of such a positioning technique into the hydraulics of a construction plant may allow automated plant control and monitoring. Real time OTF GPS could also be used to monitor the movement of structures, whether they are meant to move or not. Such structures could include stock piles, large bridges and damns. Many other applications are possible with the technology, the only limitation being able to see enough satellites to allow positioning and being able to think of the applications.

1.4 Thesis Overview

The aim of this research is to investigate the engineering applications of real time On-The-Fly (OTF) kinematic GPS, as well as the applications of OTF GPS over long ranges and the detection of cycle slips within the OTF data. The Concepts of GPS are outlined in Chapter 2, where the way in which GPS works is described. Chapter 3 discusses the Measurements and Observables available through using the GPS system, discussing their resolution, and the way in which the GPS receiver accesses the signals, and how modern GPS receivers can overcome encryption placed upon the GPS signals by the US DoD. Chapter 4 discusses the Positioning Techniques used, with accuracies ranging from ~100m to a few millimetres. Chapter 5 Discusses the concepts of OTF GPS, as well as detailing the processing techniques which can improve the technique. Chapter 6 details the problem of cycle slips with using carrier phase data, especially with kinematic data. Four techniques are discussed, which have been used by the

author to develop a FORTRAN 77 program, which detects and corrects cycle slips. Chapter 7 details trials and results carried out by the author using OTF GPS over baselines in excess of 100 km, using software developed by Hansen [1996]. Chapter 8 discusses real time OTF GPS and how the data may be transmitted through a telemetry link, resulting in a real time system. The precision of such a system as well as its advantages and disadvantages are discussed. Chapters 9 and 10 discuss engineering applications of real time OTF GPS. Chapter 9 details the use of real time OTF GPS to monitor and control construction plant. Trials were carried out by the author whereby real time OTF GPS was placed on a bulldozer, and the resulting positions analysed. Chapter 10 details the use of real time OTF GPS as a tool to measure the movement of large structures. Such structures include bridges which move due to wind loading and traffic loading, as well as the monitoring of a bridge during construction. Conclusions and recommendations are given within each Chapter.

1.5 References

HANSEN. P., 1996, *On-The-Fly Ambiguity Resolution for GPS*, PhD Thesis, The University of Nottingham, Nottingham, United Kingdom.

SUMMERFIELD, P.J. 1990. *Kinematic GPS Surveying*. PhD Thesis, University of Nottingham.

WALSH, DMA. 1994. *Kinematic GPS Ambiguity Resolution*. PhD Thesis, University of Nottingham.

WESTROP, J., 1990, *Dynamic Positioning by GPS*, PhD Thesis, The University of Nottingham, Nottingham, United Kingdom.

Chapter 2

The Concepts of GPS

2.1 Introduction

Navstar GPS is an acronym for **NA**Vigation **S**atellite **T**iming **A**nd **R**anging **G**lobal **P**ositioning **S**ystem, and is commonly abbreviated to GPS. The positioning through GPS is a form of intersection, where the user measures the distance to four satellites, which transmit their positions in orbit. The user then solves for his position (X, Y, Z or ϕ, λ, h) and clock error (Δt).

Many publications are presently available which describe the 'concepts of GPS', however, this chapter will only outline the general details of the system.

2.2 Motives Behind the GPS System

The Transit Doppler satellite navigation system was developed between 1958 and 1963 for the US Navy, and became generally available for non-military users in 1967 [ASHKENAZI *et al*, 1977], but was only able of providing accuracies in the order of 10's of metres after about one hour's observation [WALSH, 1991]. This method was not accurate and quick enough for new aircraft and missile positioning.

In the early 1970's the Unites States of America Department of Defense (DoD) decided to develop GPS, which would provide instantaneous three dimensional (3-D) positioning to a few metres anywhere in the world. The predominant reason for the system was a military one, but with the development of civilian receivers and understanding, the civilian service is now as good as that available by the forces, if not better. The positioning accuracies vary from millimetric Fiducial GPS techniques to 100m stand alone C/A-code. These accuracies depend upon the type of receiver, user dynamics, observables and processing techniques used.

2.3 The System

GPS was declared at Initial Operational Capability (IOC) in December 1993 and at Full Operational Capability (FOC) in April 1995. It was designed as an all weather, all terrain system. The number of users at any one time is infinite, as long as they have a GPS receiver. The only limitation with the system is the ability to see at least four satellites for 3-D positioning, five satellites for real time On The Fly (OTF) positioning and three satellites for two dimensional (2-D) positioning. The US DoD have placed two extra limitations upon the system as used by non military personnel, these being Anti Spoofing (AS) and Selective Availability (SA) §3.2.4. AS results in the encryption of one of the two GPS codes, and SA results in false codes being transmitted. SA became operational on the 15 March 1990, and AS in July 1992. Only Block II satellites are affected. Certain environments can produce problems and limitations, such as the effect of multipath. This is discussed more fully in chapter 6.

The system presently consists of 24 Block II satellites at a range of around 20,200 km above the earth, with approximately 11 hour 58 min orbits. Six orbital planes exist, which lie at 55° inclination. Four satellites orbit in each of the planes. Two positioning services exist, Precise positioning Service (PPS) and Standard Positioning Service (SPS). The PPS was intended for military use only, and the SPS for civilian.

GPS is split into three segments, these being

- The Control Segment
- The Space Segment
- The User Segment

2.3.1 The Control Segment

The control segment carries out the tracking, data transmission and supervision tasks necessary for the control of all the GPS satellites.

The control segment consists of five ground based monitoring stations, whose coordinates are accurately known, equipped to monitor the satellites and update the information transmitted by the satellites. These are located at Hawaii, Colorado Springs, Ascension Island, Diego Garcia and Kwajalein, figure 2.1, all of which lie close to the equator. Their configuration means that the satellites can be monitored 90% of the time. This segment is a vital part of the system, whereby each satellite is updated every hour. However, the satellite ephemeris will degrade over time, and the ephemeris should be upgraded at least every four hours [SHARDLOW, 1994]. Each tracking station possesses a dual frequency GPS receiver connected to an external caesium beam oscillator. The data from the tracking stations is transmitted to the master control station at the Consolidated Space Operations Centre, Falcon Air Force Base, Colorado Springs. Here, the satellite ephemerides and clock corrections can be predicted and uploaded to the satellites.

2.3.1.1 Satellite Ephemerides

The satellite ephemeris is a list of Keplerian elements defining the mean orbit of the satellites and correction terms for deviations from the orbits. As the satellites orbit the Earth at approximately 20, 200 km, they experience very little drag and the orbits are fairly consistent. The ephemeris may be obtained in one of two ways.

The broadcast ephemeris is transmitted as part of the Navigation message in the GPS signal [ASHKENAZI and MOORE, 1986] and [VARNUM and CHAFFEE, 1982].

Essentially, the user receives a list of 16 Keplerian elements for the satellites. From these, it is possible to determine the instantaneous orbital ellipse and the position of the satellite on that ellipse, for all epochs of observations [MOORE, 1993], [SHARDLOW, 1994]. These elements are revised every hour, but are valid without too much degradation for up to 4 hours. The updated information is uploaded to the satellites from one of the four ground antennas (GA) shown in figure 2.1. Broadcast ephemerides have accuracies in the region of 10 to 20 metres.

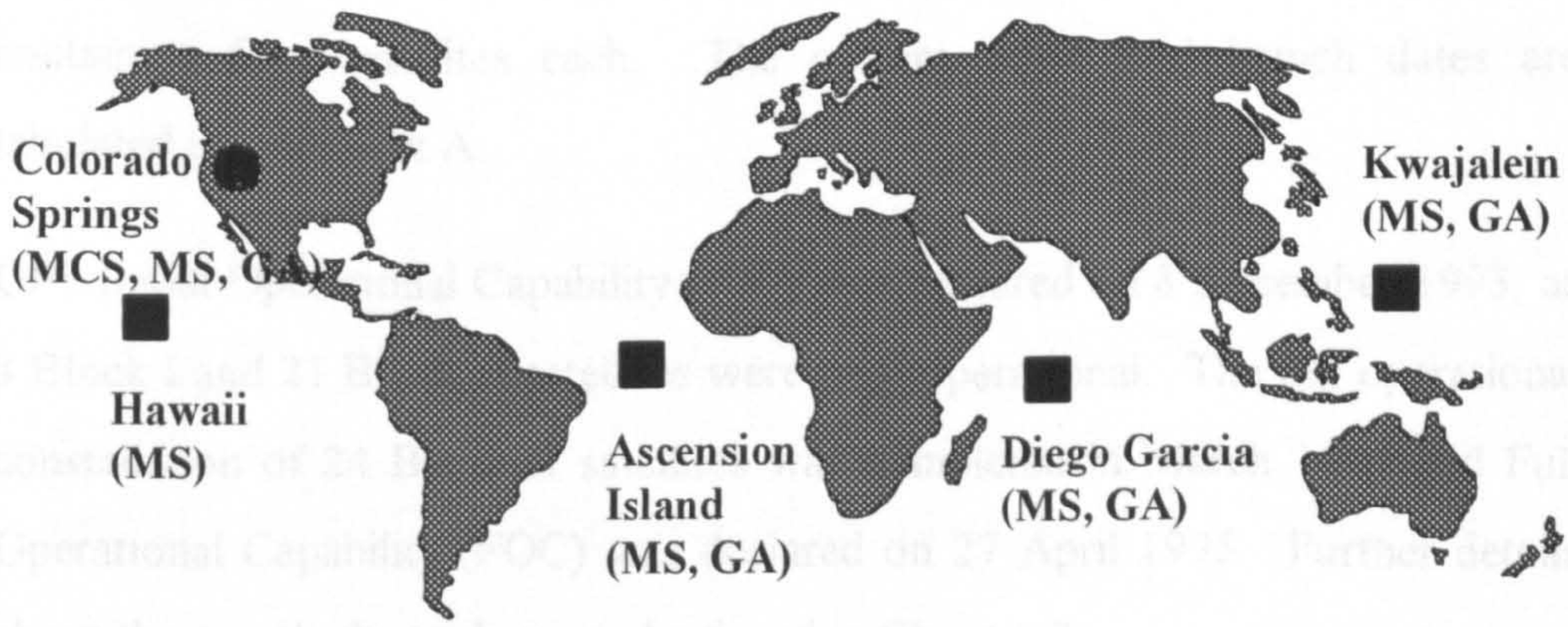

Figure 2.1

Location of the Control Segment's tracking Network.

More accurate ephemerides are generated after the event. These are termed Precise Ephemerides, and have accuracies of approximately 20 cm. Such ephemerides are obtained from organisations such as International GPS Geodynamics Service (IGS), and are freely available over the internet. The precise ephemerides are created from a world-wide network of permanently tracking GPS receivers.

2.3.2 The Space Segment

The space segment of the GPS system consists of the GPS satellite constellation.

Initially, the constellation was to consist of 24 satellites plus 3 active spares. However, due to budgetary limitations, the constellation consists of 24 satellites, orbiting the earth in such a way as to provide 24 hour coverage with at least 4 satellites being visible anywhere in the world at any time.

The satellites are in near circular orbits at nominal altitudes of 20,200 km, with a period of approximately 11 hours and 58 minutes. The satellites consist of 21 satellites with 3 spares orbiting at an inclination of 55°, with six orbital planes containing four satellites each. The current status and launch dates are tabulated in Appendix A.

GPS Initial Operational Capability (IOC) was declared on 8 December 1993, as 3 Block I and 21 Block II satellites were fully operational. The full operational constellation of 24 Block II satellites was completed in March 1994 and Full Operational Capability (FOC) was declared on 27 April 1995. Further details about the signals themselves can be found in Chapter 3.

The first Block IIR, replenishment, satellite blew up on launch on the 17 January 1997 at Cape Canaveral. It is the second launch failure on the GPS program's history, the first occurred on 18 December 1981 [GPS WORLD, 1997].

2.3.3 The User Segment

Because GPS is a passive system, an unlimited number of users can access it at any one time. The user must have a GPS receiver to access the data, which is basically a radio receiver, with an in-built data processor to calculate the 3-dimensional position. The characteristics of the receiver depend upon the accuracies of the applications. The cost of a GPS receiver dramatically

increases with accuracy. These range from a C/A-code receiver which is accurate to ~100 m 2d RMS, to geodetic receivers which can access both the carriers and pseudorange observables on L1 and L2. Numerous types of receivers have been developed which can cater for the wide range of requirements.

Further details about the techniques used within the receivers to access the signals are found in §3.3.

Two levels of GPS services are available, namely the Standard Positioning Service and the Precise Positioning Service.

2.3.3.1 The Standard Positioning Service

The Standard Positioning Service (SPS) is available to all users on a continuous world wide basis with no direct charge. This service is provided through the GPS L1 carrier frequency, supplying the C/A-code and navigation message. SPS provides horizontal positioning accuracies to within 100 m 2d RMS (95% probability) and 300 m (99.9% probability). The degraded accuracies are achieved by the US DoD placing encryption and errors onto the SPS, §3.2.1.

2.3.3.2 The Precise Positioning Service

Users authorised by the US DoD may access the Precise Positioning Service (PPS), designed to provide instantaneous and accurate positioning, velocities and timing service on both L1 and L2 carrier frequencies. It is denied to non authorised users by the encryption of the P-code to the Y-code §3.2.1, and the use of SA. PPS users can therefore access both the C/A-code and P-code.

2.4 References

ASHKENAZI, V, GOUGH, RJ, SYKES, RM. 1977. *Satellite-Doppler Positioning*, Prepared for a seminar held at the University of Nottingham 10 to 11 January, 1977.

ASHKENAZI, V. and MOORE, T., 1986, *The Navigation of Navigation Satellites.* The Journal of Navigation, Vol. 39, No. 3, pp 377 - 393.

GPS WORLD, 1997, *News and Applications of the Global Positioning System.* GPS World, February 1997, pp. 20.

MOORE, T., 1993, *GPS Orbit Determination and Fiducial Networks.* Sixth International Seminar on the Global Positioning System, University of Nottingham.

SHARDLOW, P.J., 1994, *Propagation Effects on Precise GPS Heighting,* PhD Thesis, University of Nottingham.

VARNUM, F. and CHAFFEE, J., 1982, *Data Processing at the Global Positioning System Master Control Station.* Proc. 3rd Int. Geodetic Symposium Doppler Positioning, Las Cruces.

WALSH, DMA. 1991. *Real time Dynamic Positioning*. First Year Report, University of Nottingham.

Chapter 3

GPS Measurements and Observables

3.1 Introduction

A signal transmitted at a frequency f_s will be subjected to a phenomenon known as *Doppler Shift* when received by a relatively moving receiver. This is simply *'the change in apparent time interval between two events which arise from the motion of an observer together with the finite velocity of transmission of information about the events'* [GILL, 1965].

This happening can be witnessed in everyday life for example; a moving car emits a sound at a constant frequency. Whilst the car moves towards an observer, the frequency heard increases to it's maximum value, which is the same as f_s. As the car travels away from the observer, the frequency decreases in value. The same effect is seen with emitted satellite signals, moving relative to a ground receiver. The Doppler shift effect has been evident since 1676, well before Doppler and Fizeau published their work. Here, Romer deduced the velocity of light using the apparent variation of Jupiter's satellites [GILL, 1965]. The same effect was observed from the first satellite, Sputnik, to orbit the Earth. Ever since, techniques and satellites have been developed to enable positioning using Doppler shift.

This technique has been used by the Transit Doppler system, and is now the fundamentals behind the Carrier Phase GPS method.

The Transit Satellite system was developed between 1958 and 1963 for the US Navy. A satellite Doppler receiver measures (integrated) Doppler counts, over a fixed time interval, as the satellite passes over it. Range rate equations are then derived from the Doppler measurements to lead to the receivers position. The system consisted of six operational satellites, at a nominal altitude of 1,100km [ASHKENAZI, 1977].

GPS was designed as a passive system, capable of serving a large number of users. This is achieved by taking range measurements through recording the time taken for a signal to travel from a satellite to the GPS receiver. This time will give a distance when multiplied by its velocity, the speed of light. There are, however, errors due to atmospheric effects, satellite and receiver clock errors, ephemeris errors and others such as multipath effects. The measured distance is therefore called a pseudo range, as it is not the true range due to the errors. The basic details of the GPS signal are outlined in the following chapter.

3.2 GPS Signal Structure

The signal was designed to reduce multipath and ionospheric noise and to withstand hostile interference through jamming. This was partly achieved using a spread spectrum technique, where the signal is spread over a much wider signal band than the minimum bandwidth required to transmit the information. The time and frequency generation on board the satellites is based on extremely precise atomic standards carried by all the satellites. The Block II satellites contain two rubidium and two caesium beam atomic clocks. All the GPS satellite signals are derived from this on-board atomic standard, which has a fundamental frequency of 10.23 MHz. The time of signal broadcast is stated to be accurate to within 1 microsecond and the frequency held to 1 part in 10^{12}. The atomic frequency standards are, however, affected by the motion of the satellite and its lower gravitational potential. These are collectively termed *relativistic effects* and are partly compensated for by altering the fundamental

frequency of the signal to 10.29999999454 MHz. Other relativistic effects are described in Leick [1990].

3.2.1 The Carrier

Each satellite transmits two L-band carrier frequencies L1 (1575.42 MHz) and L2 (1227.60 MHz). Navigational and identification information unique to each satellite are bi-phase modulated onto these carriers. Sub bands within the L-band have been set aside by the International Telecommunications Union, which is the radio regulation arm of the United Nations, for satellite based positioning systems [SHARDLOW, 1994].

A third L-band (L3) exists, which has classified details, and future GPS satellites (Block IIF) will include an L5 band for standard positioning service only. This is a new plan agreed by the US DOT and DOD which will try to overcome the security problems the US DOD currently face due to civilian GPS receivers being able to access the L2 P-code.

3.2.2 Pseudo Random Noise Codes

Two Pseudo-Random Noise (PRN) binary sequences are modulated onto the L-spectrum carrier signals. These are the Precise Code (P-Code), and the Coarse Acquisition Code (C/A-Code). The codes provide an unambiguous observable which enable range measurements to be made, using the time delay. The codes consist of a series of random binary digits generated by mathematical algorithms. The C/A-code is only modulated on the L1 frequency whilst the P-code is modulated onto the L1 and L2 carriers. To distinguish between the two codes on the L1 carrier, they are modulated at right angles to each other. Figure 3.1 illustrates the idea of modulating the codes onto the carrier.

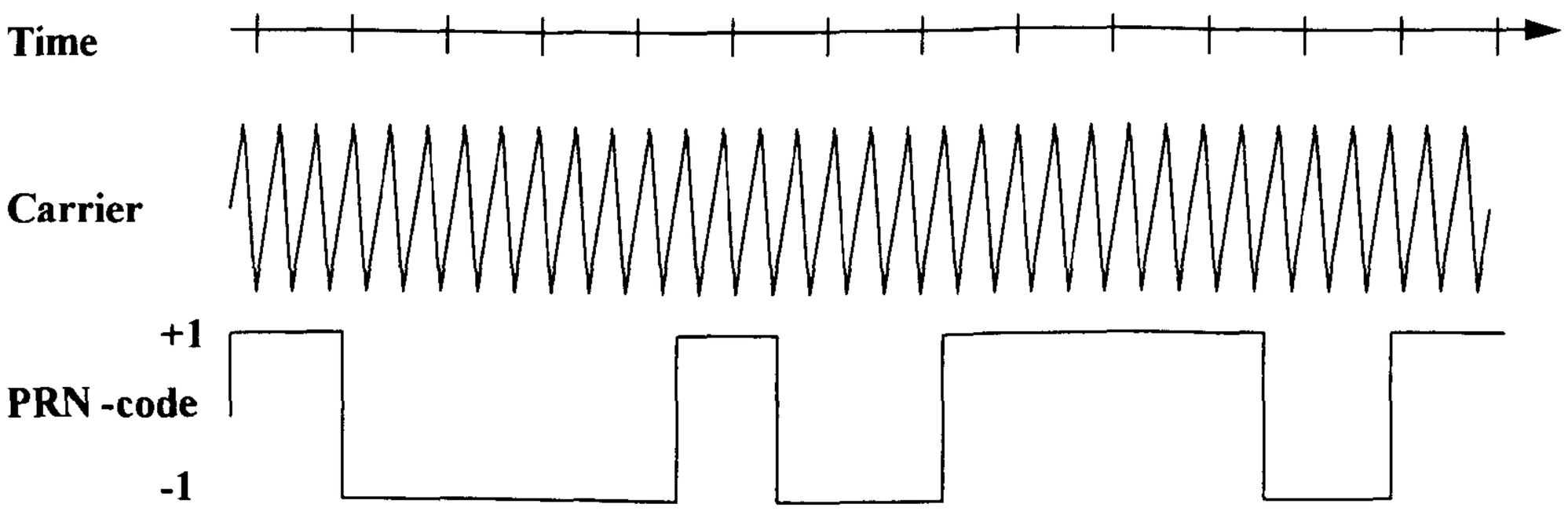

Figure 3.1

GPS Signal Structure (Reproduced from [MOORE. T , 1994])

3.2.2.1 Coarse Acquisition Code

Each satellite transmits an unique C/A-code and is represented by a given PRN number. The C/A-Code has a frequency of 1.023 MHz and under fully operational conditions will have an accuracy of 100m 2-D RMS in single stand alone positioning with SA and 30m without. The C/A-code is a sequence of 1,023 binary digits, or chips, which repeat every millisecond. It is possible to obtain a unit of measurement by multiplying the time interval by the speed at which the carrier travels through space, this being the speed of light. One millisecond corresponds to approximately 300 metres, which is the chip wavelength of the C/A-code. A GPS receiver can quickly lock onto this signal and begin to correlate the received code with an internally generated replica code, as it repeats itself every millisecond.

3.2.2.2 Precise Code

The P-Code is also a pseudo random binary sequence and is used for more precise positioning. It has a frequency (chipping rate) of 10.23 MHz, which is ten times faster than C/A-code, and a repeat period of 38 weeks. Each satellite

position, however, are provided every 30 seconds, being the ephemeris and clock offsets.

A composite signal comprising of the code and message are modulated onto the carrier. This is made up of a combination of PRN code chip stream and message data stream using modulo 2 addition. This means that if the code chip and the message bit have the same value (both 0 or both 1) the result is 0, otherwise the result is 1.

Combining the message with the PRN code is a straight forward process on the L2 carrier, as there is only the P-code. As there are two code present on L1, both C/A-code and P-code, the process is more complex. The problem is overcome by modulating the P-code onto the L1 channel in the same manner as on L2 channel. The C/A-code, however, is mixed onto the *quadrature carrier*, which means that the unmodulated carrier is shifted in phase by 90°. The signal is then combined with the P-code modulated in-phase component to result in the L1 carrier with both the C/A-code, P-code and navigation message.

3.2.4 Degradation of the GPS Signal

Both systematic and random errors can affect the GPS signal, which can be classed into satellite errors, receiver errors and signal path errors. Further to these natural inherent errors are induced errors which have been introduced into the GPS signal by the US DoD to degrade and limit the accessibility to non permitted Precise Positioning Service users i.e. SPS only users. As with all surveying techniques, setting up errors can also be present, which are important when carrier phase data is used, resulting in millimetric positioning.

3.2.4.1 Anti Spoofing

Anti-Spoofing (AS) was designed to encrypt the P-code by modulating a W-code as well as the P-code onto the carrier resulting in the Y-code. This meant that only those authorised to access the Precise positioning Service would know the structure of the W-code and be able to access full P-code positioning.

Block I satellites were exempt from AS, and at present AS is active on all Block II satellites.

3.2.4.2 Selective Availability

Selective Availability (SA) was also designed to degrade the positioning accuracies achievable. SA was implemented on 25 March 1990, and accomplishes the degradation through manipulating the navigation message *(epsilon)* and the satellite clock frequency *(dither)*.

3.3 GPS Receiver Technology

The GPS user segment's hardware consists of a GPS receiver and antenna and some form of data recorder. Two types of receivers exist, these being *Navigation* and *Geodetic*. The Geodetic receiver is detailed in this chapter, as well as explanations of how the C/A-Code is accessed and different techniques to access the encrypted Y-Code. The receivers track and store carrier and code values, either L1 only or L1 and L2.

In general, single frequency receivers access the C/A-Code and the L1 carrier phase through *code correlation*. Dual frequency receivers access the encrypted Y-Code through various means, including cross correlation, signal squaring and code tracking techniques.

3.3.1 Code Correlation

The C/A-Code is tracked by employing a *code correlation* technique, whereby the receiver generates a replica C/A-Code for each individual satellite, similarly to that used within the satellite. The internally generated code is then aligned onto the received code by delaying it, the delay time is the pseudo range. This is detailed in chapter 4. Once alignment has occurred and the pseudo range calculated, the C/A-Code can be removed from the carrier signal in order for

the receiver to access the navigation message and the carrier phase data which is used for precise carrier phase positioning §4.3. The process is used for P-code correlation when AS is not active.

3.3.2 Signal Squaring

The Trimble 4000 SST uses the most simple form of accessing L2 carrier phase when AS is on, this is called *signal squaring*. The C/A-Code and L1 carrier phase are accessed through code correlation. The L2 signal is squared, removing the phase inversions due to the codes. This results in a signal with a constant unit amplitude and a frequency twice that of the original. The L2 pseudo range can not be accessed with this technique, and squared 'half wavelength' data is produced. This means that cycle slip cleaning through triple differencing and ambiguity resolution are difficult.

With the continuous AS implementation, receiver manufacturers have devised new techniques to access the encrypted P-Code (Y-Code).

3.3.3 Cross Correlation

The Trimble 4000 SSE receiver uses a form of cross correlation to access the encrypted P-Code. This does not give an accurate value of the P-Code. A *Precise* C/A-Code is obtained, also known as narrow correlation. The resolution is not as good as the P-Code, but more so than the C/A-Code.

This technique assumes that like the P-Code, the W-Code and the Y-Code are the same on both L1 and L2. The L1 signal arrives at the receiver before the L2 signal, due to ionospheric delay, and the L1 Y-Code is accessed using the L1 signal, which is then used to access the L2 signal. The (Y2-Y1) pseudo range is measured as the delay between the two signals. The L1 precise C/A-Code is then added to the Y2-Y1 to derive a precise C/A + (Y2-Y1) pseudo

range. The L2 carrier phase observable is acquired in a similar manner, whereby the delayed L1 carrier phase observable is used in conjunction with the Y2-Y1.

3.3.4 P-W Tracking

The Ashtech Z-XII and Trimble 4000 SSI use a direct method of P-Code decryption, and is far less noisy than the cross correlation technique. The resulting P-Code pseudo range appears to be similar to that without encryption, Chapter 6. The technique used is known as *PW code tracking*, and again relies on the fact that the P-Code, W-Code and hence the Y-Code on the two frequencies are the same. Additionally, this technique make use of the fact that the W-Code is a substantially lower rate encryption, at about 50 bps. The receiver correlates the underlying P-Code in the incoming Y-Code signal with an internally generated P-Code. The receiver next estimates the current W-Code bit to remove it and leave the P-Code. This results in the C/A-Code, Y1 pseudo range, Y2 pseudo range and both full wavelength carrier phase data.

3.4 Dilution of Precision Parameters

Dilution of Precision (DOP) is the way in which the quality of a GPS position may be formally expressed, equation 3.1. The quality is dependent on the geometry of the satellites.

$$\sigma_x = \text{XDOP} \cdot \sigma_\rho$$

Where σ_x is the precision of the position, XDOP is the DOP parameter dependent on the satellite geometry and σ_ρ is the standard error of the range observation. There are a number of different DOP parameters depending on the type of positional information required, e.g.

VDOP = Vertical Position Only, 1D

HDOP = Horizontal Position Only, 2D

PDOP = Three-Dimensional Position, 3D

The final GPS constellation has been designed such that for Block II satellites, 90% of the time

HDOP ≤ 1.7

VDOP ≤ 2.8

3.5 References

ASHKENAZI, V, GOUGH, RJ, SYKES, RM. 1977. *Satellite-Doppler Positioning*, Prepared for a seminar held at the University of Nottingham 10 to 11 January, 1977.

GILL, T.P. 1965. *The Doppler Effect, An Introduction to the Theory of the Effect*. Logos Press Academic Press.

LEICK, A., 1990, *GPS Satellite Surveying.* Published by John Whiley and Sons, Inc.

MOORE, T. 1994. Royal Navy Long Hydrographic Course on GPS, Lecture Material, University of Nottingham.

SHARDLOW, P.J., 1994, *Propagation Effects on Precise GPS Heighting,* PhD Thesis, University of Nottingham.

Chapter 4

GPS Positioning Techniques

4.1 Introduction

This chapter will introduce the reader to some of the different positioning techniques which solely use either pseudorange or carrier phase observables, as well as those which use both. Absolute and relative positioning techniques are described, whose accuracies vary from ~100 m to a few millimetres.

Traditional GPS (Global Positioning System) methods have been proven accurate and efficient for many high accuracy positioning and navigation applications. Due to the often lengthy occupation times required by traditional GPS static positioning methods, terrestrial survey is frequently more competitive, particularly over a small survey area. Static GPS is more competitive over large geodetic survey areas, where a single static GPS survey for an hour's observation would be far quicker than that of a major traverse. GPS has been made more amenable to a wider range of applications through the evolution of "Rapid Static" and "Kinematic" methods and even more so with the advent of OTF real time systems.

The pseudo range observable is robust and unambiguous but has a poor resolution, ± 20 cm at best, Chapter 6. A typical DGPS position has a positional accuracy in the range 2 to 5 metres [MOORE. T, 1994]. Carrier phase readings can be read to a far greater resolution, typically better than 2mm [MOORE. T, 1994], Chapter 6, but are very fragile, ambiguous, and suffer from cycle slips, Chapter 6. Multipath can also pose a great problem with pseudo range positioning, causing errors in the magnitude of metres [SHARDLOW, 1990].

4.2 Pseudorange Positioning

4.2.1 Absolute GPS Positioning

GPS was developed by the US Department of Defence as a 24 hour, all weather global system, providing an unambiguous absolute position. Instantaneous positioning is achieved by the use of the timing codes and the navigation message. The time delay between the satellite codes and that internally generated within the GPS receiver results in a pseudorange, Chapter 3.

The GPS system was initially developed for navigation purposes, giving stand alone code receiver accuracies of ~100m for C/A-code and ~20m for P-code. Stand alone C/A-code positioning has such a poor accuracy due to the US DoD degrading the signal using SA, §3.2.1. These accuracies are more than adequate for navigating a ship or plane. Conventionally, ships and planes use instruments and radio systems such as Inertial Navigation (IN), Omega, LoranC and Doppler radar. The invent of GPS has meant that navigation accuracies have increased dramatically, in the order of kilometres, and doesn't suffer from drift as the IN system does. However, some applications, predominately surveying, require much higher accuracies. Different techniques have been developed to obtain these higher accuracies. These are mainly differencing

techniques, eliminating the errors mentioned in section §3.2, including both code and carrier observations.

In order to solve for the receiver's position, four unknowns must be calculated. these being the geocentric Cartesian coordinates (X, Y, Z) and the receiver clock offset from GPS time. Therefore, a minimum of four satellite range observations are required, as well as the coordinates of the satellites. The four ranges should be simultaneously measured to reduce errors such as SA and also to result in a single receiver clock offset. Many older receiver's share four channels between the satellites. This is either called sequencing if the timesharing is performed slowly, or multiplexing if performed quickly i.e. only a few milliseconds is spent observing each satellite. The latter is used in modern, non geodetic GPS receivers. However, it is now common for GPS receivers to have more than four channels, using the satellites with best geometry.

If, however, more than four satellites are used to position the GPS receiver, then a least squares process is used to determine the best position [CROSS, 1990], [YAU, 1986].

A satellite has a precise atomic clock operating in a satellite time frame, relative to which signals are transmitted. A GPS receiver has a less precise, but less expensive and more practical, quartz clock. The GPS receiver operates in a receiver time frame. All GPS satellite signals are received in this time frame. The true GPS time frame (T) relates to the satellite time frame (t) and receiver time frame (τ) through;

$$T = t + \delta t \tag{4.1}$$

$$T = \tau + \delta\tau \tag{4.2}$$

Where δt is the satellite clock offset and $\delta\tau$ is the receiver clock offset.

The pseudorange (PR) has already been defined as the difference between the time of transmission of the GPS signal (t^s) in the satellite time frame, and the time of reception (τ_r) of the GPS signal in the receiver time frame, when scaled by the speed of light in a vacuum [BINGLEY, 1997].

$$PR_r^s = c[\tau_r - t^s] \tag{4.3}$$

The geometrical range (true range) (ρ) is the difference between the time of transmission of a GPS signal (T^s), in the GPS time frame, and the time of reception of a GPS signal (T_r), in the GPS time frame, when scaled by the speed of light in a vacuum [BINGLEY, 1997];

$$\rho_r^s = c[T_r - T^s] \tag{4.4}$$

From equations (1) and (2), however, knowing that

$$T^s = t^s + \delta t^s \tag{4.5}$$

$$T_r = \tau_r + \delta\tau_r \tag{4.6}$$

The geometric range may be written as

$$\rho_r^s = c[[\tau_r + \delta\tau_r] - [t^s + \delta t^s]] \tag{4.7}$$

rearranging equation (4.7) results in

$$\rho_r^s = c[[\tau_r - t^s] + [\delta\tau_r - \delta t^s]] \tag{4.8}$$

By combining the definition of the pseudorange, equation (4.3) with equation (4.8), the basic pseudorange observation equation is obtained.

$$PR_r^s = \rho_r^s - c\,[\delta\tau_r - \delta t^s]] \qquad (4.9)$$

This observation equation is not, however, truly explicit as the exact time frames for each of the constituent quantities have not been defined. Errors due to the atmosphere, clock errors and satellite errors are also present, which result in

$$PR_r^s = \rho_r^s - c\,[\delta\tau_r - \delta t^s]] + \text{errors} \qquad (4.10)$$

Equation 4.10 is the basic range equation. To determine the position of a GPS receiver, the ranges form at least 4 satellites are used, three for the positional unknowns, and the fourth for the receiver/satellite clock offset.

4.2.2 Differential GPS

Differential GPS (DGPS) was developed to increase the accuracies through the elimination of the clock, atmospheric and orbital errors, due to the ephemeris as well as SA. This technique makes use of two GPS receivers where the reference receiver's WGS84 co-ordinates are known to at least a tenth of the required positioning accuracy of the roving receiver. The clock, atmospheric and orbital errors are calculated for the base receiver using the observed GPS position and the known position. The second receiver's co-ordinates are corrected for the same errors to obtain a position with accuracies in the range 2 to 5 metres [MOORE. T, 1994]. This is a form of relative positioning. For real time positioning, however, it is vital that a data link is established. This usually consists of a transmitting antenna attached to the reference receiver, which will transmit the corrections to the rover. The system can not be truly 'real time' due to the time delay during the telemetry linkage. The delay may only be in the order of a second or two, but may allow a high velocity roving receiver to cover a considerable distance during this time.

The code can be phase smoothed eliminating errors, thus allowing a higher accuracy code reading.

4.2.3 Pseudorange Differencing

An alternative method to reduce systematic errors in stand alone point positioning is to form a differenced observable. Differencing allows common errors to be cancelled out. Such errors include atmospheric, the effect of SA. Measurement noise, however is increased, and Multipath can not be reduced in any way through such a technique.

The effect of differencing is discussed further in §4.3 in relation to carrier phase measurements. For further details on pseudorange differencing, the reader is referred to Westrop [1990] and Ochieng [1993]

4.2.4 Phase Smoothed Pseudoranges

Pseudorange measurements are much noisier than carrier phase measurements, but may be smoothed using the carrier phase to reduce the noise. This idea was first suggested by Hatch [1982]. Such techniques, however, are affected by cycle slips due to the use of carrier phase.

Two such techniques have been used by Hansen [1996], and are fully detailed there. The techniques used are the ***First Epoch Algorithm*** and ***Between Epoch Algorithm***.

4.2.5 Wide Area Differential DGPS

Wide Area DGPS (WADGPS) is a similar technique to DGPS, but uses more than one reference GPS receiver. The reference receivers are widely separated

and provide corrections valid over a large area. Further details may be found in Ochieng [1993].

4.3 Carrier Phase Positioning

Pseudoranges provide an unambiguous range measurements capable of instantaneous positioning to accuracies at the metre level. This is adequate for navigation, and in some applications, has been the only possible method. For land or geodetic surveying, much greater accuracies are required. Relative positioning accuracies of between 1 and 3 ppm are achievable using the phase of the carrier wave and the broadcast ephemeris.

To access the un-modulated carrier wave, the timing codes have to be removed from the signal. Once this has been achieved, the receiver is capable of measuring the fractional part of the phase, but is unable to resolve the integer number of cycles between the antenna and satellite. Once the GPS receiver locks onto the GPS satellite, the receiver selects an arbitrary integer and is then able to keep count of the integer number of cycles being added as the range between the satellite and receiver change. Consequently, all carrier phase readings for a satellite can be referenced to the integer ambiguity at lock-on, providing loss of lock does not occur. The integer ambiguity has to be resolved for the optimal solution to be obtained. Figure 4.1 illustrates a GPS receiver having locked onto a satellite's carrier phase observable. The range between the satellite and GPS antenna is a combination of the carrier phase and the integer ambiguity. The following subsections outline the various carrier phase observables and techniques, but a complete derivation of all the observables may be found in Bingley [1997].

$\delta\tau_r(\tau_r)$ is the receiver *clock offset* for receiver r in the *receiver time frame* of receiver r.

$\delta t^s(t^s)$ is the *satellite clock offset* for satellite s in the *satellite time frame* of satellite s.

N_r^s is the *integer ambiguity* between satellite s and receiver r. his consists of a correction to the receivers arbitrary "guess" at the value of the integer ambiguity, which is in fact the difference between the "true" integer ambiguity and the receivers arbitrary "guess".

Its derivation can be found in numerous texts [SHARDLOW, 1994], [HANSEN, 1996], [BINGLEY, 1997].

The pure phase observable, as with the pseudorange observable, contains clock, orbit, SA and atmospheric errors. In the same way it is possible to form a difference between receivers to remove the satellite clock and ephemeris errors, plus the majority of the effects of SA. Some of the atmospheric errors will also be removed, if the two receivers are close enough to each other. Three differencing techniques are detailed n the following sections, these being the Single, Double and Triple differencing techniques.

4.3.2 The Single Difference Observable

The single difference observable can be between-satellite, between-receiver or between-epoch difference as illustrated in Figure 4.2.

Between receiver differencing will cancel out the satellite clock offset, orbit inaccuracies and most of the atmospheric error (over short baselines).

Since the receiver clock offset is not cancelled, the observable can be used for monitoring the relative receiver clock behaviour. The disadvantage of this observable is that the receiver clocks need to be modelled accurately. The most commonly used observable is the double difference observable, as it removes the receiver and satellite clock offsets.

4.3.3 The Double Difference Observable

By differencing the single difference observable, the double difference observable is obtained illustrated in figure 4.3. This defines the double difference observable between the two GPS receivers (A and B) and two GPS satellites (i and j). Two single difference observables may be written as

$$\Phi^{i}_{AB}(\tau) = \frac{f}{c}.\rho^{i}_{AB}(T) - \phi_{AB}(\tau) + N^{i}_{AB} \qquad (4.13)$$

and $$\Phi^{j}_{AB}(\tau) = \frac{f}{c}.\rho^{j}_{AB}(T) - \phi_{AB}(\tau) + N^{j}_{AB} \qquad (4.14)$$

Hence,

$$\Phi^{ij}_{AB}(\tau) = \frac{f}{c}.\rho^{ij}_{AB}(T) + N^{ij}_{AB} \qquad (4.15)$$

GPS, various carrier phase kinematic GPS methods have been established. These include both post processing and real time procedures. Tradition has meant that navigation systems have used real time links, whilst surveying has used post processing. The trend is now going towards real time positioning for surveying. The following section outlines some of the carrier phase positioning techniques.

4.4.1 Static Surveying

Static GPS surveying was the first technique to use carrier phase interferometery. One GPS receiver is located upon a point of known WGS84 coordinate, whilst the other is located upon the point whose coordinate is required. The two GPS receivers remain stationary whilst simultaneously recording carrier phase data. As all the techniques described in this section, positioning is made relative to a reference receiver. Post processing is carried out, usually by single or double difference, during which cycle slip cleaning is also carried out.

Most static GPS data processing software packages use double difference observables. The unknowns in the least squares adjustment program consist of the coordinates of the unknown point and the double difference integer ambiguities. As there are more unknowns than observation equations, it is not possible to directly solve the equations. If for example, four satellites are observed, there are three coordinate components, and three double difference integer ambiguities to solve for, with only three double difference observation equations at the first epoch. The equation system is therefore insoluble. A further three observation equations are available at every epoch, which can be used to solve for the six unknowns as long as cycle slips are not present. Following the second epoch, however, the satellite constellation will not have changed much, resulting in very similar observation equations. Using them to solve for the unknowns would produce an ill conditioned matrix, which could not be decomposed successfully, or would not be very stable.

In order for the observation equations to change sufficiently for the equation system to be solved for, it is necessary for the satellite constellation to change significantly. If the survey lasts long enough, between 30 minutes to one hour depending on baseline length and number of satellites, then the least squares solution will produce stable estimates of the coordinate and ambiguity unknowns. The data should also be free of cycle slips, or their values calculated.

Due to un-modelled systematic errors, the initial estimate of the integer ambiguities are non-integer in nature. For short baseline lengths (< 10 km) their values are very close to the integer value. For longer lengths, however, it may be possible to fix the integer ambiguities to an incorrect value, which would degrade the solution. It is common to use a statistical search test, as described in Chapter 5, to estimate whether the integer ambiguity value is significantly better than the next best and whether to accept it or not.

Typical accuracies for static baselines are of the order of 1 cm ± 1 ppm [TRIMBLE NAVIGATION, 1992]. The main disadvantage with this type of surveying is the need for the user to remain static for up to an hour.

4.4.2 Fiducial GPS

Fiducial GPS techniques aim to improve the precision achieved with static GPS. The aim is to maintain sub centimetre precision over hundreds of kilometres. This is achieved through increasing the precision of the satellite orbits. Baseline precisions of 1 part in 10^{-7} or even 10^{-8} are possible [BINGLEY 1997].

When performing a Fiducial survey, a number of GPS receivers are situated upon points whose inter-station separation is known to a high level of accuracy. Fiducial surveying is a two stage operation, firstly, the satellite orbits are improved through transferring the accuracy in the Fiducial network to the

satellites. The improved orbits are then used to position the unknown GPS receivers. Many techniques are available, which can either relax the orbits or integrate the orbits. Further details of the Fiducial technique can be found in [FFOULKES-JONES, 1990], [SHARDLOW, 1994] and [WHITMORE, 1994].

Since the development of the IGS, however, and the availability of precise ephemerides which are accurate to 20 cm, it is common practice to use these in preference to Fiducial techniques.

4.4.3 Rapid Static Surveying

Rapid static GPS is a similar process to static, but involves the use of pseudorange observables to decrease the occupation time. The algorithms used include some or all of dual frequency observations, precise pseudorange measurements and ambiguity searching.

The basic principle is to resolve the integer ambiguities very quickly, enabling centimetre positioning.

The observation time required depends upon baseline length, the number of satellites, the geometry of the satellites and their elevation. Table 4.1 illustrates the observation times recommended by Trimble for rapid static surveys. These times are rather conservative, but in most cases prevent the user from having to re-survey if otherwise too little data is gathered. Again, as with static surveying, rapid static is a post processing technique.

Number of Visible Satellites	*Observation Time (minutes)*
4	20
5	15
6 or more	8

Table 4.1

Rapid Static Observation Times [TRIMBLE NAVIGATION, 1992]

The effects of multipath is not reduced as much as with static, as there is less time available to allow averaging to remove the effects. Rapid static techniques are only used over short (< 20 km) baselines, ionospheric effects start to become de-correlated over this distance.

Rapid static surveying is similar to static, however, the dual frequency carrier phase data is used to produce the wide lane observable (L1 - L2) and precise pseudoranges are used. These are combined with a search technique, similar to that described in Chapter 5, to enable rapid integer ambiguity resolution.

The use of rapid static has increased productivity and is commonly used to initialise integer ambiguities for stop and go surveying.

4.4.4 Stop and Go Kinematic GPS (Semi Kinematic)

An accurate initial baseline vector to eliminate any systematic biases contained within the mathematical model is firstly required, which can be measured using fast-static. This allows the integer ambiguity to be determined quickly. Lock is maintained between the surveyed points whilst the receiver is moved. The bandwidth is widened whilst moving between the points to help keep lock, but only allows the whole number of carrier phase wavelengths to be recorded

whilst travelling between the survey points. When the receiver is placed over the survey point, the bandwidth narrows and the carrier phase can be read to a much higher order of accuracy.

Cycle slips and loss of lock pose a great problem to the system, resulting in the receiver having to be taken to the last known point where the ambiguities are recalculated. Moderm state of the art GPS systems incorporate the use of stop and go surveying with real time datalinks, allowing real time kinematic surveying through single frequency observables. The resulting coordinates, once the integer ambiguities have been correctly resolved for, are as precise as the dual frequency system as both use the L1 carrier phase for the final position.

4.4.5 Pseudo-Kinematic (Nottingham Technique)

Considering static GPS positioning using double differencing algorithms, only a few observations are required to recover the baseline vector. However, longer occupation times are required to allow the satellite geometry to change enough to enable the integer ambiguity to be calculated. It is the span of the data that is important, and not its quality. This technique takes advantage of the changing satellite geometry over a 30 minute period, as the data at the start and the end of the period is important to calculate the integer ambiguities. The roving receiver re-occupies every station twice, after an interval of ~30 minutes. This period gives the satellite geometry enough time to change significantly to allow good positioning, [SUMMERFIELD, 1990]. All the data for a single point is processed together in a static baseline adjustment.

4.4.6 Kinematic 'On The Fly' Ambiguity Resolution

The main disadvantage of the carrier phase techniques discussed are their need for static initialisation. It is not always possible to remain static to initialise the integer ambiguity, and being able to remain dynamic whilst resolving the integer

ambiguities is a great advantage. Such a technique is known as On-The-Fly (OTF) integer ambiguity resolution, and is the only true carrier phase kinematic positioning technique. OTF is the main surveying technique used by the author in the Thesis. The aims of the OTF technique are to be able to obtain centimetre relative positioning, without the need for a known start point, no requirement for the antenna to remain stationary, real time implementation should be possible and loss of lock or cycle slips should not be a problem. There should also be a high degree of integrity, where the system must not fail or produce an incorrect solution.

The OTF technique is detailed further in Chapter 5.

4.5 Conclusions and Recommendations

This chapter has outlined the surveying techniques available, giving an indication of their advantages and disadvantages. None of the techniques are superior to each other, as they all have their advantages as well as disadvantages. The technique to be used by a surveyor depends on the accuracy required, as well as the terrain, dynamics and baseline lengths required.

When planning a GPS survey, all the different techniques should be considered before using any one.

The real time aspect of GPS surveying is becomming an important issue. It is now possible to carry out real time kinematic and static surveys using both single and dual frequency receivers. The real time component is a quality control, allowing the user to witness in the field whether or not the integer ambiguities have successfully been resolved for.

4.6 References

BINGLEY, R. M., 1997. *GPS Observables and Algorithms,* Royal Navy Long Hydrographic Course - GPS, Lecture Material, University of Nottingham.

CROSS, P. A. 1990. *Advanced Least Squares Applied to Position Fixing,* Working Paper No 6, Department of Land Surveying, Polytechnic of East London (North East London Polytechnic, 1983, reprinted 1990).

FFOULKES-JONES, G. H.,1990. *High Precision GPS Surveying by Fiducial Techniques*, PhD Thesis, The University of Nottingham, Nottingham, United Kingdom.

HANSEN. P., 1996, *On-The-Fly Ambiguity Resolution for GPS*, PhD Thesis, The University of Nottingham, Nottingham, United Kingdom.

HATCH, R. R. 1982. *The Synergism of GPS Code and Carrier Measurements,* Proc. 3rd. International Geodetic Symposium on Satellite Doppler Positioning, Las Cruces, New Mexico.

MOORE, T., 1994. *An Introduction to Differential GPS,* Royal Navy Long Hydrographic Course - GPS, Lecture Material, University of Nottingham.

OCHIENG, W. Y., 1993. *Wide Area DGPS and Fiducial Network Design.* PhD Thesis, The University of Nottingham, Nottingham, United Kingdom.

SHARDLOW, P.J. 1990. *Multipath: An Investigation.* MSc Thesis, University of Nottingham.

SHARDLOW, P.J., 1994, *Propagation Effects on Precise GPS Heighting,* PhD Thesis, The University of Nottingham, Nottingham, United Kingdom.

SUMMERFIELD, P.J. 1990. *Kinematic GPS Surveying.* PhD Thesis, University of Nottingham.

TRIMBLE NAVIGATION, 1992, *Real Time Kinematic GPS Surveying Technical Overview,* Surveying and Mapping Division, 645 North Mary Avenue, Sunnyvale, California.

WALSH, DMA. 1994. *Kinematic GPS Ambiguity Resolution.* PhD Thesis, University of Nottingham.

WESTROP, J., 1990, *Dynamic Positioning by GPS,* PhD Thesis, The University of Nottingham, Nottingham, United Kingdom.

WHITMORE, G., 1994. *Coordinate reference Systems for High Precision Geodesy,* PhD Thesis, The University of Nottingham, Nottingham, United Kingdom.

YAU, J. W. Y. 1986. *Relative Geodetic Positioning Using GPS Interferometry,* PhD Thesis, The University of Nottingham, Nottingham.

Chapter 5

OTF Integer Ambiguity Resolution

5.1 Introduction

The main disadvantage of the carrier phase positioning techniques detailed in Chapter 4 is the need to be stationary for integer ambiguity determination. The need to return to a known position is a time wasting procedure, as is re-occupation, and it may not be possible or feasible to do so. (Indeed, some GPS requirements, such as navigating a plane or ship, mean that it is impossible to remain stationary for ambiguity resolution). In these situations, a method of establishing the integers whilst on the move is needed.

One such method is known as On The Fly (OTF) Integer Ambiguity Resolution. OTF requires at least five satellites for ambiguity resolution, but four can be used for positioning once the integers have been established. The following paragraph will discuss the OTF search technique, and some of the processing options which accelerate the search time. Further information may be found in [HANSEN, 1996].

Traditionally, navigation systems have used real time links, whilst positioning and surveying have used post processing. Post processing does not allow poor

readings or results to be effectively detected until the processing takes place back in the office, and corrective procedures can cost extra time and money. As such, the trend is now going towards both real time positioning and surveying.

The advantages of a real time system is that the positioning can be established whilst in the field, and any poor readings and data can be rectified and taken again. The raw data may be recorded, in addition to the positions, and the positions computed by post processing using different variables and options as well as forward and backward processing. Another advantage of a real time system is that by only recording positions, the amount of data to be archived can be vastly reduced. Assuming that the raw data is not required for post processing, this allows a real time system to function with only a small onboard memory and hence it will be smaller in size and cheaper to build and buy.

With such obvious advantages, the uses for real time OTF kinematic GPS are numerous, including mapping, attitude determination, structural deformation, high speed co-ordinate determination, approach landing, plant control, setting out and high accuracy flight path.

The following chapter discusses an OTF method of integer ambiguity resolution used to provide real time positioning results.

5.2 Integer Ambiguity Search Technique

An integer ambiguity search technique involves considering a number of possible integer ambiguity values for a number of satellites, and searching through them to find the ambiguities which are the most likely to be correct. Various techniques have been developed [HATCH, 1990], [SUMMERFIELD, 1990], [WESTROP, 1990], [WALSH, 1994], [HANSEN, 1996] and researched [MOORE, 1994].

One such technique is known as the 'modified Hatch technique' [WALSH, 1994], [HANSEN, 1996], and consists of the following steps,

1. Calculate an initial ambiguity, resulting in a search volume
2. Set up a search grid
3. Search through all the ambiguity combinations
4. Reject if the residuals are too big
5. Reject the remainder using statistical techniques
6. If one solution remains, then accept it. If more than one remains then use the next epoch's data.

The number of potential solutions for each satellite can be determined by $((2 \times \text{search range})+1)^{n-1}$. If, for example, we have a six satellite constellation, with a fixed range of ± 5 cycles on each ambiguity, the number of double difference integer ambiguity combinations to consider will be equal to 161,051 (i.e. 11^5) [HANSEN, 1996]. If there are eight satellites, then the number jumps to 19,487,171 possible combinations. This huge number of combinations and calculations can cause problems when processing this amount of data at sub-second epoch intervals, and in a real time system. It is therefore important to minimise the number of calculations required. Hatch recognised that the ambiguities are not all independent [HATCH, 1990]. Three double difference ambiguities will define a unique position in space, thus enabling the remaining ambiguities to be determined directly.

An initial position may be estimated using DGPS [HATCH, 1990], [DE LOACH *et al*, 1993], phase smoothed DGPS [REMONDI, 1992], or triple difference carrier phase [REMONDI, 1992]. This position has a calculated range error, from which a search volume can be established around the point [TEUNISSEN *et al*, 1996]. Phase smoothed DGPS and triple differencing have the disadvantage of being affected by cycle slips, and the use of DGPS in high multipath can cause positional errors in the order of metres [SHARDLOW, 1990], [SHARDLOW, 1994], [JACK, 1994]. This initial position could

therefore result in the true solution lying outside the search volume formed. Obviously the search volume must contain the true solution, so a factor of safety is used. However, the factor of safety shouldn't be so great as to dramatically increase the calculations.

Each axis of the search volume represents one of the three independent ambiguities and the values on the axes are the possible ambiguity values. These points occur where the carrier phase wave fronts cross the axes. A grid is created, around the initial estimate, of all the possible combinations of double difference integer ambiguities. This grid can be at L1, L2 or wide lane spacing. The grid is oriented so the axes are perpendicular to the three satellites used for positioning. The possible ambiguity combinations, or search nodes, are therefore at the intersection points of the three position lines. Figure 5.1 illustrates the technique, where the grid has been set up within the search window.

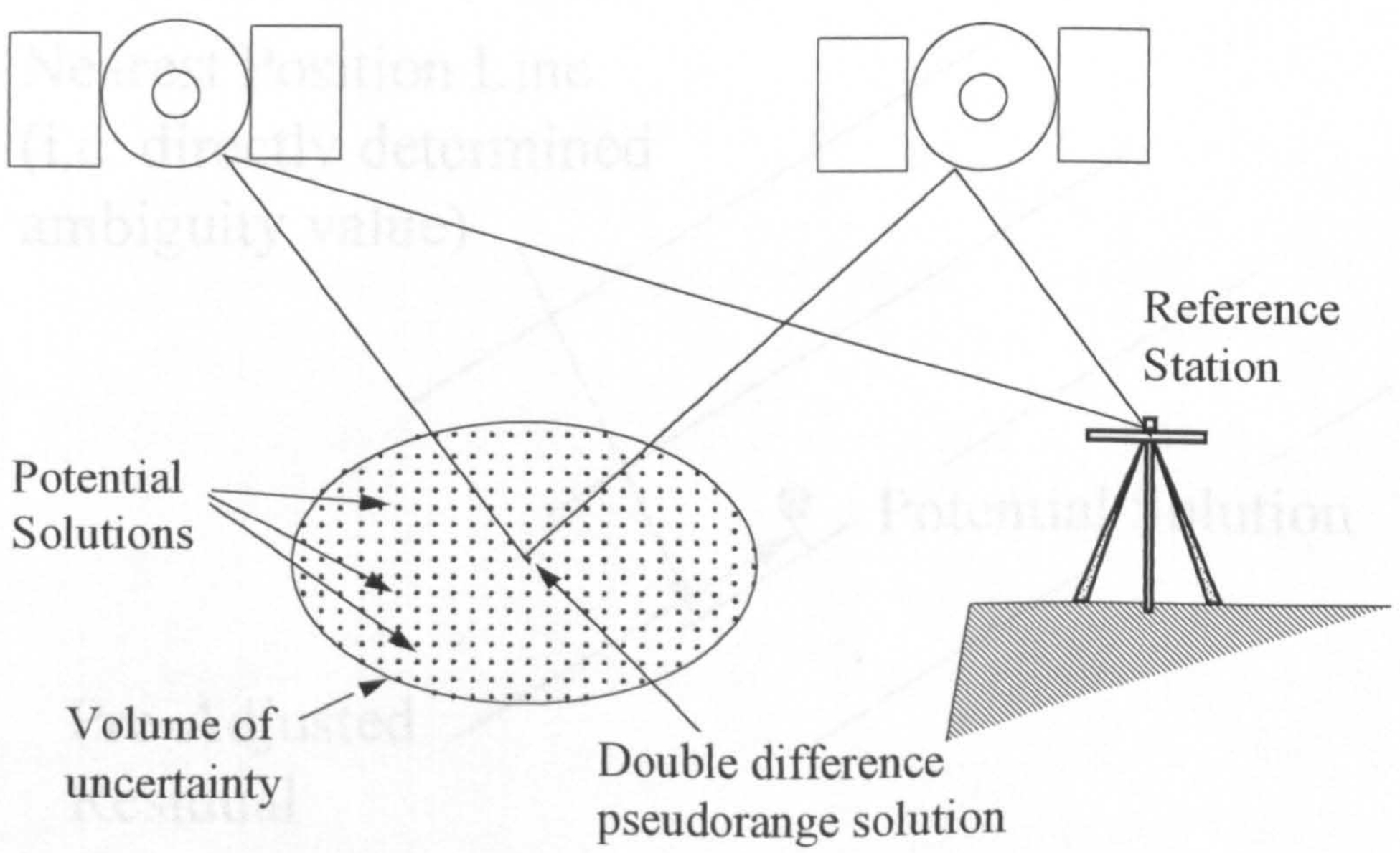

Figure 5.1

Setting up a Search Window Using DGPS for the Initial Position

Incorrect potential solutions are eliminated in two ways. Firstly, if the computed ambiguity results in the wave front lying outside the search volume, it is removed, and secondly, if the pre-adjusted residual is greater than a given tolerance, it is removed. The tolerance used has to be high enough to remove as many incorrect solutions as possible, but not so high as to remove the true solution during a noisy epoch of data. Further details about this can be found in [HANSEN, 1996].

Once the initial rejection has taken place, the true searching begins. The remainder are then compared to each other using a statistical test, such as an F-Test (Fisher Test) [HANSEN, 1996]. It assumes that all observations are independent, and uses a variance ratio test;

$$F_{u1,\,u2} = \frac{\frac{\sigma_2^2}{U_2}}{\frac{\sigma_1^2}{U_1}} \qquad (5.1)$$

where

σ_1^2 and σ_2^2 are the variances of the best and second potential solutions, and

U_1 and U_2 are the degrees of freedom of the distribution of the best and second best potential solutions respectively

The best solution is compared to the second best, and if it satisfies the statistical criteria, then it is accepted. All the satellites' data are used, and then the next epoch worth of data are used. The integers can be confidently fixed if the tests are successful, if not testing is continued. Figure 5.3 illustrates the ambiguity search technique, but in 2-D. Many variations of this method have been investigated. Further details can be found in [HANSEN, 1996].

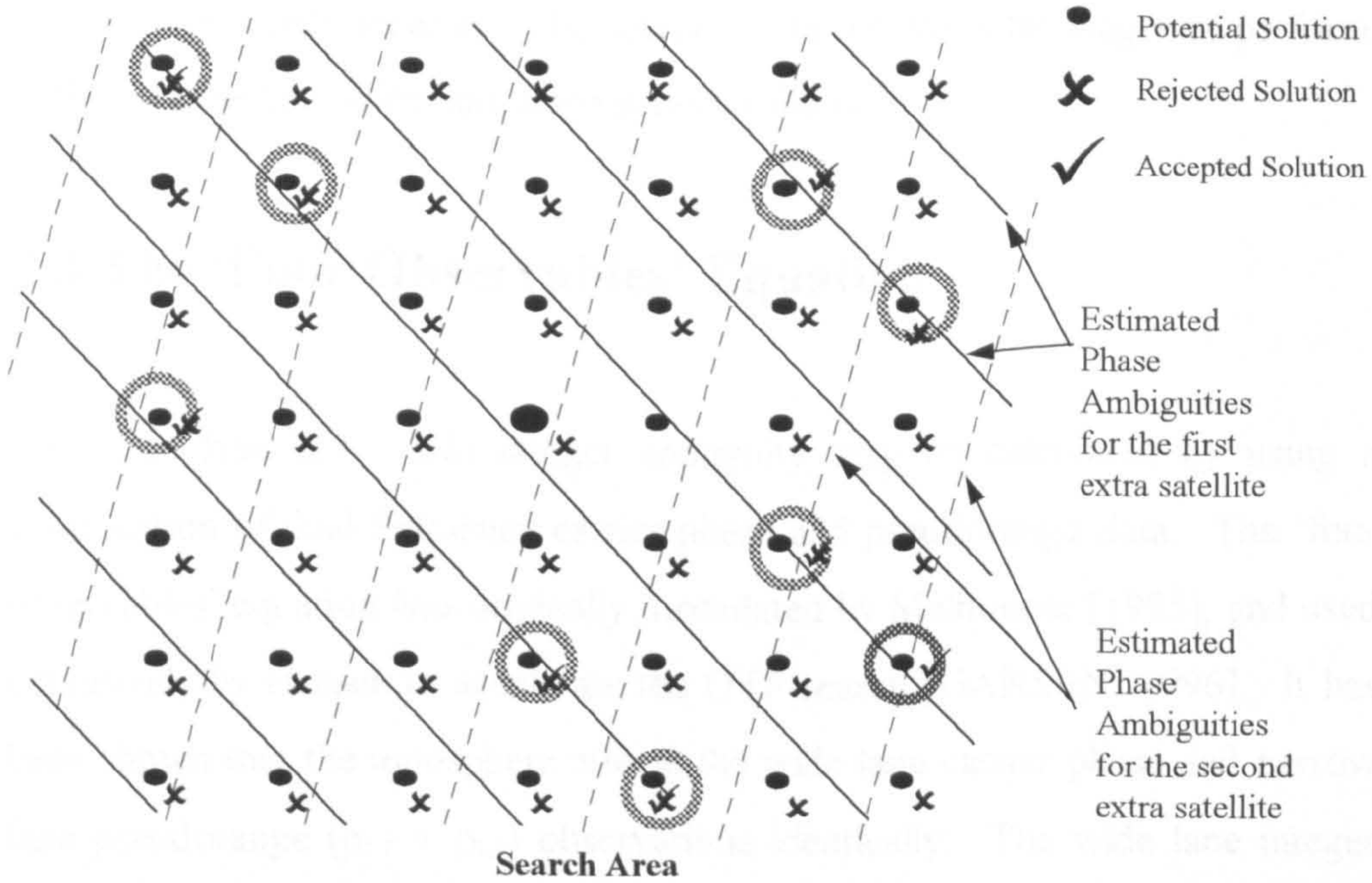

Figure 5.3

Illustration of the Ambiguity Search Technique in 2-D

Once the integer ambiguities have been resolved, they may be fixed, and precise positioning carried out.

Dual frequency accelerates the integer search, because the wide lane observable may be used (L1 - L2). This is a combination of L1 and L2 carrier phase frequencies resulting in a wavelength of approximately 86 cm. A typical sequence of events includes searching for a wide lane integer ambiguity around an initial DGPS solution, fixing it and then searching for the L1 integer ambiguity around the fixed wide lane solution. As the wide lane has a wavelength of approximately 86 cm, there are fewer possible solutions within a search volume than that provided by L1 (19 cm). The search volume produced around the wide lane solution will be far smaller than the DGPS solution, therefore resulting in fewer potential L1 solutions [HANSEN, 1996].

It is possible to use single frequency data to perform an OTF search, and once the integer ambiguities have been resolved, the L1 position is as accurate as that

of a dual frequency receiver. The search, however, takes far longer to perform, as the intermediate wide lane stage is not available.

5.3 The 'Four Observables' Equation

The wide lane (L1 - L2) integer ambiguity may be calculated by using a combination of dual frequency carrier phase and pseudorange data. The 'four observables' equation was originally formulated by Melbourne [1985], and used extensively by Hansen to accelerate the OTF search [HANSEN, 1996]. It has been shown that the ionosphere affects the wide lane carrier phase and narrow lane pseudorange ($\rho_{L1} + \rho_{L2}$) observations identically. The wide lane integer ambiguity may be stated as,

$$N_{WL} = N_{L1} - N_{L2} = \phi_{L1} - \phi_{L2} - \left(\left(\frac{f_{L1}}{c}\rho_{L1} + \frac{f_{L2}}{c}\rho L2\right)\left(\frac{\lambda L1 - \lambda L2}{\lambda L1 + \lambda L2}\right)\right) \quad (5.2)$$

A full derivation of this equation can be found in Hansen, [1996].

This equation therefore enables a direct estimation of the wide lane integer ambiguity value, which can be used in conjunction with the wide lane search, to either hasten the search, or check the results as a quality control.

This equation has only been successfully used over the past couple of years, as pseudorange measurements have become precise enough on both frequencies, whether AS is on or off. However, multipath currently limits the use of this equation, as the pseudorange values are affected more by multipath than the carrier phase, (see Chapter 6).

5.4 Multiple Reference Stations

The use of Multiple Reference Stations (MRS) has been used with some commercially available DGPS systems [ØRPEN AND BUCHANAN, 1994], [JOHNSTON, 1994] and [ALMOND AND BENNETT, 1994]. MRS has also been shown to aid ambiguity searching [CORBETT, 1994] and [HANSEN, 1996]. MRS adds more information into the integer ambiguity search, which accelerates the search and also quality controls the results, as any results should be true for all the MRS.

The use of MRS allows the baseline lengths over which OTF GPS can be implemented to be increased. As the baseline length increases, the carrier phase residuals become more noisy due to less of the ionosphere and troposphere noise being differenced, making the best solution less distinct from the others. MRS allows some of the noisy incorrect solutions to be removed, resulting in a common solution. The use of MRS for long baselines has been investigated by [HANSEN, 1996] and also in Chapter 7 of this thesis.

MRS may be implemented into the OTF search process in two ways, either as an addition to a single baseline search, or to construct independent ambiguity searches [HANSEN, 1994], [HANSEN, 1996]. The first, involves including all the information from each reference station in the least squares solution, around which a single ambiguity search is performed. The second, involves constructing separate ambiguity searches from each reference station, which are all compared to deduce the correct ambiguity combination.

5.5 Further Ambiguity Resolution Techniques

Many other techniques have been developed, which include the Ambiguity Function [REMONDI, 1984], [MADER, 1990], [MADER, 1992] and the

Sequential Square Root Information Filter [LANDAU and EULER, 1992], [WALSH, 1994]. Most of these, and others may be found in [HANSEN, 1996].

The most recent developments have seen the introduction of GPS/GLONASS systems. New algorithms and processing techniques are under development [LANDAU and VOLLATH, 1996], [WALSH and DALY, 1996] and [ROSSBACH and HEIN, 1996] which will resolve the ambiguities for both systems, allowing approximately twice as many satellites to be used, and a quality control on the results from two independent systems.

5.6 References

ALMOND, G. and BENNETT, J., 1994, *Seastar Network DGPS - Portable, Yet Fully Complementary to Conventional Inmarsat-A Based System,* Proc. third International Conference on Differential Satellite Navigation System (DSNS 94), Vol 1, Paper No. 35.

CORBETT, S.J., 1994, *GPS Single Epoch Ambiguity Resolution for Airborne Positioning and Orientation,* PhD Thesis, University of Newcastle Upon Tyne.

DELOACH, S. FRODGE, S.L., and REMONDI, B.W., 1993 *Assessment of GPS Phase Ambiguity Resolution On-The-Fly.* Paper Presented at DSNS '93, Amsterdam.

HANSEN, P., 1994, *Real Time GPS Carrier Phase Navigation,* Proc. Third International Conference on Differential Satellite Navigation Systems (DSNS 94), London, UK.

HANSEN, P., 1996, *On-The-Fly Ambiguity Resolution for GPS*, PhD Thesis, The University of Nottingham, Nottingham, United Kingdom.

HATCH, R., 1990. *Instantaneous Ambiguity Resolution.* Paper Presented at KIS Symposium 1990, Banff, Canada.

JACK, O. T. J, 1994, *Multipath Effects on GPS Observations*, MSc Thesis, University of Nottingham, Nottingham.

JOHNSTON, G. T., 1994, *Comparison of Two Multi-Site Reference Station Differential GPS Systems*, Proc. Third International Conference on Differential Satellite navigation Systems (DSNS 94), Vol 1, Paper No. 34.

LANDAU, H. , and EULER, H. J., 1992, *On The Fly Ambiguity Resolution for Precise Differential Positioning,* Proceedings of the 4th International Technical Meeting of the ION Satellite Division, pp. 607 - 613, Albuquerque, NM, October 1991.

LANDAU, H. and VOLLATH, U., 1996, *Carrier Phase Ambiguity Resolution using GPS and GLONASS Signals,* Proc. of the 9th International Technical Meeting of the ION Satellite Division, pp. 917 - 923, Kansas City, MS. September 17 - 20 1996.

MADER, G. L., 1990, *Ambiguity Function Techniques for GPS Phase Initialisation and Kinematic Solutions,* Proc. Second International Symposium on Precise Postioning with the Global Positioning System, Ottawa, Canada, pp 1234 - 1247.

MADER, G. L., 1992, *Kinematic GPS Phase Initialisatioon Using the Ambiguity Function*, Proc. Sixth International Geodetic Symposium on Satellite Postioning, Columbus, Ohio, Vol 1, pp 749 - 758.

MELBOURNE, W.G., 1985, *The Case for Ranging in GPS-Based Geodetic Systems*, Proc. First International Symposium on Precise Positioning with the Global Positioning System, 'Positioning with GPS - 1985', Vol. 1, pp 373 - 386, Rockville, Maryland.

MOORE, D., 1994, *An Examination of Two GPS 'On-The-Fly' Ambiguity Resolution Systems.* MSc Thesis, University of Nottingham.

ØRPEN, O. AND BUCHANAN, G., 1994, *Experiences Using Multiple Reference Station Position Solutions in a DGPS System*, Proc. Third International Conference on Differential Satellite navigation Systems (DSNS 94), Vol 1, Paper No. 33.

REMONDI, B.W., 1984, *Using the Global positioning System (GPS) Phase Observables for Relative Geodesy: Modelling, Processing and Results*, Doctoral Dissertation, Centre of Space Research, University of Texas, Austin, Texas.

REMONDI, B.W., 1992, *Real-Time Centimetre-Accuracy GPS Without Static Initialisation.* Presented at the Sixth International Geodetic Symposium On Satellite Positioning, Columbus, Ohio, March 17-20 1992.

ROSSBACCH, U. and HEIN, G. *Treatment of Integer Ambiguities in DGPS/DGLONASS Double Difference Carrier Phase Solutions*, Proc. of the 9th International Technical Meeting of the ION Satellite Division, pp. 909 - 916, Kansas City, MS. September 17 - 20 1996.

SHARDLOW, P.J., 1990, *Multipath: An Investigation.* MSc Thesis, University of Nottingham.

SHARDLOW, P.J., 1994, *Propagation Effects on Precise GPS Heighting,* PhD Thesis,University of Nottingham.

SUMMERFIELD, P.J., 1990. *Kinematic GPS Surveying.* PhD Thesis, University of Nottingham.

TEUNISSEN, P. J. G, DE JONGE, P. J., TIBERIUS, C. C. J. M., 1996, *The Volume of the GPS Ambiguity Search Space and its Relevance for Integer Ambiguity Resolution*, Proc. of the 9th International Technical Meeting of the ION Satellite Division, pp. 889 - 898, Kansas City, MS. September 17 - 20 1996.

WALSH, D. M. A., 1994, *Kinematic GPS Ambiguity Resolution.* PhD Thesis, University of Nottingham.

WALSH, D. and DALY, P., *GPS and GLONASS Carrier Phase Ambiguity Resolution,* Proc. of the 9th International Technical Meeting of the ION Satellite Division, pp. 899 - 907, Kansas City, MS. September 17 - 20 1996.

WESTROP, J., 1990, *Dynamic Positioning by GPS,* PhD Thesis, The University of Nottingham, Nottingham, United Kingdom.

Chapter 6

The Accurate Recovery of Cycle Slips

6.1 Introduction

GPS has been made more amenable to a wide range of applications through the evolution of "rapid static" and "kinematic" methods, and now even more so with the advent of On-The-Fly (OTF) real time systems. The occurrence of cycle slips, however, is a major limiting factor for positioning using such techniques. A major conclusion of a recent PhD thesis at the University of Nottingham was that *"... the cycle slip detection research which is underway within the IESSG should be implemented as a matter of urgency..."*. The thesis also states that cycle slip detection and correction should be conquered to allow true kinematic OTF positioning to be successful [HANSEN, 1996].

Cycle slips result from the loss of lock between the receiver and the satellite signal. They can be caused by obstructions to the satellite signal, a low Signal to Noise Ratio (SNR), incorrect signal processing within the receiver software, high antenna acceleration, interference from other radio signal sources or high ionospheric activity.

When cycle slips occur, the integer ambiguity is lost and must be re-determined, or the value of the cycle slip accurately calculated. The first option can take at least 30 one second epochs with current techniques [MOORE, D, 1994], [WALSH, 1994], [ASHKENAZI *et al*, 1996]. However, due to the evolution of new receivers with better resolution, research into new and quicker search algorithms [HANSEN, 1996], receivers that can gather true dual frequency data in the presence of AS and the capability of recording data at 5 Hz [ACKROYD, 1996], this time is continuously decreasing.

Cycle slips should be detected and corrected for the efficient and successful use of OTF kinematic GPS. To do this, it is important for their values to be accurately calculated. Sometimes a cycle slip may be detected, but not accurately corrected for. Such instances include a loss of lock, resulting in a large gap in the data of the order of minutes. Under such circumstances, the detection of the cycle slip can be flagged in the data file, in order for an OTF search to be carried out.

Various cycle slip detection and correction techniques have been developed in the past, including double and triple differencing techniques, comparing the difference between consecutive carrier phase and code values (range residual), comparing consecutive four observables equations, comparing consecutive ionospheric residuals, carrier phase curve fitting, using redundant satellites and using the GPS Doppler values. Four of these techniques have been thoroughly examined and programmed into an unmitigated cycle slip correction package by the author, which utilises the advantages of the different methods into a single cycle slip detection process. These four techniques will be discussed, outlining their advantages and disadvantages and how their combination can successfully detect and correct for cycle slips. The techniques being code minus carrier comparison (range residual), adjacent four observables comparison, the use of GPS Doppler measurements, and the ionospheric residual technique. These techniques use the data from a single receiver, not relative to another receiver by using differencing techniques. In addition to these techniques, Kalman

filtering and Signal to Noise Ratio (SNR) are used to reduce signal noise parameters.

These techniques are used to detect the presence of cycle slips, and to correct when all or most of the satellites suffer from slips. If only one satellite suffers a cycle slip, these techniques are also useful for its detection. However, it is far easier to correct for the cycle slip through using the redundant satellite technique, where the remaining clean satellites are used to position the GPS antenna, and the new integer ambiguity for the satellite affected by the cycle slip is calculated from the position at that epoch.

6.2 Code Minus Carrier (Range Residual) Comparison

Both the pseudorange and carrier phase values are measured simultaneously. These values are closely correlated, and can therefore be compared epoch by epoch. A 'range residual' is defined as the difference in the change between a concurrently measured pseudorange and carrier phase, equation [6.1],

$$RR = \left(\frac{\rho_{(i)} - \rho_{(i-1)}}{\lambda}\right) - \left(\phi_{(i)} - \phi_{(i-1)}\right) \qquad (6.1)$$

where RR = Range Residual (cycles)
ρ = Pseudorange (metres)
λ = Carrier Wavelength (metres)
ϕ = Carrier Phase (cycles)
i = Current epoch

Equation 6.1 is affected by the following four factors.

1. Clock and receiver errors
2. Cycle slips
3. Multipath
4. Observable noise

Cycle slips affect carrier phase readings, but not pseudoranges, therefore, equation [6.1] could be used to calculate a first approximation of a cycle slip. This assumes that any clock errors are eliminated and that the other factors affect pseudorange and carrier phase measurements equally. This is clearly not the case, but is a good enough assumption in order to estimate the size of the cycle slip to within a few cycles in a low multipath environment. Figures 6.1 to 6.4 illustrate typical range residual results obtained from Trimble 4000 SSE and Ashtech Z-XII dual frequency receivers located in low multipath environments.

These figures suggest that the range residual cycle slip detection technique can be as accurate as at least ± 4 cycles when using modern receivers capable of accessing the Y-code in a low multipath environment. This technique does, however, have its limitations and drawbacks which are detailed in §6.6.1. Further examples of code and carrier resolution values are shown in Appendix B and §6.6.1.

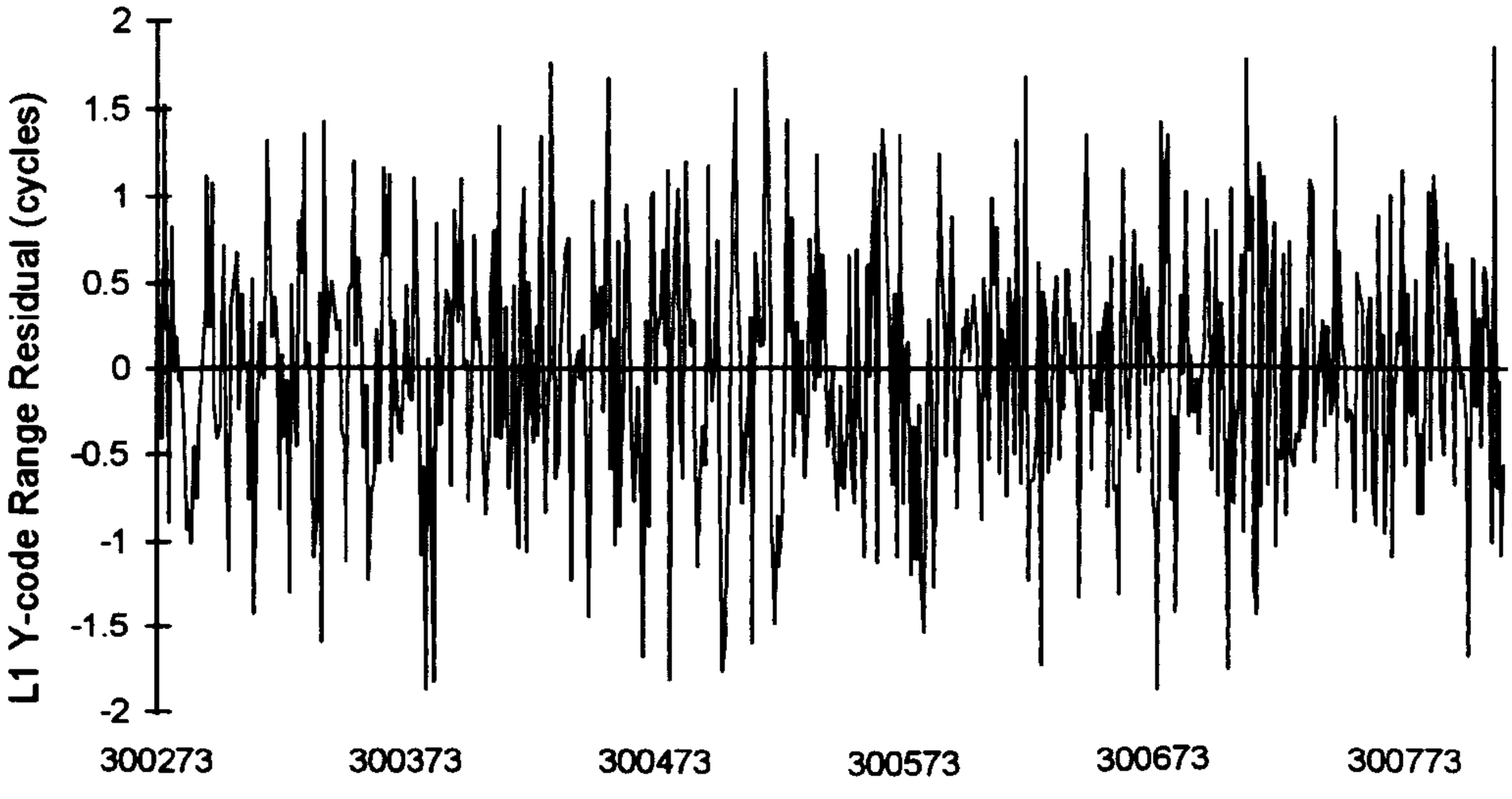

Figure 6.1

A plot showing the Ashtech Z-XII L1 Y-code Minus L1 Carrier Phase (L1 Range Residuals) for satellite 20, during the presence of AS. A scatter of about ± 2 cycles is seen for data recorded at a 1 second epoch interval

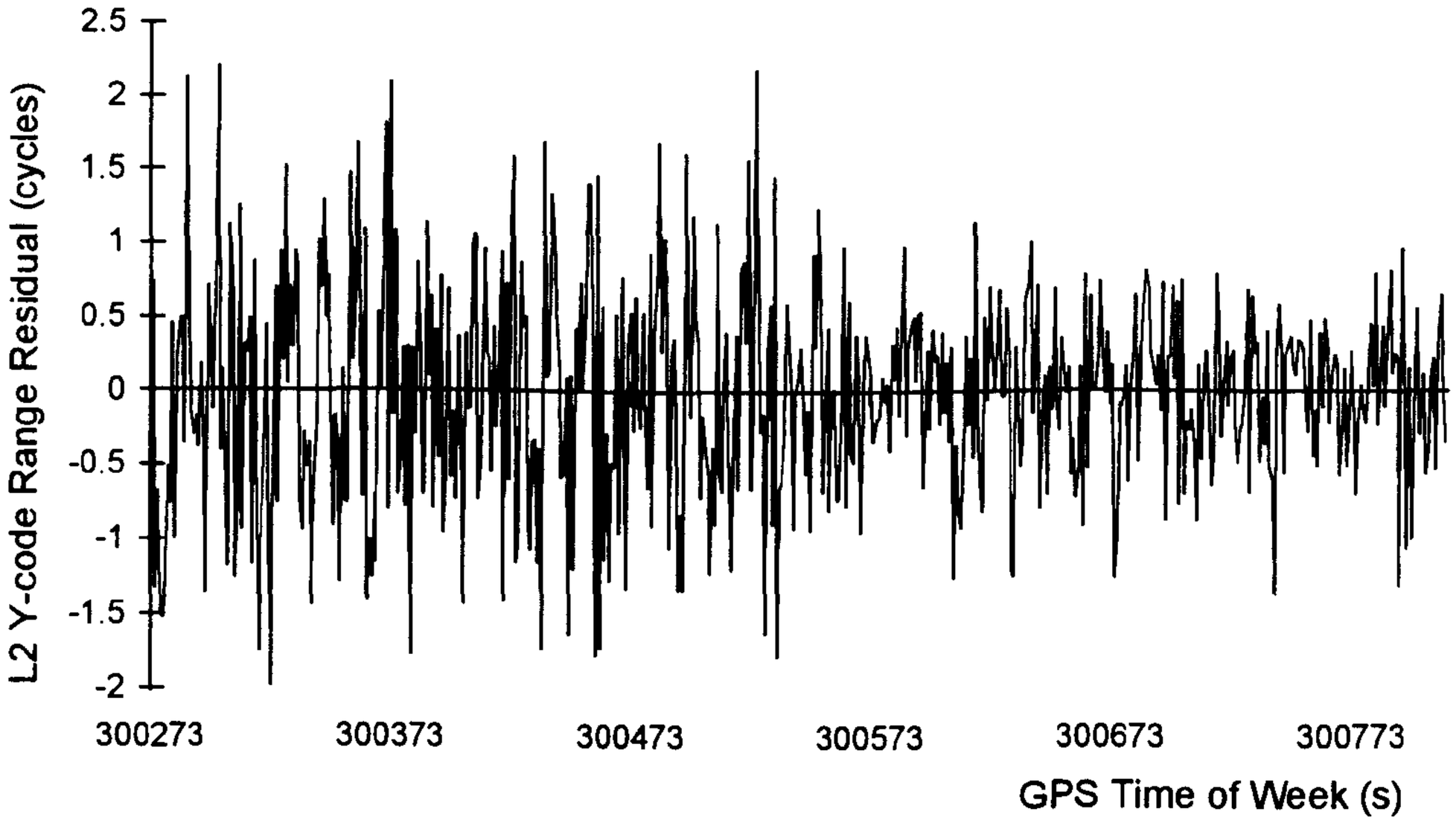

Figure 6.2

A plot showing the Ashtech Z-XII L2 Y-code Minus L2 Carrier Phase (L2 Range Residuals) for satellite 20, during the presence of AS. A scatter of about ±2 cycles is seen for data recorded at a 1 second epoch interval

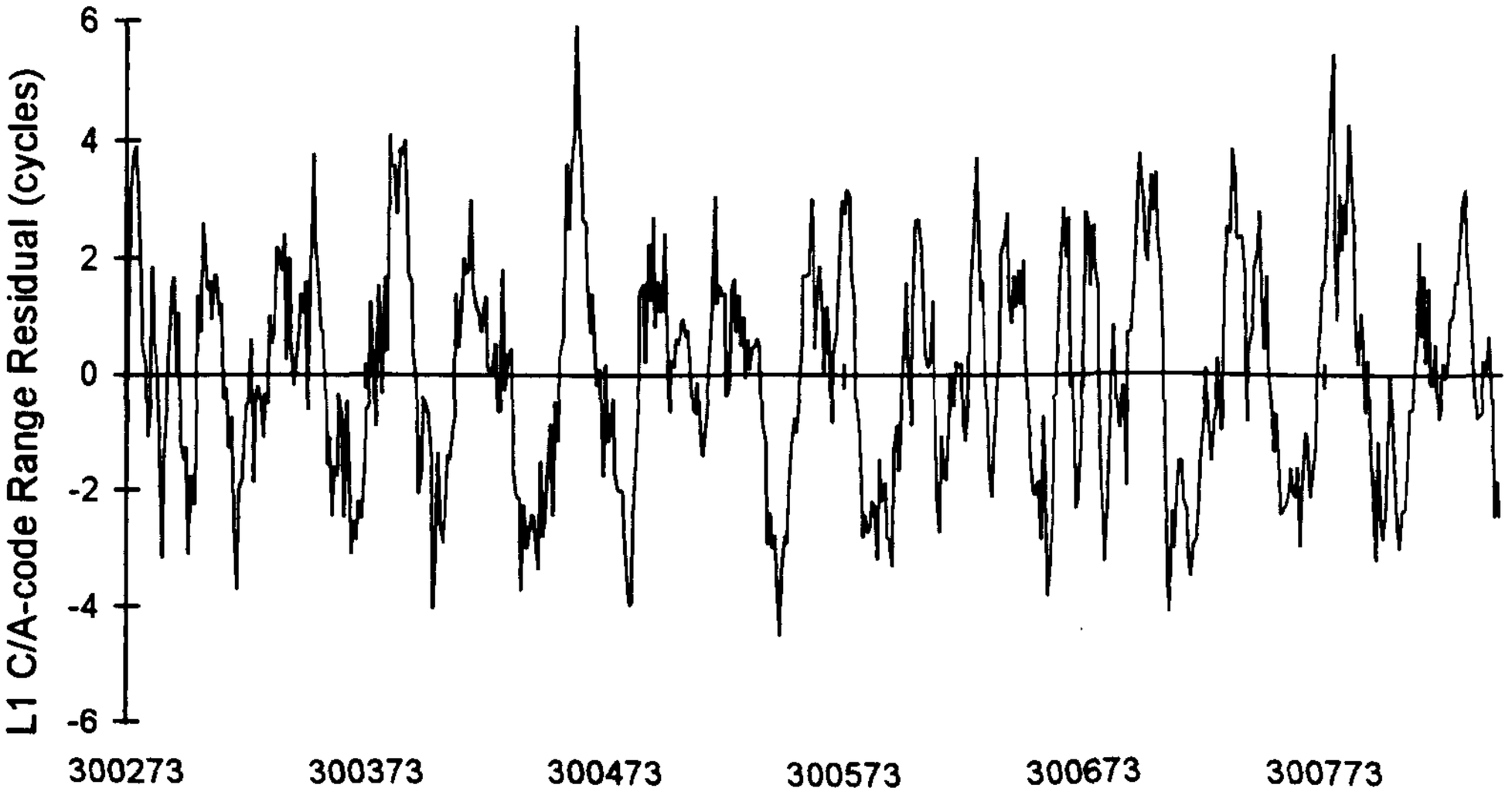

Figure 6.3

A plot showing the Ashtech Z-XII L1 C/A-code Minus L1 Carrier Phase (L1 Range Residuals) for satellite 20, during the presence of AS. A scatter of about ±6 cycles is seen for data recorded at a 1 second epoch interval

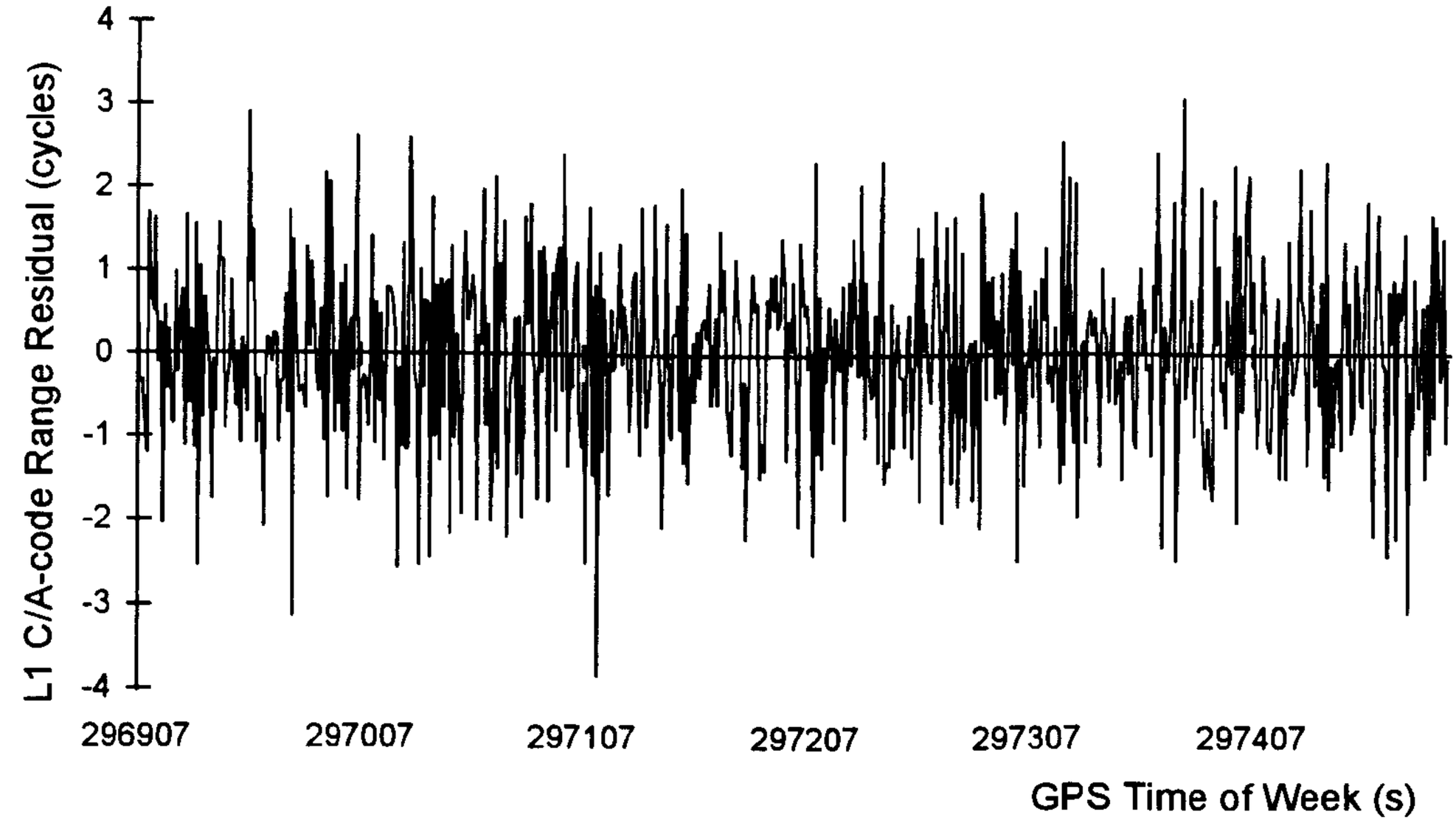

Figure 6.4

A plot showing Trimble 4000 SSE L1 C/A-code Minus L1 Carrier Phase (L1 Range Residuals) for satellite 22, during the presence of AS. A scatter of about ±4 cycles is seen for data recorded at a 1 second epoch interval

Figures 6.3 and 6.4 suggest that single frequency receivers, only capable of accessing the C/A-code may also use this range residual technique to detect such cycle slips, although they will not be able to use the wide lane and ionospheric residual techniques detailed in §6.3 and §6.5.

The C/A-code experiences a higher multipath value than the P-code, as discussed in §6.6.1.b, which would make a C/A-code range residual technique obsolete in a high multipath environment. However, this would not be a problem if the multipath could be detected and quantified, as discussed in §6.6.1.b. Figure 6.2 shows some indication of the existence of multipath, or some other source of noise. Here the range residual becomes less at approximately 300573 seconds. This shows the effect of multipath on the range residual, changing it from ± 2 cycles to ± 1 cycle in a relatively low multipath environment. Higher multipath environments will affect the range residual to a greater extent, §6.6.1.b.

6.3 Cycle Slip Detection Through the Use of the 'Four Observables' Equation

Equation [6.2], is the well known '4 Observables Equation' which is used to calculate the wide lane integer ambiguity [HANSEN, 1996], originally formulated by [MELBOURNE, 1985]. Although the formula is given as a phase range from a satellite to receiver, it is normally used in a 'double difference' mode. Generally, N_{LW} varies smoothly from epoch to epoch, and consequently a significant jump in its value can be attributed to a wide lane cycle slip. This still leaves the problem of identifying whether the wide lane cycle slip is due to a corresponding cycle slip in the L1 or L2 frequencies, or both.

$$N_{Lw} = (\phi_{L1} - \phi_{L2}) - \frac{(f_{L1} - f_{L2})}{(f_{L1} + f_{L2})} x \left(\frac{\rho_{L1}}{\lambda_{L1}} + \frac{\rho_{L2}}{\lambda_{L2}} \right) \qquad (6.2)$$

where

N_{LW}	=	Wide Lane Ambiguity (cycles)
ρ	=	L1 or L2 Pseudorange (metres)
λ	=	L1 or L2 Carrier Phase Wavelength (metres)
f	=	L1 or L2 Frequency (Hz)
ϕ	=	L1 or L2 Carrier Phase (cycles)

Wide lane cycle slip detection is a useful way of detecting the presence of cycle slips, and to check the accuracy of the L1 and L2 cycle slips detected using other methods.

Figures 6.5 and 6.6 illustrate typical four observables values for Trimble 4000 SSE and Ashtech Z-XII dual frequency receivers. The values have been derived from clean data taken at low multipath sites.

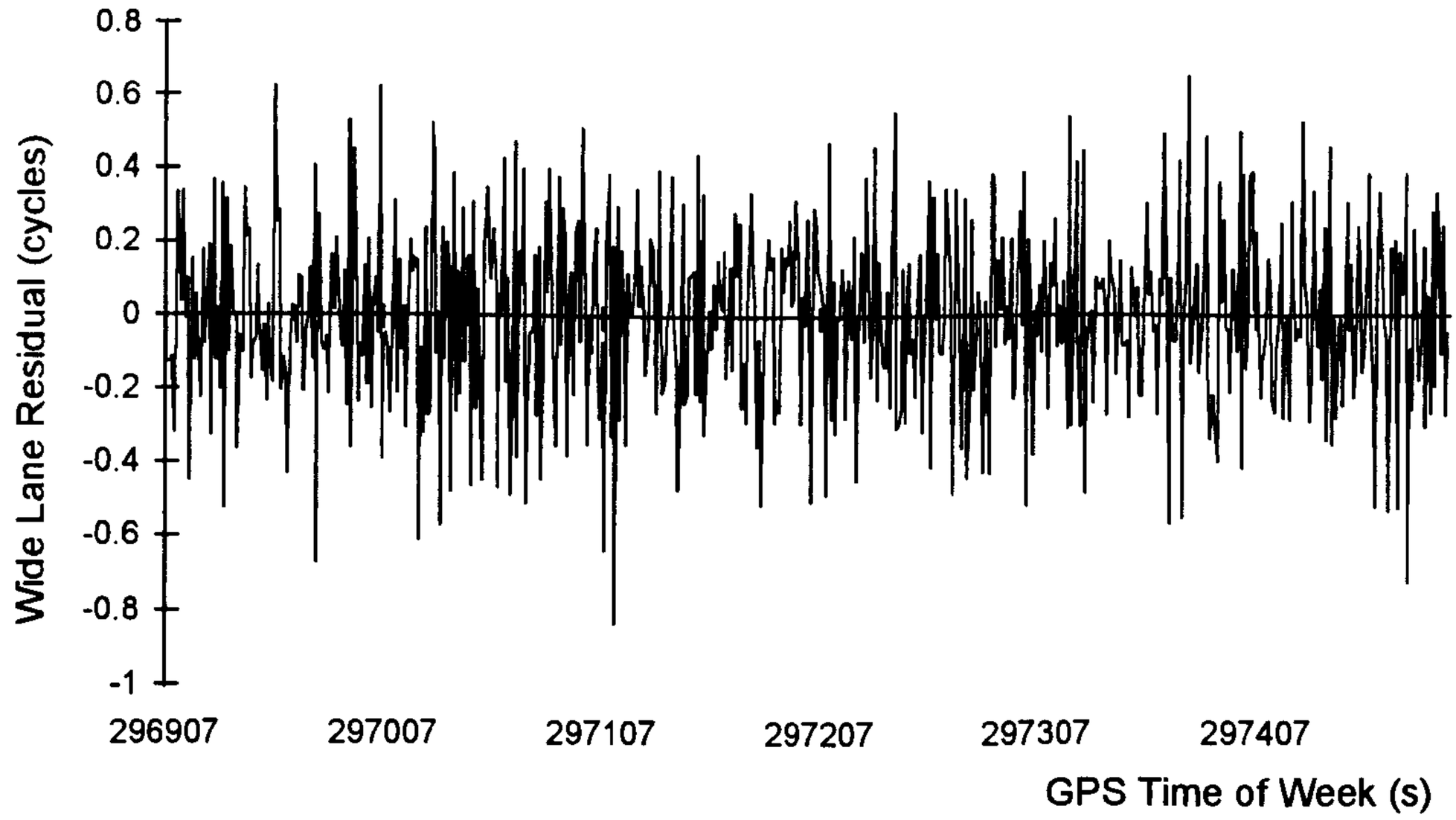

Figure 6.5

A plot of a Trimble 4000 SSE Wide Lane Residuals for satellite 22 during the presence of AS. Data recorded at a 1 second epoch interval

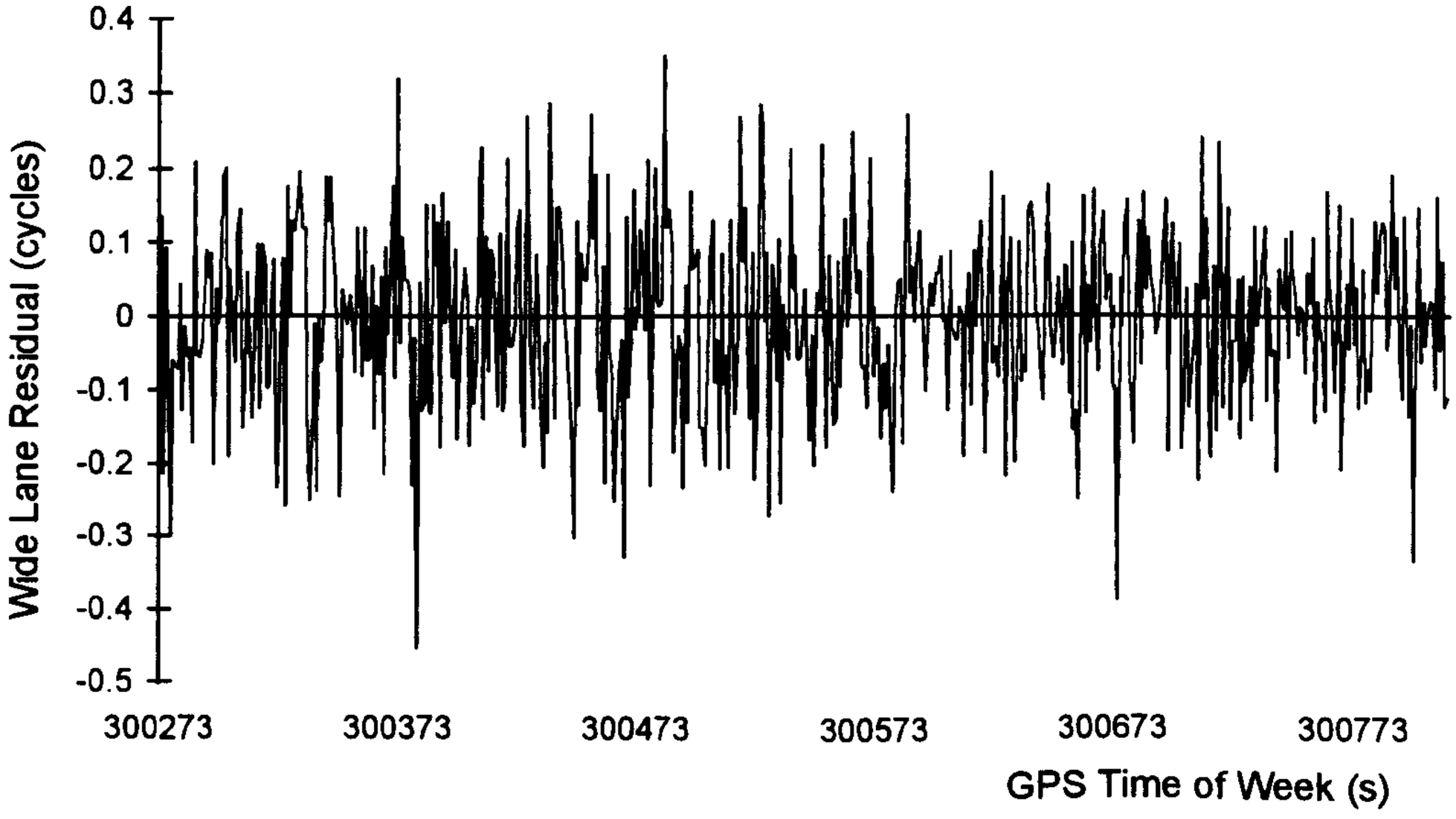

Figure 6.6

A plot of an Ashtech Z-XII Wide Lane Residuals for satellite 20 during the presence of AS. Data recorded at a 1 second epoch interval.

The figures illustrate that wide lane cycle slips may be detected to an accuracy of ± 0.4 cycles in a low multipath environment. Multipath, however, can cause

problems with this technique since pseudorange multipath is greater than that of the carrier phase, resulting in a noisy wide lane residual.

6.4 Cycle Slip Detection Through the Use of Doppler Data

In addition to carrier phase and pseudoranges, most commercial geodetic GPS receivers will also output Doppler readings at each epoch. These Doppler readings may be use to detect and calculate carrier phase cycle slips [ROBERTS *et al*, 1995]. A sample RINEX data file is illustrated in Appendix B. This illustrates the layout of a modern RINEX data file, including the Doppler data as well as the code and carrier data, and SNR values.

The Doppler data has been explained to the author [HOGARTH, 1996] as being the value of a third order curve fitted to the last three carrier phase values. The derivative of the curve is known as "Doppler".

In cases where carrier phase data does not exist, the Doppler data may well be present, and can be used to detect any cycle slips present. This can be seen in the RINEX data file in Appendix B. Here, there are instances where the Doppler data are present, but the carrier phase data are not. Appendix B contains examples of graphs illustrating Doppler changes over time.

Figure 6.7 illustrates the relationship between Trimble 4000 SSE L1 Doppler and L1 carrier phase data. Clearly, the slip in the carrier phase reading does not affect the Doppler values. Further examples of cycle slips within GPS Doppler and Carrier phase data can be seen in Appendix B.

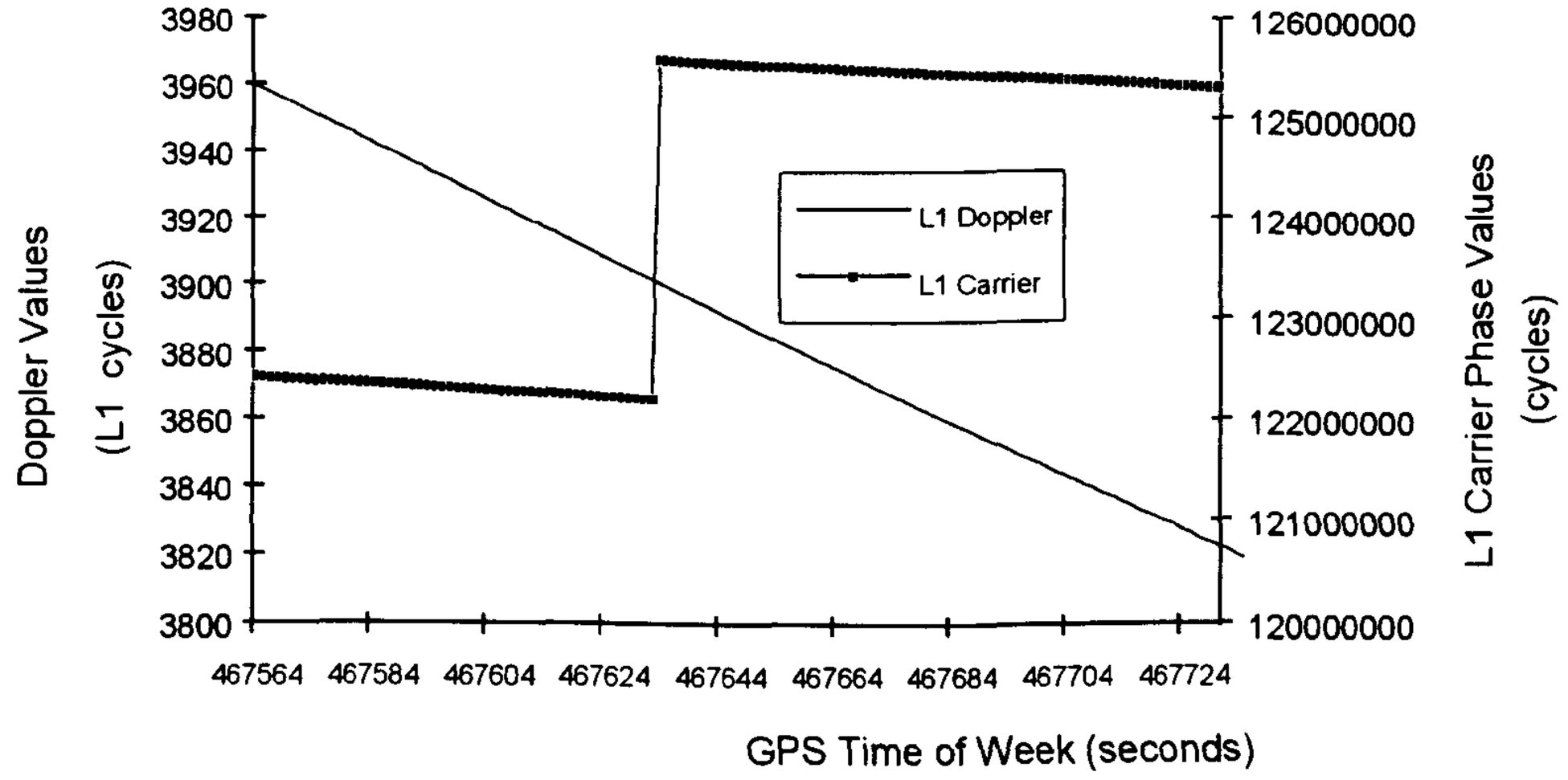

Figure 6.7

The Effect of a Cycle Slip Upon Carrier Phase and Doppler Data for a Trimble 4000 SSE receiver. Data recorded at a 1 second epoch interval.

The Doppler data can be used to detect and calculate carrier phase cycle slips, through forward predicting the carrier phase values. Any deviations between the predicted and actual carrier phase values are due to;

1. Cycle slips.
2. Measurement noise.

Equation [6.3] illustrates an equation derived by the author to calculate cycle slips using the L1 Doppler value.

$$DR = \phi_{(i)} - \left(\frac{\phi_{(i-1)} - (Dopp_{(i)} + Dopp_{(i-1)}) * (\Delta t)}{2} \right) \qquad (6.3)$$

where

DR	=	Doppler residual (carrier phase cycles)
Dopp	=	Doppler count (carrier phase cycles)
Δt	=	Epoch separation (seconds)
ϕ	=	Carrier phase measurement (cycles)

L2 carrier phase data may be predicted in a similar way to L1, using the L1 Doppler or the L2 Doppler, if this exists in the data file. Equations [6.4] and [6.5] are used to calculate the L2 Doppler when cross correlation and signal squaring are used, respectively, to obtain the L2 carrier phase data during Anti Spoofing (AS).

$$L2Doppler = L1Doppler \times \frac{120}{154} \qquad (6.4)$$

$$L2Doppler = L1Doppler \times \frac{120}{77} \qquad (6.5)$$

Figures 6.8 to 6.11 illustrate typical values obtained for clean data, recorded at a one second epoch intervals using both an Ashtech Z-XII receiver and a Trimble 4000 SSE receiver. It can be seen that the noise value is in the region of ± 0.2 cycles for the Ashtech receiver, and ± 0.04 cycles for the Trimble receiver. Similar results for a Trimble 4000 SSI receiver can be found in Appendix B.

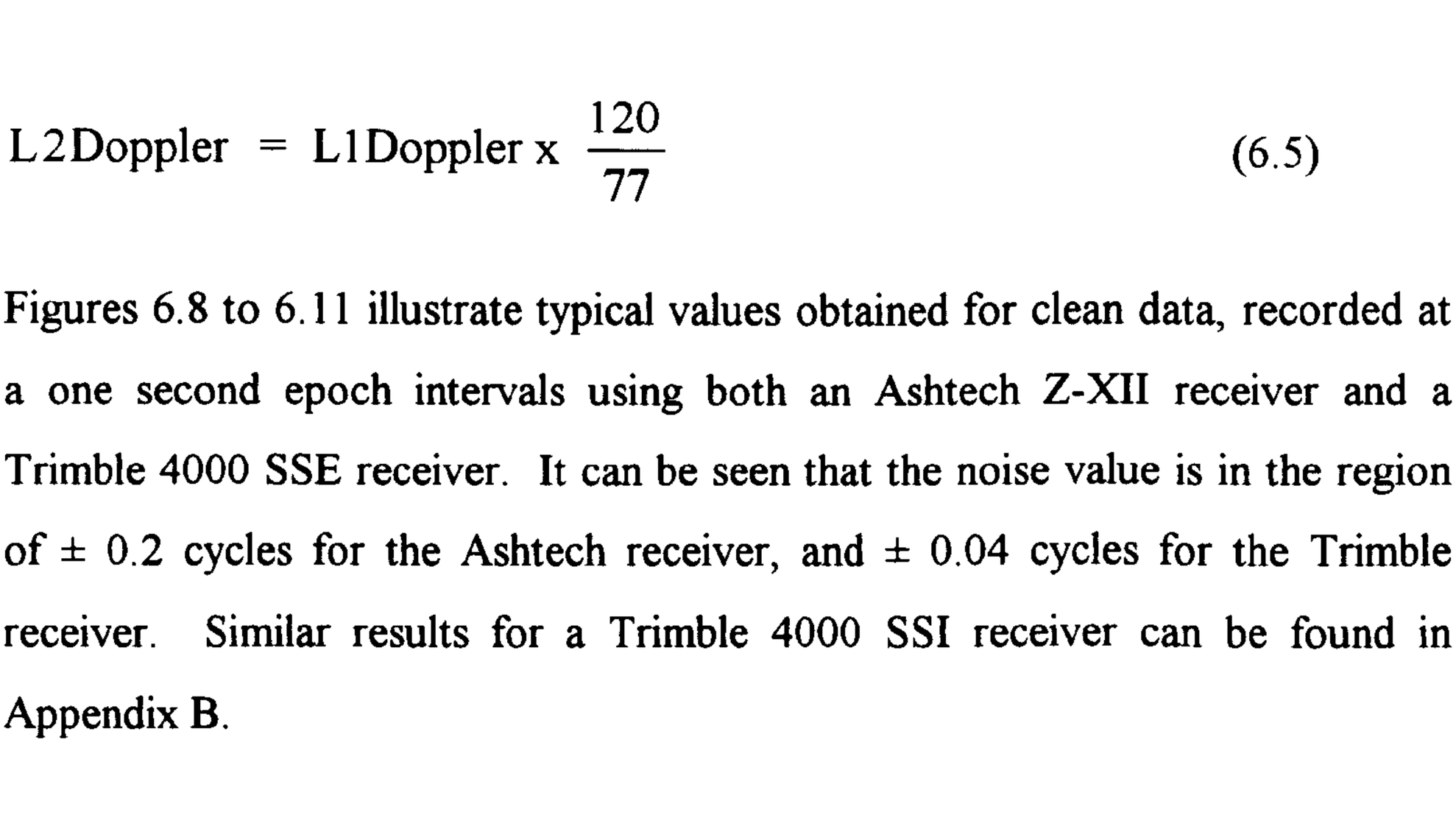

Figure 6.8

A plot of an Ashtech Z-XII L1 Doppler Residuals for satellite 26 during the presence of AS. Data recorded at a 1 second epoch interval.

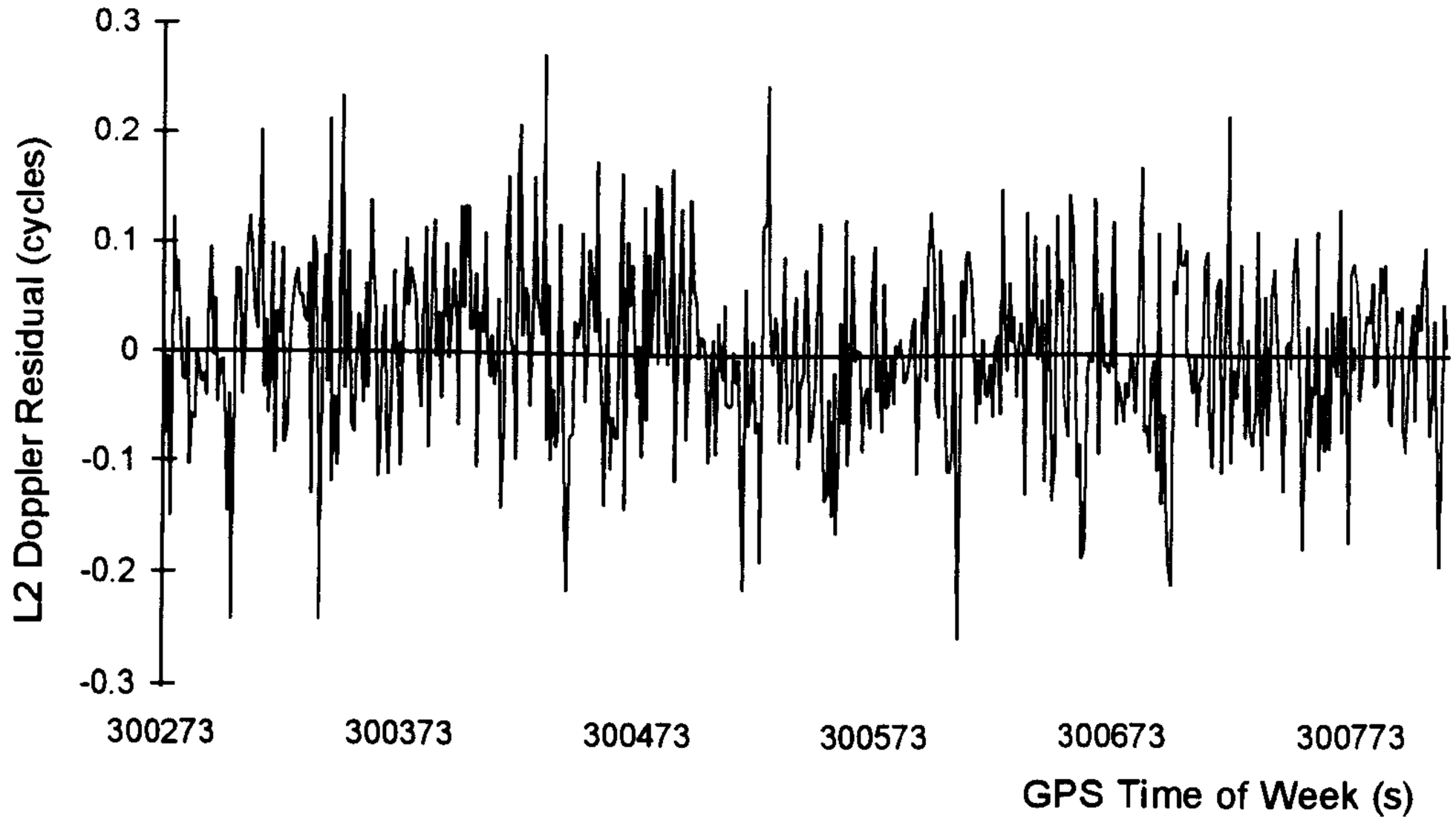

Figure 6.9

A plot of an Ashtech Z-XII L2 Doppler Residuals for satellite 26 during the presence of AS. Data recorded at a 1 second epoch interval.

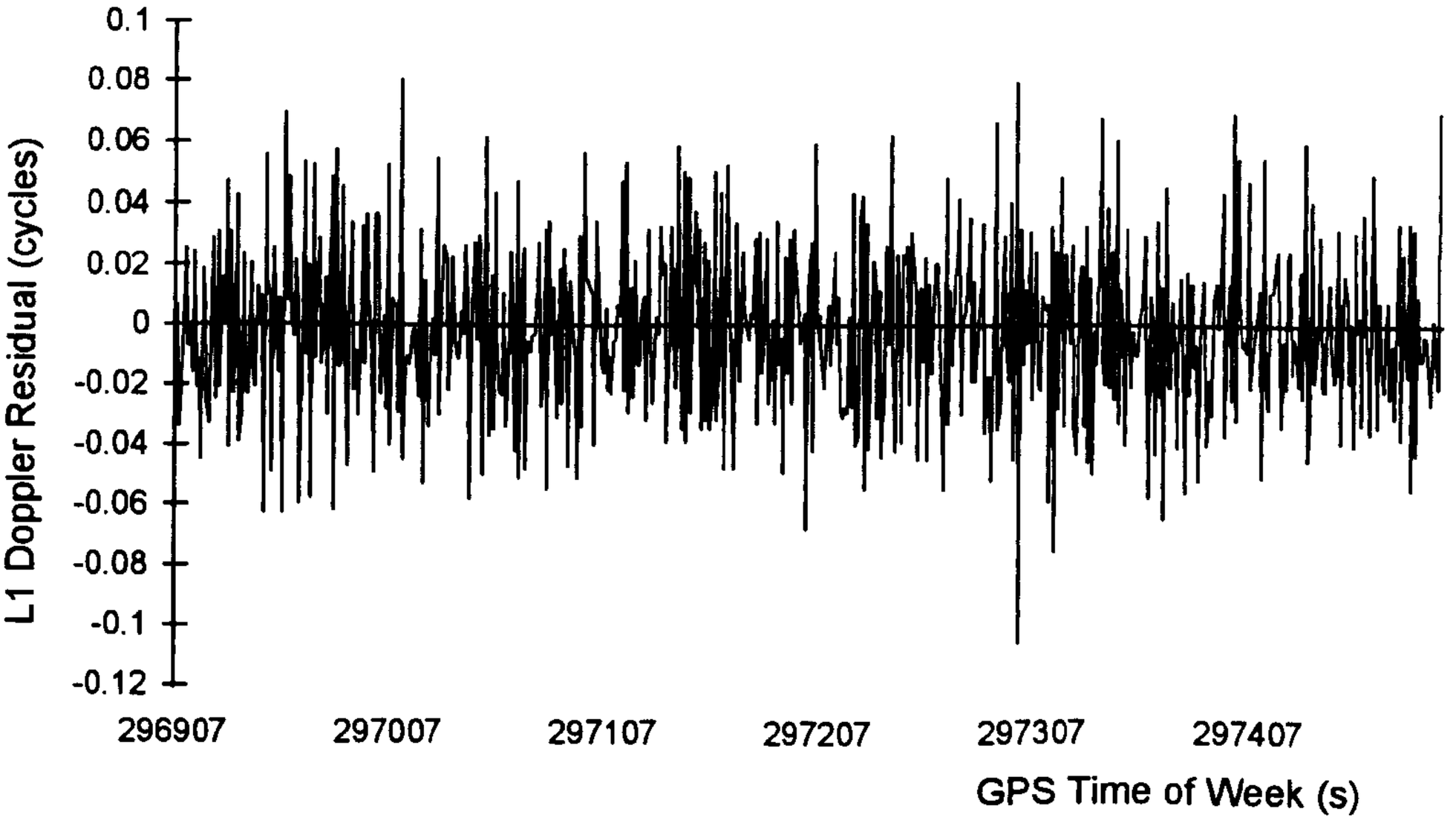

Figure 6.10

A plot of a Trimble 4000 SSE L1 Doppler Residuals for satellite 22 during the presence of AS. Data recorded at a 1 second epoch interval.

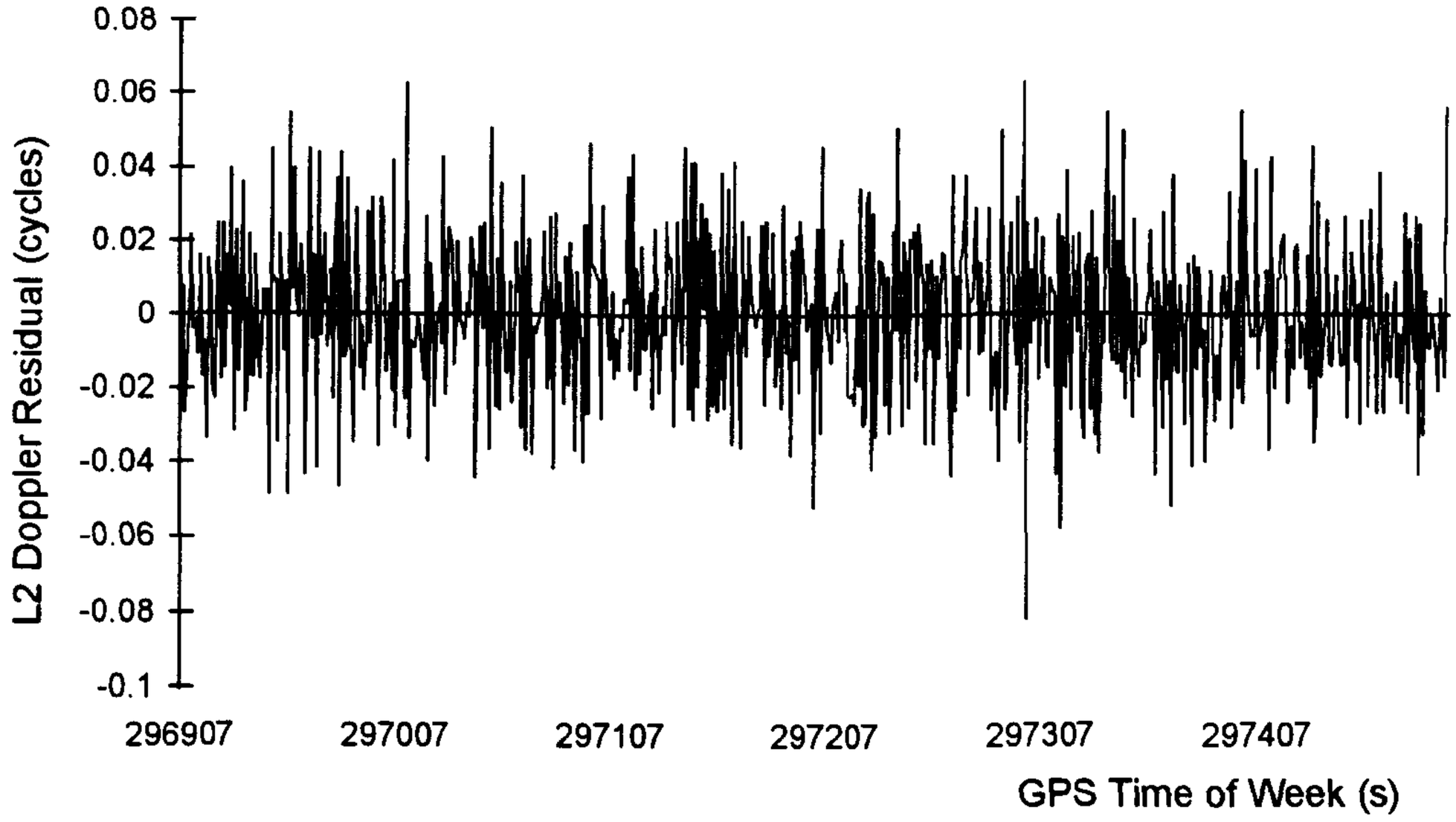

Figure 6.11

A plot of a Trimble 4000 SSE L2 Doppler Residuals for satellite 22 during the presence of AS. Data recorded at a 1 second epoch interval.

6.5 Cycle Slip Detection Through the Use of the Ionospheric Residual

The L1 and L2 carrier phase observations simultaneously measure the change in range between two epochs from the receiver to the satellite. Consequently, a phase observation can be determined, from the other, to an accuracy of less than half a cycle, given that the other observation is free from cycle slips [WESTROP, 1990]. The following is a derivation of the relationship between the two frequencies;

Starting with the simple equation;

$$C = f \lambda$$

c = speed of light (m/s)

Considering L1 and L2 frequencies;

f = frequency (Hz)

$$C = f_{L1} \lambda_{L1} = f_{L2} \lambda_{L2}$$

λ = wavelength (m)

$$\therefore \qquad \frac{1}{\lambda_{L1}} = \frac{f_{L1}}{f_{L2}} \frac{1}{\lambda_{L2}}$$

ϕ = carrier phase value (cycles)

Multiplying both sides by the range (D) between the satellite and receiver,

$$\frac{D}{\lambda_{L1}} = \frac{f_{L1}}{f_{L2}} \frac{D}{\lambda_{L2}}$$

where $\phi = \frac{D}{\lambda}$

$$\phi_{L1} = \phi_{L2} \frac{f_{L1}}{f_{L2}}$$

Systematic errors in the observables due to the ionosphere are frequency dependent and will not be completely removed by differencing observations. The remaining effect is known as the ionospheric residual, $\delta\phi$, and will change with time according to the change in ionospheric activity [GOAD, 1986]. The ionospheric residual changes very slowly with time, of the order of 1 L1 cycle per minute. A cycle slip exhibits itself as a sudden jump in this value.

Equation [6.6] details the calculation of the ionospheric residual between the L1 and L2 carrier phases, whilst that between the L1 and widelane carrier phases is shown in equation [6.7].

$$\delta\phi_{L1} = \phi_{L1} - \frac{f_{L1}}{f_{L2}} \phi_{L2} \qquad (6.6)$$

$$\delta\phi_{L1} = \phi_{L1} - \frac{f_{L1}}{f_{L1} - f_{L2}} \phi_{Lw} \qquad (6.7)$$

where

$\delta\phi$	=	Ionospheric residual (L1 cycles)
ϕ_{Lw}	=	widelane carrier (cycles)

ϕ_{L1} = L1 carrier phase (cycles)
ϕ_{L2} = L2 carrier phase (cycles)
f_{L1} = L1 frequency (Hz)
f_{L2} = L2 frequency (Hz)

Equations [6.6] and [6.7] both contain two unknowns and hence have an infinite number of solutions. An approach to their solution involves the generation of approximate values for the unknowns, which are used to compute a value for the ionospheric residual. These approximate values for the unknowns are called Refinement Integers. Different combinations of these refinement integers, RmL1 and RmL2 are then used to find the solution which gives the closest agreement between the observed and computed ionospheric residuals [WESTROP, 1990]. A search is conducted, using different refinement integer combinations to calculate which combination correspond to the ionspheric residual value. The combination of L1 and widelane was used rather than the L1 and L2 combination ionospheric residual, as the resulting values are more distinct. Table 6.1 illustrates the Rm_{L1} and Rm_{Lw} values derived from equation [6.7].

Rm L1 \ RmLw	-5	-4	-3	-2	-1	0	1	2	3	4	5
-5	17.65	13.12	8.59	4.06	-0.47	-5.00	-9.53	-14.06	-18.59	-23.12	-27.65
-4	18.65	14.12	9.59	5.06	0.53	-4.00	-8.53	-13.06	-17.59	-22.12	-26.65
-3	19.65	15.12	10.59	6.06	1.53	-3.00	-7.53	-12.06	-16.59	-21.12	-25.65
-2	20.65	16.12	11.59	7.06	2.53	-2.00	-6.53	-11.06	-15.59	-20.12	-24.65
-1	21.65	17.12	12.59	8.06	3.53	-1.00	-5.53	-10.06	-14.59	-19.12	-23.65
0	22.65	18.12	13.59	9.06	4.53	0.00	-4.53	-9.06	-13.59	-18.12	-22.65
1	23.65	19.12	14.59	10.06	5.53	1.00	-3.53	-8.06	-12.59	-17.12	-21.65
2	24.65	20.12	15.59	11.06	6.53	2.00	-2.53	-7.06	-11.59	-16.12	-20.65
3	25.65	21.12	16.59	12.06	7.53	3.00	-1.53	-6.06	-10.59	-15.12	-19.65
4	26.65	22.12	17.59	13.06	8.53	4.00	-0.53	-5.06	-9.59	-14.12	-18.65
5	27.65	23.12	18.59	14.06	9.53	5.00	0.47	-4.06	-8.59	-13.12	-17.65

Table 6.1

Computed Ionospheric Residuals Using L1 and Lw

It can be seen in table 6.1 that most values are greater than 0.5 cycles, which is far greater than the expected receiver noise. The theoretical 3σ confidence noise value is 0.04 cycles for L1/L2 and 0.41 for L1/Lw.

It can be seen in the table, however, that the values of the ionospheric residual within the range ± 4 RmLW and ± 4 RmL1 are very significant from each other. As the table is expanded, however, many of the ionospheric residual values become very similar in magnitude to each other. Table 6.1 illustrates this fact. The resulting ionospheric residual values for the RmLw/RmL1 combinations of -2/-4 and 0/5 differ from each other by only 0.06 L1 cycles. As the table is further expanded, these similarities become more frequent, and the ionospheric residual numbers less distinct. This is looked at further in §6.6.3.a.

Figure 6.12 shows the effect of introducing a cycle slip of one cycle on L1. A jump of 3.53 cycles is observed in the ionospheric residual value indicating a slip of one cycle on L1, one cycle on Lw, both from table 6.1, and hence zero cycles on L2.

Figures 6.13 and 6.14 illustrate the ionospheric residual results for both a Trimble 4000 SSE and Ashtech Z-XII receiver respectively. It can be seen that the noise value is far less than the theoretical 3σ confidence value of 0.41 cycles.

6.6.1.1 Measurement Noise

Tests were carried out to investigate the typical pseudorange and carrier phase measurement noise expected from the receivers used, these being the Trimble 4000 SSE and Ashtech Z-XII. Zero baseline data were gathered by connecting two GPS receivers to a single antenna via a two way splitter. The resulting data were relatively multipath free, and not affected by clock errors. The data were then processed using the IESSG GPS Analysis Software (GAS) [STEWART *et al*, 1995], by fixing the two receiver station coordinates to the same values, so that the resulting double difference residuals would be due to the noise of the system.

Typically, the measurement noise was seen to be different for the two receivers, and different for the P-codes during the presence of AS. The narrow correlated C/A-code is also shown to have a far better resolution than the previously available C/A-code. Figures 6.15 to 6.20 illustrate the noise values obtained from the zero baseline tests for the two receivers, both with and without the presence of AS.

It can be seen in figures 6.15, 6.16 and 6.17 that the Y-code, the C/A-code and the P-code on the Ashtech Z-XII have all roughly the same magnitude of noise, about ± 0.4 m, which corresponds to ± 2 cycles. This shows that the presence of AS with this receiver has little or no effect. A comparison of figures 6.16 and 6.18, with figure 6.21, indicates that the narrow correlation technology has improved the resolution of the C/A code dramatically. From figure 6.20, the '*C/A + (Y2-Y1)*' technique of 'cracking' the encrypted Y-code, can be seen to be noisier than the C/A-code, the P-code and the direct method of cracking the code. This is because the '*C/A + (Y2-Y1)*' technique consists of an accumulation of the C/A-code and both the Y-codes' pseudorange noise values.

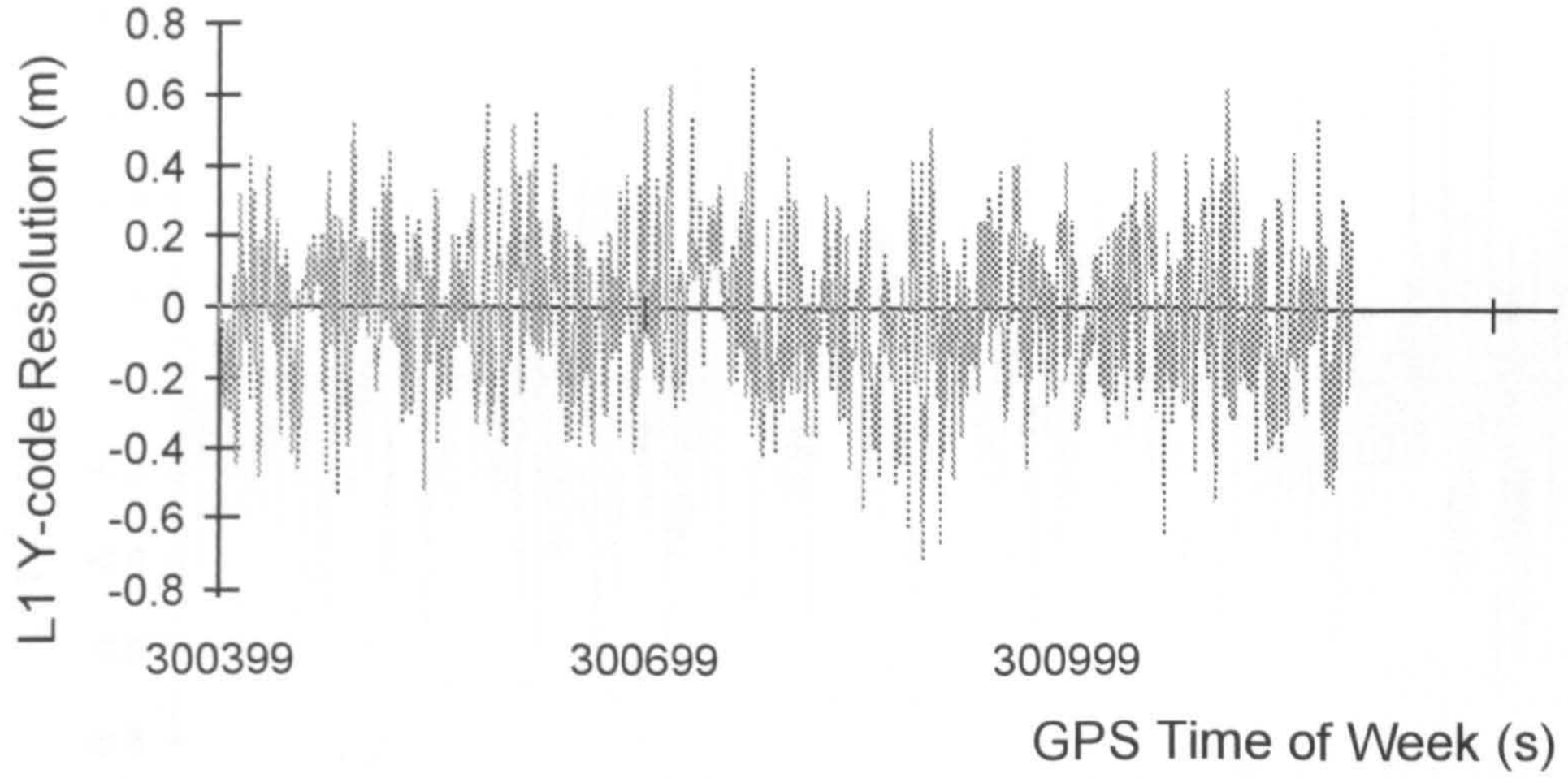

Figure 6.15

Typical Noise Value Obtained from a Zero Baseline for an Ashtech Z-XII L1 Y-Code for Satellite Combination 22, 6. AS was on during the Experiment.

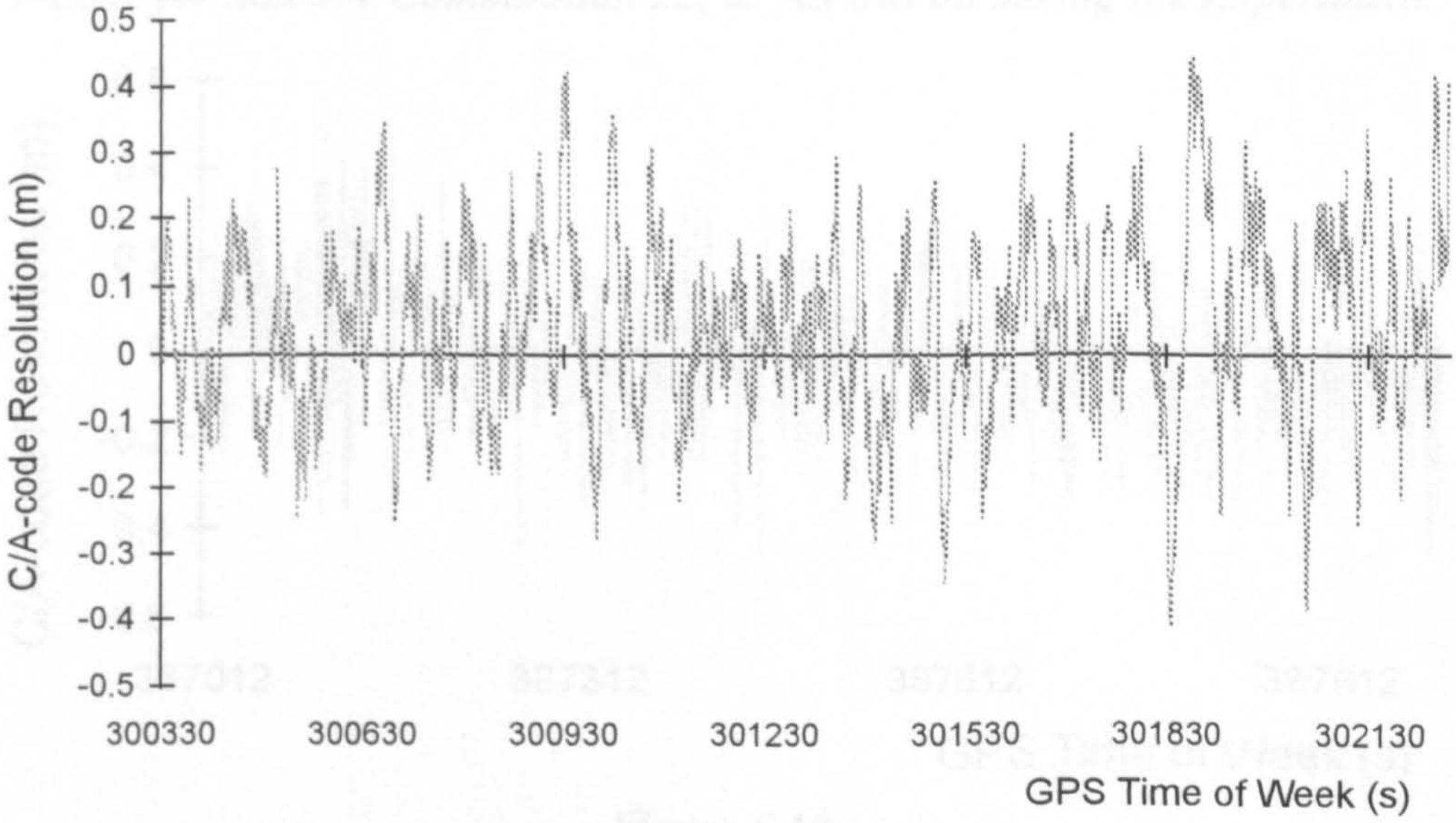

Figure 6.16

Typical Noise Value Obtained from a Zero Baseline for an Ashtech Z-XII L1 C/A-Code for Satellite Combination 22, 6. AS was on during the Experiment.

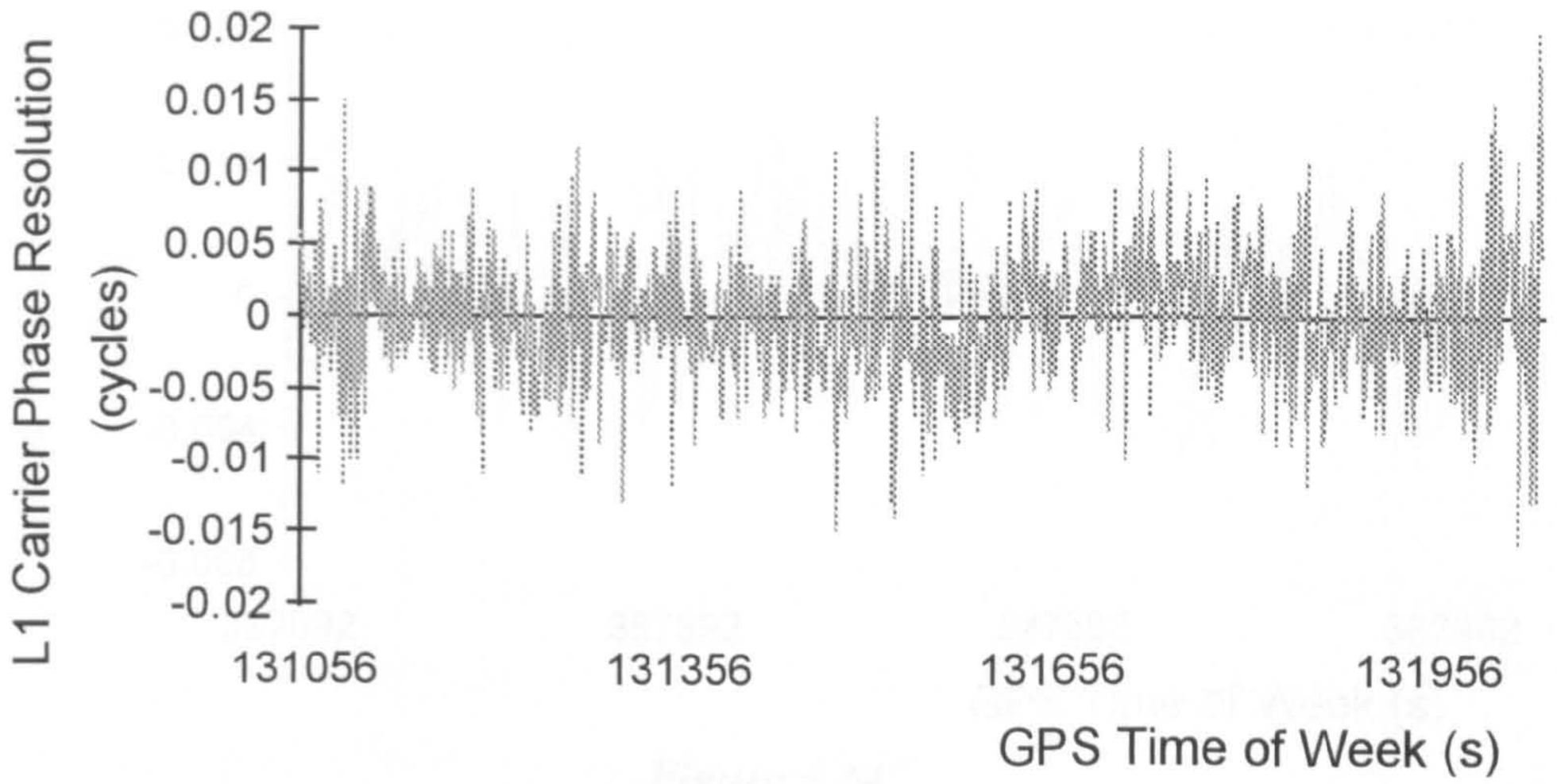

Figure 6.22

Typical Noise Value Obtained from a Zero Baseline for a Trimble 4000 SST L1 Carrier Phase for Satellite Combination 26, 5. AS was on during the Experiment.

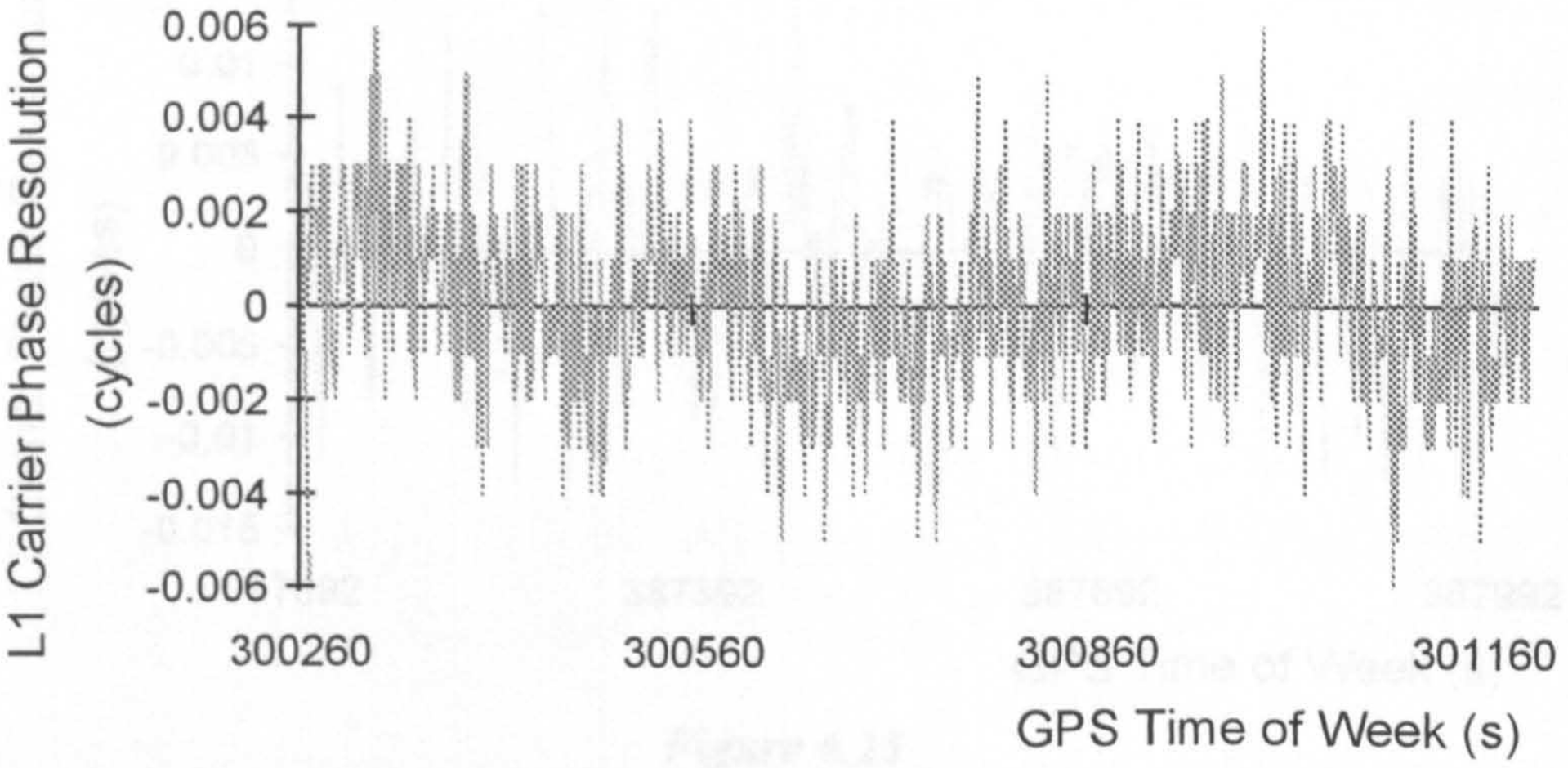

Figure 6.23

Typical Noise Value Obtained from a Zero Baseline for an Ashtech Z-XII L1 Carrier Phase for Satellite Combination 26, 6. AS was on during the Experiment.

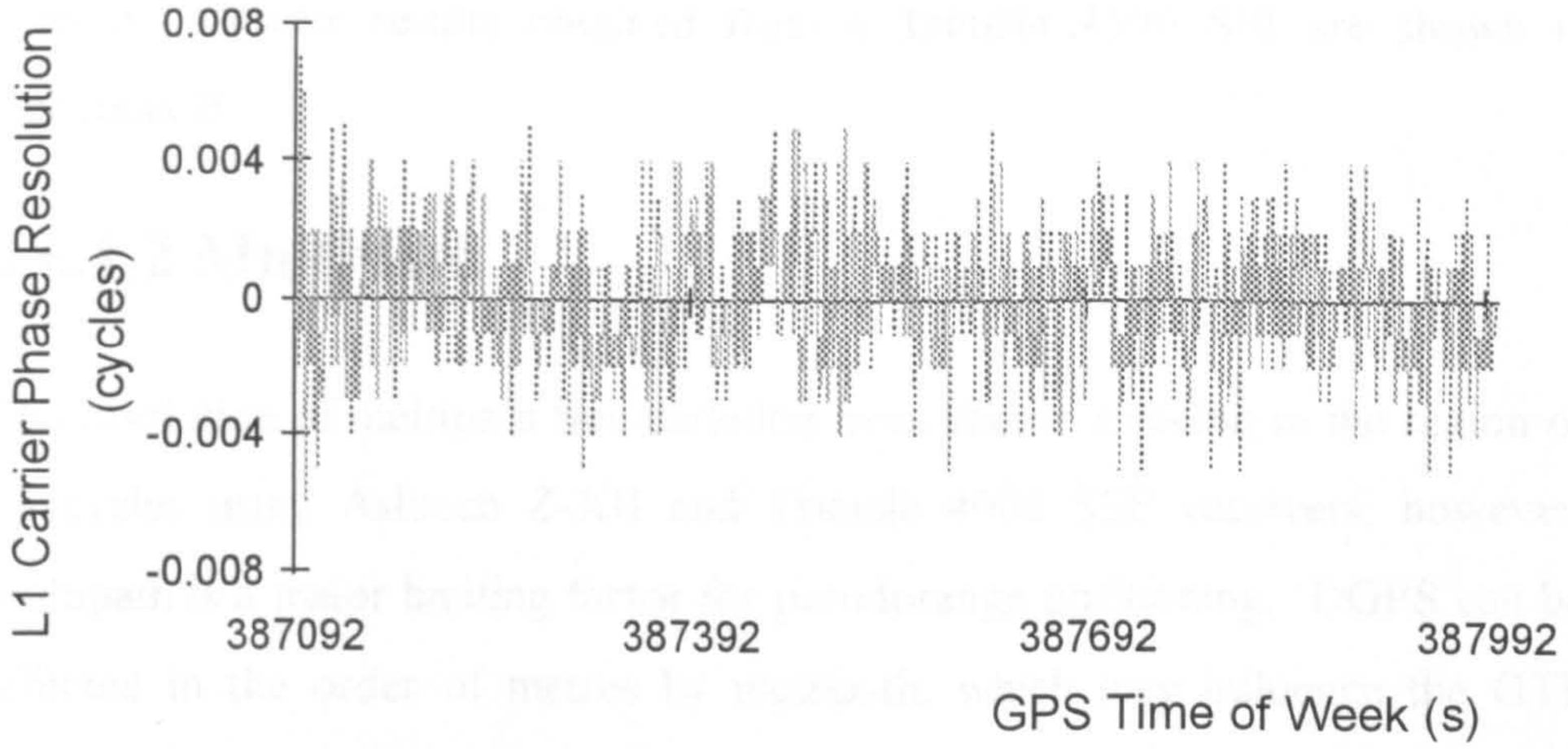

Figure 6.24

Typical Noise Value Obtained from a Zero Baseline for a Trimble 4000 SSE L1 Carrier Phase for Satellite Combination 26, 23. AS was on during the Experiment.

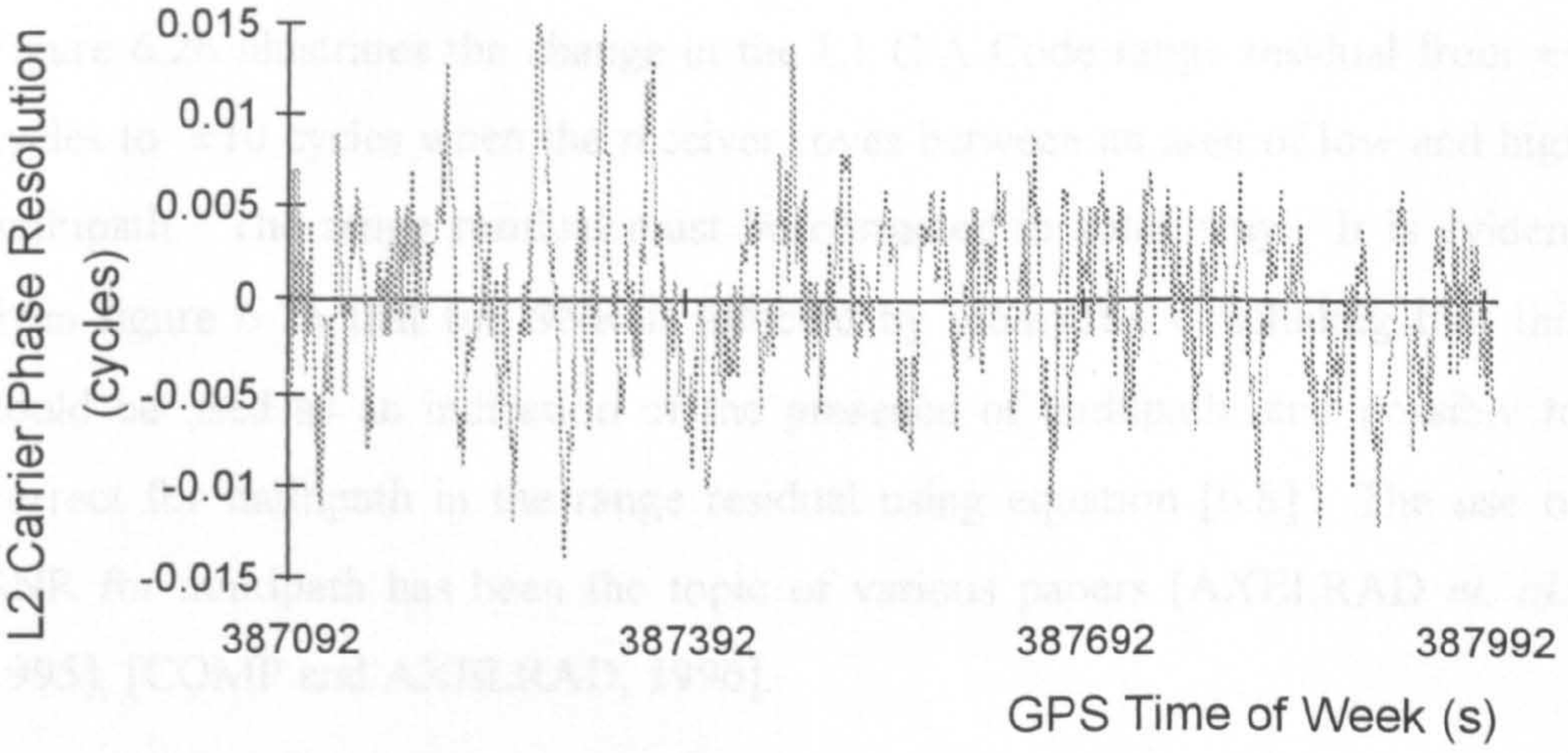

Figure 6.25

Typical Noise Value Obtained from a Zero Baseline for a Trimble 4000 SSE L2 Carrier Phase for Satellite Combination 26, 23. AS was on during the Experiment.

By comparing the resolution of the pseudorange to that of the carrier phase, as shown in figures 6.22 to 6.25, it can be seen that the range residual noise is mainly affected by the pseudorange, apart from when a cycle slip exists. It can also be seen that the higher quality resolution of the Ashtech Z-XII and Trimble 4000 SSE result in better resolution carrier phase values. This is due to the resulting carrier phase being 'cleaner' due to a more precise code being stripped

from it. Similar results obtained from a Trimble 4000 SSI are shown in Appendix B.

6.6.1.2 Multipath

The resolution of multipath free code has been shown as being in the region of ±4 cycles using Ashtech Z-XII and Trimble 4000 SSE receivers, however, multipath is a major limiting factor for pseudorange positioning. DGPS can be affected in the order of metres by multipath, which may influence the OTF ambiguity search [JACK, 1994]. The cycle slip detection methods based upon the use of codes may also introduce false cycle slips, when in fact multipath is the cause of any large deviation in the range residual or the four observables equation.

Figure 6.26 illustrates the change in the L1 C/A-Code range residual from ±4 cycles to ±10 cycles when the receiver roves between an area of low and high multipath. The range residual must be corrected in some way. It is evident from figure 6.26 that the SNR is affected by multipath, concluding that this could be used as an indication of the presence of multipath, and possibly to correct for multipath in the range residual using equation [6.8]. The use of SNR for multipath has been the topic of various papers [AXELRAD *et. al.*, 1995], [COMP and AXELRAD, 1996].

The SNR can therefore be used to correct for the range residual multipath via an empirical relationship derived by the author. In equation [6.8], the range residual affected by multipath is corrected using the SNR of the affected signal and that of the same satellite signal received at the reference GPS receiver.

$$RR_{Clean} = RR_{MP} \left(\frac{SNR_{Rove}}{SNR_{Base}} \right)^{(SNR_{Base} - SNR_{Rove})} \qquad (6.8)$$

where;

RR_{Clean} = Range Residual Corrected Using SNR (cycles)

RR_{MP} = Range Residual Affected by Multipath (cycles)

slight increase in noise, as shown in figure 6.27, but not as much as that seen in figure 6.26.

Multipath is a function of wavelength [SHARDLOW, 1994], [LANGLEY, 1996]. The C/A-code chip space is 300 m, and the P-code is 30 m. Multipath is a percentage function of these values, therefore, 10% multipath would introduce 30 m error on C/A-code and 3 m on P-code (and Y-code). Carrier phase, however, can have multipath errors in the region of centimetres, as the wavelengths are approximately 19 cm and 24 cm respectively for L1 and L2. Figures 6.26 and 6.27 show that the C/A-code range residual multipath is greater than the P-code. The Y-code is seen to have only slight multipath, however, the C/A-code multipath is far greater in magnitude.

Figures 6.28 and 6.29 illustrate the range residuals and SNR for the C/A-code and the P-code respectively. The GPS antenna was located in a low multipath environment. The data used for these figures were recorded simultaneously to those collected for figures 6.26 and 6.27. It is evident from these two figures that the SNR value is constant, and the range residual scatter is of a low order. The C/A-code and Y-code range residual scatters are of the order of ± 3 cycles and ± 1 cycle respectively. It is possible to correct for the range residual multipath noise through using the two SNR values as detailed in equation [6.8].

6.6.2.1 Measurement Noise

The Doppler technique has been shown in §6.4 to have a resolution of the order of ± 0.2 cycles. The Doppler noise must be small enough to make accurate cycle slip calculations possible. However, as the epoch separation becomes larger, the Doppler becomes un-representative of the carrier phase data. The larger the gap in the data the more inaccurate the Doppler-residual becomes.

Figures 6.31 to 6.33 illustrate the L1 Doppler residual value for an Ashtech Z-XII receiver, operating at 1 second, 5 second and 15 seconds epoch intervals respectively. The three figures are drawn using the same data but filtered to the required epoch separation. The data were recorded in a low multipath location, with the antenna remaining static throughout.

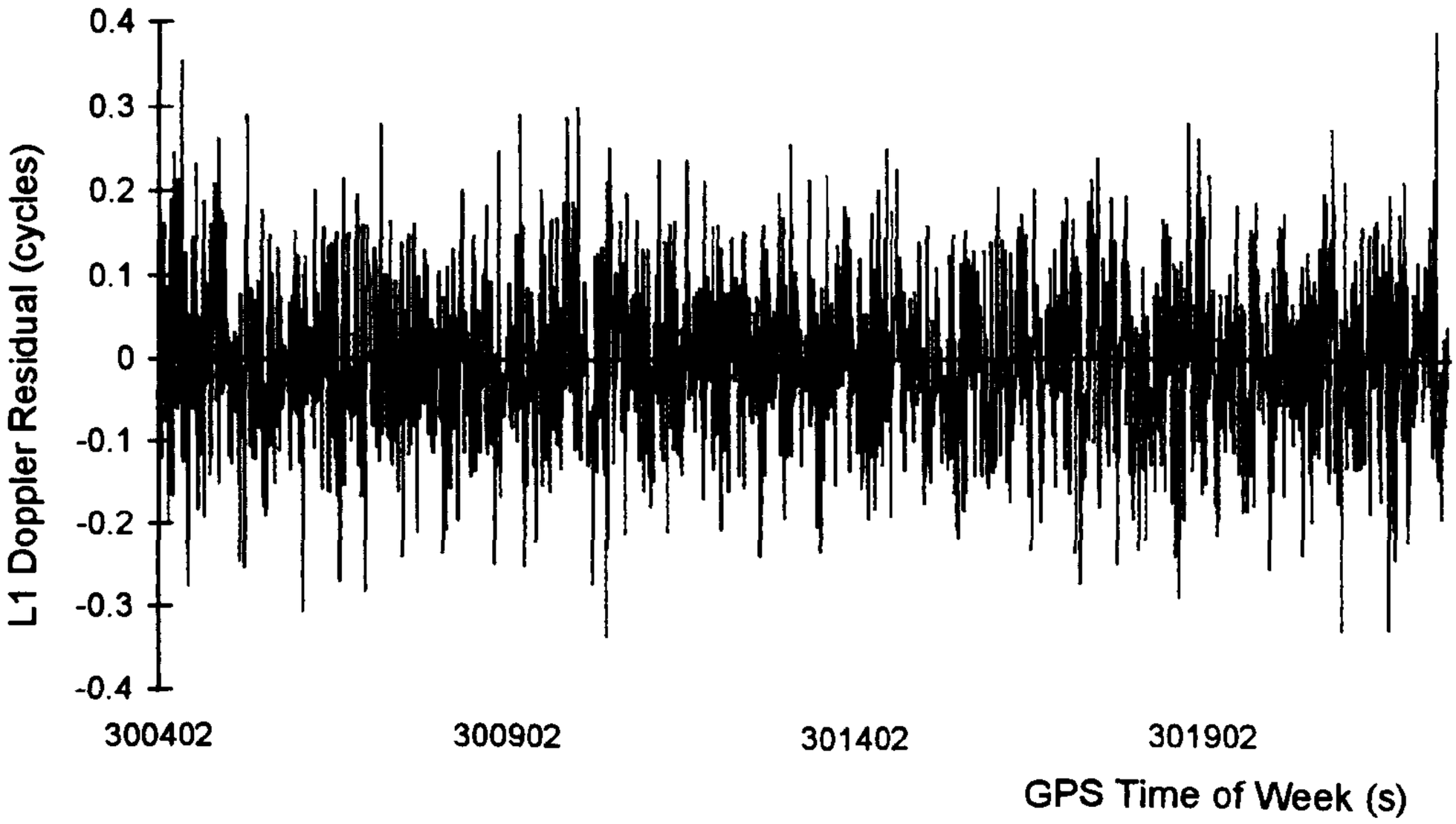

Figure 6.31

A Plot of an Ashtech Z-XII Doppler Residuals for Satellite 6 During the Presence of AS. Data Recorded at a 1 Second Epoch Interval.

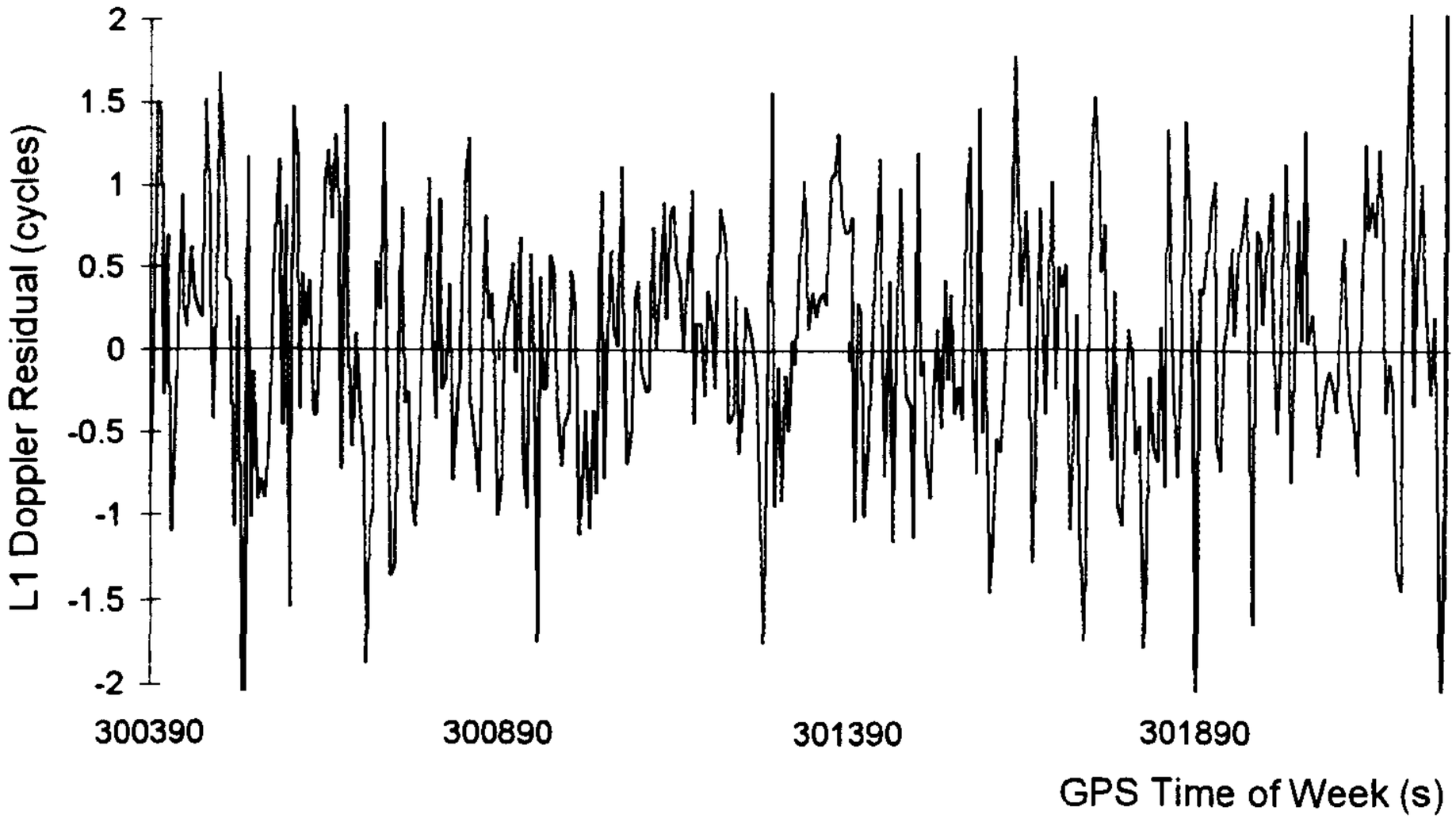

Figure 6.32

A Plot of an Ashtech Z-XII Doppler Residuals for Satellite 6 During the Presence of AS. Data Recorded at a 5 Second Epoch Interval.

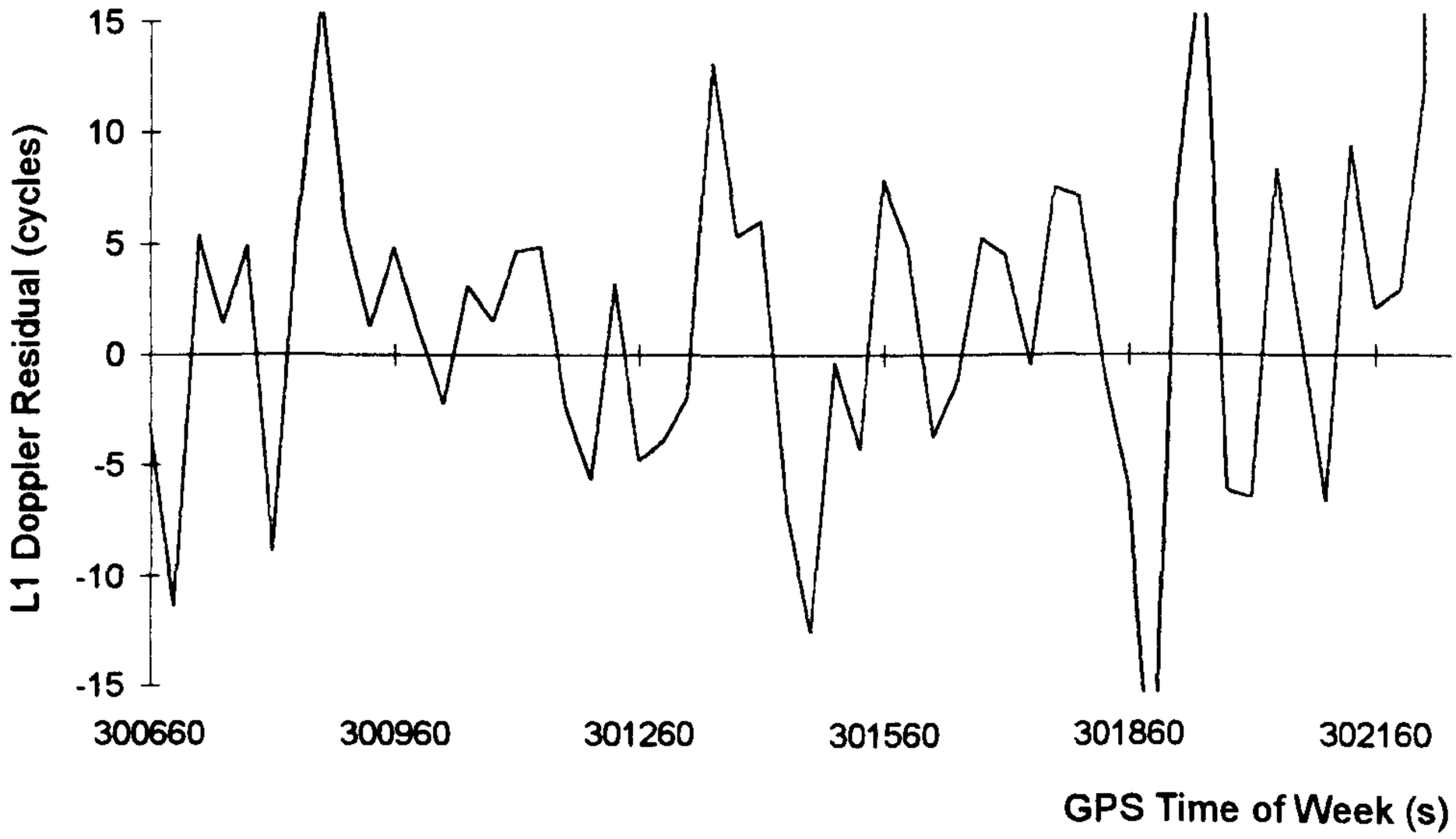

Figure 6.33

A Plot of an Ashtech Z-XII Doppler Residuals for Satellite 6 During the Presence of AS. Data Recorded at a 30 Second Epoch Interval.

It can be seen that the greater the epoch separation, the noisier and more unreliable this technique becomes. Therefore, in order for this technique to be useful, it should only be used on data with small epoch intervals, and should only be relied when gaps in the data are not greater than a few seconds. The

noise value over large epoch intervals or data gaps makes the technique unreliable and could end up introducing cycle slips into clean data.

6.6.2.2 Velocity Changes

The Doppler measurement is a function of the relative velocity of the receiver to the satellite. A static receiver, or one with constant velocity, will experience a constantly changing Doppler count. If, however, the receiver's velocity changes, then the Doppler count will not change at a constant rate. Any large velocity deviations may cause the Doppler residual technique to wrongly suggest the presence of a cycle slip.

Figure 6.34 illustrates the increase in noise level due to a sharp change in velocity as an aeroplane accelerated to take off, during the long baseline trails, detailed in Chapter 7. The data were recorded at a 2.5 second epoch interval using an Ashtech Z-XII GPS receiver.

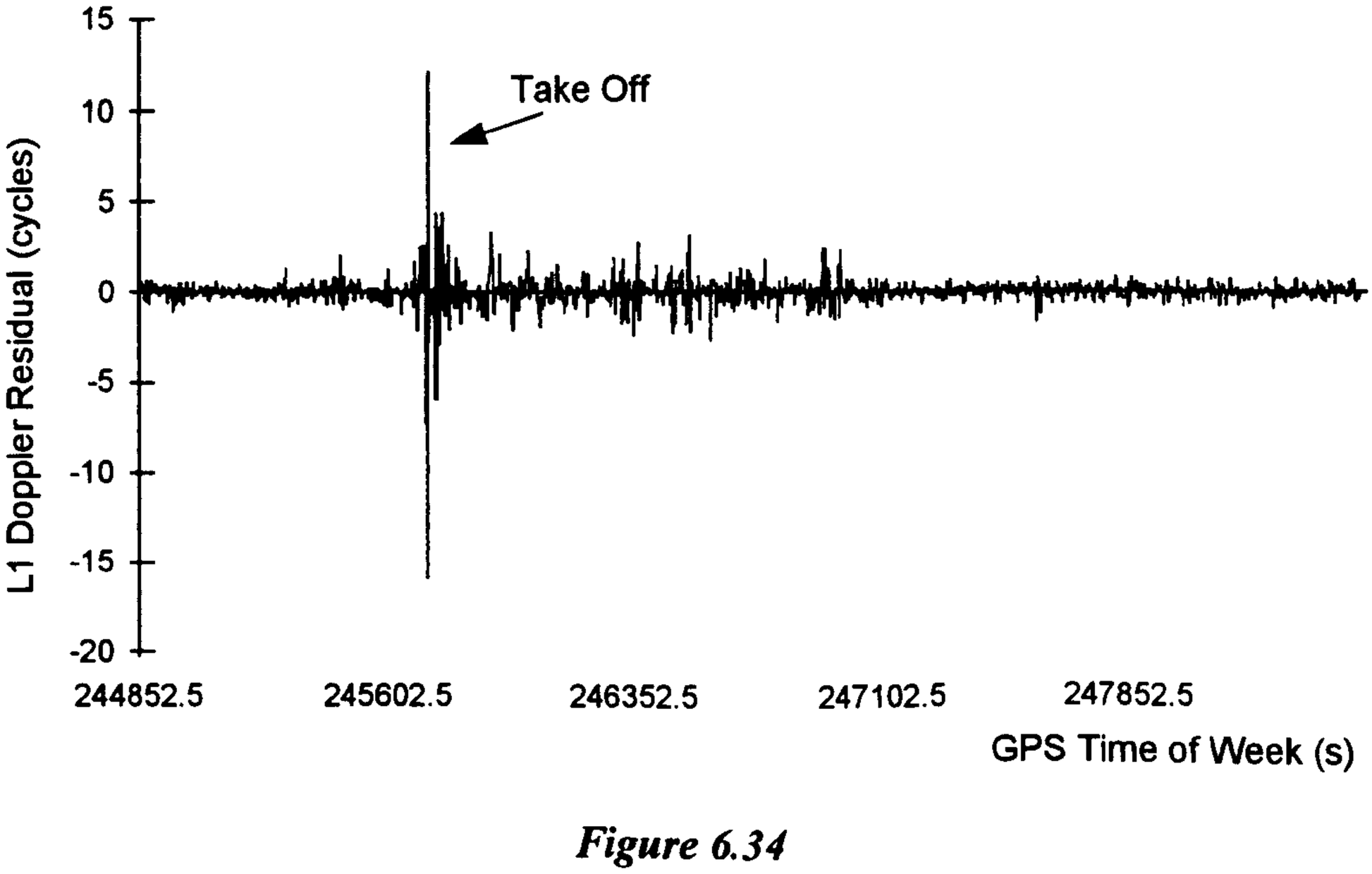

Figure 6.34

A Plot of an Ashtech Z-XII Doppler Residual Values for Satellite 4 During the Presence of AS. Data Recorded at a 2.5 Second Epoch Interval.

In this case if the Doppler technique was used it could introduce cycle slips into clean data.

6.6.2.3 Spurious Doppler Values

The continuity of the Doppler values is not affected by cycle slips, however, during the occurrence of cycle slips, spurious instantaneous Doppler values may be generated. Due to the Doppler value being a third order curve fitted to the carrier phase data, it should be affected by cycle slips. The effect should, however, only be a problem during the cycle slip. Following the cycle slip the Doppler value should continue as before without any problems. This spurious value may affect the calculated cycle slip at that point, although the Doppler value at the following epoch will counter correct.

The foregoing discussion has demonstrated that the Doppler residual technique may be relied upon to detect a cycle slip, or in fact show data to be clean, most of the time. The technique does, however, have its limitations and a secondary technique should be used to complement it and verify that a cycle slip has indeed occurred.

6.6.3 Ionospheric Residual Constraints

Two problems exist with this method.

a) The measurement noise in the carrier phase data may be so great that a wrong slip combination is chosen.

b) Certain cycle slip combinations will result in an ionospheric residual jump close to zero.

6.6.3.1 Measurement Noise

The ionospheric residual noise must not be greater than the difference between various ionospheric residuals obtained from equations [6.6] and [6.7], otherwise distinct solutions will not be found.

Assuming a measurement resolution of 0.01 cycles (~2 mm) for each phase reading, the theoretical ionospheric residual noise value may be calculated. It

follows that the expected ionospheric residual measurement noise is $\sqrt{2}$ x 0.01 cycles (0.014 cycles), and the 3σ confidence level corresponds to approximately 0.04 cycles. [WESTROP, 1990]. Taking a noise value of ~19.4 mm for the Trimble 4000 SSE wide lane [TALBOT, 1992] then the ionospheric residual measurement noise is $\sqrt{2}$ x 0.097 cycles (0.14 cycles), and the 3σ confidence level corresponds to approximately 0.41 cycles. It has been shown, however, in §6.6.1.a, figure 6.23, that modern GPS receivers can generate carrier phase observables with a resolution better than 0.005 cycles. This means that the computed ionospheric residual values must be distinct from one another by at least 0.04 cycles for the L1/L2 technique, or 0.41 for the L1/Lw technique. The distinction becomes less as the values of the refinement integers increase.

It can be seen in table 6.1, §6.5, that the two values corresponding to L1/Lw slips of -4/-2 and 5/0 have values which are distinct by 0.06 cycles. As the range in the table increases, then the values become less distinct. The distinction therefore dictates the possible extent of the table, i.e. the table may only be used to detect cycle slips in the range ±4 cycles for L1, and ±8 cycles for Lw. In practice, however, ±4 cycles for both L1 and Lw is used, as indicated by the outlined area in table 6.1.

6.6.3.2 Ambiguous Cycle Slip Combinations

The difference in two frequencies results in a new *beat* frequency being generated. The ionospheric residual should, theoretically, have an infinite wavelength due to the Lw frequency having been scaled to L1. In reality, however, the frequency combination factor in equation 6.7 is approximated, and similar values for the ionospheric residual are computed when the *Rm* integers adopt multiples of 9 and 7 for Rm_{L1} and Rm_{L2} integers, and hence 2 for Rm_{Lw}.

By considering the 3σ measurement noise level earlier derived as 0.04 cycles, then any combination of the refinement integers that produce a value close to zero within this tolerance will give ambiguous estimates of δϕ. Table 6.2

illustrates the values of $\delta\phi$ obtained from equations 6.6 and 6.7 using multiples of 9 and 7 for the L1 and L2 integers for both the L1/L2 and L1/Lw ionospheric residual tables.

RmL1	RmL2	$\delta\phi_{L1/L2}$	$\delta\phi_{L1/Lw}$
0	0	0	0
9	7	0.017	-0.059
18	14	0.033	-0.118
27	21	0.05	-0.176

Table 6.2

$\delta\phi$ Resulting from Various Multiples of 9L1 and 7L2 Integers.

It can be seen that the effect is not as noticeable for the wide lane method, but more noise exists in the wide lane due to the summation of the L1 and L2 noise. The noise on the wide lane can be 19.4 mm, compared to that of 3.0 mm and 3.9 mm for the L1 and L2 carriers respectively [TALBOT, 1992]. The constraint on the solution to equation 6.7 is that the values of the cycle slips, and hence the corresponding integers, must not take values of greater than ±8 L1 cycles and ±6 L2 cycles.

The foregoing discussion has illustrated that this method can only be relied upon to detect any combination, apart from the ambiguous combinations. However, it can only be relied upon to calculate the magnitude of cycle slips in the range ± 4 L1 and L2 cycles from the truth. It is therefore necessary for another method to correct cycle slips of any value to an accuracy of ±4 cycles, before the ionospheric residual technique may be implemented, resulting in a two stage process. The range residual, wide lane residual and Doppler techniques may be used for this reason, as long as the required accuracy of ±4 cycles can be relied upon.

Furthermore, the ionospheric residual's noise is dependent upon the ionospheric activity, which in turn is mainly affected by the sun. The activity is least during

the night, and at a maximum when the 11 year sunspot cycle reaches its maximum, as illustrated in figure 6.35 which was generated using data obtained from the Sacramento Peak Observatory's World Wide Web page [SPO, 1997]. Sunspot activity is now approaching a low (January 1997), but will next be at its maximum in 2002. This drawback should be noted, and considered in the future through taking shorter epoch separations, so as to reduce any sudden jumps between epochs, so decreasing the likelihood of wrongly detecting the presence of cycle slips. This predicted increase in sun spot activity may also increase the occurrence of cycle slips. The increase in ionospheric activity may introduce cycle slips into the GPS data, which may result in difficult data to process during this high sunspot activity.

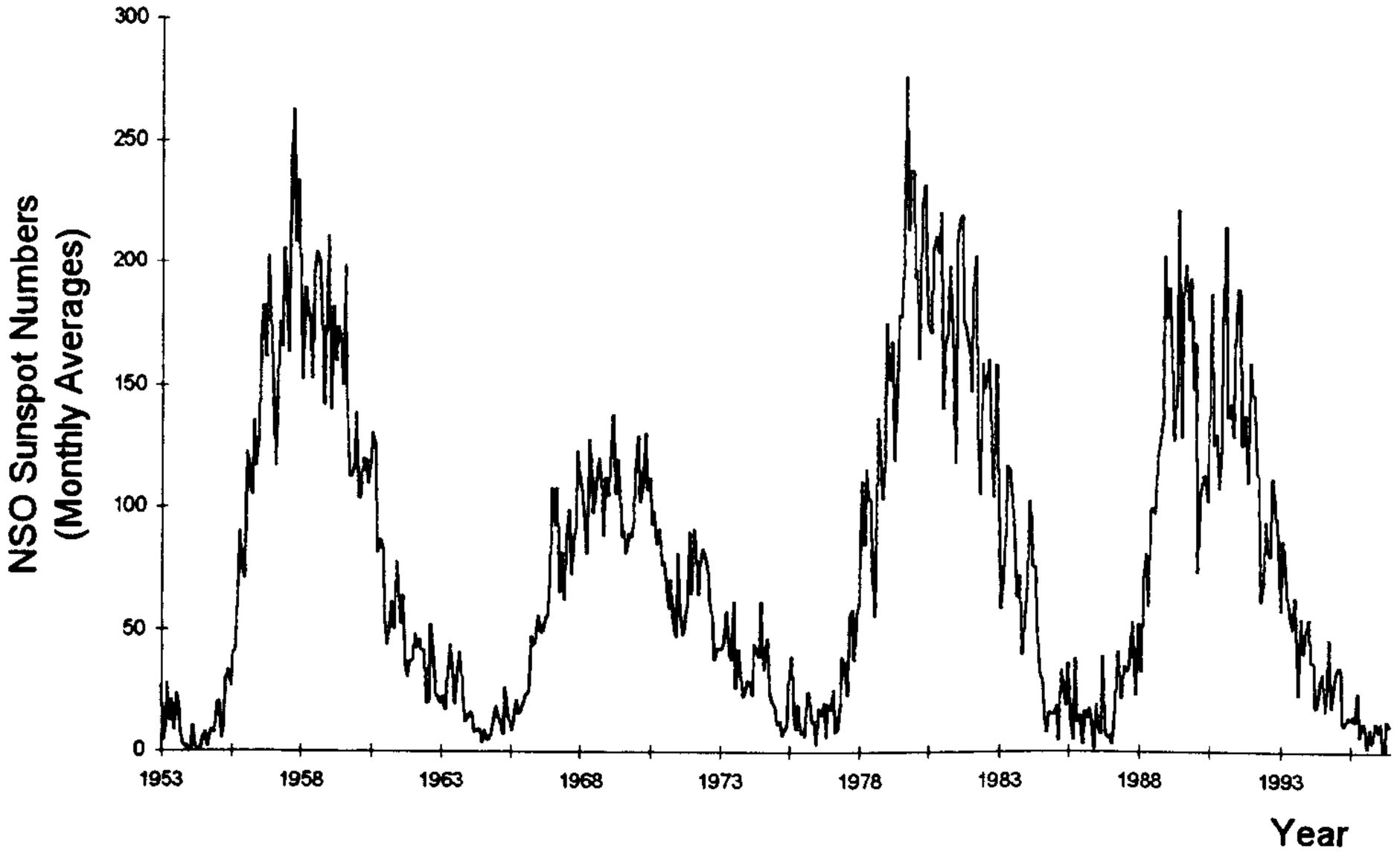

Figure 6.35

Monthly mean sunspot numbers. January 1953 - December 1996.

6.7 Implementation and Testing of the Cycle Slip Detection Techniques

The four cycle slip detection techniques discussed have been shown to have their advantages as well as their disadvantages. All the techniques are liable to wrongly detect cycle slips in certain conditions. However, a combination of all the techniques results in a more reliable method of detecting, and correcting cycle slips.

The four techniques have been implemented into a combination of FORTRAN 77 subroutines within the GAS pre-processing program, FILTER [STEWART *et al*, 1995], which previously detected cycle slips using only the code minus carrier comparison technique.

The subroutines are designed to analyse the GPS data independently of each other, resulting in independent estimates of cycle slips. The various 'residuals' are then examined to determine whether or not a cycle slip has occurred, or whether the noise in any of the 'residuals' is in fact due to other reasons, such as multipath, or any of the other constraints discussed in §6.6. These constraints become less of a problem by combining all the techniques. Once an anomaly has been detected, and it has been determined to be a cycle slip, it is calculated, and corrected for in the GPS data file. Cycle slip details are recorded in separate files, allowing user intervention and further manual analysis to be possible.

The GPS data is analysed using the four techniques, all of which have tolerances to take into account for receiver noise. If the tolerance of any method is exceeded, then the data are analysed to determine whether or not a cycle slip does in fact exist, and quantify it if possible. Analysis takes place by taking into account the other cycle slip detection techniques. The estimates of the cycle slip are inspected for each technique, and corrected for if appropriate.

The Doppler residual, range residual and wide lane technique are all used to coarsely correct the cycle slip. The ionospheric residual is then re-calculated for the new coarsely corrected carrier phase values, and then the remaining cycle slip is corrected for through this manner. Figure 6.36 illustrates a flow diagram of how the program operates.

To truly test this program's capabilities, the following data were analysed

1. Analysis of clean data, ensuring that the program recognises the data as being clean, and does not in fact introduce cycle slips.

2. Analysis of data with synthetic cycle slips introduced. This will enable the program to detect cycle slips of known values.

3. Analysis of data with real cycle slips. This is the ultimate test, whereby the program will detect cycle slips in real data.

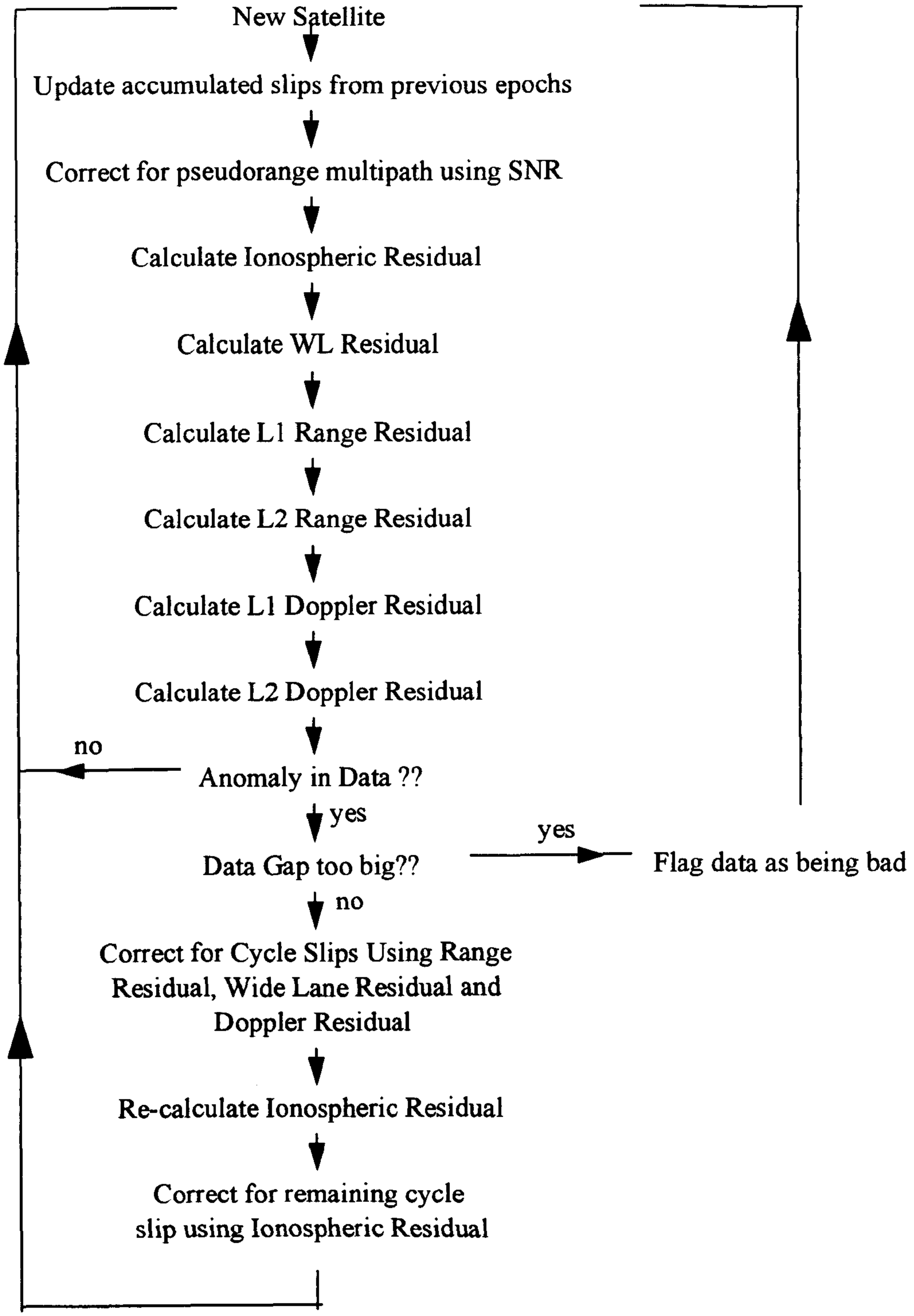

Figure 6.36

A Flow Diagram Showing the Principles Behind the Cycle Slip Correction Program.

In order to test the cycle slip detection techniques, synthetic cycle slips were introduced into clean data. The cycle slips were introduced by manually altering the carrier phase value by an integer number. The following section illustrates some of the results, showing that the combined techniques can indeed detect and correct for cycle slips. Table 6.3 shows the times and magnitudes of the cycle slips introduced into satellite 16 data.

Intro Slip GPS Time of Week (s)	L1 Cycle Slip (cycles)	L2 Cycle Slip (cycles)
300255	100	0
300270	0	100
300280	1	0
300290	0	1
300300	1	1
300310	10	0
300320	1000	0
300330	-1	0
300340	-1	-1
300350	9	7
300360	-9	-7

Table 6.3

Times and Magnitudes of the Synthetic Cycle Slips for Satellite 16.

GPS Time of Week (s)	L1 Range Residual (cycles)	L2 Range Residual (cycles)	Ionospheric Residual (cycles)	L1 Doppler Residual (cycles)	L2 Doppler Residual (cycles)	Wide Lane Residual (cycles)	L1 Cycle Slip (cycles)	L2 Cycle Slip (cycles)
300255	99.562	2.413	-352.948	100.070	0.052	100.247	100	0
300270	0.924	100.448	452.953	-0.070	99.948	-99.832	0	100
300280	0.951	1.357	-3.538	0.985	-0.014	1.164	1	0
300290	0.027	2.075	4.520	-0.007	0.993	-0.861	0	1
300300	1.257	0.595	0.982	0.809	0.847	-0.014	1	1
300310	10.189	0.786	-35.297	10.075	0.058	10.122	10	0
300320	998.119	0.340	-3529.414	999.884	-0.091	999.809	1000	0
300330	0.187	-0.358	3.526	-0.930	0.053	-0.896	-1	0
300340	-0.333	-2.608	-1.010	-0.945	-0.959	-0.114	-1	-1
300350	7.009	5.990	-0.055	9.015	7.013	1.627	9	7
300360	-8.549	-5.383	0.078	-8.832	-6.864	-1.748	-9	-7

Table 6.4

The Synthetic Cycle Slips as Detected by the Various Techniques, and the Programs Overall Estimate of their Values.

Table 6.4 illustrates the values obtained by the various cycle slip detection techniques. It can be seen that the overall slip detection is successful, even

though individual techniques may not always detect the cycle slip. The large cycle slips are detected by all the methods. The small cycle slips, in this case of a magnitude of ± 1 cycle, are only detected by the ionospheric residual and Doppler techniques, as the noise of the code minus carrier range residual is too great.

Similarly, the 9 L1 and 7 L2 cycle slip combinations are not detected by the Ionospheric Residual technique, but are detected using the others. Again, the noise level of this technique prevents the cycle slip from being detected.

It is evident that the combination of techniques allows the cycle slips to be detected, and in most cases, corrected for. The program developed by the author has been implemented upon various real data series. Examples and illustrations of real cycle slips are shown in Chapter 7. An example of data being cleaned can be found in Appendix B.

6.8 Conclusions and Recommendations

The cycle slip detection techniques have been shown to operate, but all have their disadvantages. These disadvantages have been overcome somewhat by utilising all the techniques into a single cycle slip detection and correction package.

The detection of cycle slips is an important process. Even if the cycle slips cannot be quantified, it allows an OTF integer ambiguity search to be carried out. The detection of cycle slips is an important process for the use of OTF processing to be successful, especially in a real time manner.

Ideally, the cycle slips should be calculated within the GPS receiver. Also, if the user were to record data at a 30 second epoch interval, for instance, then cycle slips would be difficult to detect even in a post processed sense. The GPS

receiver, however, would be sampling data at a far higher rate, allowing easier cycle slip detection. Any cycle slip detected should, however, be flagged, allowing post processing to take this into account, and be cautious during such instances.

Further work needs to be carried out into the detection and possible quantification of multipath. This would be useful for both the techniques which rely on the pseudorange data to detect cycle slips as well as multipath detection in general.

The future use of combined GPS and GLONASS receivers may make cycle slip detection and correction less of a problem, as the two systems may check one another. The combination of the two systems may also decrease the integer ambiguity search time, due to the increased number of satellites. The increase in satellite numbers may also mean that single frequency GPS/GLONASS receivers may be able to resolve the integer ambiguities in as short a time as a dual frequency GPS receiver.

6.9 References

ACKROYD, N., 1996, *GPS and Civil Engineering*, Published in the Civil Engineering Surveyors GIS/GPS Supplement, Autumn 1996.

AXELRAD. A., COMP. C., MACDORAN. P., 1995, *Use of Signal-To-Noise Ratio for Multipath Correction in GPS Differntial Phase Measurements: Methodology and Experimental Results*. Proceedings of Institute of Navigation, ION95 GPS Conference.

ASHKENAZI, V., HANSEN, P., LOWE, D.P., MOORE, T., ROBERTS, G.W. and SMITH, M.J., 1995, *Novel Applications of On-The-Fly GPS*, Proc. Fourth International Conference on Differential Satellite Navigation

Systems (DSNS 95), Bergen, Norway, April 1995, Volume 2, Poster No. 3.

ASHKENAZI, V., DODSON, A.H., HANSEN, P., ROBERTS, G.W., 1996, A new cycle slip recovery technique and its use for long range OTF measurements. Proc. Fifth International Conference on Differential Satellite Navigation Systems (DSNS'96), St.Petersburg, Russia.

COMP. C and AXELRAD. P., 1996, *An Adaptive SNR Based Carrier Phase Multipath Mitigation Technique*. Paper presented at of Institute of Navigation, ION96 GPS Conference.

GOAD, C., 1986, *Precise Positioning with the GPS*. Proceedings of the CERN Accelerator School of Particle Acceleration, CERN, Geneva.

HANSEN, P., 1994, *Real Time GPS Carrier Phase Navigation,* Proc. Third International Conference on Differential Satellite Navigation Systems (DSNS 94), London, UK.

HANSEN. P., 1996, *On-The-Fly Ambiguity Resolution for GPS*, PhD Thesis, University of Nottingham.

HOGARTH, B., 1996, Personal communication.

JACK, O. T. J, 1994, *Multipath Effects on GPS Observations,* MSc Thesis, University of Nottingham.

LANGLEY. R. B., 1996, Propagation of the GPS Signals. *In: Lecture Notes in Earth Science; GPS for Geodesy. Edited by Alfred Kleusberg and Peter J. G. Teunissen, pp 132 - 135, Springer-Verlag, Berlin.*

MELBOURNE, W.G., 1985, *The Case for Ranging in GPS-Based Geodetic Systems*, Proc. First International Symposium on Precise Positioning with the Global Positioning System, 'Positioning with GPS - 1985', Vol. 1, pp 373 - 386, Rockville, Maryland.

MOORE. D., 1994, *An Examination of Two GPS 'On The Fly' Ambiguity Resolution Systems*, MSc Thesis, University of Nottingham.

ROBERTS, G.W., ASHKENAZI, V., and DODSON, A.H., 1995, *The Use of Doppler to Calculate Cycle Slips,* Oral Presentation at UKGA-19. Abstract to be found in 'The JAG Newsletter, UKGA-19 Abstracts.'

SHARDLOW, P.J., 1994, *Propagation Effects on Precise GPS Heighting,* , PhD Thesis, University of Nottingham.

SPO, 1997, Sacramento Peak Observatory Sunspot numbers, *ftp://ftp.sunspot.noao.edu/pub/sunspots*

STEWART, M. P., FFOULKES-JONES G. H., OCHIENG, W. Y. and SHARDLOW, P.J., 1995, *GAS: GPS Analysis Software User manual. Version 2.3.* IESSG Publication, University of Nottingham.

TALBOT, N.C., 1992, *Recent Advances in GPS Surveying.* Presented at the National Conference on GPS Surveying, conducted by the Department of Land Information, RMIT, and the School of Surveying, UNSW, Sydney, Australia. June 22 - 26, 1992.

WALSH., D.M.A., 1994, *Kinematic GPS Ambiguity Resolution,* PhD Thesis, University of Nottingham.

WESTROP, J., 1990, *Dynamic Positioning by GPS*, PhD Thesis, University of Nottingham.

Chapter 7

Long Range OTF Kinematic GPS

7.1 Introduction

OTF GPS has been shown to be useful over short baselines (< 20 km), [HANSEN, 1996]. The following chapter will show that it is possible to use OTF GPS over longer baseline lengths, in the order of hundreds of kilometres. Such a system would allow many more applications to be able to use precise kinematic GPS. Predominately, the applications to gain from such a system would be the offshore industry and aviation for precise navigation. The need for such precision for navigation may not be necessary, but may prove productive for offshore work. This, however, would be more applicable if real time OTF was possible over such distances. This issue is discussed at the end of the chapter, section 7.4, where various suggested answers to the problem are looked at.

Research at the IESSG [HANSEN, 1996], [WALSH, 1994], has lead to the development of OTF software at the IESSG. The current software [HANSEN, 1996] allows the use of multiple reference stations (MRS), which in turn speeds up the ambiguity search, Chapter 5, and increases the baseline length.

The following chapter will detail two sets of experiments carried out by the author over long baselines, using the MRS technique. This software is known as the Nottingham OTF software (NOTF)

Section 7.2 details an experiment and some results obtained from an experiment carried out over a baseline length of 134 km. Four reference stations were used over this distance, whilst a fifth reference station was located some 9 km from the roving receiver as a quality control.

Section 7.3 details an experiment carried out, using three reference stations during the ARIES 96 Polar flight. The three reference stations were placed at the US airbase at Thule in Greenland, whilst the roving receiver was located on an RAF Comet test plane which flew from Thule to the North Pole and back again.

7.2 134 km Baseline Tests

7.2.1 Test Set-up

The test was conducted using 6 Ashtech Z-XII dual frequency GPS receivers. Four static reference receivers were based near Oxford (ASH1, ASH2, ASH3, ASH4), approximately 134 km from the roving receiver. A fifth reference receiver was placed at Nottingham (NOTT) some 9 km from the rover (HUCK), this being the sixth receiver. The four receivers at Oxford had previously been positioned relative to NOTT over an 11 hour static occupation, using a precise ephemeris and ionospherically free fixed integer ambiguity observable. The relative accuracy of such a baseline length and positioning techniques has been shown to be in the order of 10 to 15 mm in height and sub centimetre in plan [BEAMSON, 1995].

GPS Time of Week (s)	Comments	GPS Time of Week (s)	Comments
468660	Antenna on Tripod	470029	Accelerate to 50 mph
468850	Antenna placed on vehicle	470084	Retard and turn through 180 degrees
468900	Travel at 20 mph	470154	Accelerate to 70 mph
469028	Turn through 180 degrees	470204	Retard and turn through 180 degrees
469156	Turn through 180 degrees	470269	Accelerate to 70 mph
469170	Accelerate to 50 mph	470654	Retard to 50 mph
469320	Accelerate to 70 mph	470729	Retard to 30 mph
469367	Retard and turn through 180 degrees	470814	Turn through 180 degrees
469375	Accelerate to 70 mph	470879	Accelerate to 40 mph
469427	Antenna on Tripod	471035	Accelerate to 50 mph
469769	Antenna placed on vehicle	471147	Antenna on tripod
469829	Accelerate to 30 mph	471419	Move antenna onto vehicle and accelerate to 50 mph
469935	Turn through 180 degrees	471779	Stop

Table 7.1

Vehicle speeds during the trial.

The kinematic data was collected at 2 Hz over a period of approximately 50 minutes. HUCK was placed upon a minibus, roving on an open runway at speeds of up to 70 mph. On three occasions during the trial, the antenna was carefully detached from the minibus, and placed upon the same tripod for a number of minutes, hence establishing an absolute truth and repeatability criteria for the results. Table 7.1 illustrates the speeds and corresponding times during the trial, and the times considered during the next sections (highlighted).

The short and long baselines were then independently processed using NOTF, then analysed and compared to each other.

7.2.2 Short baseline results

For the long baseline to be compared to the results of the short, it was first necessary to establish the accuracy of the short baseline. Fast static processing was carried out for the three times the HUCK receiver was placed upon the tripod. The resulting solution for the three occupations was used to compare the short baseline results. The RMS radial difference between the fast static and

short range OTF solution was calculated at 0.025m. Over 900 OTF positions were taken into account.

7.2.3 Long Baseline Results

The cycle slip detection techniques worked successfully on the data sets. The data sets being HUCK, NOTT, and ASH1 to 4. The following illustrates some of the results for HUCK. Figures 7.1 and 7.2 respectively show the L1 and L2 range residuals for satellite 07. It is seen that these are accurate to approximately ±4 cycles as expected, but do have a couple of peaks at locations of high multipath. Figures 7.3 and 7.4 illustrate the L1 and L2 Doppler residuals respectively for satellite 07. These can be seen to be accurate to ±0.1 cycles whilst the vehicle is static. However, this accuracy soon decreases when the vehicle accelerates, but is still accurate to approximately ±0.5 cycles. Figure 7.5 illustrates the ionospheric residual plot for the considered data for satellite 7. The plot suggests that the ionospheric residual is by far the most accurate means of detecting cycle slips, although it does have spikes at acceleration times.

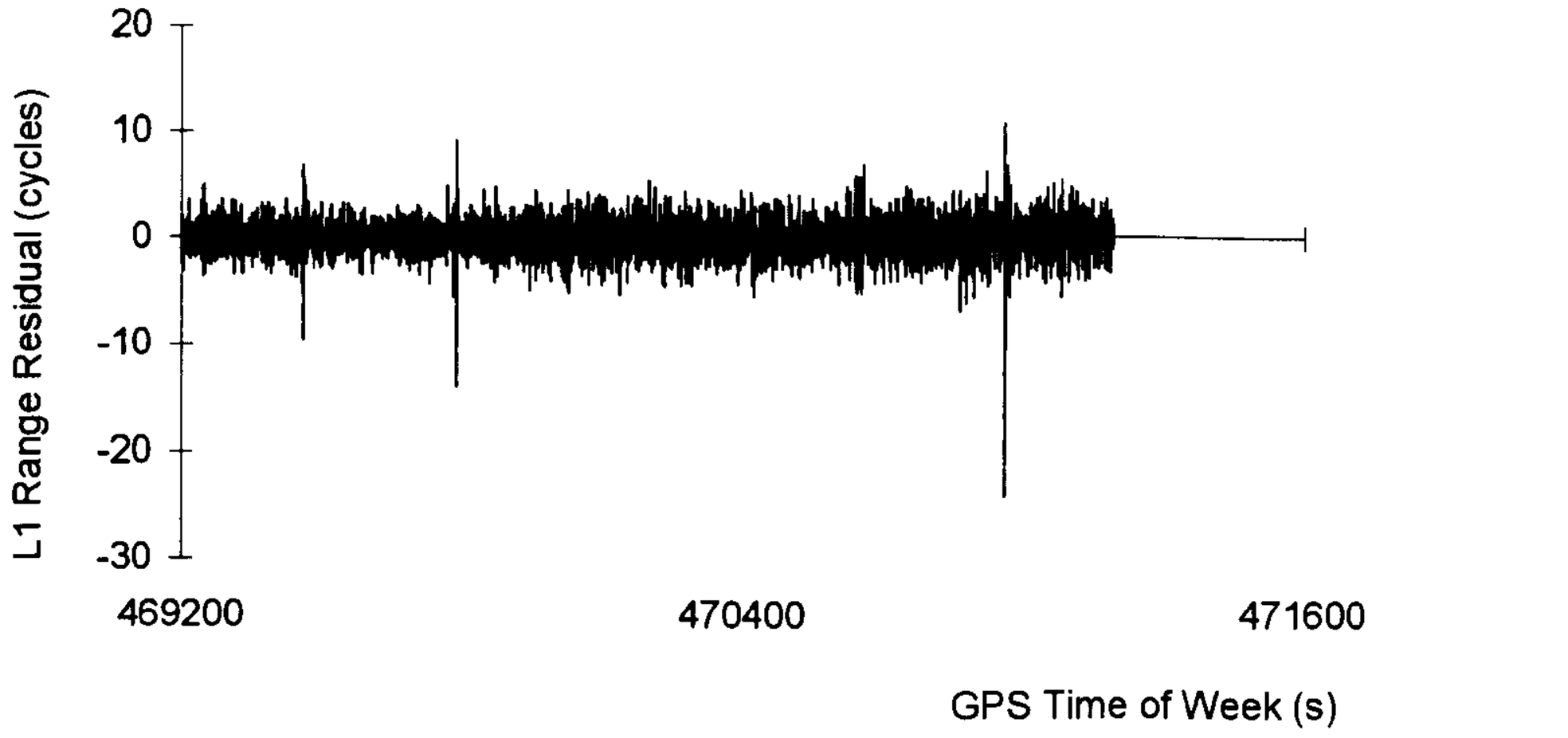

Figure 7.1

Satellite 07 L1 Range Residual Showing Spikes at High Multipath.

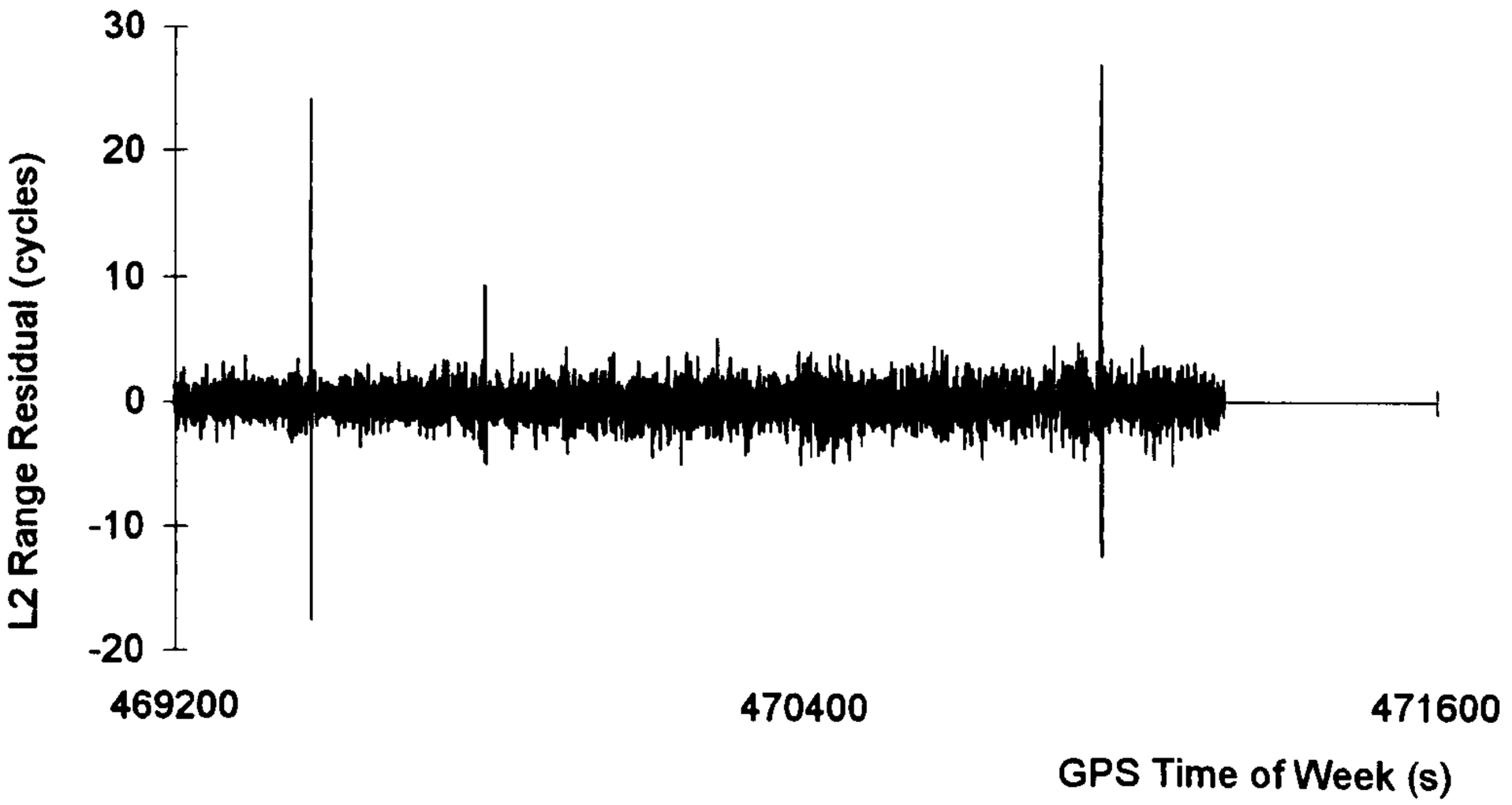

Figure 7.2

Satellite 07 L2 Range Residual Showing Spikes at High Multipath.

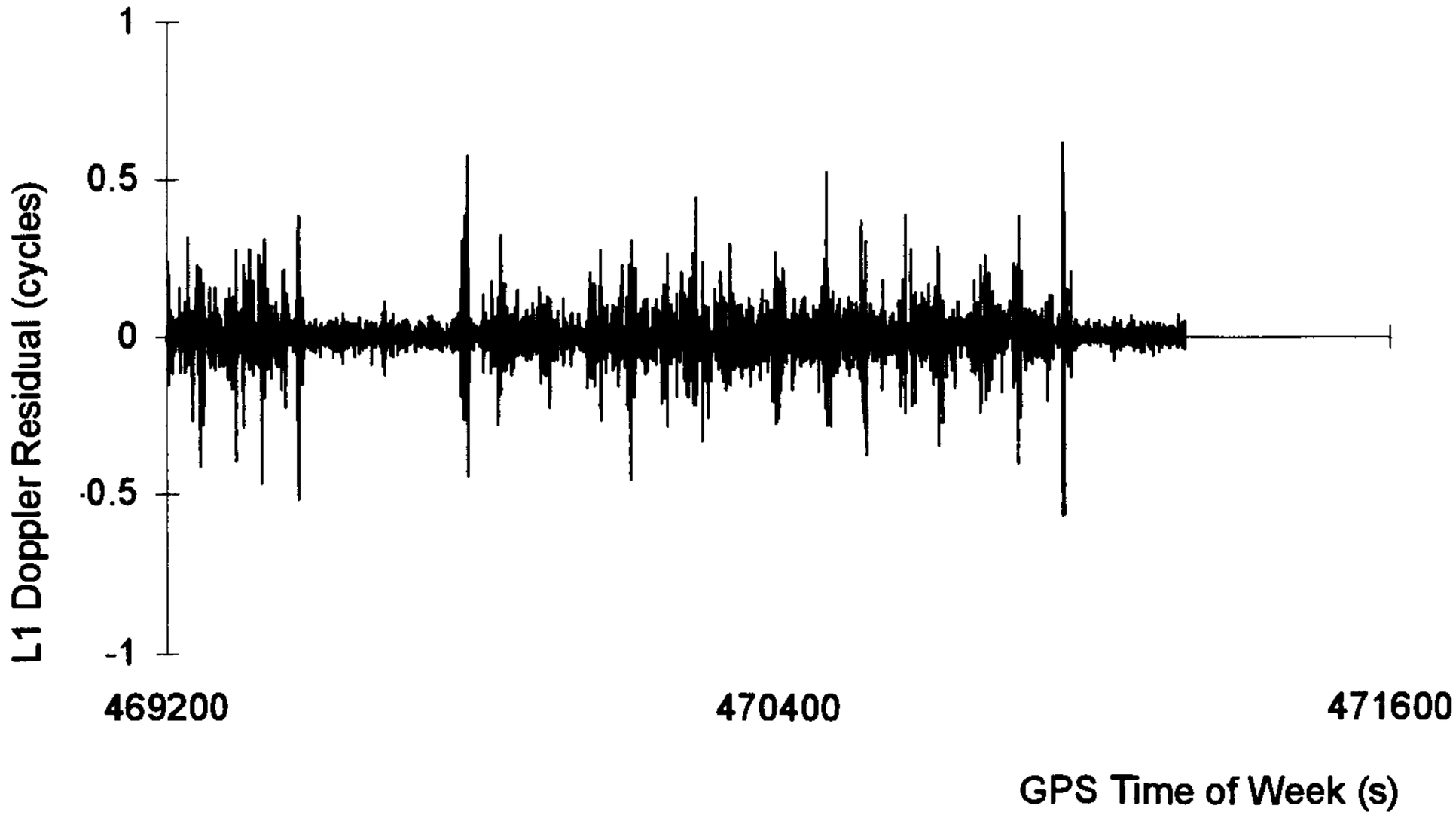

Figure 7.3

Satellite 07 L1 Doppler Residual, Showing Higher Resolution at Constant Velocities.

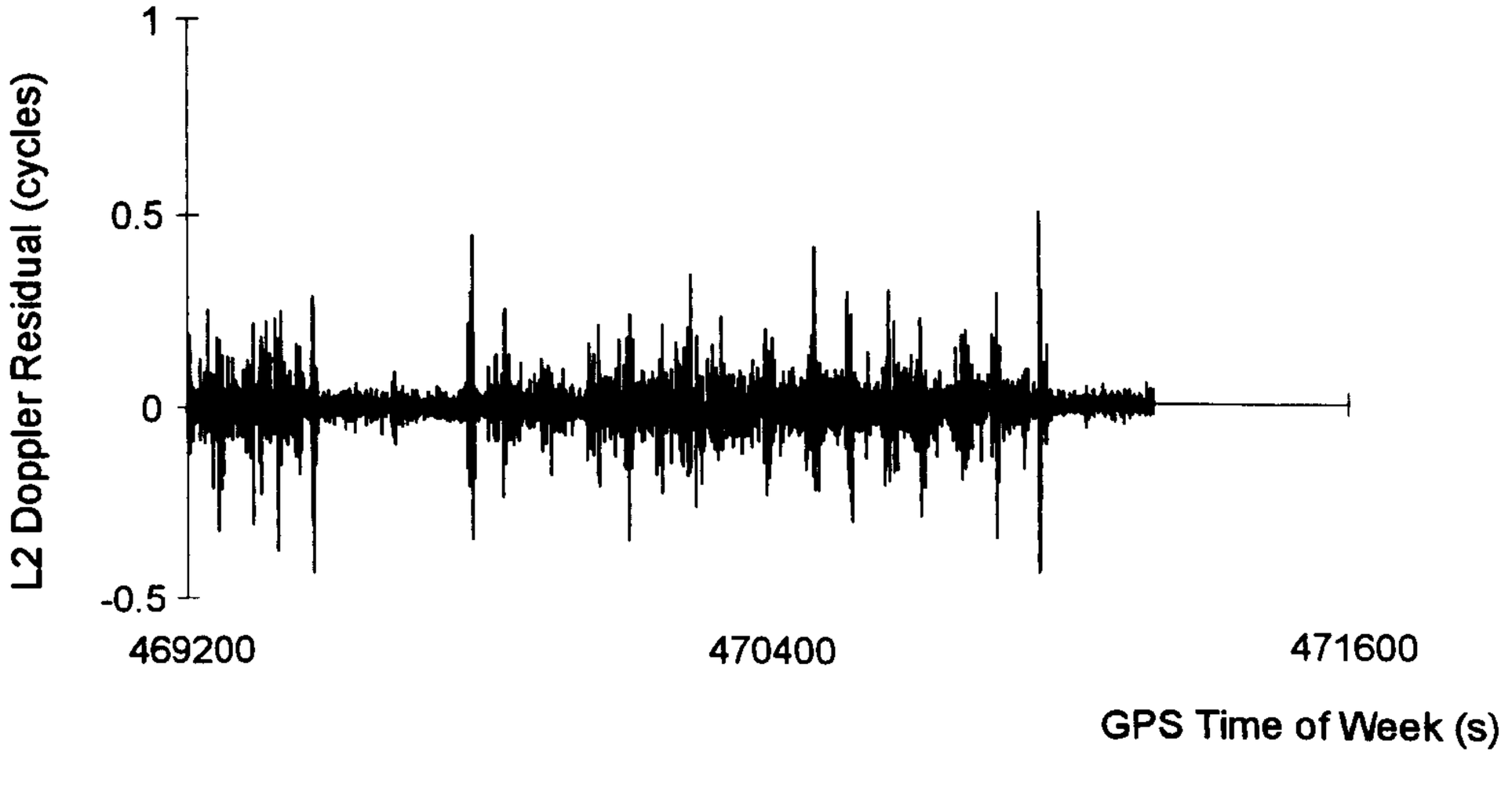

Figure 7.4

Satellite 07 L2 Doppler Residual, Showing Increased Accuracies at Constant Velocities.

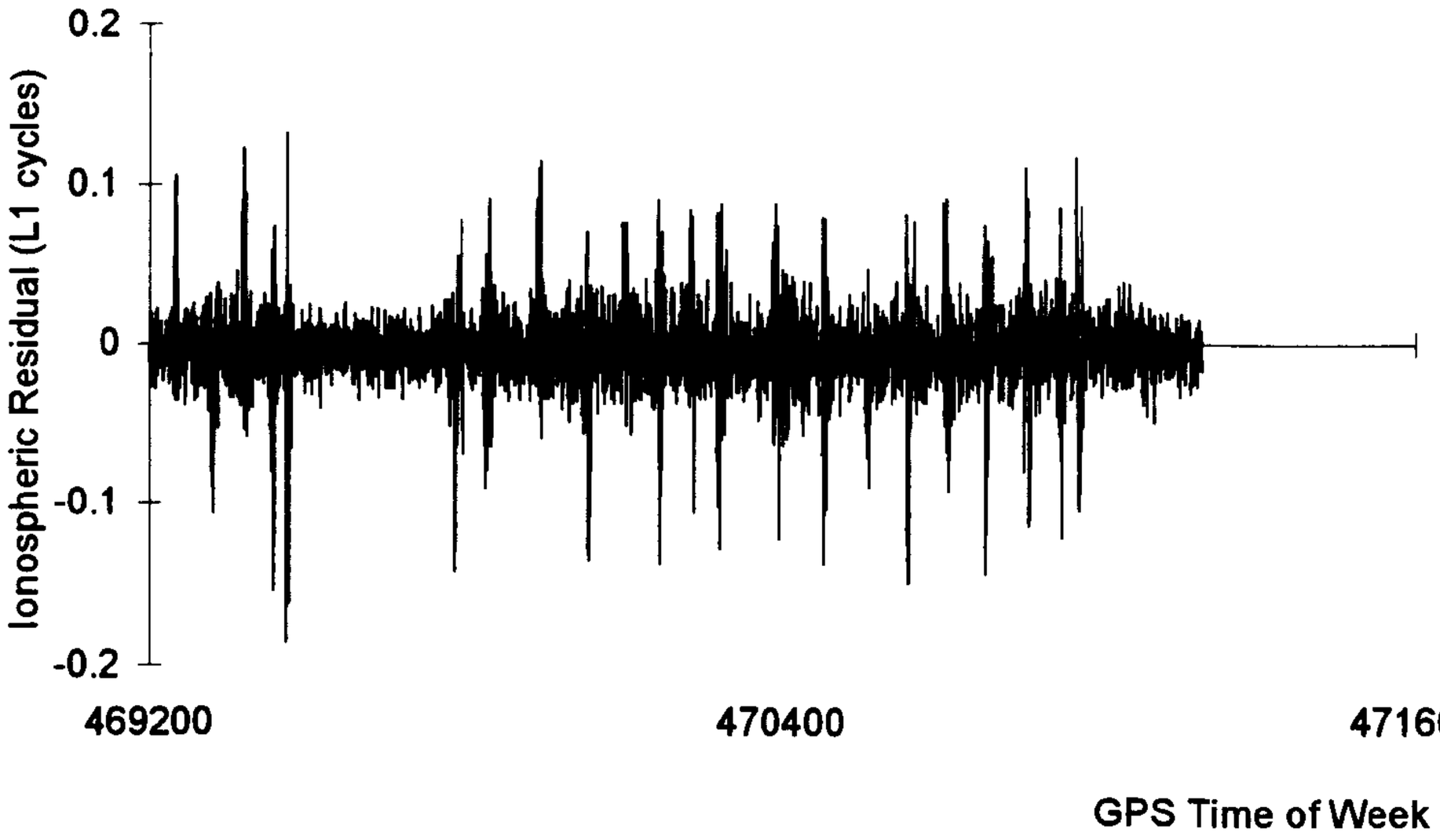

Figure 7.5

Satellite 07 Ionospheric Residual for the Considered Data.

Figure 7.6 illustrates the radial difference between the long and short baseline L1 solution results for a sample of the data, with rover speeds of up to 70 mph. Figure 7.7 illustrates the difference between the L1 short baseline results and the long baseline wide lane results for the same data.

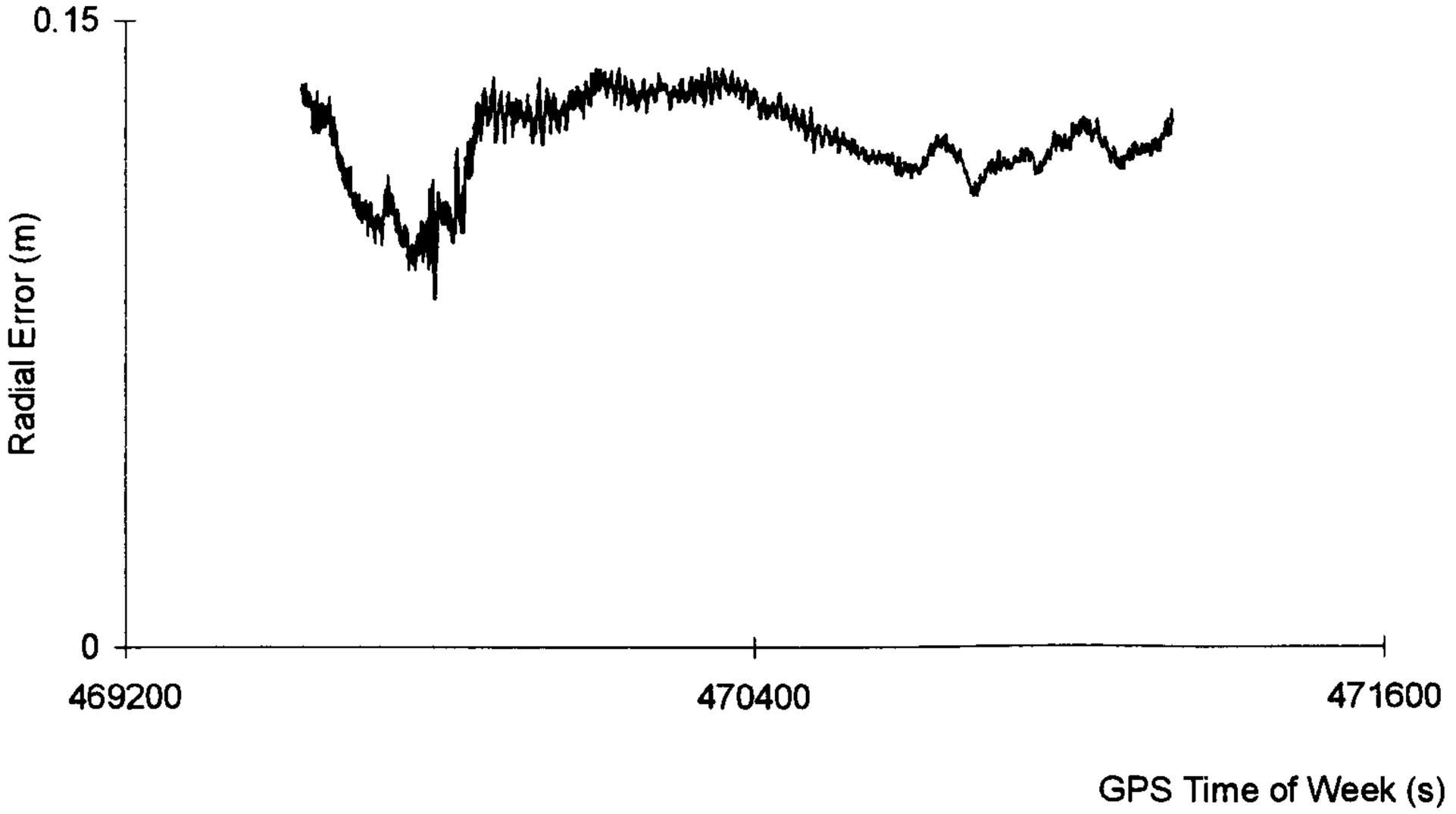

Figure 7.6

Short Baseline L1 minus Long Baseline L1 Radial Error for the Kinematic Trial.

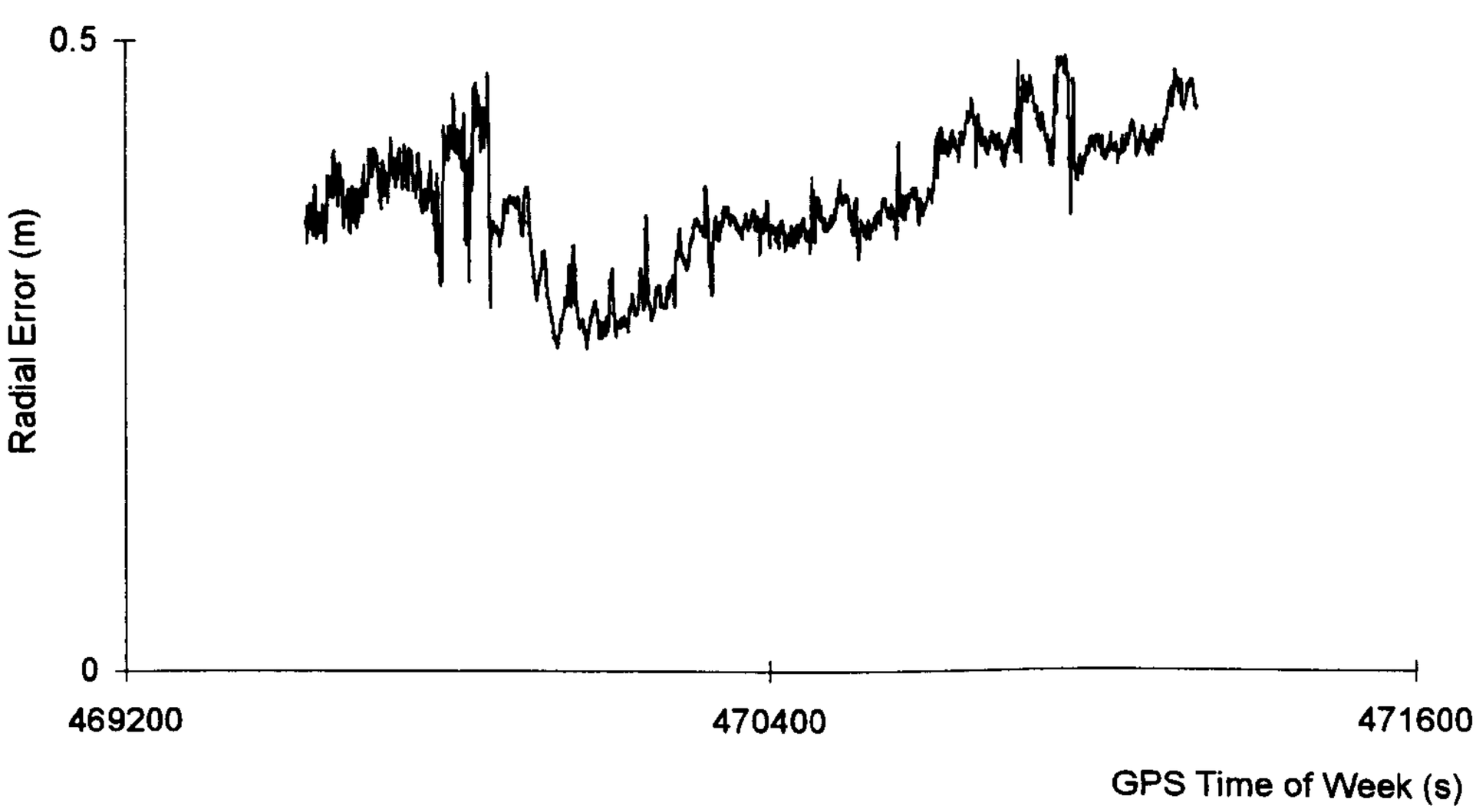

Figure 7.7

Short Baseline L1 minus Long Baseline Lw Radial Error for the Kinematic Trial.

The RMS errors for the L1 and wide lane solutions are 0.121m and 0.378m respectively. The radial errors in Figures 7.6 and 7.7, appear to be offset from the truth. This offset may be due to the relative positioning accuracy of ASH1-

4 and NOTT, carried out through an 11 hour static carrier phase occupation processed using a precise ephemeris. The relative accuracy, however, has previously been shown [BEAMSON, 1995] to be in the order of a centimetre for such a static positioning technique. The ionospheric noise is more likely to be the cause of the offset. OTF positioning using an ionospherically free observable rather than L1 would increase the positioning accuracy.

The time to resolution is an important factor for OTF. It has previously been demonstrated that the Nottingham OTF technique can resolve wide lane integer ambiguities over minimum baseline lengths of 130 km within approximately 3 epochs [ASHKENAZI *et al*, 1996]. Tests carried out on the long range data showed that a mean resolution time of 14 half second epoch intervals, or 7 seconds, was taken to resolve the L1 ambiguities.

The curve in Figure 7.6 exhibits two distinct features. Firstly there is an offset of approximately 0.12m from the truth, and secondly there is some fluctuating bias within the graph. The offset of the curve in Figure 7.6 may be a result of the ionospheric activity, whilst the shape of the curve may be due to the Tropospheric delay.

The data were processed from ASH1 to NOTT in static mode during the 50 minute kinematic trial, using L1 and ionospherically free (L0) frequencies. The results from the two frequency tests, Table 7.2, show the effects the ionosphere can have on the coordinate differences.

Frequency	Integer	Dx from truth (m)	Dy from truth (m)	Dz from truth (m)	Radial Error(m)
L1	Free	-0.260	-0.720	-0.440	0.883
L0	Free	-0.112	-0.005	-0.127	0.169

Table 7.2

Baseline differences due to ionospheric activity.

The results in Table 7.2 suggest that the ionospherically free observable is closer to the truth than when using L1 only.

As a means of quantifying the affect of the troposphere on the results, a second test was performed. The coordinates of both stations were fixed to the truth, and the data was processed solving only for the troposphere. Figure 7.8 illustrates the total zenith delay for the kinematic data set during the trial. It can be seen that there is a correlation between the shape of the graph presented in Figure 7.6 and that presented in Figure 7.8.

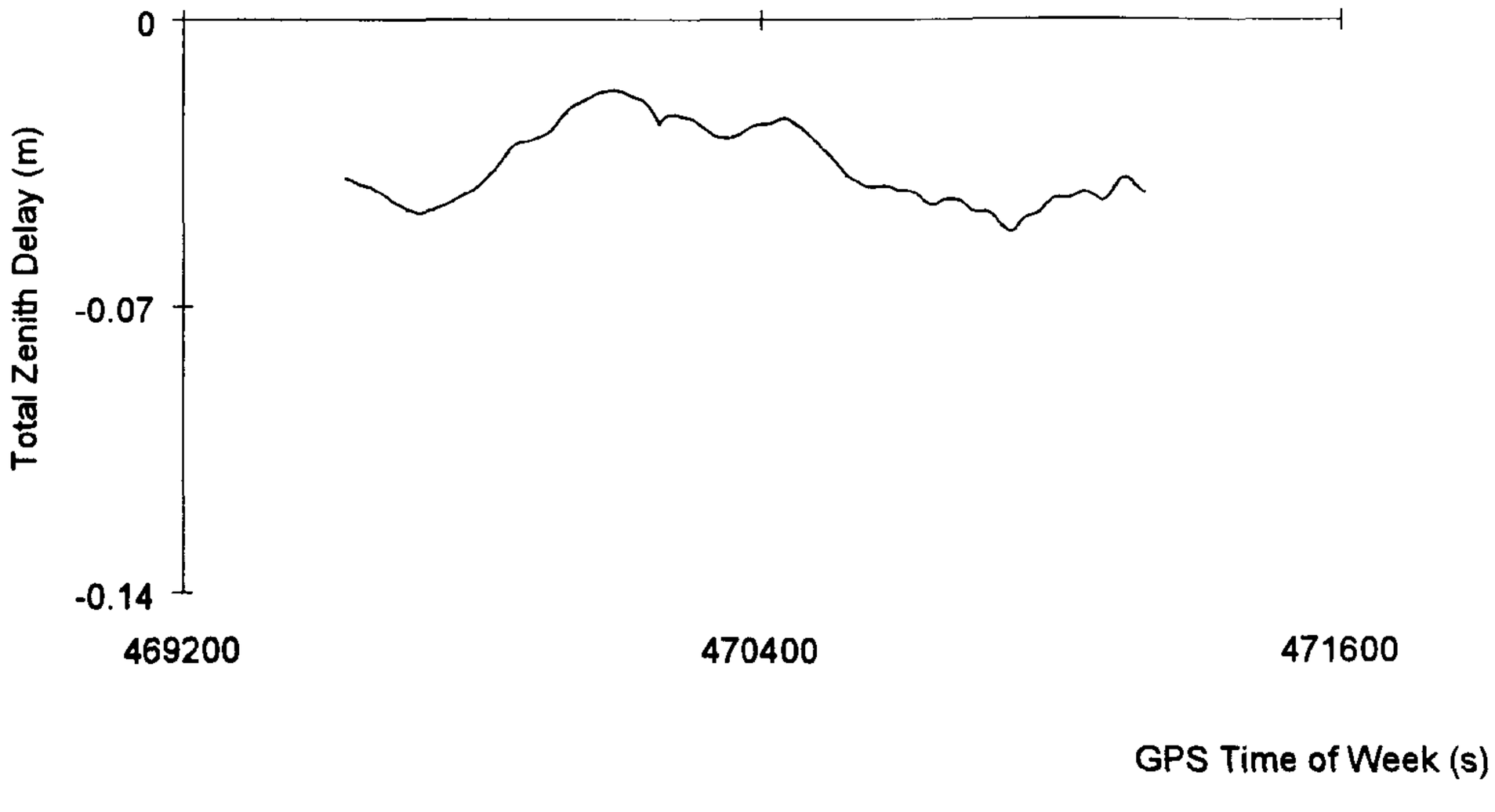

Figure 7.8

Total Trpopspheric Zenith Delay for Kinematic Trial.

Both the ionospheric activity and tropospheric delay are the limiting factors for this technique at present. They are both the subject of research at the IESSG, and their affect on OTF is under investigation.

7.3 ARIES 96 Polar Flight Results

The author was kindly invited to attend the RAF ARIES'96 test flight, a certificate of attendance can be seen in Appendix C. This flight is part of the RAF GD Aero Systems Course held at RAF Cranwell, where the students are flown in the plane from the UK to the North Pole and back. During the flight, the students are allowed to operate and view the various navigation system on

board. These systems included various GPS receivers, both military and civilian, as well as inertial navigation systems (INS), combined INS and GPS systems and gyro compass systems. Amongst these systems was one of the IESSG Ashtech Z-XII GPS receivers. All the data gathered was analysed by the students after the flight as part of their course. The data gathered by the IESSG's Z-XII receivers was used by the author to assess the use of OTF GPS for such a long flight. During the flight from the UK to Greenland, there was no reference station data available. The data was processed using pseudorange positioning, carrier phase smoothed pseudorange positioning and using a precise ephemeris. This data was supplied to the students at RAF Cranwell to examine and analyse against the other systems available. Figure 7.9 illustrates the Comet plane used during the ARIES'96 flight.

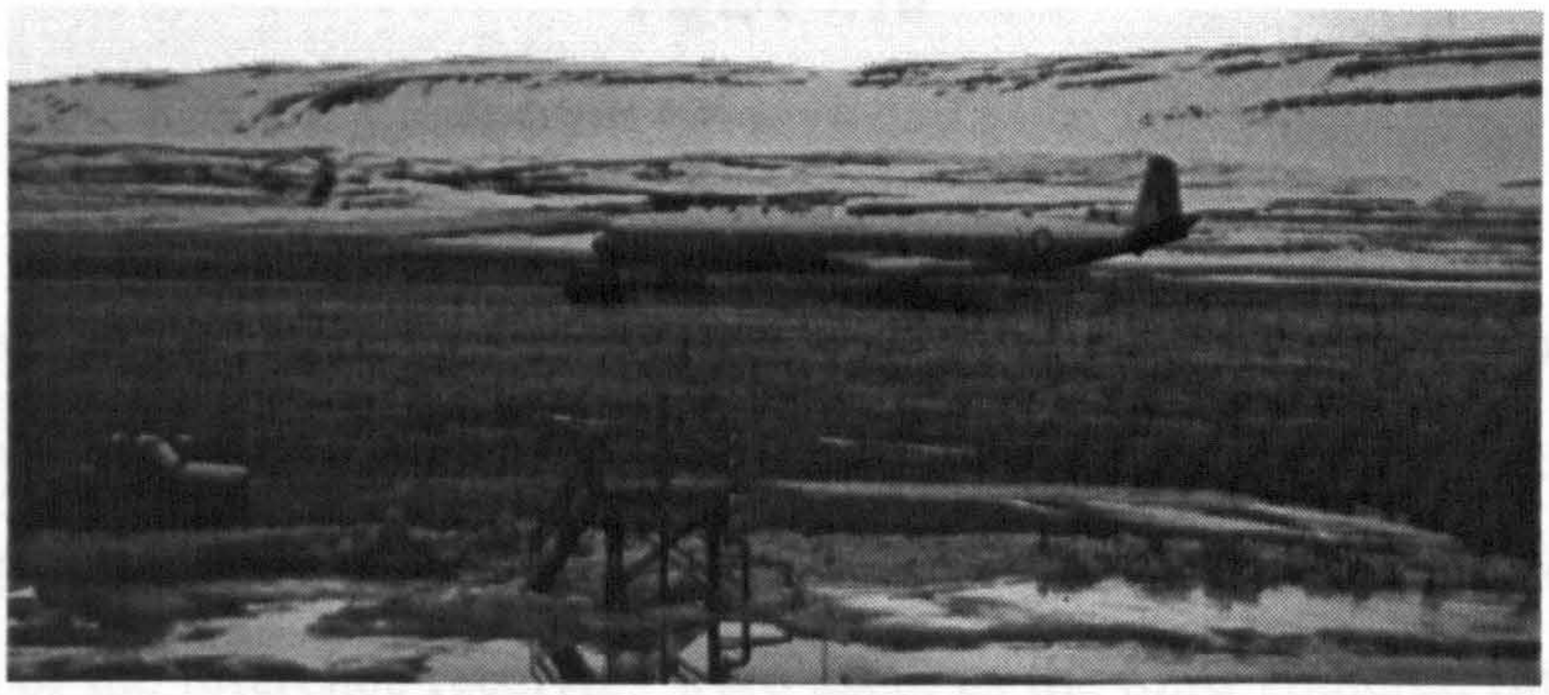

Figure 7.9

The Comet Plane.

During the flight from Greenland to the pole and back to Greenland, three reference receivers were located at the airforce base station at Thule. This flight was analysed closely by the author, and processed in an OTF manner using all the data possible.

The following section details the results obtained for the flight Thule - Pole - Thule. During the flight, the author had set up three reference stations at Thule, which had been coordinated to the IGS station at Thule using 8 hours of static

7.3.1 Cycle Slip Analysis

The data was analysed using the software and techniques detailed in Chapter 6. The reference receivers were found to be clean of cycle slips, and the data from the plane was found to have very few cycle slips. Cycle slips were not, therefore, seen as being a problem for this data. The cycle slip detection technique, however, did manage to satisfy the author that cycle slips were not a problem.

The flight itself was over a distance of 1,500 km. The whole data was, processed, showing that NOTF could in fact be used for such long distances. The resulting accuracy, however, could not be established as there was no other technique available to the author to compare the results with. Figure 7.11 illustrates a view from the plane during the flight over the North Pole.

Figure 7.11

A View of the North Pole.

7.3.2 Positioning Through OTF GPS

The data gathered was processed using the IESSG's NOTF processing package [HANSEN, 1996]. The package allows the use of Multiple Reference Stations (MRS), helping with the search and also allowing longer range searches to be performed. NOTF will allow the user to position using DGPS, Wide Lane Carrier Phase positioning, L1 and L2 positioning as well as narrow lane positioning. The author used the package in a MRS manner, in firstly a 'real time' type manner. The 'real time' processing was carried out by allowing the program to run through the data once, as if it were carried out in real time.

Figure 7.12 illustrates the WGS84 Cartesian X and Y components for the resulting L1 position. X and Y were used as these are the main plan components and Z the height at such a high latitude.

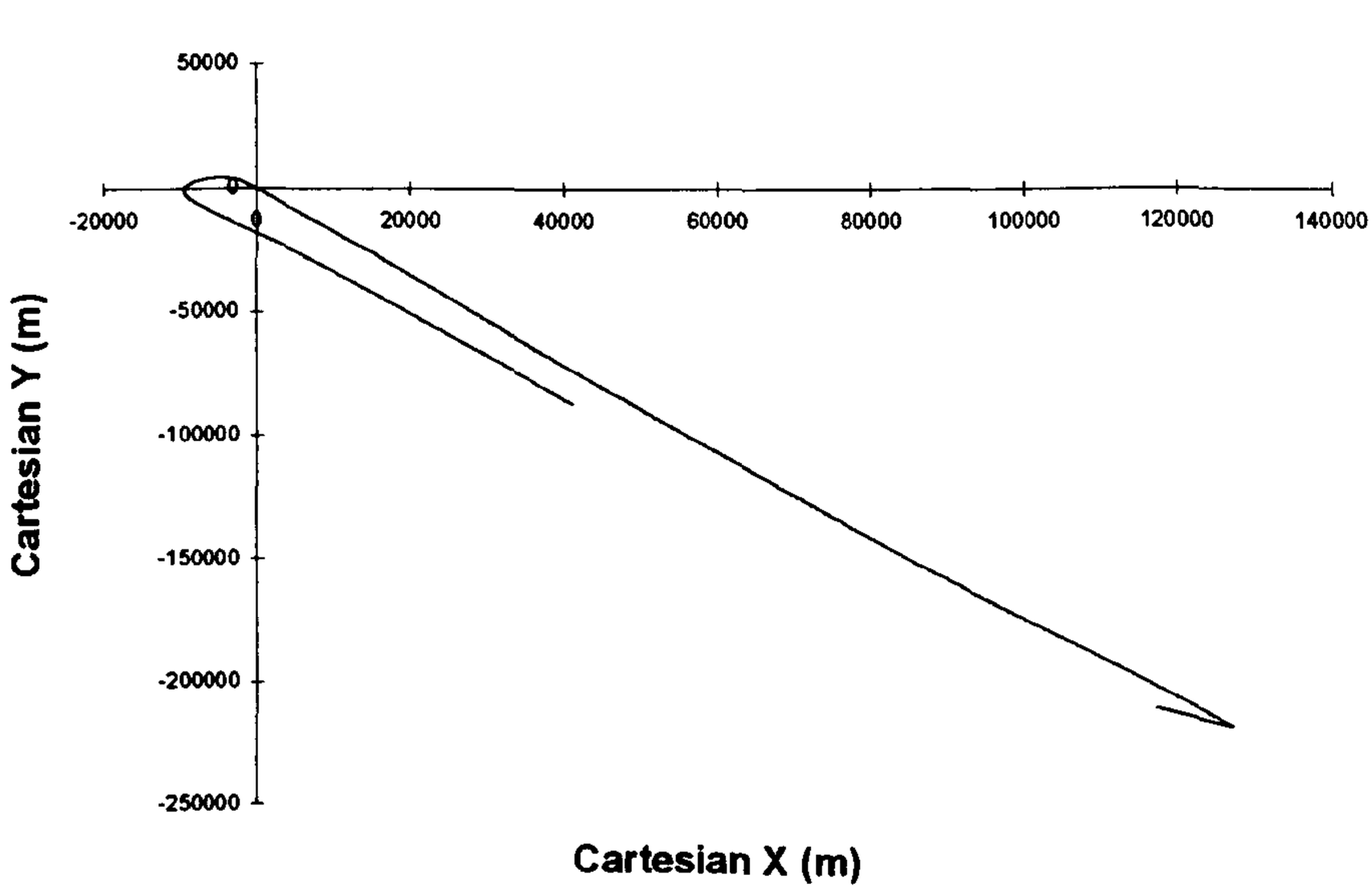

Figure 7.12

The Resulting L1 Integer Fixed Position.

Figure 7.13 shows the resulting L1 integer fixed position at the pole, showing that the antenna passed within metres of the WGS84 north pole.

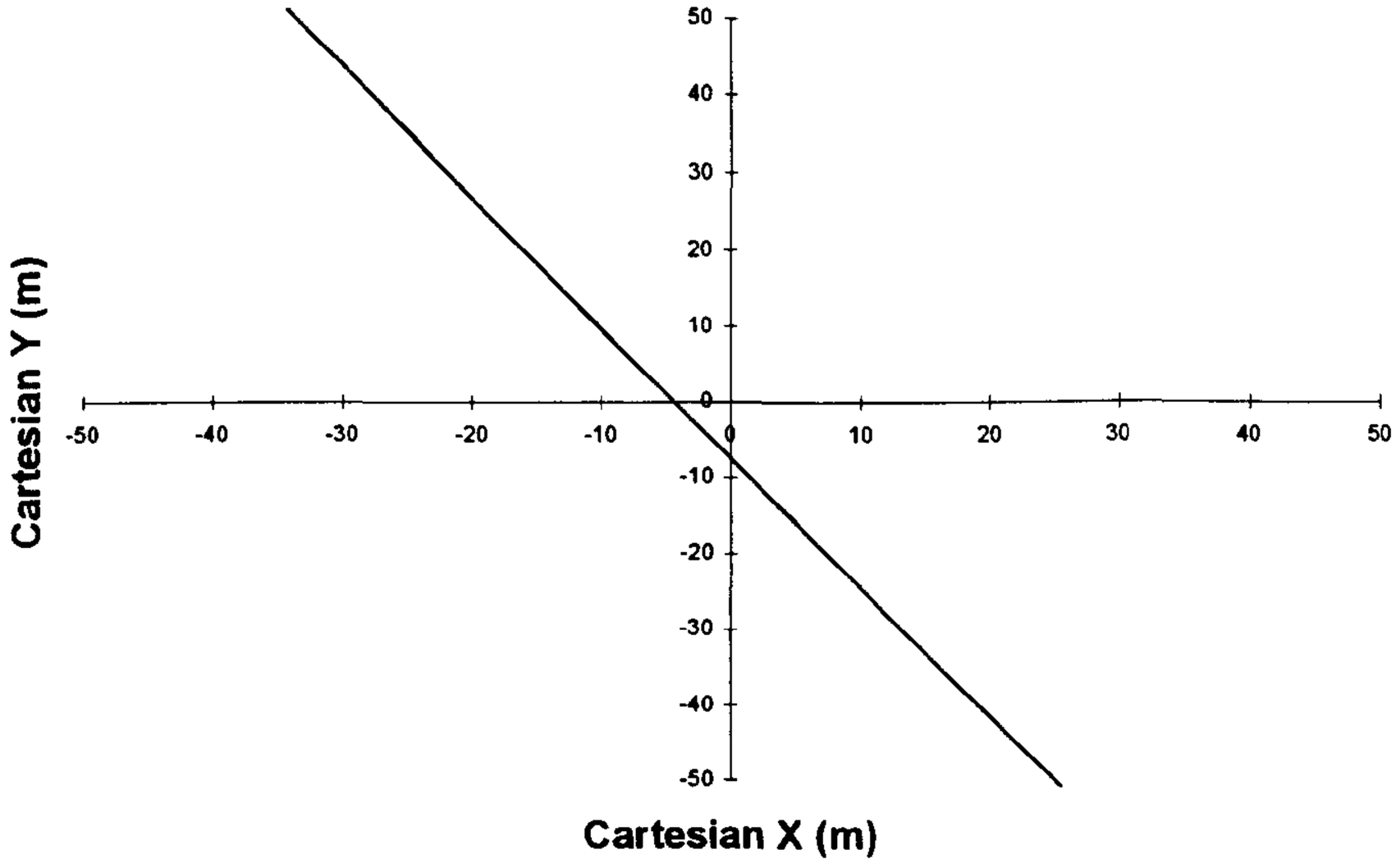

Figure 7.13

The L1 Integer Fixed Solution at the North Pole.

7.4 Conclusions and Recommendations

The results for the 134 km trial have shown that the MRS technique can be used over long ranges to fix the integer ambiguities quickly and reliably, resulting in coordinates with a precision of 12 cm.

The resulting L1 solution, however, is affected by the ionosphere and troposphere, and these need to be modelled into NOTF.

The polar flight showed that NOTF could be used over long distances, but no means of comparison was available. Future trials should include more than one roving GPS receiver on the plane, which could be positioned, and the resulting vector between them analysed.

The real time aspect of such a system needs further investigation. Current telemetry links available are low powered UHF radios, and have a very short range of about 10 km. Alternative links should be looked at, which could include cellular telephones, which could increase the range. Other alternatives include satellite communications for the telemetry links.

7.5 References

ASHKENAZI, V., DODSON, A.H., HANSEN, P., ROBERTS, G.W., 1996, A new cycle slip recovery technique and its use for long range OTF measurements. Proc. Fifth International Conference on Differential Satellite Navigation Systems (DSNS'96), St.Petersburg, Russia.

BEAMSON, G.A., 1995, *Precise Height Determination of Tide Gauges Using GPS.* PhD Thesis, University of Nottingham.

HANSEN, P., 1994, *Real Time GPS Carrier Phase Navigation,* Proc. Third International Conference on Differential Satellite Navigation Systems (DSNS 94), London, UK.

WALSH., D.M.A., 1994, *Kinematic GPS Ambiguity Resolution,* PhD Thesis, University of Nottingham.

Chapter 8

Real Time OTF System Description

8.1 Introduction

Real Time OTF ambiguity resolution and subsequent centimetric positioning is the ultimate GPS positioning technique. Real time OTF allows near instantaneous positioning without the need for post processing, or the requirement to remain stationary for initialisation. The real time capability also allows the user to quality control the survey, as it is possible to determine real time whether the integer ambiguities have been resolved and if a cycle slip or loss of lock has been experienced.

The real time system, as used by the author, consists of two GPS receivers and antennas, which receive GPS satellite data in a similar manner to post processed GPS. The data, however, is transmitted from one receiver to the other through the use of a telemetry link, where the data from both receivers is processed real time, thus allowing the user to check whether OTF initialisation has successfully taken place. This real time check becomes a quality control for the user. In contrast, where GPS data is only post processed, the user does not have this real time information, and may have to carry out the survey again if OTF

initialisation fails, or if a cycle slip or loss of lock occurs at a vital time during the survey.

The real time aspect of OTF GPS allows the position to be used in many more applications which require the near instantaneous nature of the system. Such applications include monitoring structures or the monitoring and control of a construction plant.

Monitoring structures using real time OTF GPS could allow the user to monitor and detect whether the structure was failing or moving in a dangerous nature. For example, the author has used OTF GPS to monitor the movement of the Humber Bridge. The results are detailed in Chapter 9 and indicate that wind and traffic loading did in fact cause the bridge to move. Such a system could be used 24 hours a day, allowing future bridge designs to be assessed, and in addition allow the monitoring of the bridge for dangerous movements.

Another application is the use of real time OTF GPS for construction plant control. For example, GPS on a bulldozer could be used to position the machine and it's blade, allowing precise and quick laying of aggregate. Such experiments have been carried out by the author and are detailed in Chapter 9.

Many more applications are possible, some of which are currently in use. One such application presently being used by Stena Sealink is to position their HSS 1500 Catamaran ferry during docking. The ship is a high speed ferry catamaran, 126 metres long and 40 metres wide. It is capable of carrying 1,500 passengers, and has space for up to 375 cars, with a service speed of 40 knots. The ship will use DGPS which is claimed to have an accuracy of ± 10 m for general navigation [STENA LINE, 1996]. During docking, however, "....*a more finely-tuned differential GPS network is used, and it can calculate the ferry's position accurately to within a distance of as little as one metre.*" [STENA LINE, 1996]. The use of real time OTF GPS has accelerated the

docking procedure itself, the ferry now having a fast turn around at the port of 30 minutes. Figure 8.1 illustrates the HSS in the process of docking at the port of Holyhead.

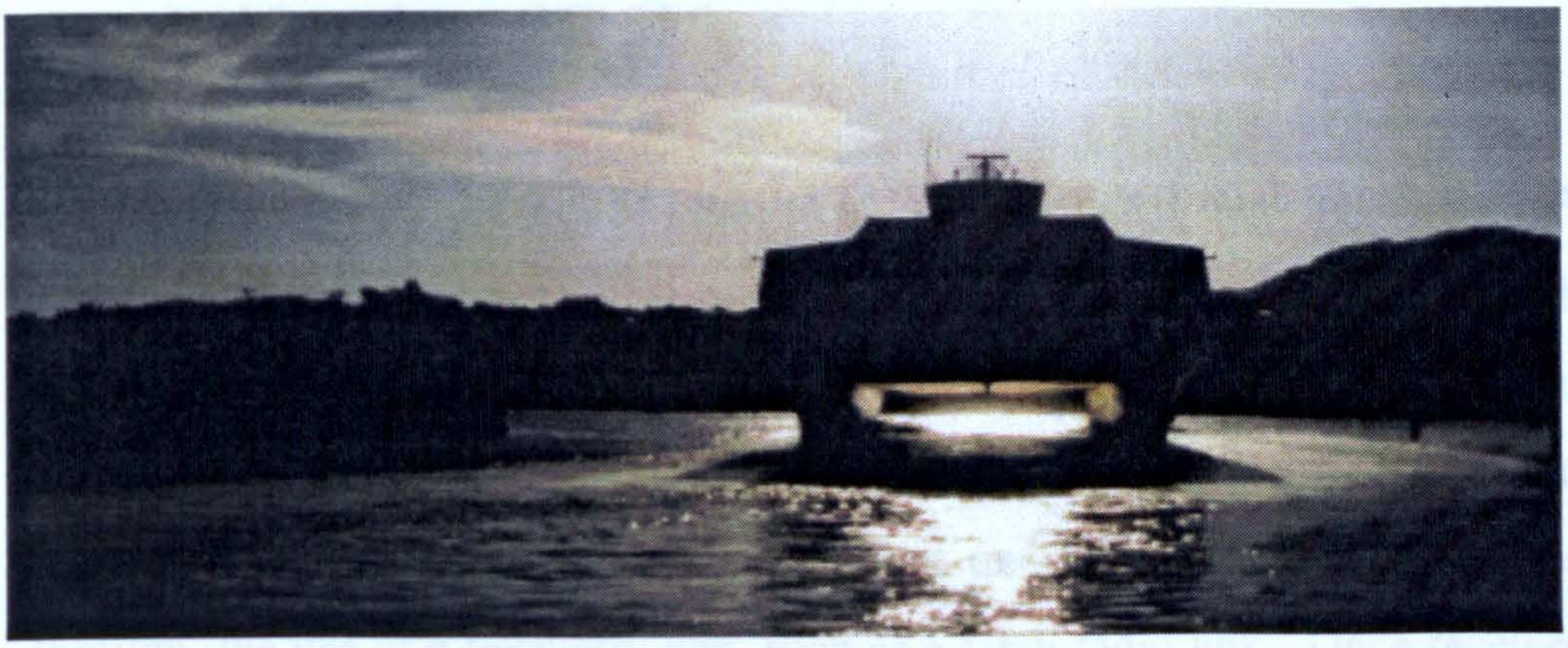

Figure 8.1

The Stena Line HSS 1500 Catamaran docking at Holyhead. The use of real time OTF GPS allows this procedure to be accelerated.

Once real time OTF is acknowledged as being reliable and trusted, its applications are extensive. This chapter will describe the system used by the author during tests that have been carried out as part of this research, details of which can be found in Chapters 9 and 10. In addition other systems which are currently available will be discussed. Results obtained by the author enabling the accuracy and reliability of the system to be determined will also be presented.

8.2 Real Time OTF GPS Hardware

Real time OTF GPS hardware consists of at least two GPS receivers and antennas which track GPS pseudorange and carrier phase data. The commercial GPS manufacturers allow their conventional post processed receivers to output the necessary data for real time OTF GPS positioning. In

addition to the GPS receivers and antennas, the OTF GPS system consists of some form of telemetry link to transmit all the GPS data from one receiver to the other. This is a similar idea to DGPS. However, DGPS only transmits corrections to the pseudoranges in contrast to all the GPS observables being transmitted for real time OTF GPS.

The system used by the author consists of Ashtech Z-XII dual frequency GPS receivers. These receivers will output a DBEN file [ASHTECH (i), 1994]. The DBEN file is a binary file which contains all the GPS receivers observables and satellite ephemeris information, and is output from a port at pre-set epoch intervals. The data is then transferred from one GPS receiver to the other through the use of a telemetry link, such as a UHF radio link. Once received, the data is processed using OTF algorithms, allowing real time integer ambiguity resolution and positioning.

8.2.1 Telemetry Links

The telemetry links used by the author are Racal Deltalink II UHF radio links. These can either be receiver/transmitter units or transceivers, which can be set up as either receivers or transmitters. Figure 8.2 illustrates the telemetry units used as well as the telemetry antennas, along side an Ashtech Z-XII GPS receiver. The units operate within the 400 - 500 MHz frequency band and have seven available channels. The power output of the units is 500 mW, which is the maximum permitted within the UK without the need for a broadcasting licence. Further specifications may be found in the units' user manual [RACAL, 1995].

Figure 8.2

The Real Time System's Telemetry Links. Shown, from left to right, are the receiving telemetry link antenna, the receiving datalink, the GPS receiver, the transmitting telemetry link antenna, the transmitting datalink and a 12 V power supply for the transmitting datalink.

The data may be transmitted from the reference receiver to one or more roving receivers, where processing and OTF positioning is carried out, and where the real time position is displayed. This is ideal for applications such as setting out, docking a ship, landing a plane or real time plant control. The GPS data may, however, be transmitted from the roving receiver to the reference receiver where subsequent OTF processing is carried out, and where the resulting position is available. This method could be used for remotely monitoring the OTF position of the roving GPS receiver. Applications for such a system include the monitoring of large structures such as stockpiles, bridges, tall buildings and reservoirs. The user would be able to monitor the real time position of the structure, or even multiple locations on the structure. For

example, a number of positions on a long bridge could be monitored at the reference station, which could be located in the users office. Other applications could include using remotely operated vehicles in dangerous locations such as military mine or bomb disposal vehicles.

Ideally, the real time OTF coordinate would be transformed a more user friendly format for the user to interpret. This could be a graphical display, or the coordinates could be transformed from WGS84 (X, Y, Z or ϕ, λ, h) into a local system.

8.2.2 Real Time Processing Using a Laptop PC

Once the data has been transmitted, processing may be carried out in one of two ways. Firstly, the OTF initialisation and positioning may be carried out on a laptop PC. This system has been used by the author on numerous occasions, and is illustrated in figure 8.3. Here, the author is seen using the system during a field trip in Llangollen, North Wales. The GPS antenna is located on top of the bipole and is centred and levelled using a pond spirit level bubble. The Ashtech Z-XII GPS receiver is located inside the orange ruck-sack. The data collected by this roving receiver is output from the receiver through an RS232 cable to a COM port at the rear of the laptop. The reference receiver's data is transmitted from the reference station and received by the telemetry link antenna seen at the top of the ruck-sack. This data is sent via the Deltalink receiving unit to a second COM port at the rear of the laptop.

A real time version of Ashtech's PNAV processing package was used for OTF initialisation and positioning. In addition, the raw GPS data may be gathered at each GPS receiver for post processing purposes. However, it is also possible to switch off this option as raw 0.5 second epoch data can fill a substantial portion of the GPS receivers memory. The real time position and other parameters, such as position quality and ambiguity search parameters are all displayed on

the laptop's screen. This data is also recorded into a data file on the laptop, allowing the user to analyse the coordinates after the survey. This technique has been utilised by the author, where real time data was gathered and analysed using Microsoft Excel after the survey. An example of the raw OTF coordinate datafile is shown in Appendix D.

Figure 8.3

The Real Time OTF system used by the Author. The GPS antenna is situated upon the bipole. The GPS receiver is housed inside the rucksack, as is the telemetry link unit. The telemetry link antenna is situated on top of the rucksack, where it receives the GPS data from the reference GPS receiver. The data from the two GPS receivers is processed within the laptop computer in a real time manner.

The laptop computer used by the author is a Pentium 90 MHz machine, with a 500 Mb hard disk, operating with 8 Mb of RAM.

Figure 8.4 illustrates the real time system as used with a laptop computer to process the OTF position, showing the components used.

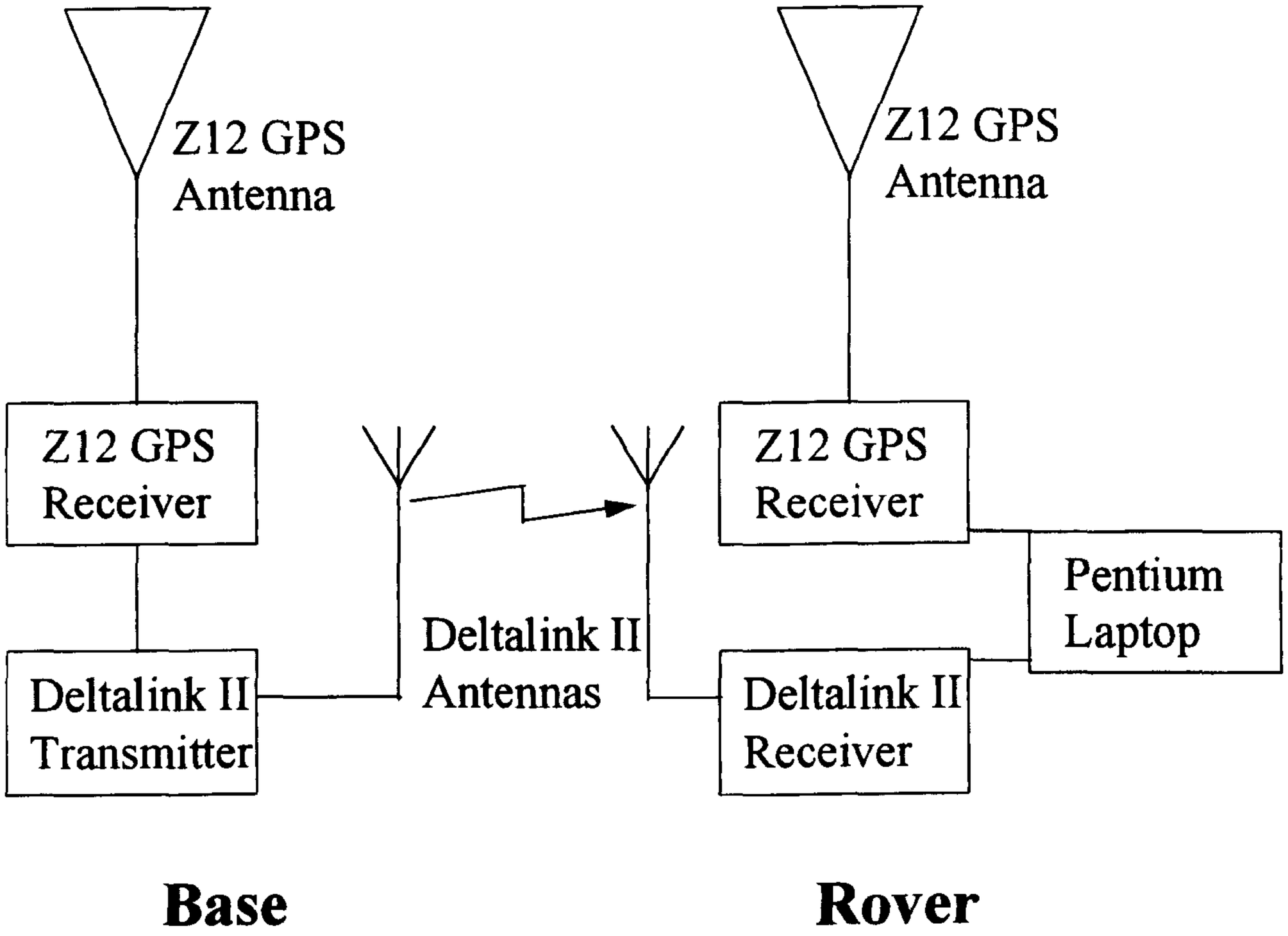

Figure 8.4

The Real Time System Using a Laptop Computer for Processing and OTF Positioning.

Figure 8.5 shows the main processing screen within the PNAV package. The screen illustrates, from top to bottom, the time and date of processing, as well as the PDOP. The base (or reference) receiver's coordinates are next displayed, all in the pink section. The next line, in red, illustrates the rover GPS receiver's coordinates, which are updated every epoch. The following line in pale blue, illustrates the vectors between the reference and rover receivers and their

corresponding RMS values in grey. The remainder of the screen illustrates the processing status. The satellites that are in view and used are displayed, with the reference satellite illustrated in red. The corresponding CHI square data and residuals are also illustrated. On the right of this is an indication of whether the integer ambiguities have been resolved. The final blue row illustrates the L1 and L2 double difference residuals. The bottom area illustrates the activities taking place, such as cycle slip fixing.

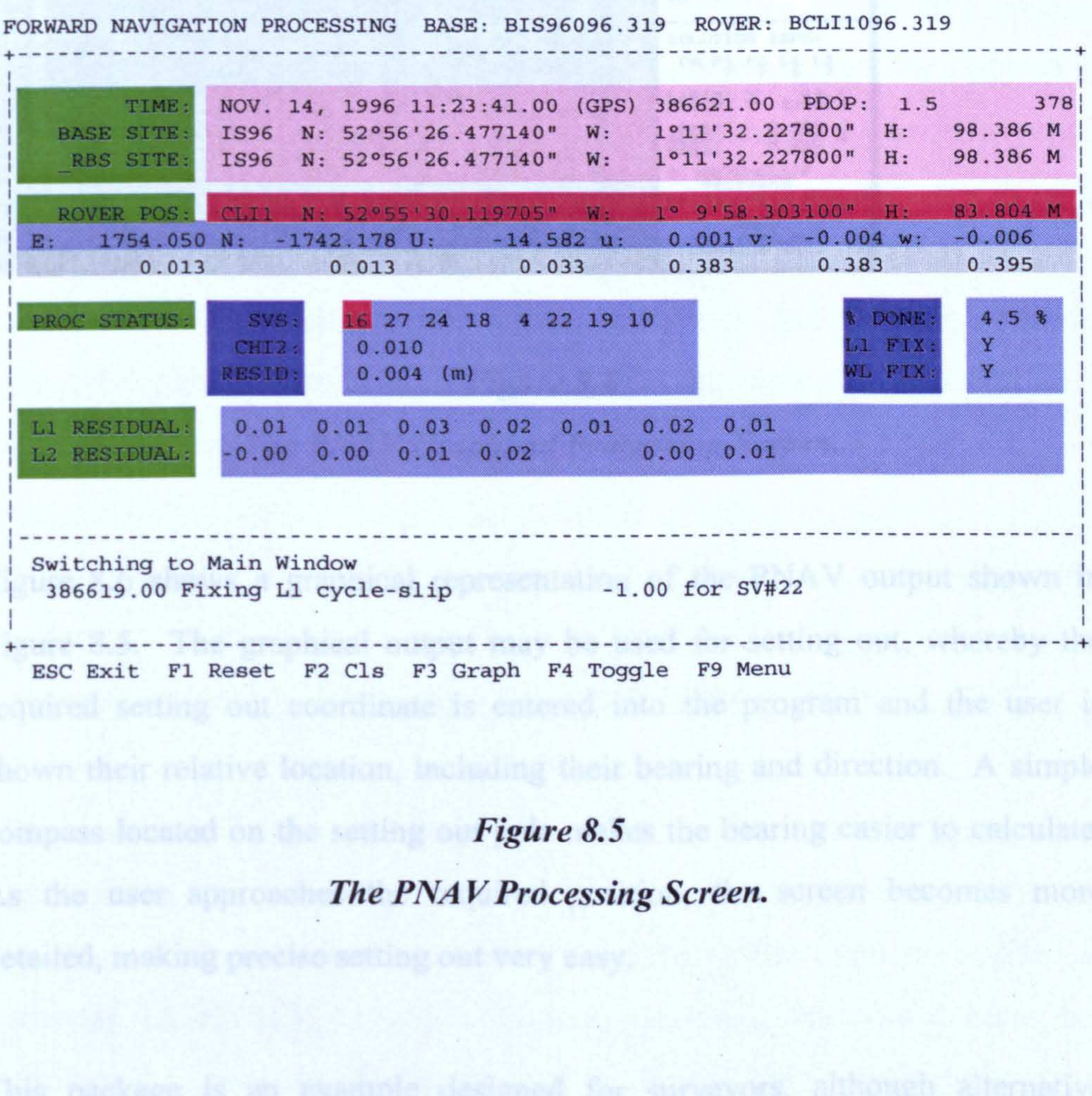

Figure 8.5

The PNAV Processing Screen.

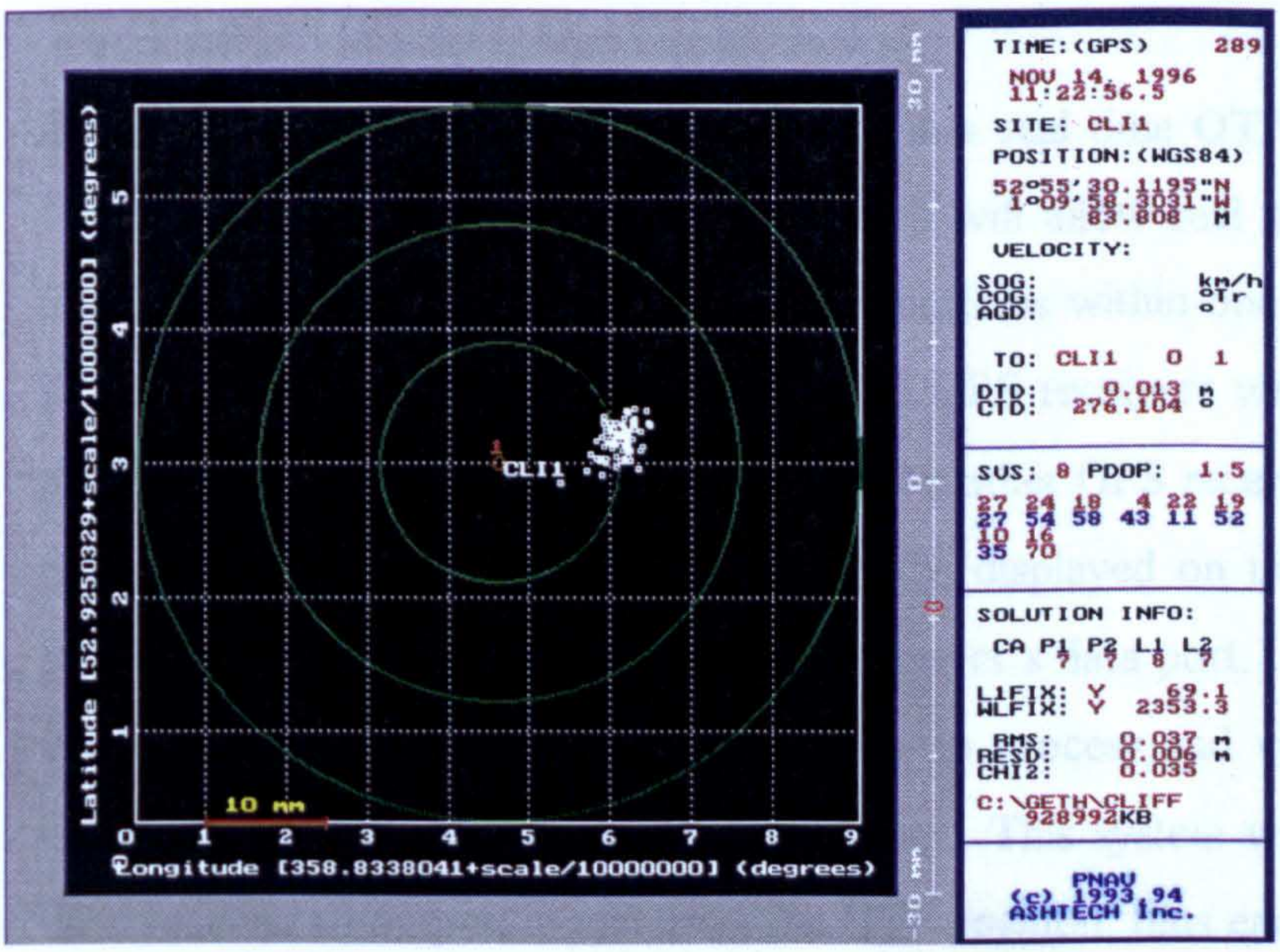

Figure 8.6

The PNAV Graphical Processing Screen.

Figure 8.6 shows a graphical representation of the PNAV output shown in Figure 8.5. The graphical output may be used for setting out, whereby the required setting out coordinate is entered into the program and the user is shown their relative location, including their bearing and direction. A simple compass located on the setting out pole makes the bearing easier to calculate. As the user approaches the required position, the screen becomes more detailed, making precise setting out very easy.

This package is an example designed for surveyors, although alternative packages are available, which will allow the user to set out in a conventional manner, giving bearings and directions, as well as coordinates [TRIMBLE, 1997].

8.2.3 Real Time Processing Within the GPS Receiver

As well as being able to process the data in a real time OTF manner using a laptop PC, systems are also available which will allow real time OTF integer ambiguity resolution and positioning computations within one of the two GPS receivers. This means that one of the two GPS receivers will track the GPS data as well as record it, and also process the other GPS receivers data with its own, in real time. An OTF solution is then displayed on the GPS receivers screen and may also be output from the receiver's data port. The Ashtech RZ system works in this way, it being possible to process and view the resulting OTF position at one of either GPS receivers. This system will also allow the GPS receiver to output, in real time, the OTF position, thus enabling the user to integrate the OTF position within a real time system. For example, integrating the OTF position into a bulldozer, (§10) could allow the bulldozer to be controlled automatically.

It is also possible to utilise the real time OTF position into a real time computer program. Such programs may be run inside small rugged computers, for example, for real time setting out [TRIMBLE, 1996], [TRIMBLE, 1997].

The time taken for the GPS data to be tracked by the receiver, transmitted and received by the telemetry links, travel through the telemetry links, and subsequently be processed produces a delay which can be in the region of 2 seconds [ASHTECH, 1995]. Various processing techniques have been developed to overcome the latency factor. Firstly, the data can be processed allowing a 2 second latency in viewing the results. This is the more precise method, as the true GPS data is processed from both receivers in a real differenced manner. Some real time applications do not require true real time data, as in the case of most survey applications, and a latency of 2 seconds would not be a problem.

The second technique is to use prediction models and kalman filters to predict some of the data for real time output. The prediction is usually carried out for the reference receiver's observables, as these observables should change with a definite trend over time due to the receiver remaining static. Whereas, the roving receivers data may not contain a definite trend due to sudden changes in its velocity. Furthermore, the effects of SA, however, are not correctly accounted for in this technique.

The data rate is an important factor for the successful use of real time OTF GPS. If re-initialisation of the integer ambiguities is required, then this must take place over as short a time period as possible. Many of the new GPS receivers allow the user to carry out real time OTF at a rate of 5 Hz and even 10 Hz [ACKROYD, 1996], [TRIMBLE, 1997]. This not only allows positioning at a higher rate, which is ideal for fast moving vehicles, but also enables OTF integer ambiguity resolution over a shorter period.

Figure 8.7 illustrates the real time system where the processing is carried out within one of the GPS receivers, eliminating the need for a separate computer. This type of system is likely to be quicker in processing as there are no handshakes or buffers to be set up through communicating to an external processor.

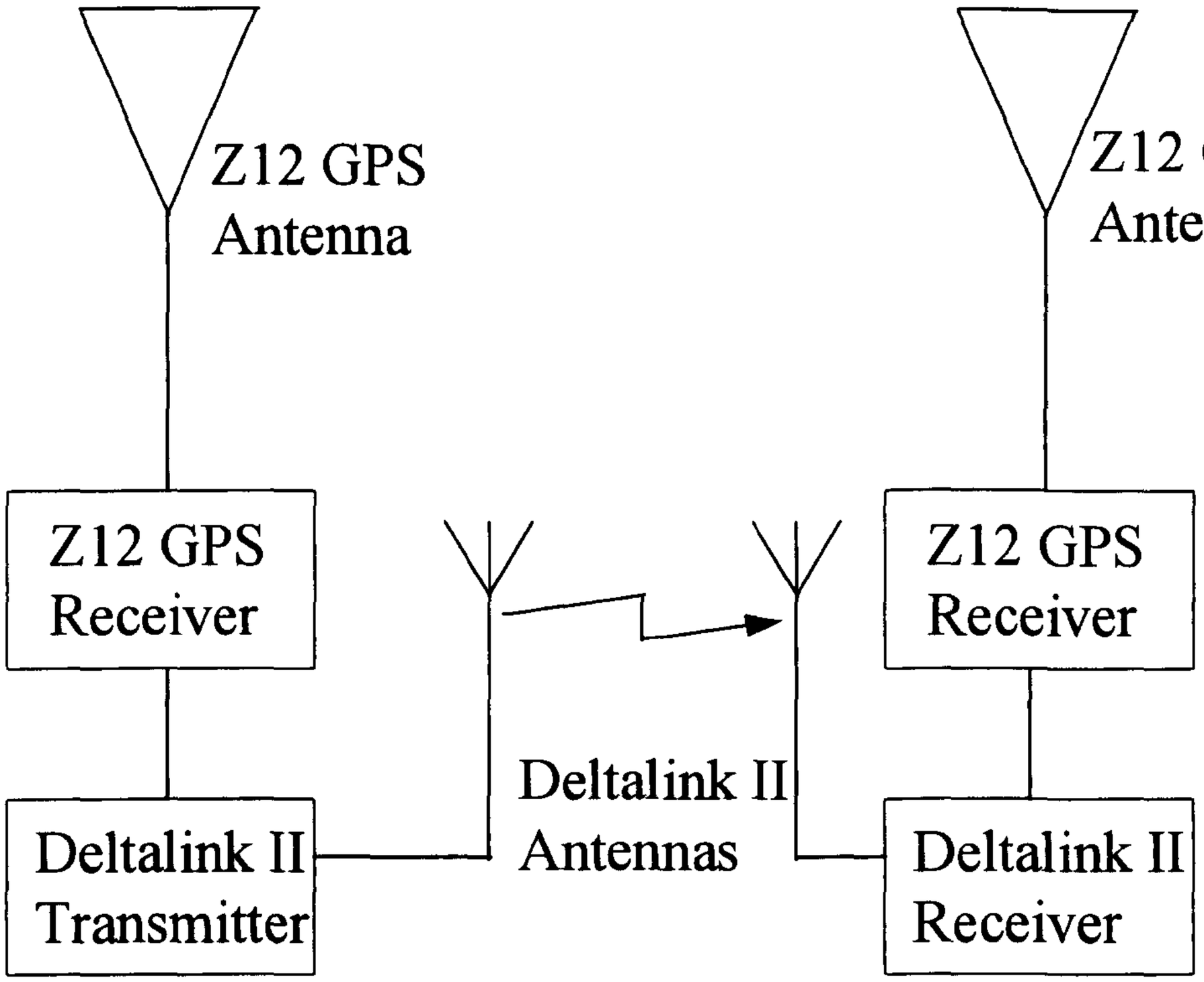

Figure 8.7

A Real Time OTF System, Using one of the GPS Receivers to Process the Data.

8.3 Alternative Telemetry Links

The telemetry links used by the author are 0.5 Watt, UHF telemetry links, which are typical low powered units. The range specifications for these units operating at the required baud rate (9600) for real time OTF GPS is in the region of ~20 km [RACAL, 1995]. This range, however, dramatically decreases when line of sight is not available. The cable which connects the telemetry link antenna to the radio unit can also cause loss in signal strength, all of which result in a weak signal or no signal at all reaching the destination.

There are various alternatives to using a 0.5 Watt UHF radio link. These include the use of VHF frequencies, the use of relay stations and even the use of a cellular telephone system or the Internet. Longer ranges and the elimination of the need for line of sight may be possible with such links, resulting in real time OTF GPS being a more useful positioning tool.

The use of a relay station has been investigated by the author as a method of overcoming the problem of having to maintain line of sight between the two GPS receivers. This increases the possible baseline length to approximately twice the distance of that without a relay station. A relay station consists of a pair of receiver/transmitter telemetry links which receive the transmitted GPS data from the reference GPS receiver and re-transmit it to the other GPS receiver. Figure 8.8 illustrates the idea behind the relay station, showing the telemetry link signal travelling via the relay station. The frequency on which the data is transmitted from the relay station, should not be the same as that received by the relay station, in order to reduce the likelihood of interference. If both the reference station and the relay station were to transmit at the same frequency, then the roving receiver may receive data from two sources.

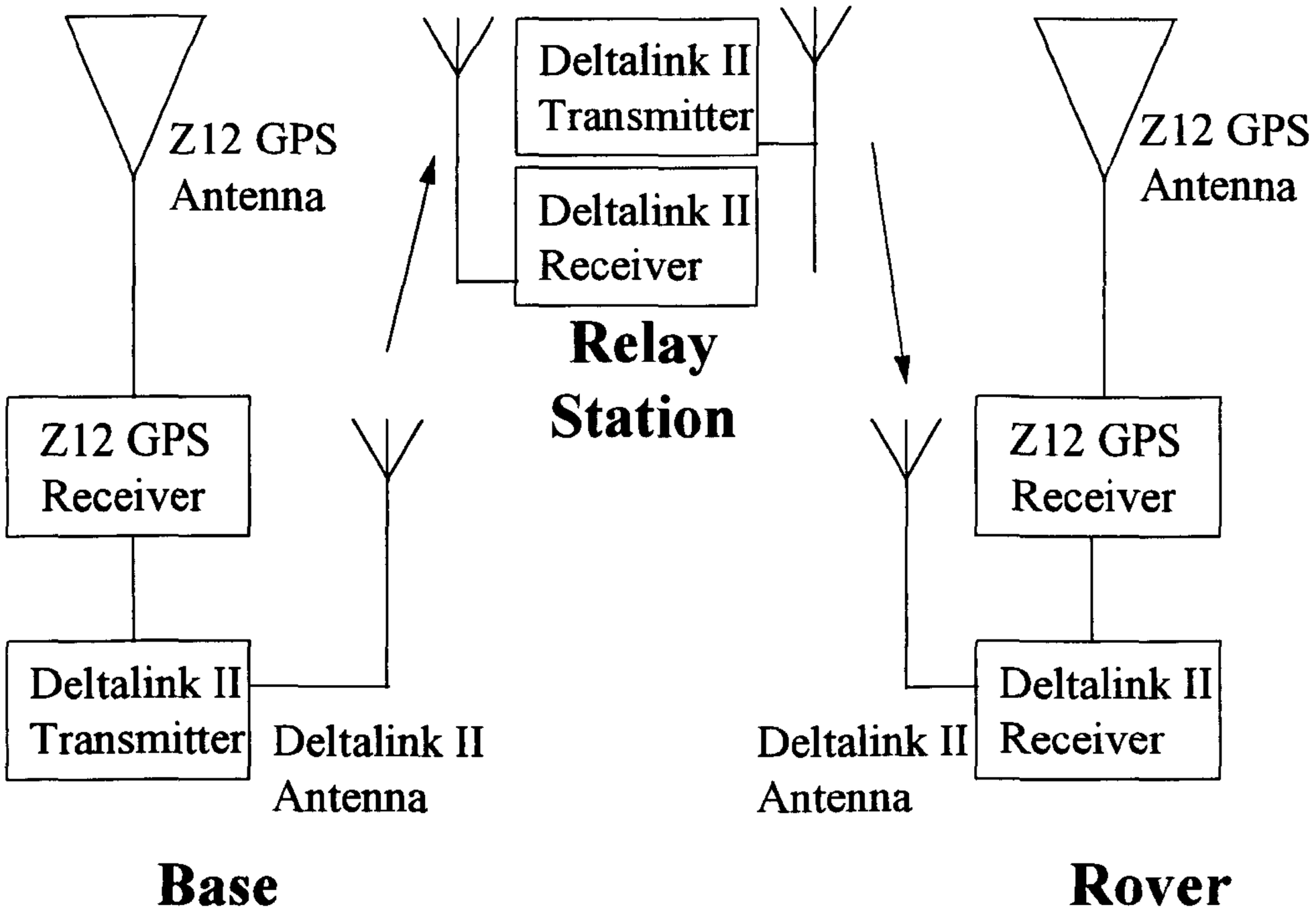

Figure 8.8

A Schematic of the Principles Behind the Relay Station. This Allows the Transmission of Data to be Carried Out Even Without Line of Sight.

An alternative to the UHF telemetry links is the use of cellular telephone system, thus allowing a wider coverage. Line of site would not be a problem with such a system, and may be the solution to making real time long range OTF GPS a reality (§7).

8.4 Resolution of the Real Time System Through the use of a Zero Baseline

The potential accuracy of the real-time OTF technique, over short distances and under low dynamics, has been first determined through a zero baseline test. The zero baseline was established upon the turret on the IESSG building. This consisted of a single Ashtech ground plane GPS antenna with a two way

splitter, allowing the data to be fed into two GPS receivers. The real time processing was carried out using Ashtech's RTPNAV program, within a P-90 laptop PC. There were no true coordinates available for the location of the antenna, thus very coarse coordinates were used for initial processing. One of the two GPS receivers was chosen as the reference, and given the coarse coordinates within the RTPNAV program. The integer ambiguities would not fix; this was thought to be due to the fact that the reference receiver's coordinates were incorrect. This is further investigated in §8.5.

Data was gathered on one of the GPS receivers over a 3 hour period. This data was then processed in an accumulated pseudorange solution using the GAS package. This coordinate was then used for the zero baseline test, even though it was thought to be only accurate to a few metres. The reference receiver's coordinates were fixed to these new values, and the initial unknown (rover) GPS receiver's coordinates were entered as being about 100 m away from the truth.

The second attempt to process the zero baseline in a real time manner was successful, and the integer ambiguities were established within about a minute. Once the integer ambiguities were fixed, it was evident that the baseline length was seen as being only a few millimetres by the RTPNAV program. The telemetry links were not used during this trial, as the GPS receivers were located next to each other. The RTPNAV program outputs a coordinate file, in WGS84 (latitude, longitude and height). The next stage was to transform these into OSGB36 national grid coodrinates and height. In order to make the resulting position easier to visualise. This was achieved through using WinCODA, which is a windows version of the DATUM package [EUROCONTROL, 1993]. Examples of the real time WGS84 Latitude, Longitude and ellipsoidal height file and the OSGB36 National Grid Eastings, Northings and ellipsoidal height files can be found in Appendix D.

Figures 8.9, 8.10 and 8.11 illustrate the Northings, Eastings and ellipsoidal height components of the results. It can be seen that the plan results are precise to ± 2 mm, and the height to ± 3 mm. As expected, the height component is not as precise as that of plan, due to GPS satellite geometry.

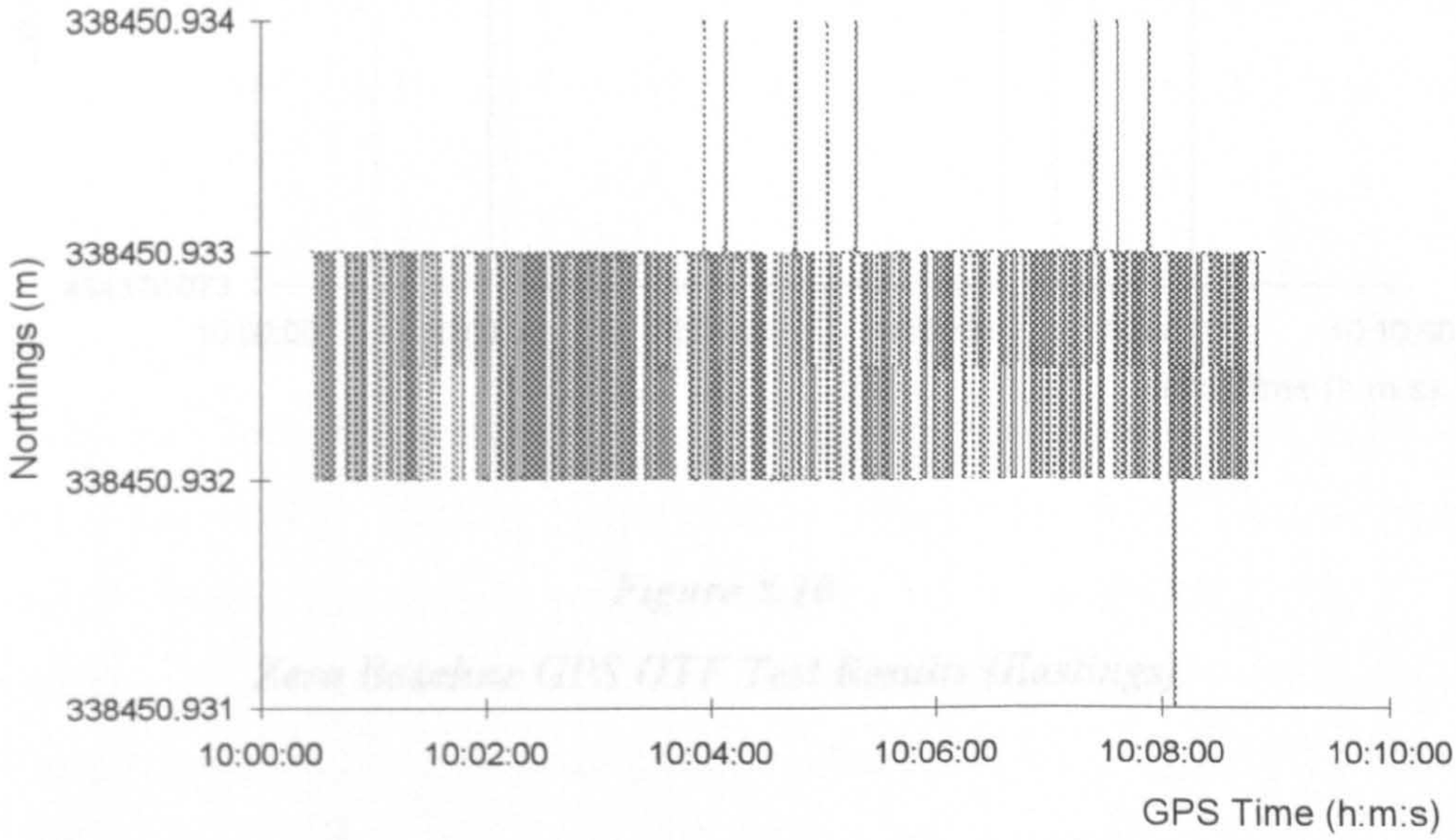

Figure 8.9

Zero Baseline GPS OTF Test Results (Northings).

8.5 Short Baseline Results

Further trials were carried out to establish the expected precision from the real time system. The zero baseline test showed remarkable precision, however, due to the absence of multipath, it was not a true representation of the expected results. To enable a true representation to be established, a further trial was conducted.

This trial consisted of placing a reference GPS receiver over a known coordinate. Two GPS antennas were located at a typical location, this being on top of the IESSG building, approximately 70 metres from the reference receiver. One of the antennas was connected directly to an Ashtech Z-XII GPS receiver, whilst the other was connected to two Ashtech Z-XII GPS receiver through a two way splitter. The two antennas located on top of the IESSG building were situated approximately 2 metres apart. Figure 8.12 illustrates the set-up used.

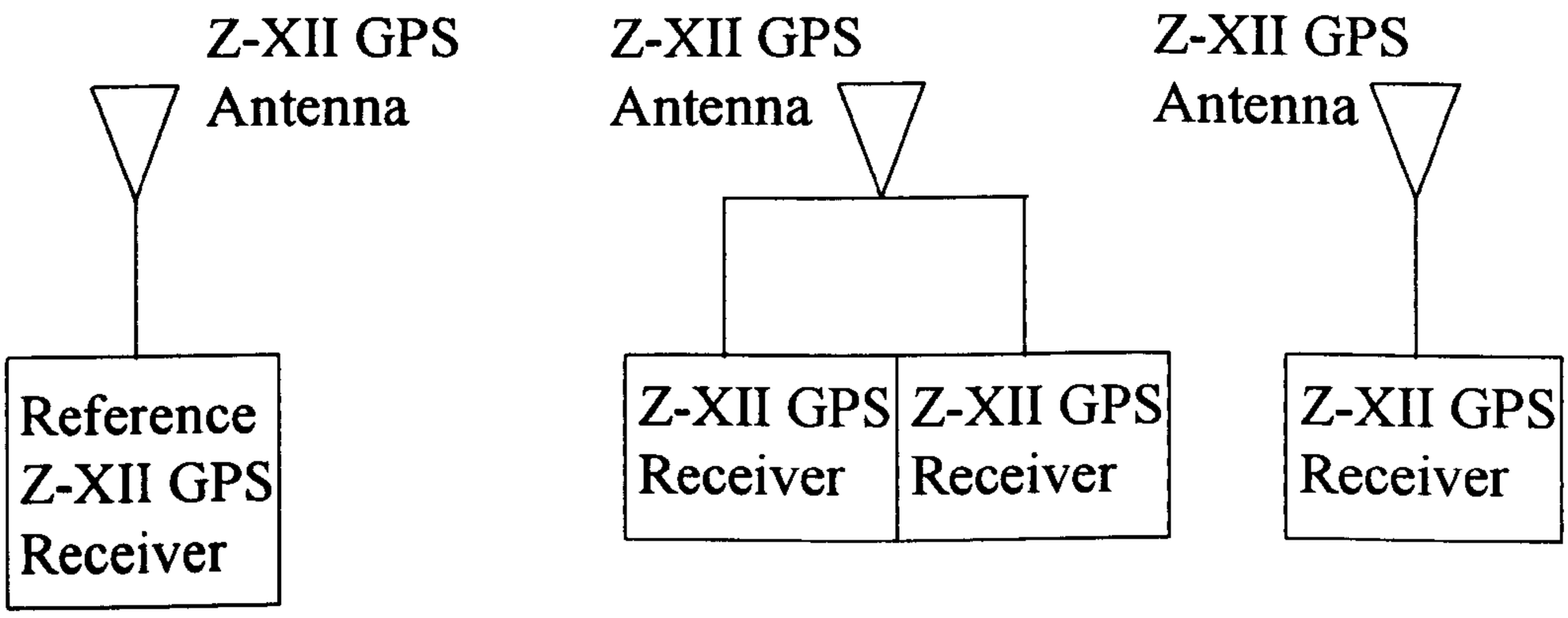

Figure 8.12

The GPS Receivers' Set-up Used for the Short Baseline Trial.

Data was gathered simultaneously at a single second epoch separation at all four GPS receivers, and post processed using PNAV in forward processing,

walking mode, similar to that of real time OTF GPS. The resulting coordinates at each receiver were then analysed, and compared to each other at every epoch. Again, the resulting WGS84 Latitude, Longitude and ellipsoidal height coordinates were transformed into OSGB36 Eastings, Northings and ellipsoidal height using the IESSG's WinCODA package, resulting in coordinates which could be easily understood and analysed in metres rather than degrees, minutes and seconds.

Once processed and transformed, the data for each antenna was entered into a spread sheet, and analysed relative to each other. The vector between each receiver was examined for the data period. Figure 8.13, 8.14 and 8.15 illustrate the Eastings, Northings and height components of one of the GPS receivers. It can be seen from these figures that the resulting integer fixed OTF solution has a precision of ± 3 mm in Eastings, ± 5 mm in Northings, and ± 10 mm in height. The Eastings, Northings and height components of the remaining two GPS receivers can be found in Appendix D. There is, however, a cycle slip evident in the results, at around 10:45:00, where the coordinates jump by around 10 mm in Eastings, 20 mm in Northings and 20 mm in height. This anomaly occurred for all the resulting OTF GPS coordinates, which suggests that the cycle slip occurred either for all three unknown GPS receivers, or just at the reference receiver.

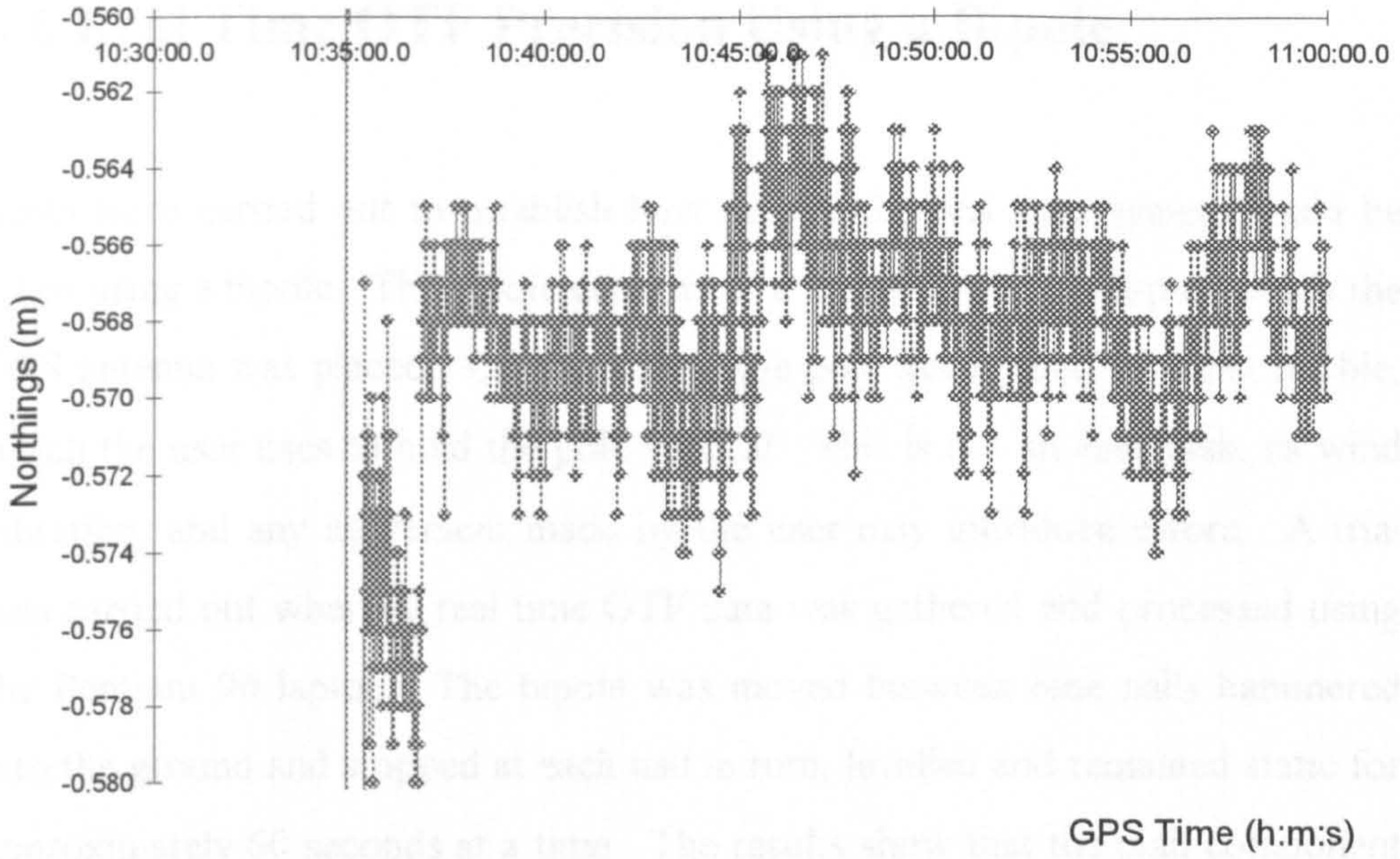

Figure 8.17

The Northings Component of the OTF Vector for the Short Baseline Trial.

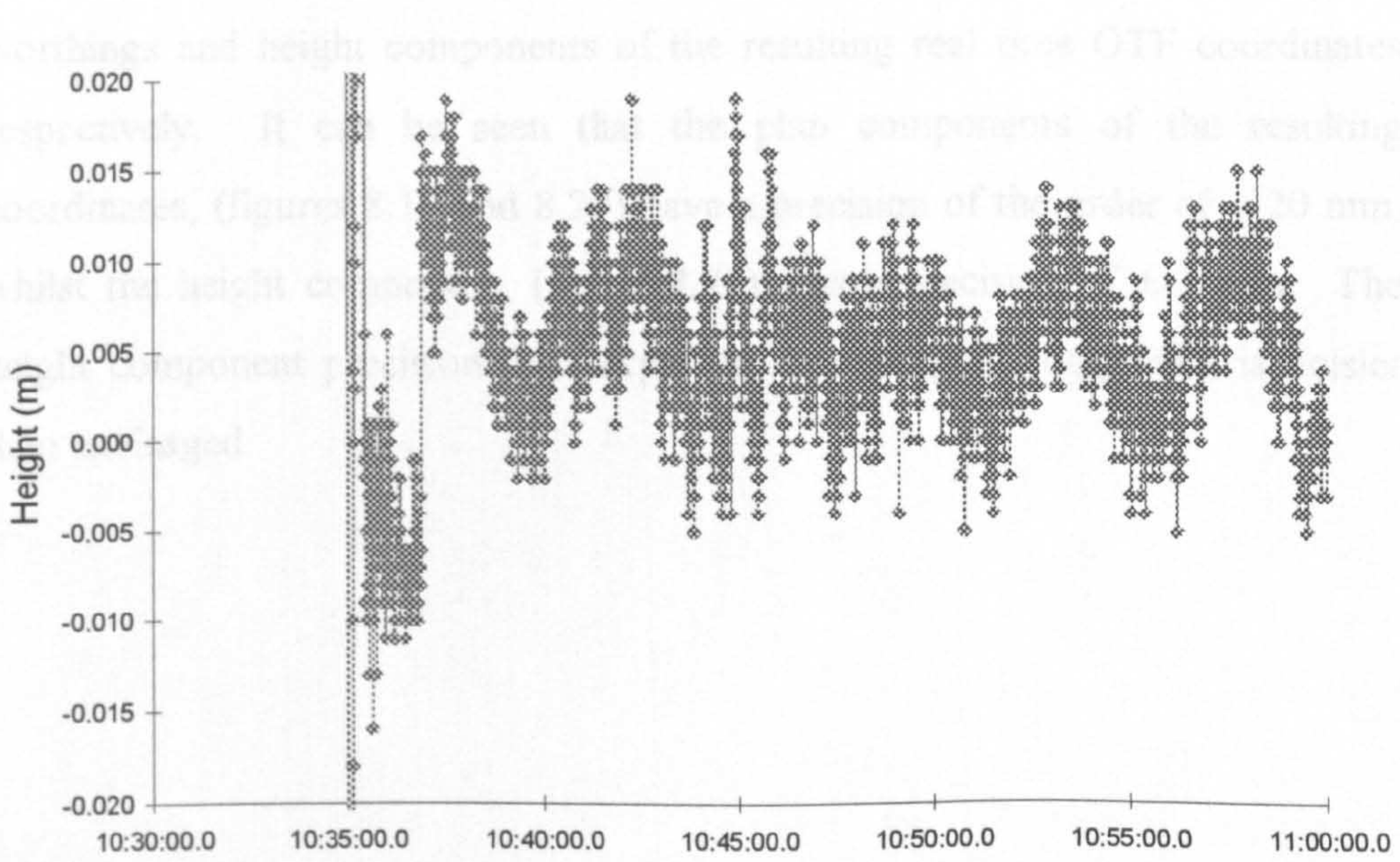

Figure 8.18

The Height Component of the OTF Vector for the Short Baseline Trial.

8.6 Real Time OTF Precision Using a Bipole

Tests were carried out to establish how precise the real time system could be when using a bipole. The bipole consists of a 2 metre pole, on top of which the GPS antenna was placed. On the side of the pole lies a pond levelling bubble, which the user uses to hold the pole vertical. This is not an easy task, as wind vibration, and any movement made by the user may introduce errors. A trial was carried out whereby real time OTF data was gathered and processed using the Pentium 90 laptop. The bipole was moved between nine nails hammered into the ground and stopped at each nail in turn, levelled and remained static for approximately 60 seconds at a time. The results show that the plan component of the resulting integer fixed OTF solution is less precise than that of the height. This is not usually the case, but can be explained since the instability of the bipole is the major error source of this technique. Figures 8.19, 8.20 and 8.21 illustrate the change from one epoch to the next epoch for the Eastings, Northings and height components of the resulting real time OTF coordinates respectively. It can be seen that the plan components of the resulting coordinates, (figures 8.19 and 8.20) have a precision of the order of ± 20 mm, whilst the height component, (figure 8.21), has a precision of ± 7 mm. The height component precision is as expected, but the plan component is noisier than envisaged.

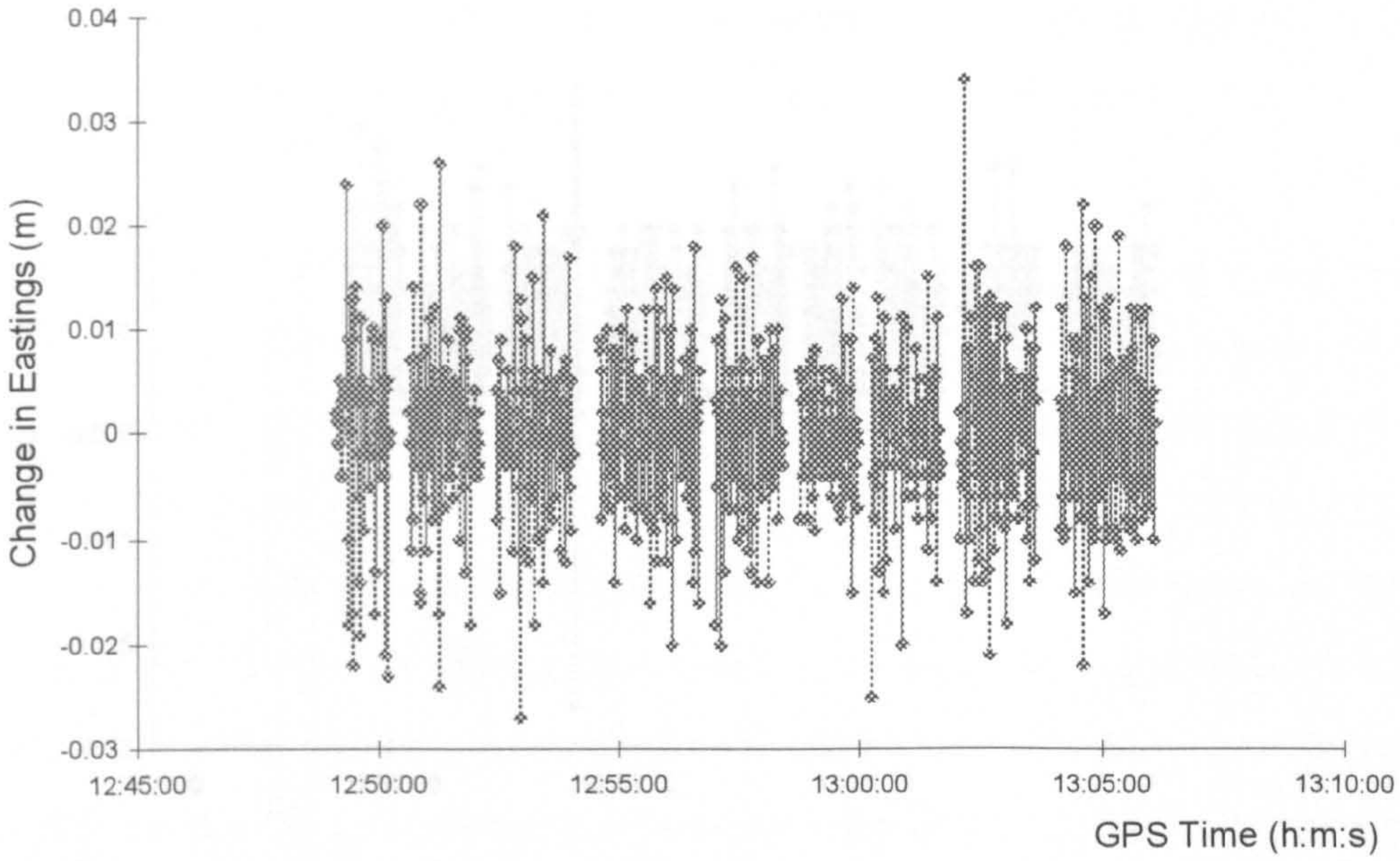

Figure 8.19

The Eastings Component of the OTF Positions for the Bipole Trial.

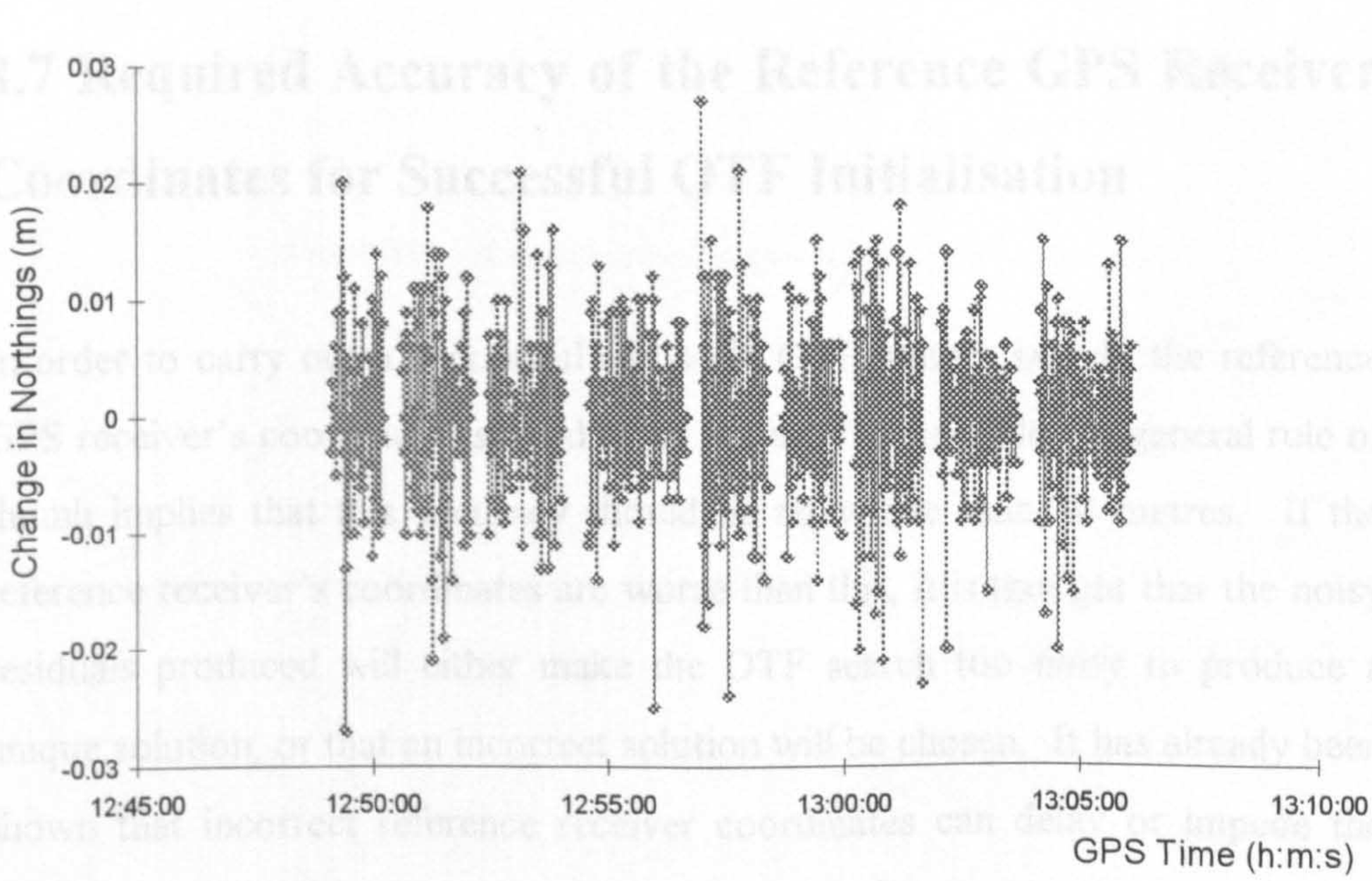

Figure 8.20

The Northings Component of the OTF Positions for the Bipole Trial.

addition whether or not incorrect integer ambiguities could be chosen. The following section details the trial, and some of the results obtained.

Two GPS receivers were set up, approximately 11 km apart. One of which was on a known ETRF89 position on the IESSG building, which is a tie in point to the Nottingham (Z095) EUREF established position [ASHKENAZI *et al*, 1996]. Data was recorded at ½ second epoch intervals, for a period of 45 minutes. This data was then post processed from the known reference receiver, using firstly the true coordinates, and then by varying the coordinates from the truth. The same data set was used with varying reference receiver coordinates so that exactly the same data and parameters were present for each processing run. These were compared to the truth, which was established using static GPS processing. Figure 8.22 illustrates the radial error at every epoch when the correct reference receiver coordinates were used.

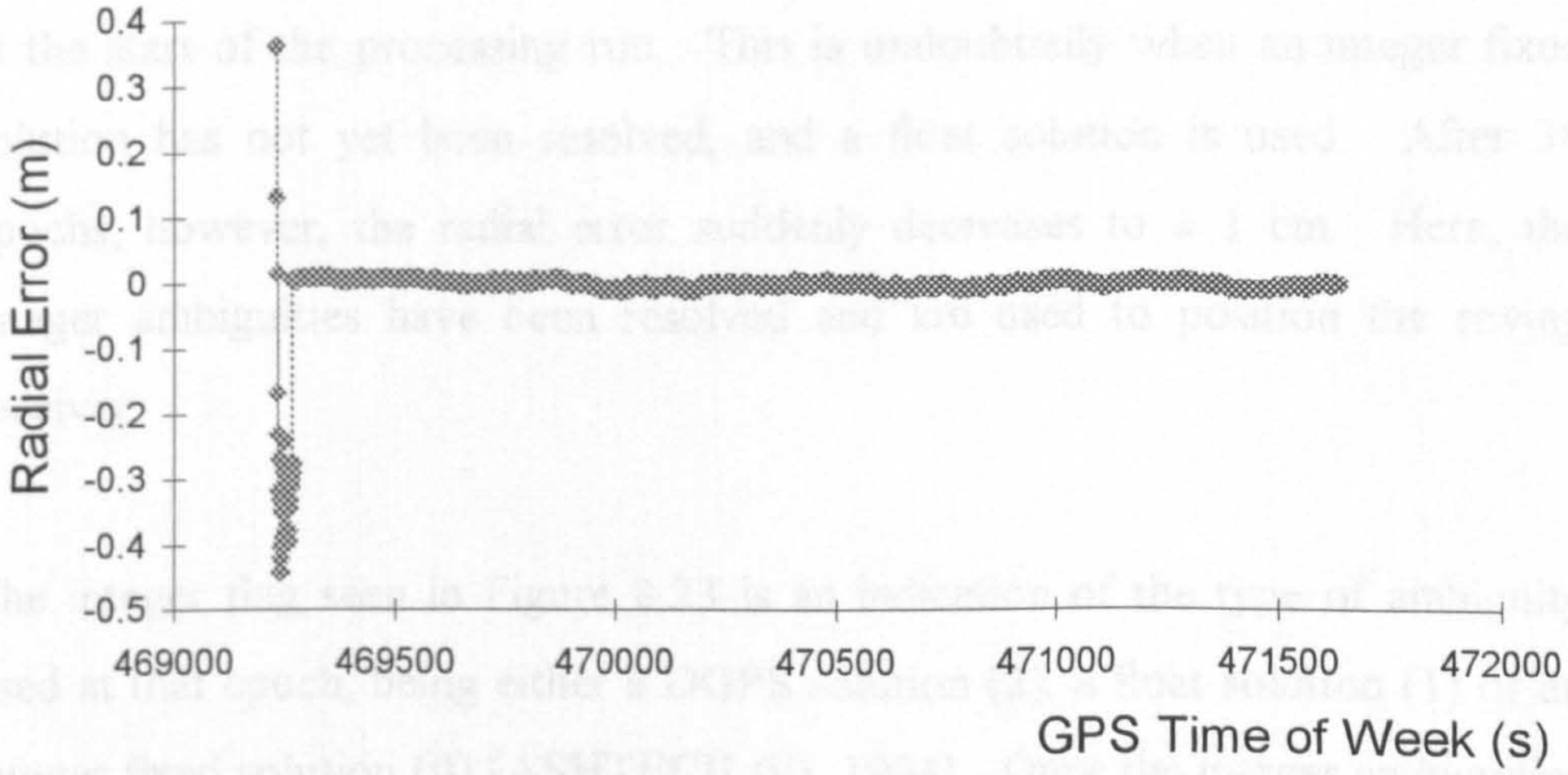

Figure 8.22

Radial Error for an OTF Position Resulting from Entering the True Reference Receiver's Coordinates.

Figure 8.23 illustrates the integer fix flag at every epoch through using the correct coordinates for the reference receiver.

decreases. This is due to the least squares float solution gradually working its way to the true value. It is also evident that the integer search was not as quick (1068 epochs) as when the true reference receiver's coordinates were used.

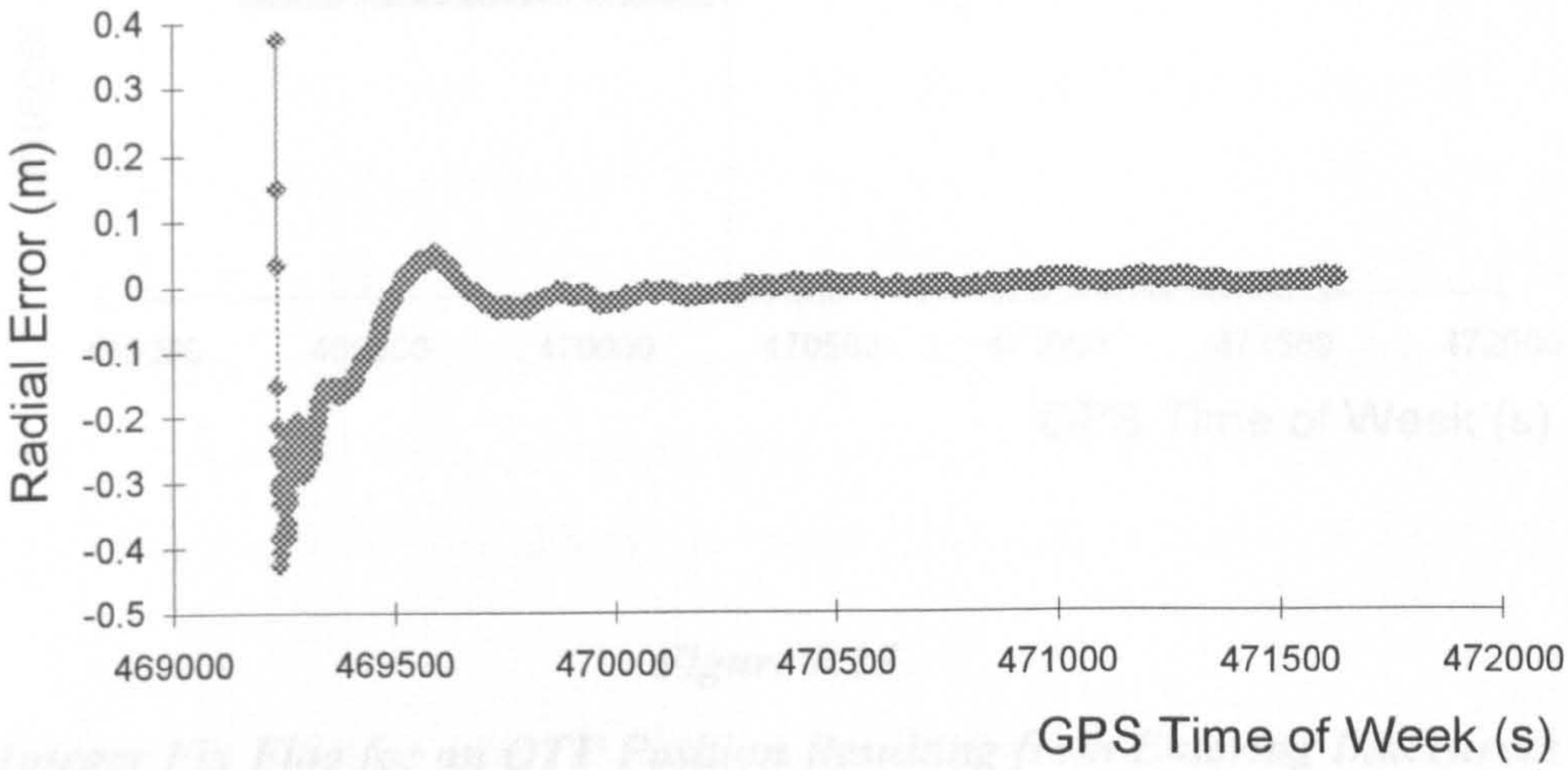

Figure 8.24

Radial Error for an OTF Position Resulting from Entering Inaccurate Reference Receiver's Coordinates.

Other sources of error can also include the method with which the GPS antenna is fixed to the object to be positioned. For example, a surveyor may use a bipole with a spirit bubble attached to it to enable real time setting out. The bipole may be 2 metres in length, the surveyor positioning its base over the point to be coordinated, and levelling the pole using the spirit bubble. The GPS antenna would be located on top of the pole. Any movements in the pole, held as steady as possible by the surveyor, may introduce errors into the solution, which may be of the order of a couple of centimetres, (§8.6). Similarly, if the GPS antenna was to be used to position a large structure, (Chapter 10), it should be clamped to the structure itself, as rigidly as possible, thus reducing any vibrations. The effect of such vibrations are detailed in Chapters 9 and 10.

8.9 Conclusions and Recommendations

It has been shown in this chapter that real time OTF GPS can be precise to a few millimetres once the integer ambiguities have been resolved.

The reference GPS coordinates should be as accurate as possible, thus allowing quick and accurate integer ambiguity resolution. Initial trials detailed in this chapter have suggested that using reference GPS receiver as inaccurate as a stand alone GPS positioning (~100 m) can impede the OTF search. This may only be true for baseline lengths of ~ 10 km or greater; shorter baseline lengths, < 1 km, may work with inaccurate reference receiver coordinates. Further work should be carried out in this region, comparing satellite numbers, satellite geometry, baseline lengths and coordinate accuracies with the success of the resulting OTF search. This would then allow a user to be able to decide the order of accuracy of the reference receiver's coordinates required for successful OTF initialisation.

The real time aspect of such a system may cause problems when using a 0.5 Watt UHF data link. The signal transmitted from such low powered telemetry

links may not be powerful enough, and signals are easily lost due to obstructions or interference. Other forms of data links should be researched, such as the use of cellular telephone links.

8.10 References

ACKROYD, N. 1996, *GPS and Civil Engineering,* Civil Engineering Surveyor GIS/GPS Supplement, Autumn 1996. pp 27 - 29.

ASHKENAZI, V., Bingley, R., Codd, B., Cory, M., *Results and Analysis of the EUREF EIR/GB95 GPS Campaign.* Report on the Symposium of the IAG Subcommision for the European Reference Frame (EUREF) held at Ankara 22 - 25 May 1996. ISSN 03407691, ISBN 7696 9620 4.

ASHTECH, 1994 (i), *Ashtech Z-12 Receiver Operating Manual,* Document number 600224, revision B, May 1994. Ashtech Inc, 1170 Kifer Road, Sunnyvale, CA 94086

ASHTECH, 1994 (ii), *Ashtech Prism Precision Survey Software, Vol I.* Publication date 17 march 1994, Document Number 600116, Revision B. . Ashtech Inc, 1170 Kifer Road, Sunnyvale, CA 94086

ASHTECH, 1995, *Ashtech Supplement to Z-12 Receiver Operating Manual Covering RTZ Functions,* Document number 600292, revision A, March 1995. Ashtech Inc, 1170 Kifer Road, Sunnyvale, CA 94086

EUROCONTROL 1993, *Datum: A Report and Software Package for the Transformation and Projection of Coordinates.* Eurocontrol Experimental Centre. EEC Report No. 237. Issued December 1990, revised December 1993.

JACK, O. T. J, 1994, *Multipath Effects on GPS Observations*, MSc Thesis, University of Nottingham.

RACAL, 1995, *Deltalink II Operating Manual,* ref no STM1320, Racal Survey Ltd, Burlington House, 118 Burlington Road, New Malden, Surrey. KT3 4NR.

SHARDLOW, P.J., 1990, *Multipath: An Investigation,* MSc Thesis, University of Nottingham.

SHARDLOW, P.J., 1994, *Propagation Effects on Precise GPS Heighting,* PhD Thesis, University of Nottingham.

STENA LINE, 1996, *The Story Behind the Building of the First Stena HSS - Facts and Information.* News Release, Stena Line Ltd, Communications Department, Charter House, Park Street, Ashford, Kent. TN24 8EX.

TRIMBLE, 1996, *GPS For Civil Engineering & Construction,* Application and technical notes, Trimble Navigation Europe Ltd, Trimble House, Meridian Office Park, Osborn Way, Hook, Hampshire, RG22 4BQ. TID 10839 (3/97)

TRIMBLE, 1997, *GPS Awareness in Civil Engineering and Construction,* Seminar notes, Trimble Navigation Europe Ltd, Trimble House, Meridian Office Park, Osborn Way, Hook, Hampshire, RG22 4BQ. March 1997.

Chapter 9

Construction Plant Control and Monitoring by GPS

9.1 Introduction

Some research has already been documented on the use of real time OTF kinematic GPS for plant control and monitoring [ACKROYD, 1996], [AL-SHAMMARI, 1996], [SANSOME, 1996], [UREN 1996]. However, this work is limited and there appears to be scope for a great deal more investigation and research into this topic. GPS, however, is not suitable for all plant control applications, such as using plant in built up areas where multipath and limited sky view is a problem. One answer to the latter problem may be the use of GPS/GLONASS receivers, which should allow the user to view at least 4 satellites even in urban environments.

The use of terrestrial surveying techniques, such as levelling, can allow the accurate control and monitoring of construction plant [SPECTRA PHYSICS]. Levelling, for example, can be used to control the height of a bulldozer's blade and allows aggregate to be precisely graded. However, this is a lengthy and manual procedure which usually slows the machinery down in order to keep pace with the surveying.

Laser levels are now frequently used to monitor and control the heighting of plant [KELLY], [SINBAD], [UREN, 1996], [SPECTRA PHYSICS], [SPECTRA PHYSICS, 1995]. Due to the continuous readings taken by a laser level, automated heighting is possible. These systems, however, only enable height control, with a crude distance measurement provided by the use of a measuring wheel attached to the plant. The use of real time OTF GPS for plant control and monitoring has been investigated by the author as being a useful addition to the laser level system, and even as a possible replacement, providing both precise height and positional information.

The following chapter will detail the current laser level techniques used to control plant. Results obtained from real time OTF GPS tests carried out by the author are also given. The tests include the use of real time OTF GPS on bulldozers for monitoring and control purposes. The GPS results are compared to other surveying methods, such as laser levels and digital levels, showing that real time OTF GPS precision to a few millimetres is possible over short baseline lengths.

9.2 The Use of Laser Levels and Ultra Sonic Devices for Plant Control

Laser levels are now frequently used to monitor and control the heighting of plant [KELLY, 1995(i)], [SPECTRA-PHYSICS, 1995], [SINBAD], [UREN, 1996], [UREN and PRICE, 1997], [SPECTRA-PHYSICS], [PRICE and UREN, 1989]. Due to the continuous readings taken by the laser level, automated heighting is possible. This in turn allows quick, cost effective and precise use of plant.

For example, by placing a laser level receptor onto a mast attached to the blade of a bulldozer, it is possible to continuously monitor its height. Laser levels can also be used to calculate the tilt of a blade. This is achieved by placing two

laser level receptors, one on each end of the blade. By knowing the distance between the receptors, and the difference in height between the two masts, the tilt can be calculated.

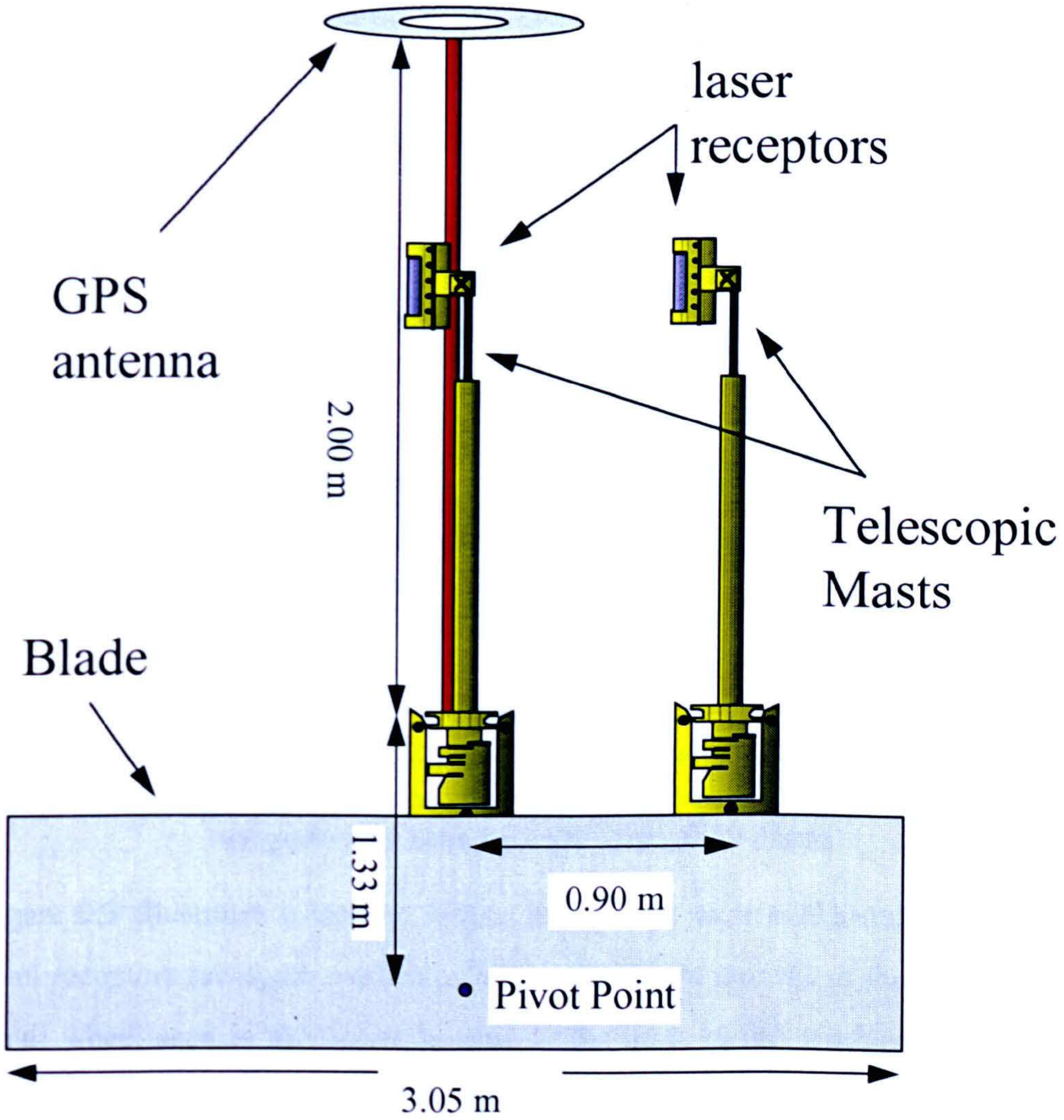

Figure 9.1
A Schematic Showing the Dimensions of the Blade Used for the Trials. The Diagram Shows the Laser Level Receptors Situated on top of the Extendible Masts, as well as the GPS Antenna Situated on One of the masts.

Figure 9.1 shows a schematic diagram, illustrating the principles behind the laser level system, as used on a bulldozer's blade. The diagram is based upon the specifications of the plant used by Sinbad Plant Hire Ltd, upon which the real time OTF GPS tests were carried out.

Figure 9.2 illustrates the use of a laser level to measure the height and tilt of the grading machine's blade. The laser level is seen mounted on top of a tripod on the left hand side of the picture, whilst the two laser level receptors are visible on either end of the blade. The laser level emits a plane of light, which the receptors detect. The laser level readings have been combined into an integrated system, whereby the level readings can be used to control the hydraulics of the blade, thus automatically adjusting the blades height and tilt where necessary.

Figure 9.2

A grader using a laser level for the control of height and tilt of the blade. The laser itself is seen on the left side of the photo, whilst the two laser level receptors are seen on each side of the blade.

Figure 9.3 illustrates a similar system being used on a bulldozer. Two laser level receptors are again used to calculate the height and tilt of the blade. The small wheel seen in the figure located at the back of the machine, is used to measure distance. This system is called the 'Laser Curve Control Computer' [KELLY, 1995(i)]. The wheel will only measure distance, and will not measure direction. The Curve Control is frequently used in conjunction with the laser level to allow coarse positioning as well as heighting.

Figure 9.3
A laser level being used to control height and tilt on a bulldozer. The wheel at the back of the bulldozer is used to measure distance.

By carefully monitoring and planning the track which the bulldozer is to take, it is possible to cover the working area in straight parallel runs. Resulting in a grid of distances along a run with corresponding laser level height values.

Figure 9.4
A Laser Level being used to control an Asphalt Paver.

In addition to the laser level, ultra sonic devices are available to control height. Such a device can be seen, in figure 9.4. The ultra sonic device will measure the distance between itself and a solid object, such as an existing road surface, a string line or a pavement [SPECTRA PHYSICS, 1994], [SPECTRA PHYSICS, 1995]. As with the laser level, the ultra sonic device may be integrated with the hydraulic system of the plant, allowing automatic height control in a similar manner.

Other uses for the laser level and 'curve control' systems include the monitoring of road and railway lines. Over time, road surfaces and railway tracks may sink

into the underlying ground, causing an uneven surface, and poor travelling conditions. A simple system used to detect these height anomalies consists of a laser level and 'curve control' system mounted onto a trailer unit, towed behind a motorcar. Any anomalies detected may then be matched up to a distance along the road or rail track, and then easily located for repair. Such a system being used to monitor a road surface is seen in figure 9.5, taken from [KELLY, 1995(ii)]

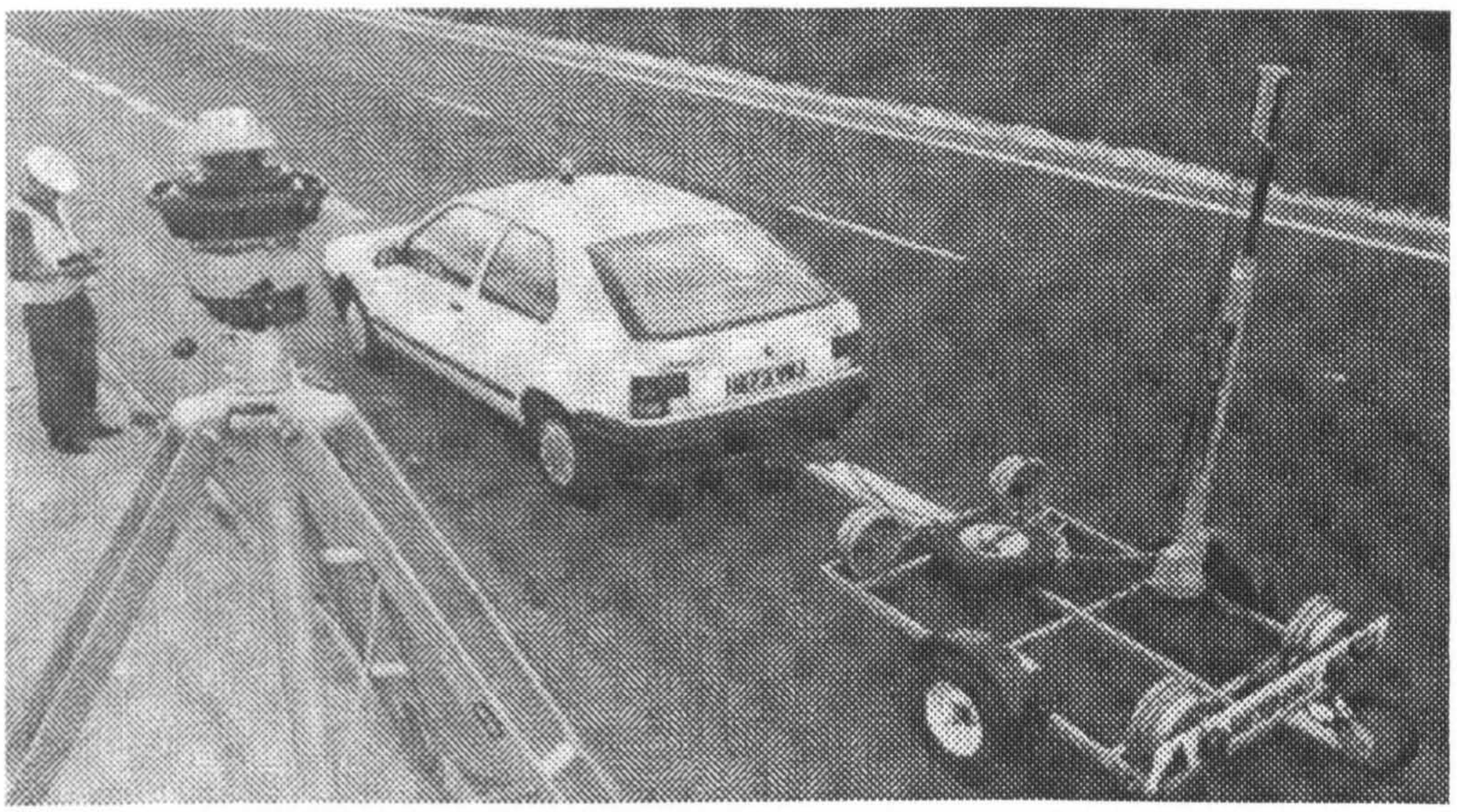

Figure 9.5
The laser level System being used in conjunction with the 'Curve Control' System to measure anomalies in the road's surface [KELLY, 1995(ii)].

9.3 The Use of Real Time OTF for Plant Control

Section 9.2 has introduced the use of laser levels and ultra sonic devices for plant control. These systems, however, only provide height control with a possibility of measuring distance using the 'Curve Control' system. Some applications may only require height control, say, when levelling aggregate during the construction of a level car park. Whilst others, such as the construction of a banking road, require the height or tilt of the road to change with position.

The use of real time OTF GPS would result in heighting, similar to the laser level system, but also position information. The 3-D position obtained through using OTF GPS would allow a quality control of the levelling to be achieved. The coordinates of every level could be recorded, which could be checked later.

Real time OTF GPS has many advantages over the laser level. As well as obtaining a 3-D position, the GPS system may be implemented over longer distances. Due to the curvature of the Earth, the Spectra Physics model 1142 laser level is quoted as being accurate to ± 4.5 mm per 100 m at standard atmospheric conditions [SPECTRA PHYSICS, 1995]. The inaccuracies increase as the distance between the laser and receptor increase. In addition, the laser level system has a limited range due to the range of the laser itself. This is stated as being of up to the order of 350 m, [SPECTRA PHYSICS, 1995]. Furthermore, the laser level system has another drawback in that the speed at which the system can travel is limited. This is due to the latency experienced from waiting for the mast holding the receptor to adjust itself to the laser level's light plane.

The experiments to assess the use of real time OTF GPS as a positioning tool for construction plant are detailed in §9.4 and § 9.5. Tests were carried out by placing GPS receivers onto strategic points of a bulldozer. The bulldozer was then operated in a normal manner, to test the real time OTF GPS to its full extent. Section 9.6 will detail and show the results obtained from the experiments, and conclusions are drawn in §9.7.

The experiments were conducted at the plant storage site which belongs to Sinbad Plant Hire Ltd in Stapleford, Notts. The plant used was a bulldozer, which Sinbad Plant Hire Ltd currently use in conjunction with a Laser-Plane laser system, and 'curve control' computer. The plant storage site was by no means a "GPS friendly" site, due to the adjacent buildings and the constant flow of lorries and construction plant. This in turn, however, helped to demonstrate

that even in such a difficult environment, real time OTF GPS can be successfully used.

The reference station at the site was coordinated from a known ETRF89 position on the IESSG building, some 6 km away, using static GPS processing with GAS [STEWART *et al.* 1995].

9.4 The Use of a Single GPS Antenna on a Bulldozer Blade

The first two tests consisted of attaching a single GPS antenna to the bulldozer's blade. The GPS receiver used was an Ashtech Z-XII dual frequency receiver, using an Ashtech GPS antenna with a ground plane. The antenna was attached to a pole, which in turn was fixed to the central laser level receptor's mast. The antenna was situated some 1.5 m above the height of the bulldozer's cab, to reduce multipath and allow more satellites to be viewed. The laser level was in full operation at all times using both masts, which in turn controlled the height and tilt of the blade.

A Leica NA2000 digital level was also used in conjunction with the GPS and laser level. The NA2000 has a quoted standard deviation of 1.5 mm (1 km double run levelling), and is classed as a precise level [LEICA, 1990]. The readings from the NA2000 were taken as the truth, from which the other two systems were compared. Digital level readings were taken at timed instances at the same position on the blade. These instances occurred, however, only when the bulldozer was static, as trying to take readings whilst moving proved difficult or impossible.

Figure 9.6 shows the bulldozer with the GPS antenna, laser level receptors and digital level staff attached to the two masts fixed to the blade. The reference GPS receiver can be seen in the background of figure 9.6, as can the

transmitting telemetry link. The roving GPS receiver is located in the orange ruck sack, along with the receiving telemetry link. The laptop PC seen in the figure was used to enable real time OTF processing.

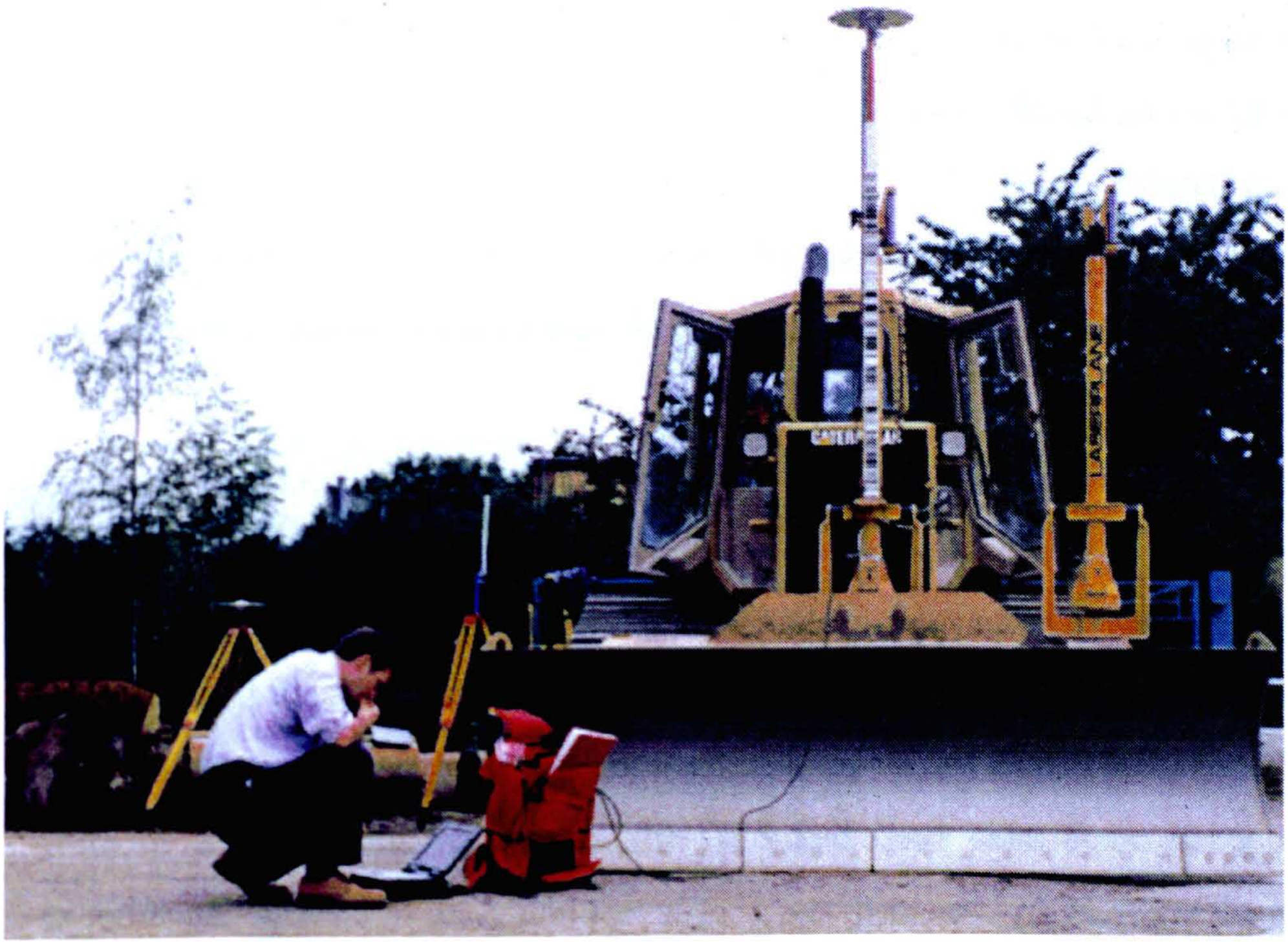

Figure 9.6
Diagram showing the GPS Antenna and a Leica NA2000 Digital Levelling Staff Located on the Laser Level Receptor's Mast on the Bulldozer's Blade.

The bulldozer was operated in a normal manner at the yard, where it was manoeuvred backwards and forwards, altering the blade's height and tilt at recorded times.

The bulldozer was manoeuvred up to some 40m away from the GPS reference station. GPS data was collected at 0.5 second epochs, and transmitted to the bulldozer using the Racal Deltalink II telemetry links. The real time processing was carried out using a Pentium-90 laptop PC. The results from these experiments are shown and analysed later in this chapter.

9.5 The Use of Three GPS Antennas on a Bulldozer

The third test consisted of a similar set-up to the first two, but this time three GPS antennas were placed upon the bulldozer. The GPS receivers used were all low powered Ashtech Z-XII receivers. Two antennas were located on the blade itself via the laser level receptor masts, and the third placed on top of the driver's cab. The two antennas placed on the blade were ground plane antennas, whilst the antenna placed upon the cab was a choke ring antenna. The reference receiver antenna was also a choke ring antenna.

During this experiment, the data collected at 0.5 second epochs was post processed as it was not possible to carry out real time processing on all three receivers. The post processing was carried out using Ashtech's PNAV software, and the data then analysed using a Microsoft Excel spread sheet. This time, however, the laser level was not used, and only a few digital level readings were recorded. The precision of the GPS had been determined using the experiments detailed in §9.3, and this experiment was used to examine the use of numerous roving GPS receivers on a single item of plant. The experiment allowed the position of the blade and cab antennas to be calculated. Figure 9.7 illustrates the three GPS antennas situated upon the bulldozer. The antenna located on top of the driver's cab has been named S1. The antenna located on the left side of the blade (as the driver looks out of the cab) named S2, and the antenna located on the right side of the blade S3. The two ground plane antennas are seen attached to the masts on the machines blade. The choke ring antenna can be seen located on top of the driver's cab. Choke ring antennas were not used on the blades as they may have proved too heavy for the mast. The three GPS receivers were situated inside the cab. The reference receiver was situated some 10 m behind the bulldozer, out of the photograph's range.

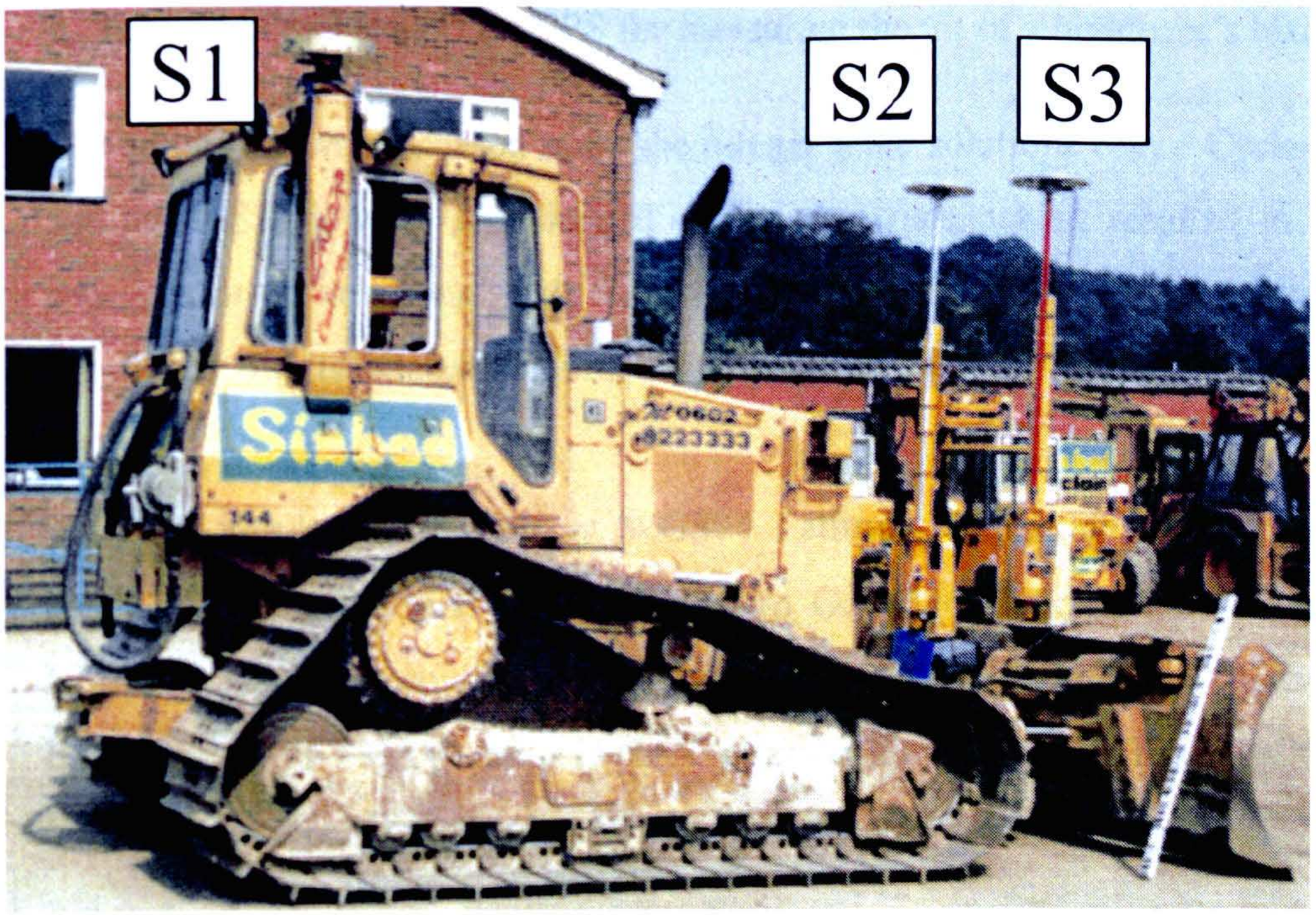

Figure 9.7
Diagram showing the Bulldozer with three Ashtech GPS Antennas Attached at Key Locations.

The NA2000 digital level's staff was manually placed on the blade at each measurement. The analysis and results of this experiment are detailed in the following section.

9.6 OTF GPS Positioning Results

The remainder of this chapter will discuss the results obtained from the tests described in §9.4 and §9.5, and hence the potential of using real time OTF GPS on such a piece of construction plant.

The results are discussed through analysis of:

1. The height accuracy of the system
2. The positional accuracy of the system
3. The system noise

4. The use of real time OTF GPS for measuring the tilt of a bulldozer's blade

The results shown are based upon the integer fixed solutions only. Cycle slips and loss of lock were experienced during the trials, which resulted in float solutions or no solutions at all for a few epochs. Such instances are seen as gaps in the results, allowing the reader to see the frequency of such obstacles.

The GPS results were given in WGS84 Latitude, Longitude and ellipsoidal height. These were then all converted into OSGB36 National Grid Eastings, Northings and ellipsoidal height using the IESSG WinCODA software. Examples of the PNAV and RTPNAV position files as well as the WinCODA OSGB36 National Grid files can be seen in Appendix E.

The Eastings and Northings were then converted into distance along and across the track which the bulldozer was travelling on. This allows the motion of the antennas, vehicle and blade to be analysed in these directions, which would ultimately be used to guide a vehicle operator in an automated system. Figure 9.8 illustrates the theory used to determine the along and across track components of the results. Equations [9.1] and [9.2] show the calculations used for the same respectively.

$$\text{Distance along the track, } x' = E \cos a + N \sin a \qquad (9.1)$$

$$\text{Distance across the track, } y' = N \cos a - E \sin a \qquad (9.2)$$

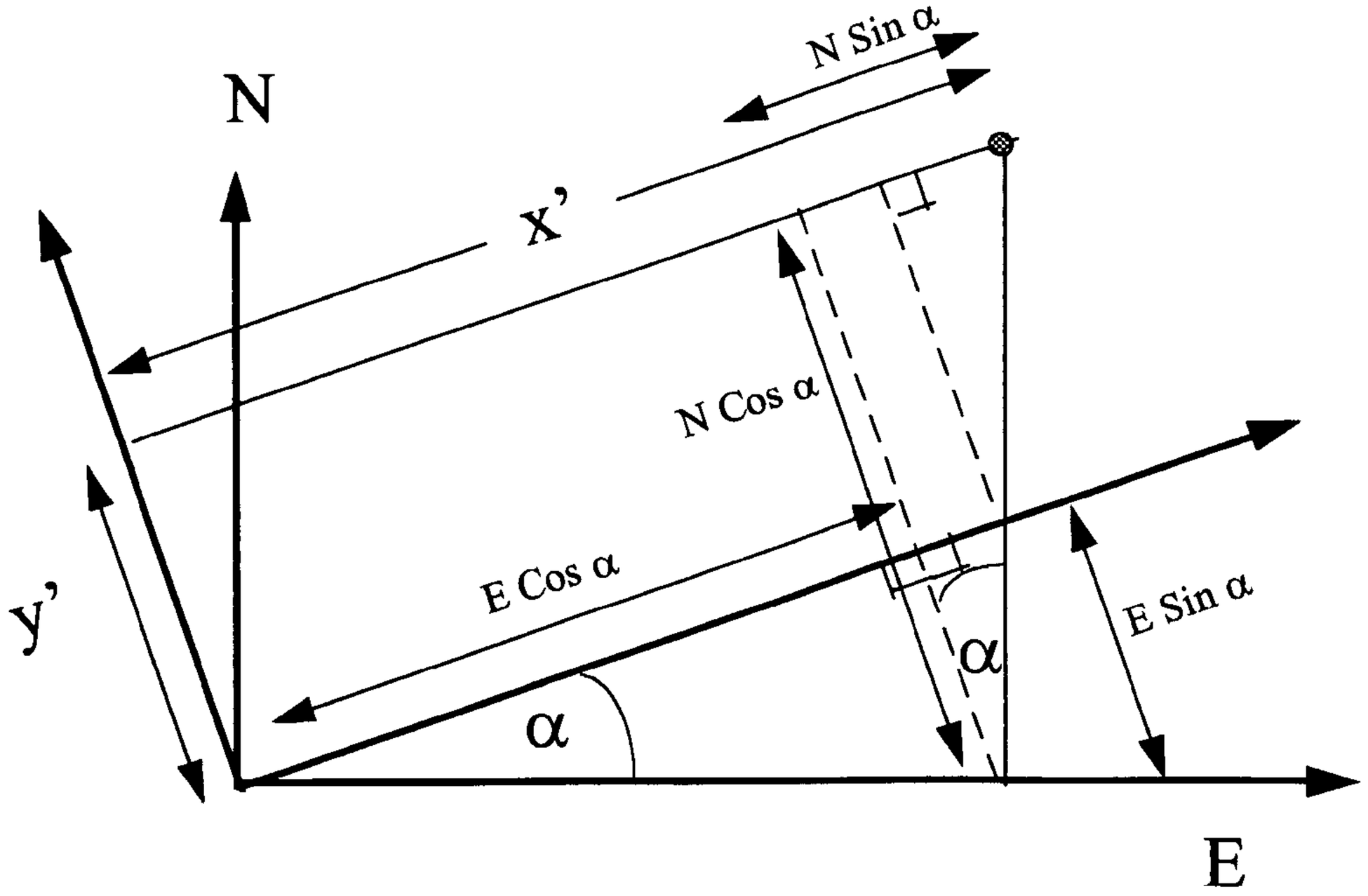

Figure 9.8
Illustration showing the conversion from Eastings and Northings to Along Track (x') and Across Track (y').

9.6.1 Height Precision of the Fixed Integer OTF GPS Solution

As described in §9.4 and §9.5, the GPS height component was compared to the laser level used on the bulldozer and a Leica NA2000 digital level.

Figure 9.9 illustrates the height component of the GPS antenna located over the driver's cab (S1) during trial 3. It can be seen that the bulldozer's height is precisely measured. The bulldozer during this period moved slowly forward, stopping four times between the times of 14:17:00 and 14:34:30. Following this initial manoeuvre, the bulldozer was then reversed to approximately the same starting location. The bulldozer was then moved forward and backwards a further four times, starting and stopping at approximately the same positions.

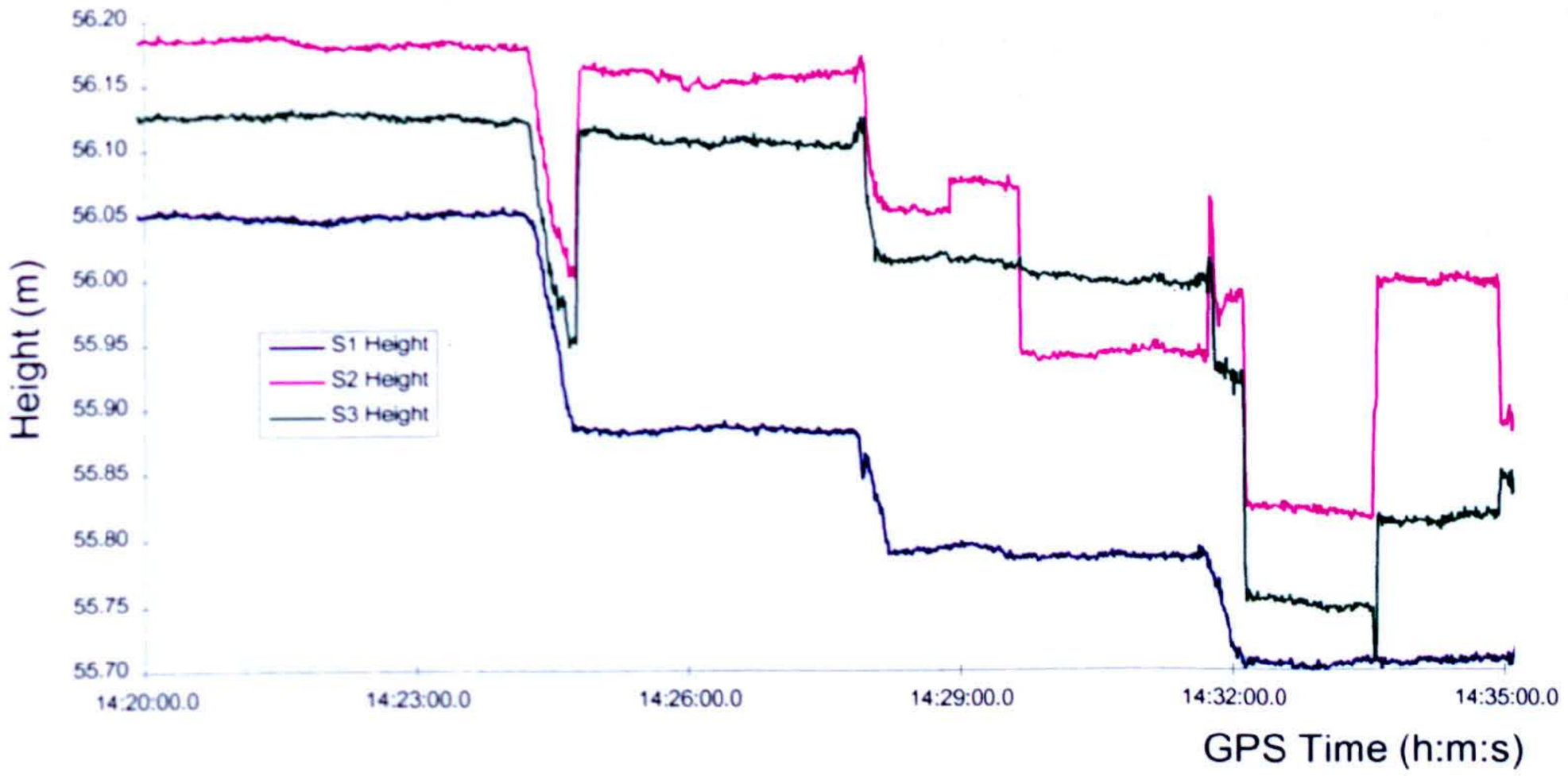

Figure 9.10
The GPS Height Component of all Three Antennas Located on the Bulldozer During Trial 3.

Figure 9.10 illustrates the height component for all three GPS receivers located on the bulldozer during trial 3. It can be see that the three components remain parallel to each other with time. This is true for all manoeuvres, apart from the tilt movements. Tilt movement can be seen at approximately 14:29:00, 14:31:30, 14:34:00 and 14:35:00. The tilt experiments are detailed in section 9.6.5. The parallel nature shows that the three independently processed baselines agree with each other. The GPS height differences between S1 and S2 and the GPS height differences between S1 and S3 have an RMS of 0.007 m and 0.009 m respectively. These values were calculated for the time span from 14:19:36 to 14:24:08. These values do, however, have the system noise of two baseline results, but still show the potential accuracy of the system. The bulldozer's engine was running during this period, causing some vibration. The effects of vibration is detailed in §9.6.4. Some vibration noise is seen at certain instances in the figure. These are noticeable at approximately 14:27:40, for example, on S2 and S3, as well as other times when the blade is moved. The vibration is probably due to the flexible poles used to attach the antennas to the blade. The fact that S1 does not show as much vibration strengthens this argument. This phenomena is detailed and discussed in §9.6.2.1.

Figure 9.11 illustrates the noise for the height component of the OTF GPS solution. This is the height component for the antenna located over the driver's cab, S1, during trial 3. It can be seen that the height deviates by ± 5 mm. The bulldozer was stationary during this time, but did have the engine switched on at intervals. The blade was also manoeuvred at periods during this time. It is noticeable that there is more noise at the start of the graph. This corresponds to when the bulldozer's engine was running, and switched off at approximately 14:32:11. At approximately 14:33:10, the engine was switched back on, and the blade raised and lowered, possibly causing some vibration or cantilever movement in the cab antenna, S1 due to the blade moving. The graph does, however, illustrate the precision of the GPS height component.

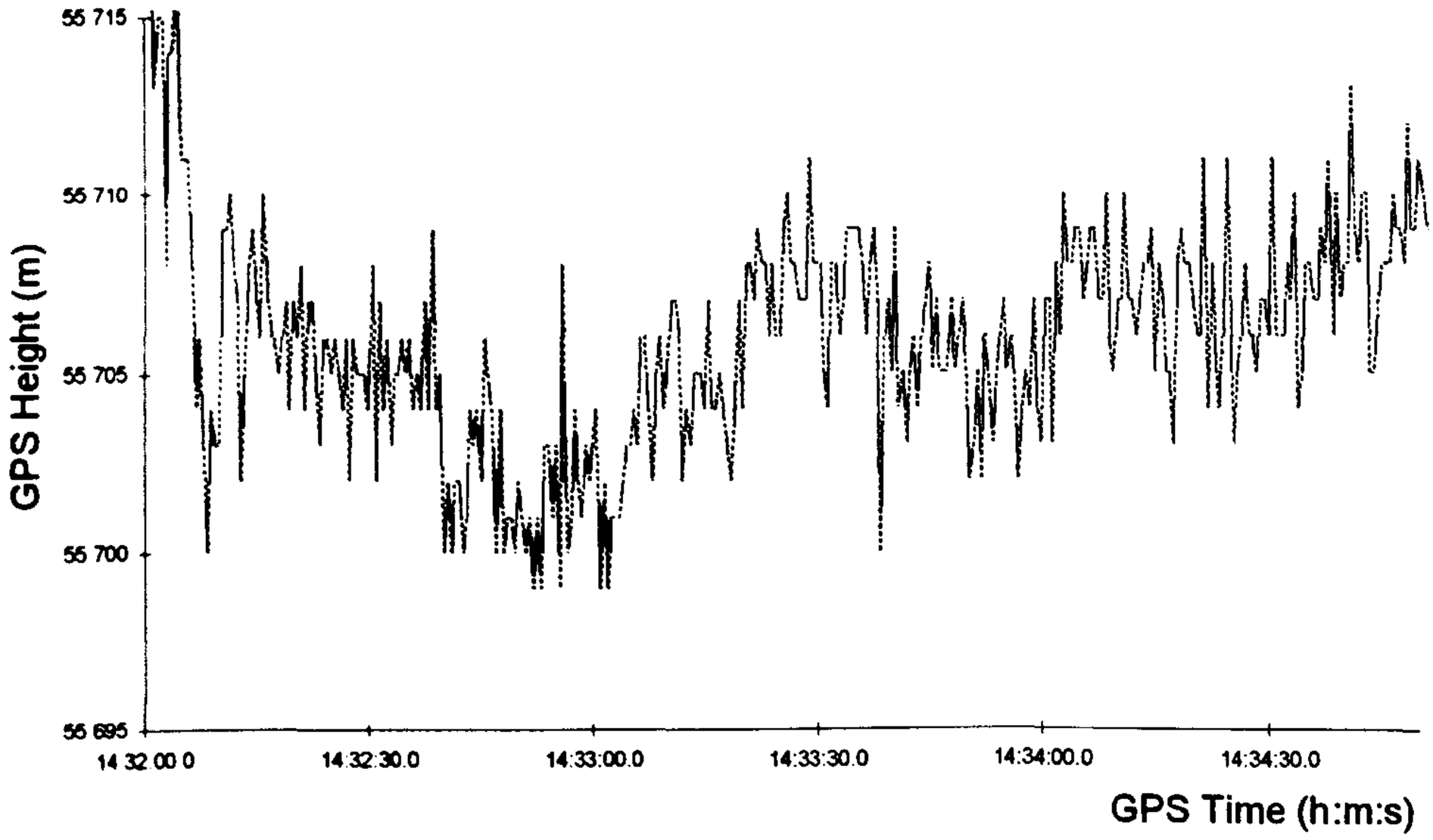

Figure 9.11
Graph Showing the Noise Level for the GPS Height of the Antenna Located on the Bulldozer's Cab During Trial 3.

9.6.2 Comparison of OTF GPS Height With a Digital Level

A Leica NA2000 digital level was used to check the GPS height. As described in §9.4 and §9.5, the digital levelling staff was placed upon the bulldozer's blade and levels taken at recorded times. The digital level height was then compared to that of the GPS in order to determine the GPS accuracy. Tables 9.1 illustrates the height component derived for the GPS and digital level, as well as the change in level and GPS height. The antenna movement across and along the track is also shown for levels and heights taken before and after blade height movements. The tilt error due to the along and across track values are shown in the last column, and detailed in §9.6.2.1.

Trial No	Digital Level (m)	Δ level (m)	GPS Height (m)	Δ Height (m)	Movement Across Track (m)	Movement Along Track (m)	Tilt Error (m)
1	1.166		56.55				
	1.167	0.001	56.553	-0.003			
	1.166	-0.001	56.556	-0.003			
	1.162	-0.004	56.552	0.004			
	1.163	0.001	56.548	0.004			
	1.162	-0.001	56.555	-0.007			
	1.159	-0.003	56.545	0.01			
	1.158	-0.001	56.548	-0.003			
	1.155	-0.003	56.549	-0.001			
	1.257	0.102	56.462	0.087	0.184	0.032	0.005
	1.262	0.005	56.457	0.005			
	1.26	-0.002	56.461	-0.004			
	1.258	-0.002	56.459	0.002			
	0.632		56.455				
	0.632	0	56.458	-0.003			
	0.633	0.001	56.459	-0.001			
	0.632	-0.001	56.459	0			
		-0.632	56.459	0			
	0.635	0.635	56.459	0			
	0.64	0.005	56.458	0.001			
	0.642	0.002	56.461	-0.003			
	0.645	0.003	56.462	-0.001			
	0.644	-0.001	56.46	0.002			
	0.645	0.001	56.466	-0.006			
	0.541	-0.104	56.558	-0.092	-0.173	-0.063	0.005
	0.543	0.002	56.555	0.003			
2	0.531		56.451				
	0.632	0.101	56.363	0.088	0.181	0.019	0.005
	0.684	0.052	56.319	0.044	0.098	-0.001	0.001
	0.735	0.051	56.276	0.043	0.079	0.023	0.001
	0.736	0.001	56.271	0.005			
	0.788	0.052	56.227	0.044	0.085	0.001	0.001
*	0.58	-0.208	56.405	-0.178	-0.352	-0.017	0.019
	0.58	0	56.406	-0.001			
	0.788	0.208	56.231	0.175	0.371	0.021	0.021
	0.787	-0.001	56.228	0.003			
	0.738	-0.049	56.278	-0.05	-0.075	0.007	0.001
	0.686	-0.052	56.317	-0.039	-0.089	-0.015	0.001
3	2.127		56.123				
	2.1	-0.027	56.11	0.013			
	2.197	0.097	56.013	0.097			
	2.176	-0.021	55.994	0.019			
	2.521	0.345	55.751	0.243			
	2.425	-0.096	55.819	-0.068			

Table 9.1
Digital Level Readings Compared to the GPS Height.

It can be seen, that the difference between the levels and GPS height is in the order of a few millimetres, except for when the blade is raised or lowered. During these instances, the difference can be anything up to 3 cm, starred (*) in Table 9.1. First impressions suggest that the fixed integer ambiguity results are only accurate to a couple of centimetres. However, this inaccuracy is thought

to be due to the fact that the blade tilts backwards when lifted or dropped. This tilt would then affect the vertical component of the GPS antenna staff, i.e. the GPS antenna's staff has a tilt component introduced into the height.

9.6.2.1 Tilt Correction Calculation

Figures 9.12, 9.13 and 9.14 illustrate typical along track, across track and GPS height graphs against time, respectively, during instances where the blade was lowered twice by 100 mm, and then raised twice by 100 mm during trial 1. From these graphs, it is evident that the blade not only moves vertically, but is also tilted along and across the track. The vibration of the pole is also evident as the movement starts and ceases. The vibration is more noticeable in plan, figures 9.12 and 9.13, than in height, figure 9.14.

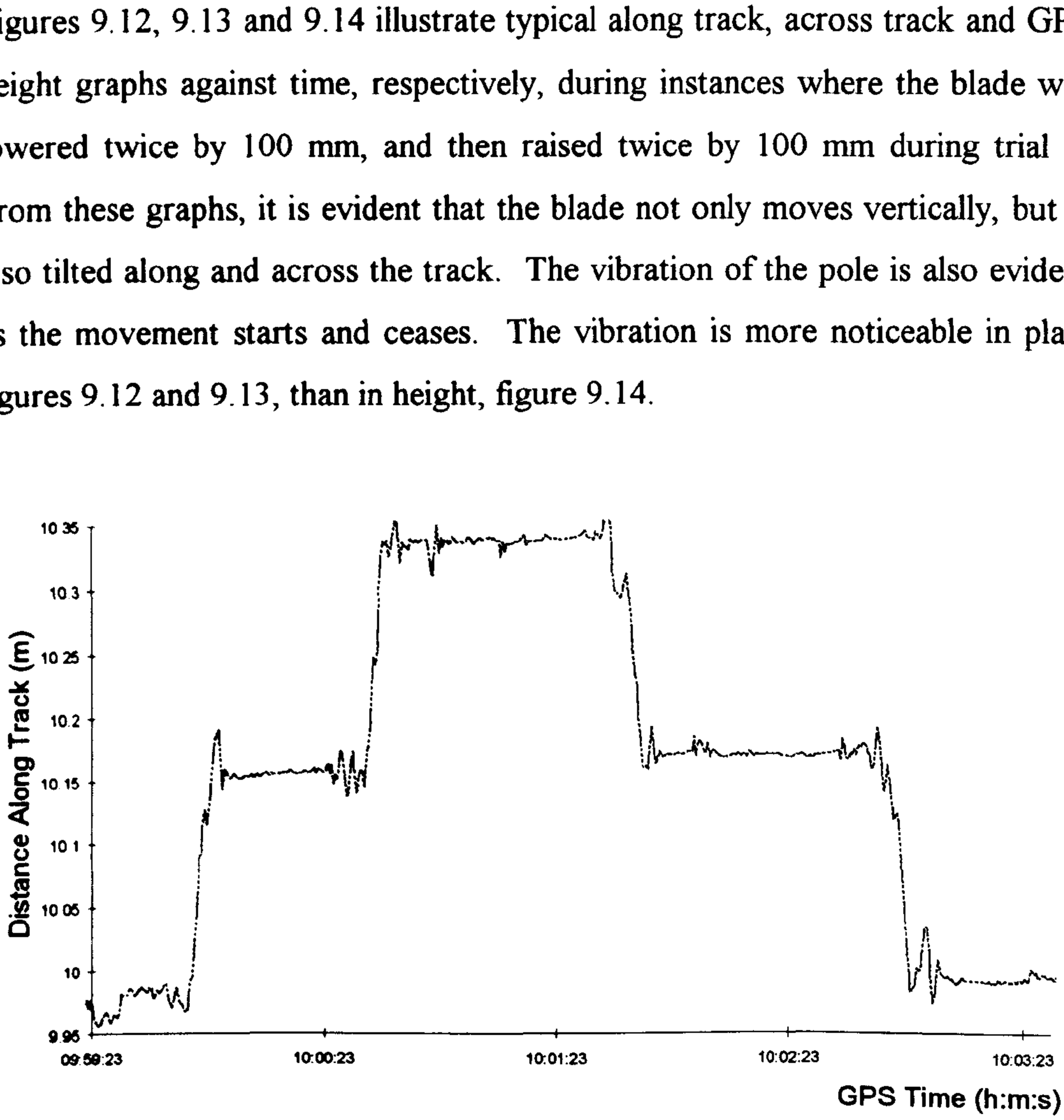

Figure 9.12
Along Track Plot During Trial 1, During which the Blade was Moved Down Twice by 100 mm at a Time, then up Twice by 100 mm at a Time.

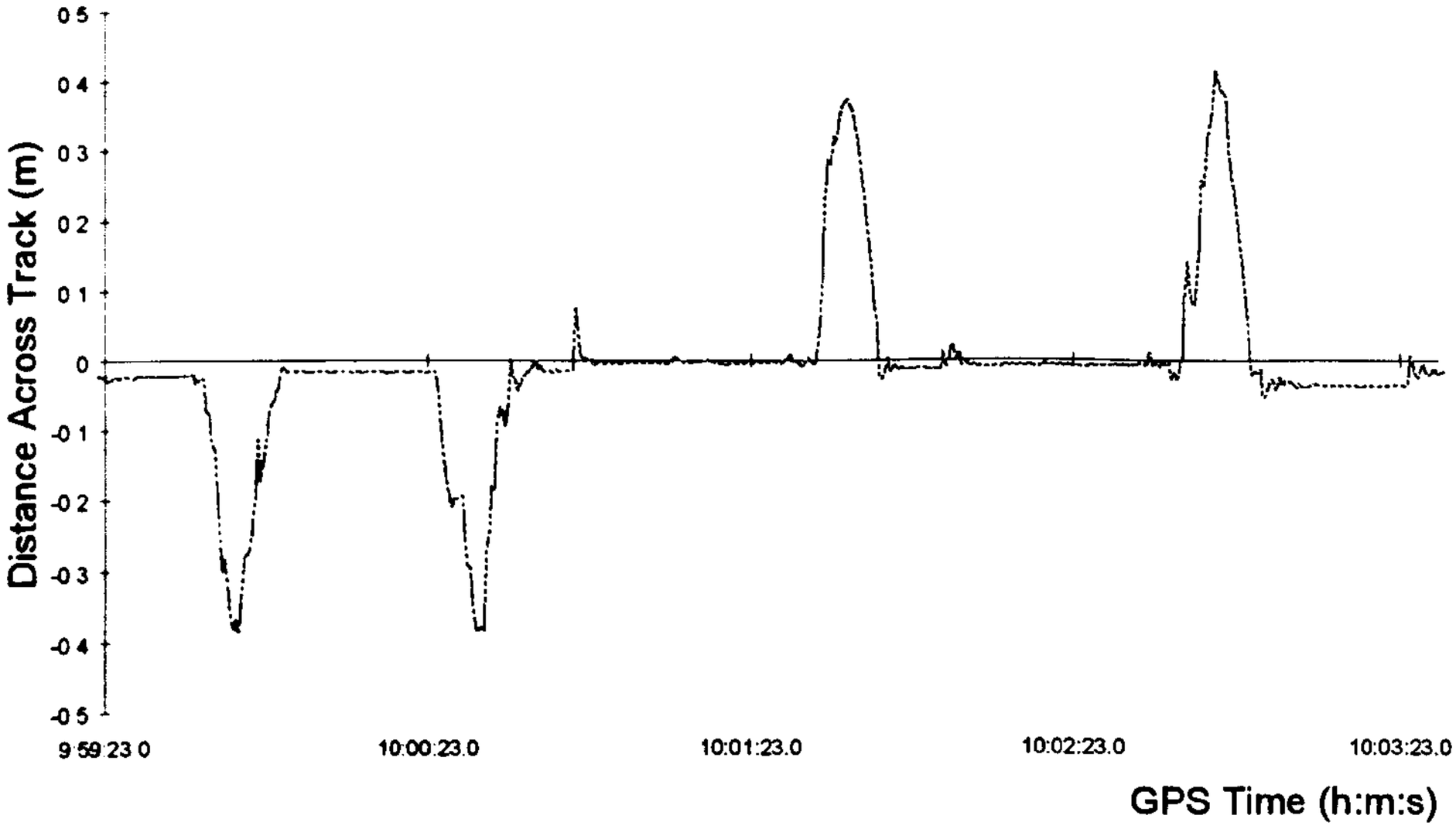

Figure 9.13
Across Track Plot During Trial 1, During which the Blade was Moved Down Twice by 100 mm at a Time, then up Twice by 100 mm at a Time.

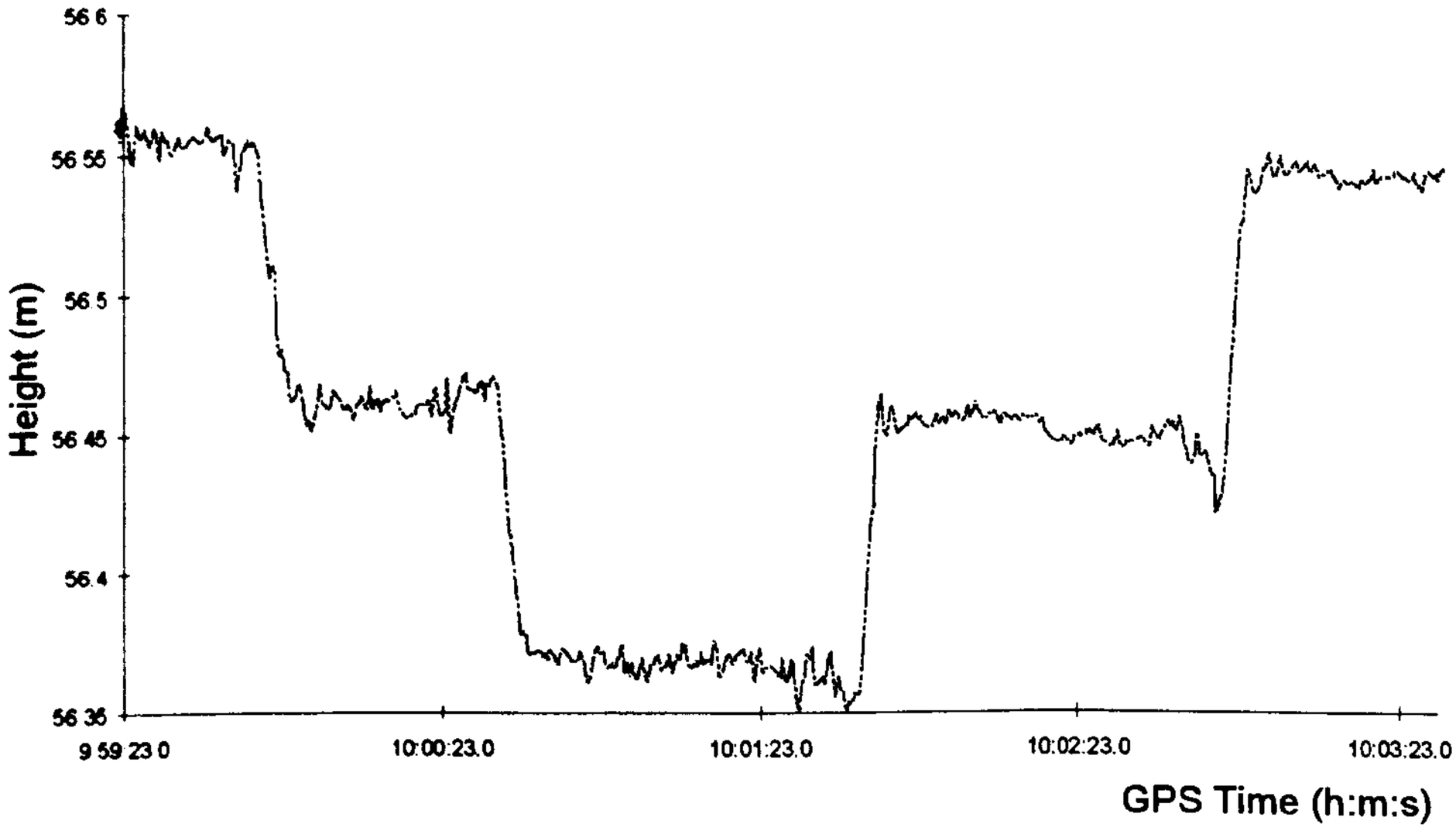

Figure 9.14
GPS Height Plot During Trial 1, During which the Blade was Moved Down Twice by 100 mm at a Time, then up Twice by 100 mm at a Time.

Figure 9.15 illustrates the plan view of this movement for the same period. It is possible to see from this figure that the right side of the blade is lowered before the left. Similarly, when raising the blade, the left side is raised first. Further

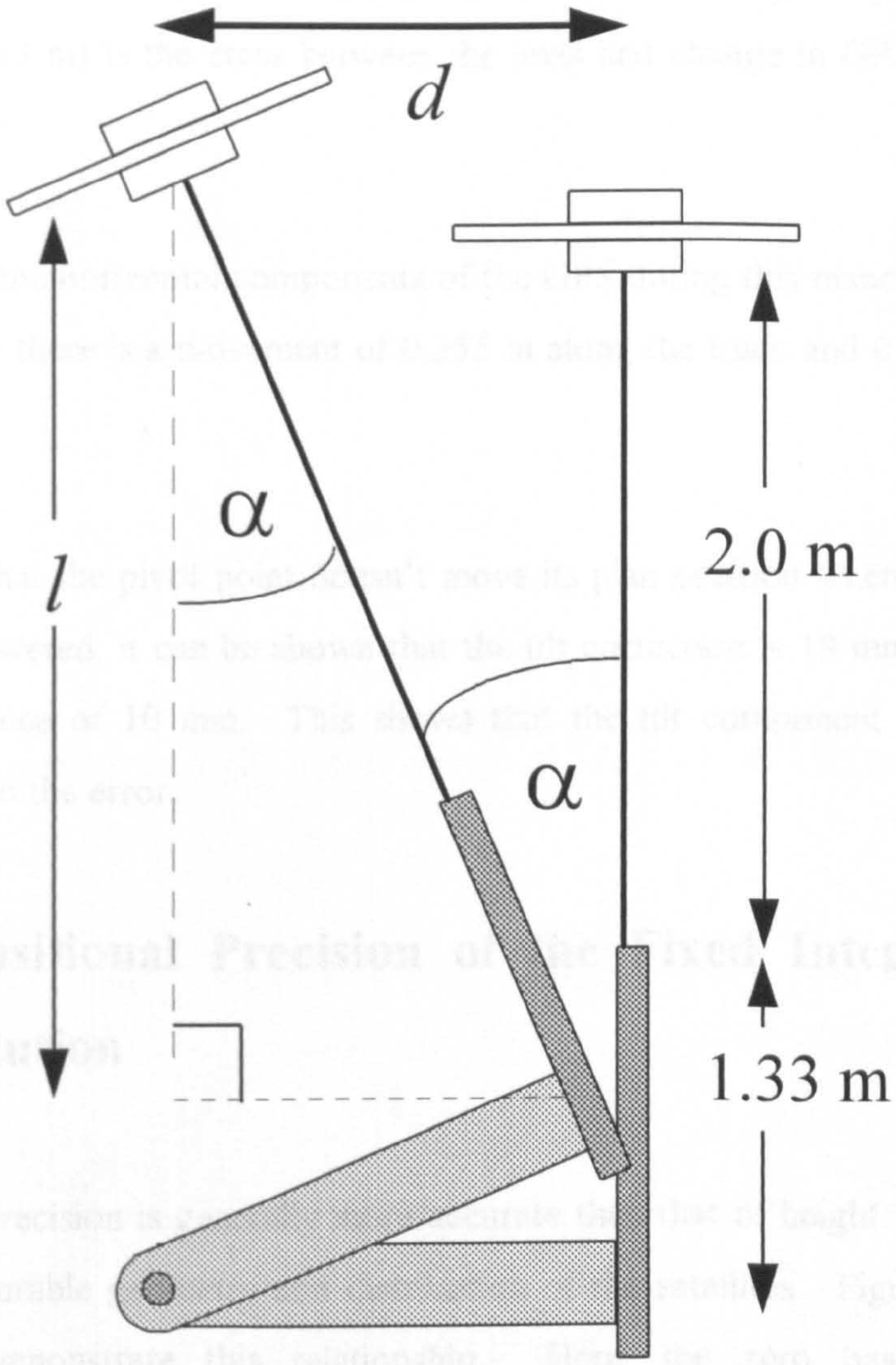

Figure 9.16
Illustration of the Dimensions and Angles Involved During Blade Movement.

Assuming that the pivot point does not move significantly in plan position, when the blade tilts back or forward, the angle of tilt, α, may be calculated from the change in plan position (d) of the antenna. Hence, the vertical component of the pole may be calculated from equation [9.3].

$$l = \sqrt{3.33^2 - d^2} \qquad (9.3)$$

The difference between *l* and the distance between the pivot point and the antenna (3.33 m) is the error between the level and change in GPS height, i.e. the tilt error

Looking at the horizontal components of the GPS during this manoeuvre, it can be seen that there is a movement of 0.355 m along the track and 0.01 m across the track.

Assuming that the pivot point doesn't move its plan position when the blade is raised or lowered, it can be shown that the tilt correction is 19 mm. Resulting in a difference of 10 mm. This shows that the tilt component does indeed contribute to the error.

9.6.3 Positional Precision of the Fixed Integer OTF GPS Solution

GPS plan precision is generally more accurate than that of height. This is due to the favourable geometry and distribution of the satellites. Figures 8.4, 8.5 and 8.6 demonstrate this relationship. Here, the zero baseline height component is shown to be in the order of ± 3 mm whilst the plan component is in the order of ± 1 mm.

Figures 9.17, 9.18 and 9.19 show the across track component of the GPS position whilst the bulldozer is static for the antennas S1, S2 and S3 respectively.

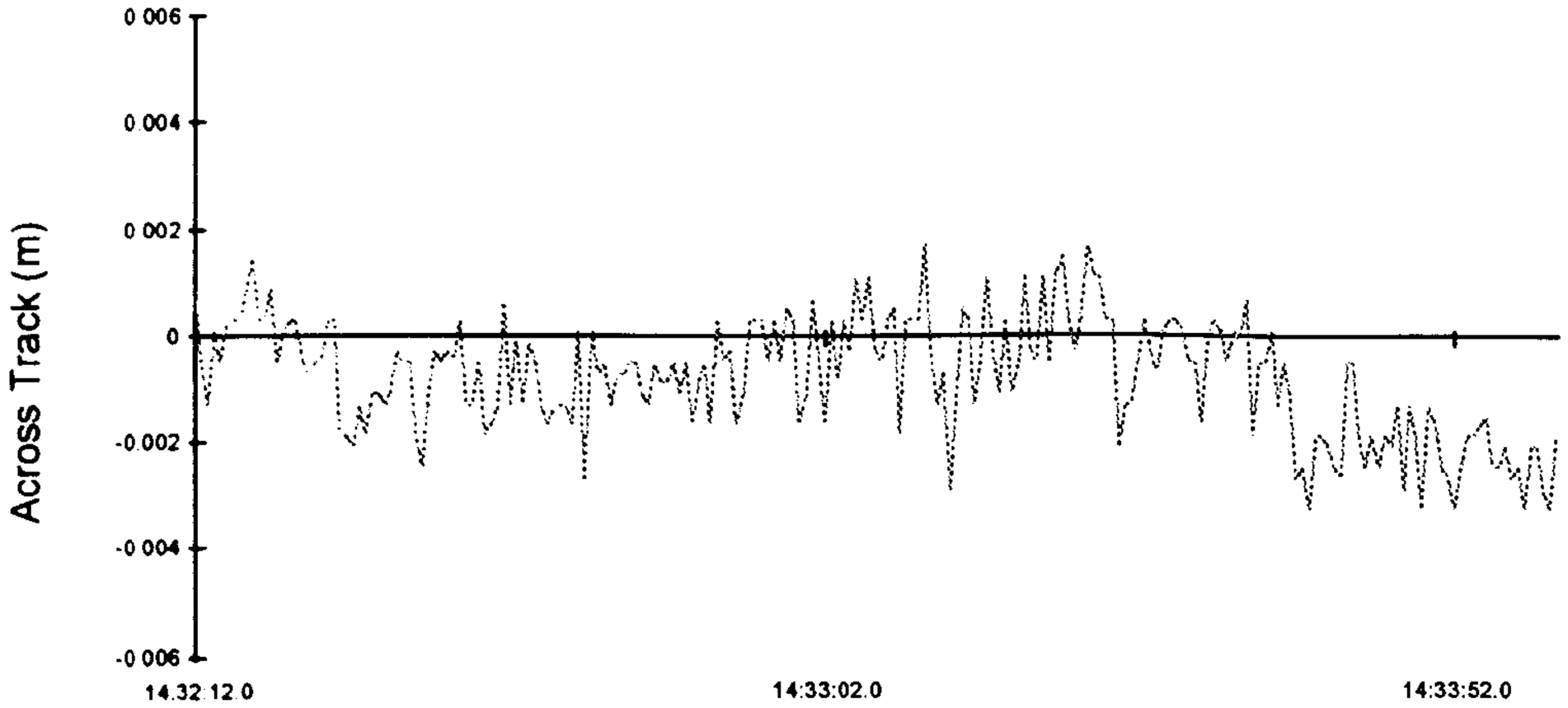

Figure 9.17
Across Track Plot for S1 During Trial 3 Illustrating the Precision of the System.

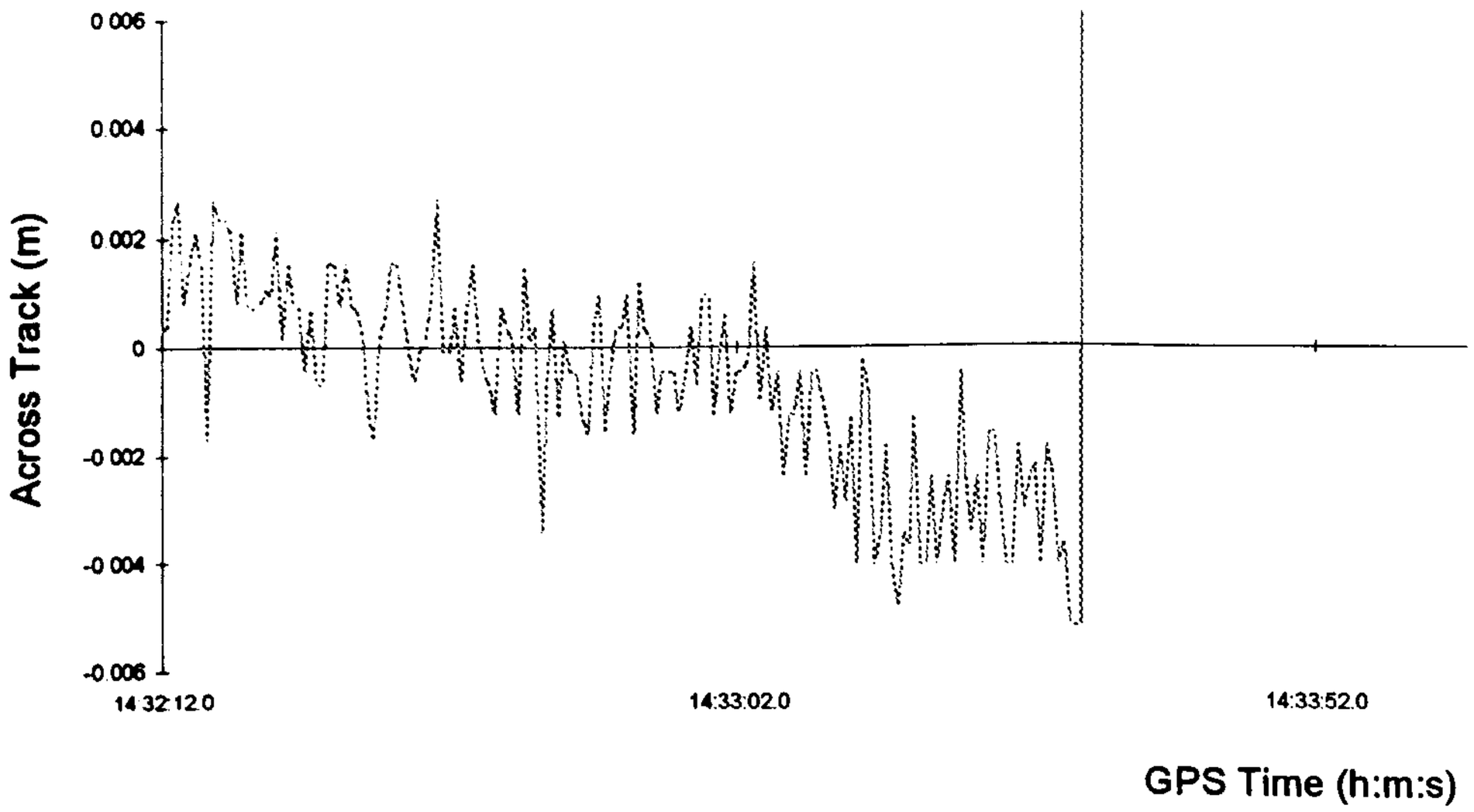

Figure 9.18
Across Track Plot for S2 During Trial 3 Illustrating the Precision of the System.

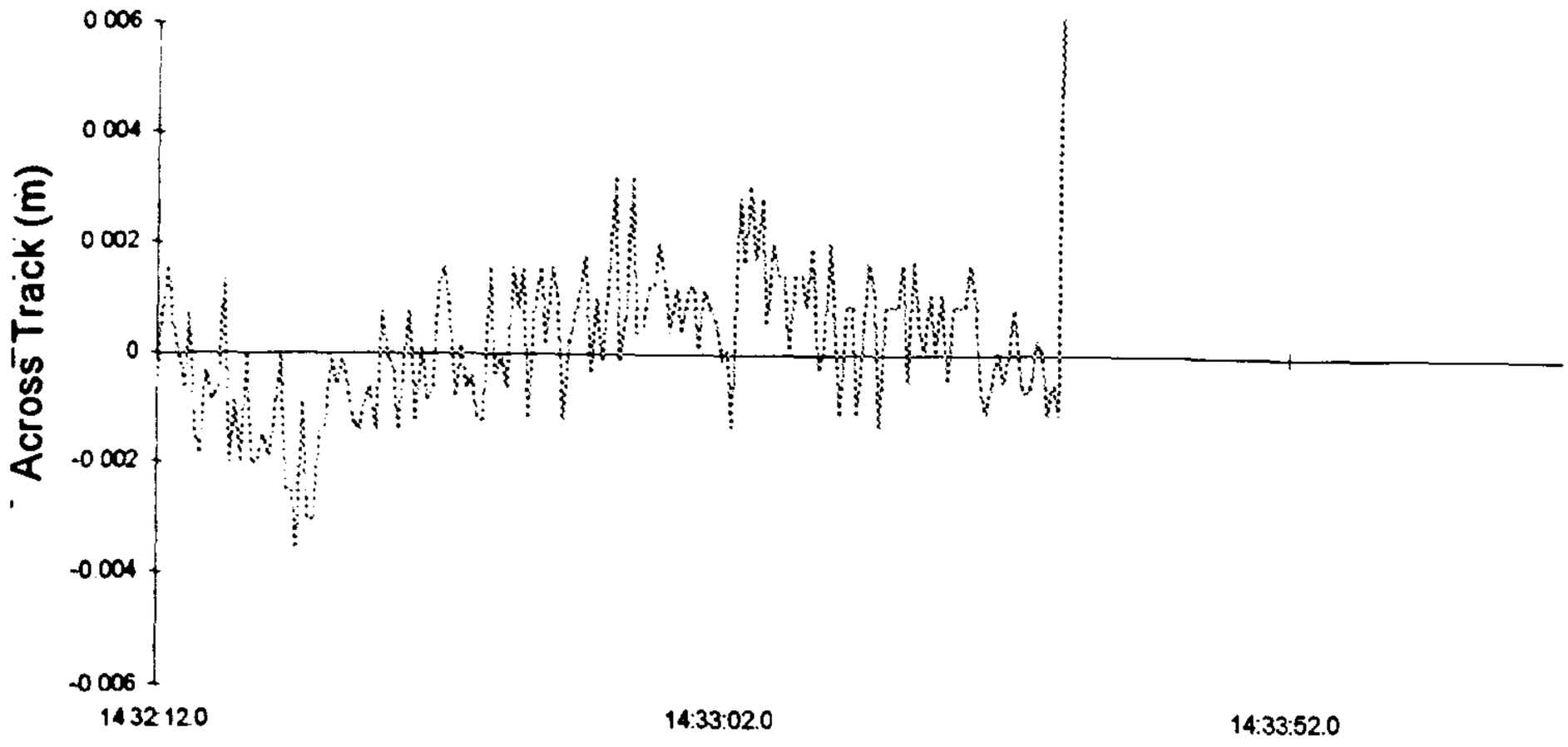

Figure 9.19
Across Track Plot for S3 During Trial 3 Illustrating the Precision of the System.

These figures show that the plan precision is in the region of ± 2 mm. Figures 9.18 and 9.19 show that the two antennas located on the blade itself move, and are both slightly noisier than the antenna located on the cab. Two reasons for this increase in noise include the fact that firstly, the cab antenna is a choke ring antenna, reducing multipath noise. Secondly, the two antennas located on the blade were located on poles which had a tendency to vibrate. This vibration is discussed in §9.6.4. However, it can be concluded that the plan precision is in the region of ± 3 mm for the ground plane antennas, and ± 2 mm for the choke ring antenna.

9.6.4 System Noise

It is evident from some of the graphs and discussion that there is vibration within the system. Some of the vibration is directly due to the whole bulldozer vibrating. Other sources of vibration include that of the flexible poles which attach the antennas to the blade. The following section will discuss and quantify these problems, giving some suggested remedies.

Figures 9.20 and 9.21 illustrate the vector S1 to S2 and S1 to S3 respectively. From these, it can be seen that there is vibration. Table 9.2 details the bulldozer's movements during the period of the graphs.

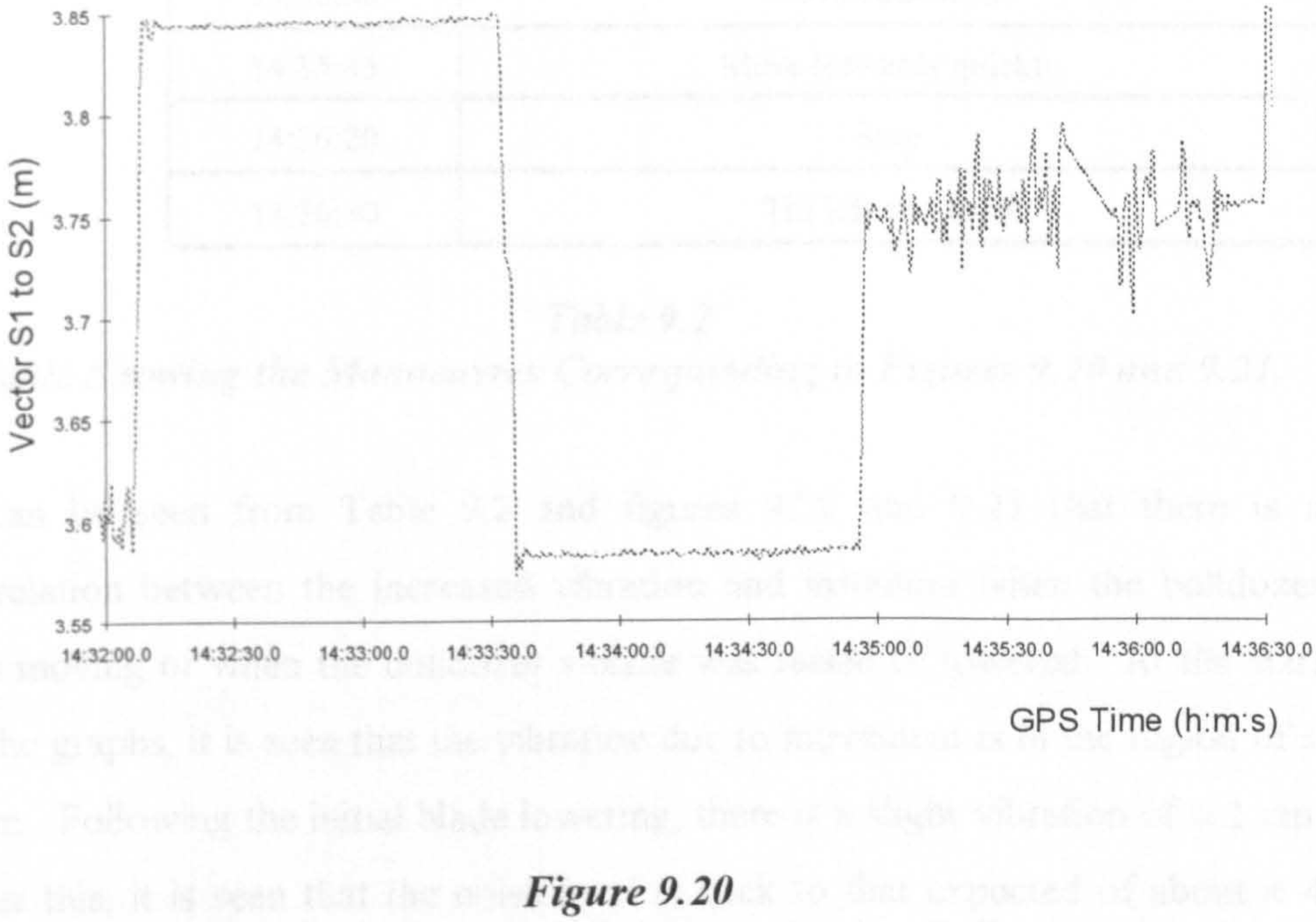

Figure 9.20
Vector S1 to S2 Showing Increased Vibration During Bulldozer Movement.

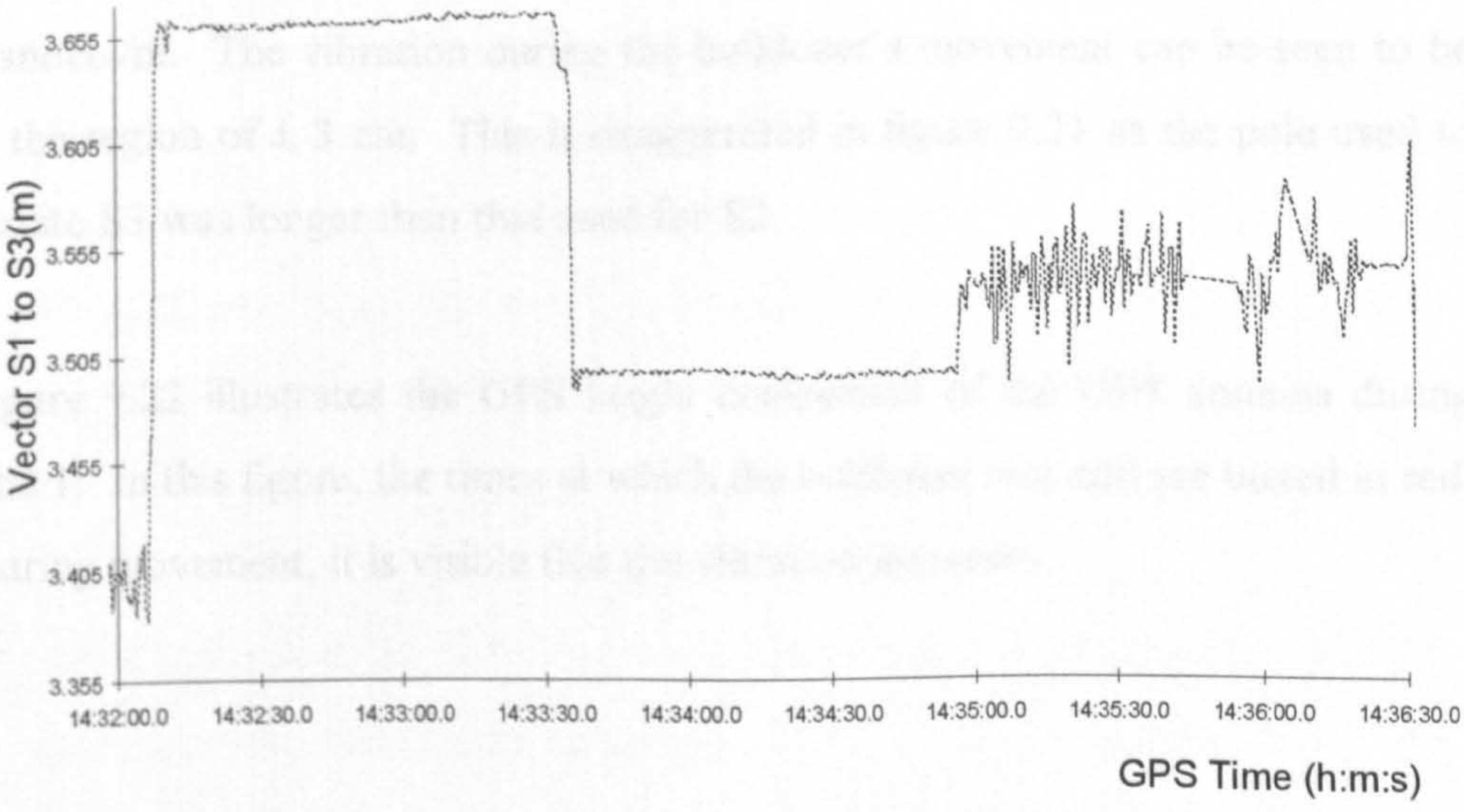

Figure 9.21
Vector S1 to S3 Showing Increased Vibration During Bulldozer Movement.

GPS Time (h:m:s)	Description of Motion
14:31:30	Move forward
14:32:10	Lower blade, stop engine
14:33:25	Start engine, move blade down, up, tilt then stop engine
14:35:00	Move backwards
14:35:45	Move forwards quickly
14:36:20	Stop
14:36:30	Tilt left and right

Table 9.2
Table Showing the Manoeuvres Corresponding to Figures 9.20 and 9.21.

It can be seen from Table 9.2 and figures 9.20 and 9.21 that there is a correlation between the increased vibration and instances when the bulldozer was moving or when the bulldozer's blade was raised or lowered. At the start of the graphs, it is seen that the vibration due to movement is in the region of ± 2 cm. Following the initial blade lowering, there is a slight vibration of ± 1 cm. After this, it is seen that the noise level is back to that expected of about ± 4 mm, which includes the noise of two GPS receivers. Following the second blade movement at 14:33:25, there is a small vibration again at the end of the manoeuvre. The vibration during the bulldozer's movement can be seen to be in the region of ± 3 cm. This is exaggerated in figure 9.21 as the pole used to situate S3 was longer than that used for S2.

Figure 9.22 illustrates the GPS height component of the GPS antenna during trial 1. In this figure, the times at which the bulldozer was still are boxed in red. During movement, it is visible that the vibration increases.

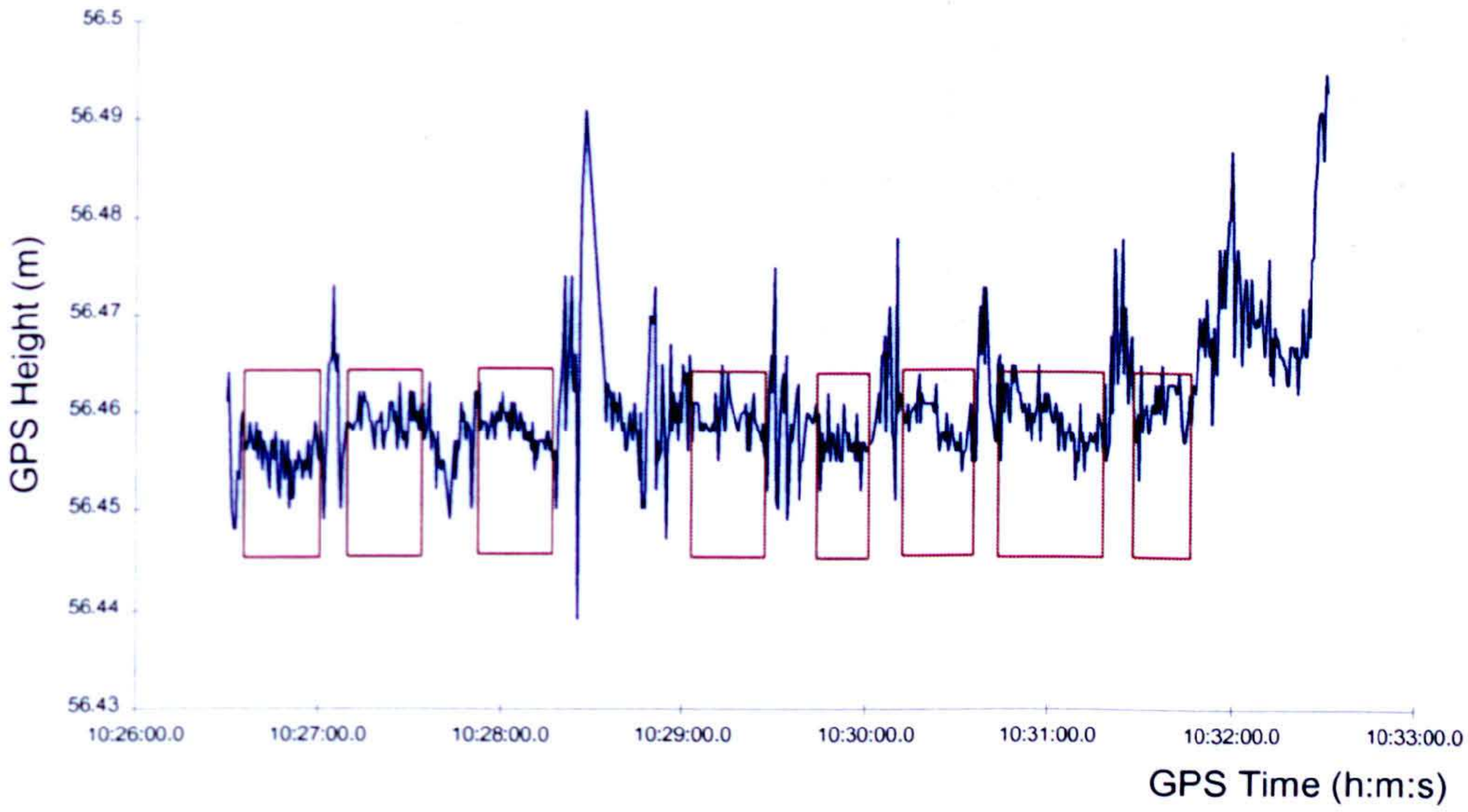

Figure 9.22
Graph Showing GPS Height Against Time During Trial 1. The Red Boxed Portions of the Graph Represent Times when the Bulldozer was Standing Still, Showing a Smaller Vibration Noise.

The trials were experimental, set up in a temporary nature. By fixing a more sturdy mast system to the blade, the mast vibration may be reduced or eliminated. An ideal location for the GPS antenna would be directly fixed to the blade. This, however, would result in poor signal quality, due to multipath, and reducing the number of satellites in view, due to the bulldozer's body being in the way. Locating the antenna near to where the blade makes contact with the aggregate may also result in damage to the antenna. Further work should be carried out to seek a better system of attaching the GPS antenna to the blade.

These trials and results do show, however, that real time OTF systems operated over such short baselines can be precise to the order of millimetres. The precision is such that the vibration of the bulldozer and the antenna masts can be quantified, and hence may be reduced through the use of Kalman filters on the GPS data.

9.6.5 The Use of Real Time OTF to Measure the Tilt of the Bulldozer Blade

The use of laser levelling to measure the tilt of the bulldozers blade requires two laser level receptors. The difference in laser level height between the two receptors, at a known distance apart from each other, is calculated. From this, the tilt of the blade may be calculated. Such systems are currently used, §9.2. Tilt determination is also possible using two GPS receivers in a similar manner. It is also possible, however, to determine the tilt of the blade using only a single GPS antenna on the blade.

The tilt of the mast, due to changing the height of the blade, can be calculated and corrected for, §9.6.2. Following the same idea, it is possible to calculate the across track and along track tilt of the blade through using the coordinates before and after the tilt.

There is only a difference of 3 mm between the GPS derived tilt and that derived by the laser level, which should also incorporate the noise of both systems. There is a problem with this technique, however, as the blade must be level before the tilt can be calculated. This was achieved during the experiment though using the laser level system to level the blade, although several possibilities are available to level the blade.

The first option would be to integrate the GPS output with that of a tilt sensor. The tilt sensor could be used to level the blade. The integration of GPS and tilt sensors has already been shown to be successful at the IESSG [ASHKENAZI *et al.*, 1996].

The second option, which is perhaps more expensive, would be to use either the laser level system as well as the GPS or use two GPS receivers in order to determine the difference in height between the two masts. This would then make a single antenna method of tilt measurement redundant and unnecessary.

The third option, and the simplest, requires no additional equipment apart from the single antenna already discussed. The idea would be to tilt the blade one way and then back the other, allowing the antenna to rock through its highest position. This being a similar principle to rocking a surveying levelling staff during reading. The coordinates which correspond to the highest location are where the blade is level, assuming that the blade and the antenna's mast lie perpendicular to each other. If this system was set up, the operator would simply rock the blade to and fro to enable the highest point to be found, allowing the blade to be levelled, possibly automatically. Once the blade has been levelled, a pre determined tilt could easily be achieved as discussed earlier.

Figure 9.25 shows a photograph taken whilst the bulldozer's blade was being tilted during trial 3. Here the bulldozer was moved forward, whilst tilting the blade backwards and forwards. The antennas on the blade, located on the top

of the poles attached to the masts on the blade, did vibrate during this movement.

Figure 9.25
The Bulldozer Travelling with a Tilted Blade During Trial 3.

During the trials, this manoeuvre was frequently carried out both whilst the bulldozer was moving and stationary. The blade was moved from a left hand tilt to a right hand tilt and back again. Figures 9.26, 9.27 and 9.28 illustrate the GPS height, along track distance and across track distance, respectively, all plotted against time for such a tilting manoeuvre performed whilst the bulldozer was stationary. Figure 9.26 shows that during the manoeuvre, the GPS height is seen to fluctuate to a minimum height, to a maximum and then down and back up again. This corresponds to the along and across track plots, figures 9.27 and 9.28 respectively, indicating the position at which the GPS antenna is at its maximum height. This in turn indicates the coordinates of the antenna at which the blade is level.

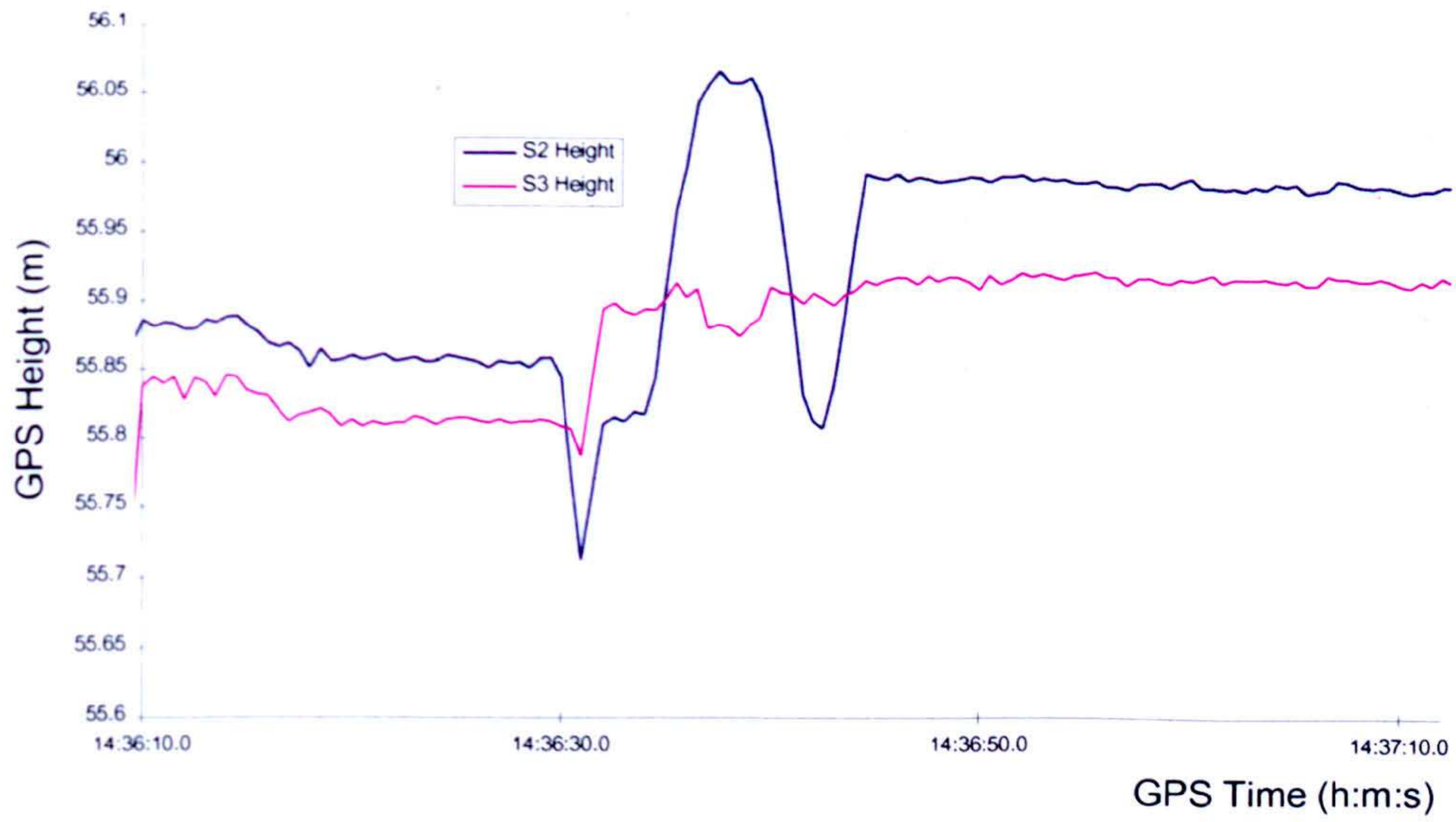

Figure 9.26
The GPS Height Component During a to and fro Tilting Manoeuvre, where the Blade was Moved from Left Hand Tilt to a Right Hand Tilt and Back Again.

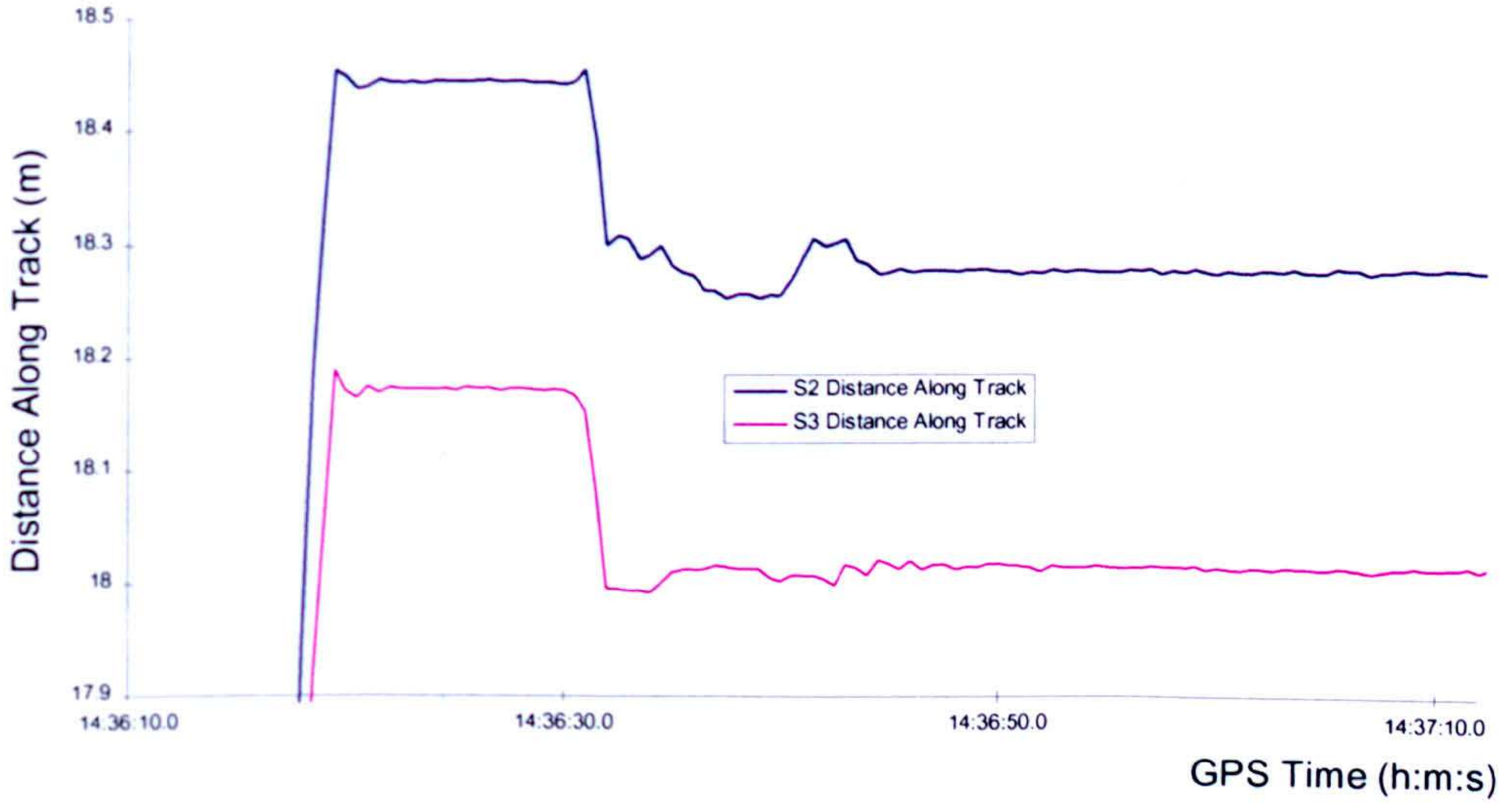

Figure 9.27
Distance Along the Track During a to and fro Tilting Manoeuvre, where the Blade was Moved from Left Hand Tilt to a Right Hand Tilt and Back Again.

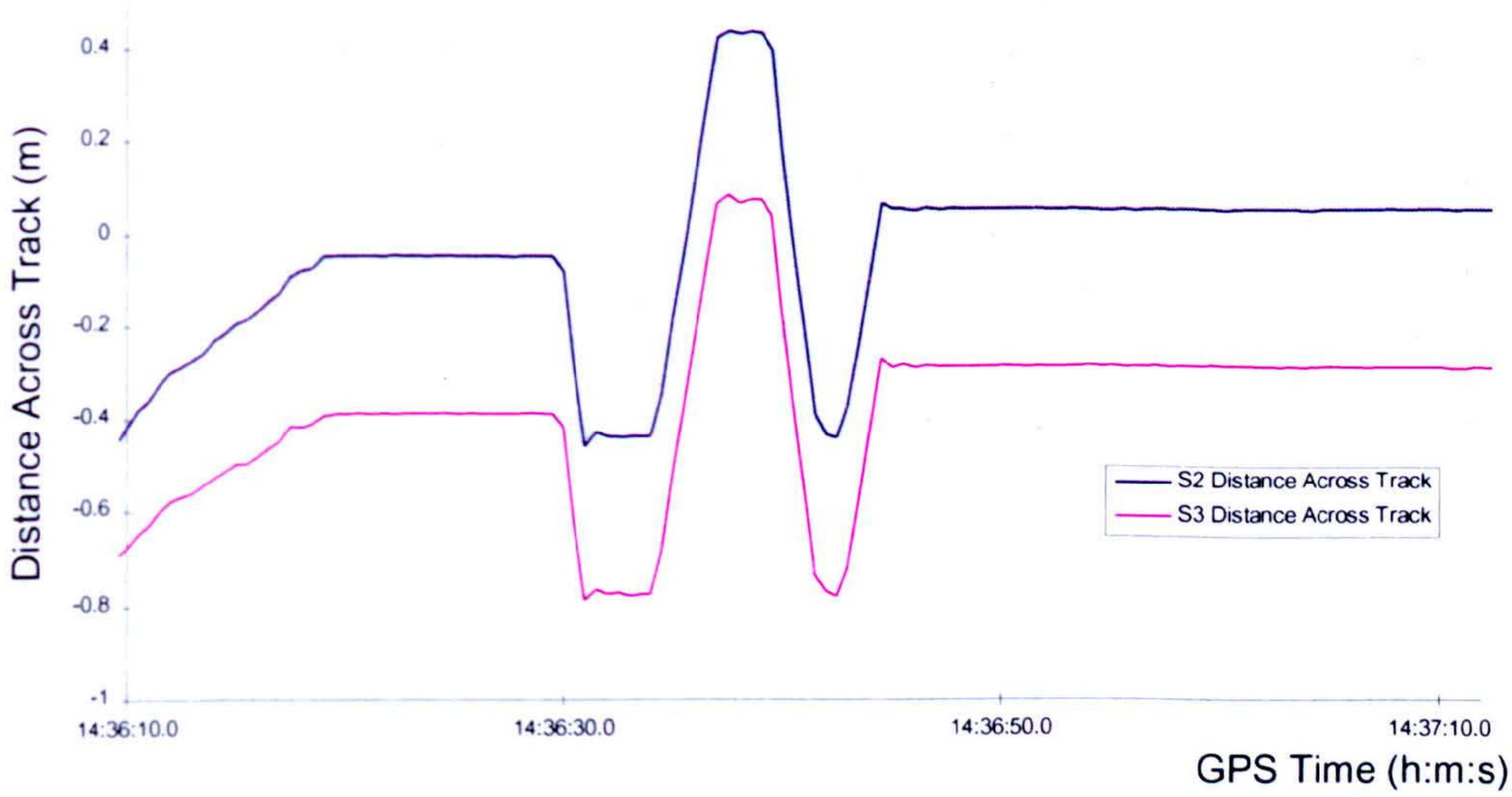

Figure 9.28
Distance Across the Track During a to and fro Tilting Manoeuvre, where the Blade was Moved from Left Hand Tilt to a Right Hand Tilt and Back Again.

The antenna located at S3 was situated over the pivot point, and S2 off-set to this by 0.9 metres. During this manoeuvre, it can be seen in figure 9.26 that the height of the antenna situated on location S2 is seen to change more than S3. This is to be expected, as S2's base would in fact drop its height, whilst S3's wouldn't, and would simply pivot about it's base. It can be seen, however, that even though the change in height at S2 is far more noticeable than S3, the latter does in fact show a change in height.

One possibility with this technique would be to locate the GPS antenna off set from the pivot point, as S2. The distance across the track plot, figure 9.28, shows that both antennas do move by the same amount during the manoeuvre. This is to be expected as they are both located upon the same blade. It is, however, evident from the results that this technique could be used for such a purpose.

9.7 Conclusions and Recommendations

The experiments and results discussed in this chapter have indicated that real time OTF GPS has potential positional precision to an order of a few millimetres. This means that it could be used for plant control and monitoring to a high order of precision.

The vibration due to the engine and plant movement is clearly evident in the results. The noise is amplified in these experiments due to the flexible poles used to attach the GPS antennas to the blade. These noise sources and other possible methods of attaching the antennas to the bulldozer should be examined, as well as the use of filtering algorithms to smooth out the data.

A working real time system which incorporates the OTF GPS data could be set up in a similar manner as that currently being used with the laser level system. Here, the real time OTF GPS coordinates would be used to control the blades height, according to its position, via the hydraulics of the bulldozer.

Multipath was not evident during the trials. This is thought to be because the antennas were located above the body of the bulldozer. This error source, however, is shown to be a problem with kinematic OTF GPS positioning in chapter 10. The positioning of the antennas is an important aspect of being able to successfully monitor and control construction plant by GPS.

The antennas used during these trials were geodetic and choke ring antennas. These proved adequate for the trials, but due to their weight may have caused a lot of the vibration. The use of smaller antennas would make this type of application more practical, however, these types of antennas can suffer more from multipath. Further research is necessary in this field.

Further work should also be carried out to investigate the use of tilt sensors and compasses to aid the GPS positioning of the blade. Such systems could help a single antenna on a blade to determine the direction of travel of the plant as well as the tilt of the mast.

The use of GPS/GLONASS receivers should be investigated in future trials. Currently, commercial GPS/GLONASS receivers are limited to single frequency. Dual frequency receivers are required for quick OTF GPS integer ambiguity resolution. When future dual frequency GPS/GLONASS receivers are made available, these would be very useful in environments where large buildings and foliage mask satellite signals. The use of a combined system would also give a quality control, as the two systems are separate, allowing possible positioning from both.

9.8 References

ACKROYD, N. 1996, *GPS and Civil Engineering,* Civil Engineering Surveyor GIS/GPS Supplement, Autumn 1996. pp 27 - 29.

AL-SHAMMARI, R. M. 1996, *Real Time Construction Plant Positioning by 'On-The-Fly' GPS*, MSc Thesis, University of Nottingham.

ASHKENAZI, V. MOORE, T. LOWE, D. MOORE, D. WOODWORTH, P. RAE, J. 1996, *Offshore Sea Measurement Using GPS,* Civil Engineering Surveyor GIS/GPS Supplement, Autumn 1996. pp 21 - 23.

KELLY, 1995(i), *Laser Curve Control Method,* Information Pamphlet, John Kelly Lasers, Broombank Road, Chesterfield Trading Estate, Chesterfield. S41 9QJ. ref JK SP11/95.

KELLY, 1995(ii), Data Sheet Number 2, *Laser Survey System,* Information Pamphlet, John Kelly Lasers, Broombank Road, Chesterfield Trading Estate, Chesterfield. S41 9QJ. ref JKL DS2/95.

KELLY, *Rideability Starts at Ground Level,,* Information Pamphlet, John Kelly Lasers, Broombank Road, Chesterfield Trading Estate, Chesterfield. S41 9QJ.

LEICA, 1990, *Wild NA2000 User Manual,* Leica Heerbrugg Ltd, CH-9435 Heerbrugg, Switzerland. ref G2159e-VII.90.

PRICE, W. F. and UREN, J., 1989, *Laser Surveying,* Van Nostrand International, ISBN 0 7476 0023 6.

SANSOME, B. W. W. 1996, *Real Time Construction Plant Control by 'On-The-Fly' Global positioning System Attitude Determination*, MSc Thesis, University of Nottingham.

SINBAD, *Sinbad Plant,* Information Package, Sinbad Plant Ltd, Hickings Lane, Stapleford, Nottingham. NG9 8PJ.

SPECTRA PHYSICS, *Road Construction - the Easy Way, Investment Pays!,* User manual, Spectra-Physics Laserplane, Mensura House, Blackstone Road, Huntington, Cambs. PE18 6EF.

SPECTRA PHYSICS, 1994, *Screed-Pro™ Modular Control System*, Information Pamphlet, Spectra-Physics Laserplane, Mensura House, Blackstone Road, Huntington, Cambs. PE18 6EF.

SPECTRA PHYSICS, 1995, *Laser Technology for the Construction Industry*, Information Pamphlet, Spectra-Physics Laserplane, Mensura House, Blackstone Road, Huntington, Cambs. PE18 6EF.

STEWART, M. P., FFOULKES-JONES G. H., OCHIENG, W. Y. and SHARDLOW, P.J., 1995, *GAS: GPS Analysis Software User manual. Version 2.3.* IESSG Publication, University of Nottingham.

UREN, J., 1996, *Controlling Construction Plant,* Engineering Surveying Showcase, February 1996. pp 13 - 16.

UREN, J., and PRICE, W. F. 1997, *Lasers in Construction - the Evolution Contimues.* Proceedings of the Institution of Civil Engineers, Civil Engineering, February 1997. pp 27 - 35. ISSN 0965 089 X.

Chapter 10

Monitoring Large Structures by Real Time OTF GPS

10.1 Introduction

The practical applications of real time OTF GPS are numerous. Chapter 9 has already detailed its use for precise plant monitoring and control. Another possibility includes measuring the movements due to deformations of large engineering structures (e.g. bridges, dams, tall buildings, chimneys, oil rigs, retaining structures and stock piles). Such analysis could allow safe future structure designs to be achieved, and also allow any dangerous or abnormal deformations to be detected instantly. Furthermore, real time OTF GPS could assist the positioning of large structural components during construction, thereby reducing times and resources when compared to conventional surveying techniques.

The following chapter details a range of OTF tests and results carried out by the author on a selection of large structures throughout the UK. The use of real time OTF as a monitoring tool for the movements of the Humber Bridge is detailed in §10.2. The use of real time OTF to position the deck of the Dee River Second suspension bridge under construction near Chester is detailed in

§10.3. The use of real time OTF to monitor the movements of the Clifton Bridge, over the River Trent, in Nottingham is detailed in §10.4.

The results demonstrate the potential for such techniques to provide a real-time monitoring system, precise to the order of a few millimetres, once the integer ambiguities have been resolved. Furthermore, the tests show that multipath is a major limiting factor and the location of the GPS antenna upon the structure is vital for precise positioning.

10.2 Real time On-The-Fly GPS monitoring of the Humber Bridge

This section describes the way in which the Humber Bridge was monitored using real time OTF kinematic GPS. The results show remarkable precision of the order of a few millimetres in plan components with a slightly worse precision in the height component. They demonstrate that the technique allows the collection of real-time deflection data which could be used to determine the deformation characteristics of the bridge and eventually provide a 'structural failure alarm' capability.

The Humber Bridge is located across the Humber Estuary on the east coast of England. Consisting of three sections, in an approximately North-South direction, the bridge spans 2220 m, supported by two towers 155.5 m in height. The bridge has been designed to withstand movements of up to ±4 m. The main span is amongst the longest in the world at 1410 m, compared to those of the Severn and Bosporous at 988 m and 1074 m respectively [THE HUMBER BRIDGE BOARD (i)], [THE HUMBER BRIDGE BOARD (ii)].

To enable real-time monitoring of the Humber Bridge by OTF kinematic GPS, several GPS antennas were located on strategic points on the bridge deck and

the support towers. The movements of each antenna were then continuously positioned relative to a reference receiver, situated 1.5 km away from the bridge, on top of the bridge's control tower. This had initially been coordinated through static GPS from a known ETRF89 coordinate on the IESSG building, using 6 hours of static data, and a precise ephemeris and the IESSG's GPS Analysis Software (GAS) [STEWART *et. al*, 1995].

The equipment used for the Humber Bridge monitoring experiment consisted of Ashtech Z-XII dual frequency GPS receivers, Racal Delta Link II UHF telemetry links [RACAL, 1995], and a real time version of Ashtech's PNAV processing software run on a Pentium-90 laptop PC as detailed in §8.2. Post processing analysis of the data was also carried out.

The analysis of the results suggest that the bridge's lateral movement at the mid span is of a simple harmonic nature, probably due to wind loading. The bridge deck also deforms in a vertical direction, but considerably less than that along the length of the bridge. The following section describes these initial tests, and illustrates the potential of 'kinematic GPS' for the real time in-situ monitoring of large structures. In all, three separate field trials were carried out on the Humber Bridge, using a variation of GPS antenna types, variations in the method of attaching the antennas to the bridge and different processing techniques.

The data analysis was carried out to assess the precision of the real time OTF system on such structures, and indeed whether real time OTF GPS would work on structures with large overhead obstacles such as cables. Movements are obviously seen in the results, and the author has tried to assess their causes. The author was not, however, trying to calibrate the movement of the bridge against external forces such as wind, water and traffic.

10.2.1 Bridge Deck Real Time Deformation Results - Trial 1

A GPS receiver was attached to the west side rail of the bridge deck, at approximately the mid span. This location would theoretically experience the greatest displacement. The GPS antenna was situated on top of a bipole, 2 m in length, which in turn was clamped to the rail. This test was carried out using the real time system, whereby the processing was carried out using the real time version of the Ashtech PNAV software described in §8.2, running on a Pentium 90 laptop PC.

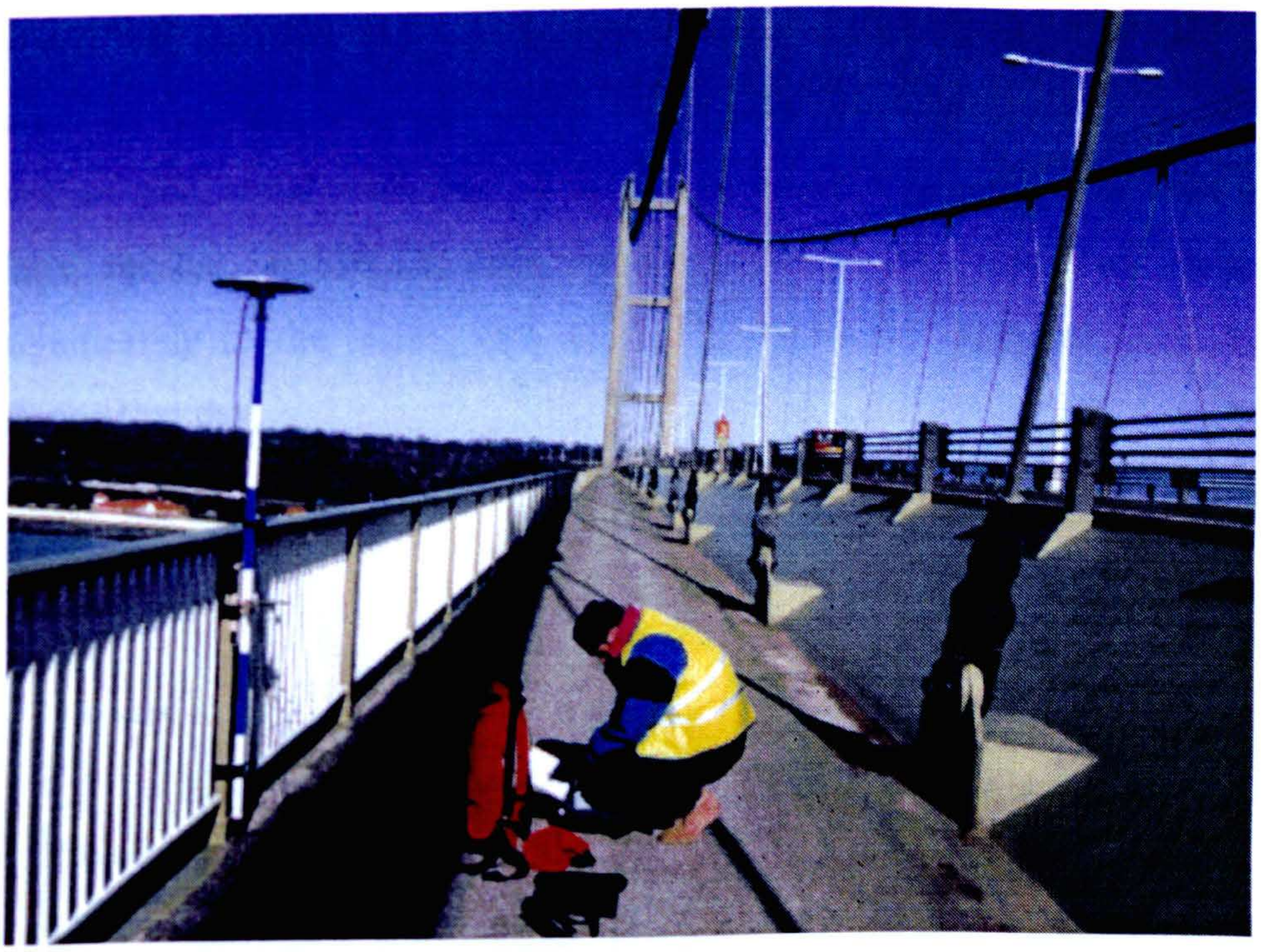

Figure 10.1

The equipment located at the mid span of the Humber Bridge. The GPS antenna is attached to the bridge via a bipole, firmly attached to the barrier. The Ashtech Z-XII GPS receiver was located inside the orange rucksack, which also houses the UHF telemetry link. The real time OTF processing was carried out on a Pentium-90 laptop PC, loaded with Ashtech's Real Time PNAV software.

The data links for this configuration presented no problems. The only signal loss which was experienced was due to very high-sided vehicles obstructing the signal path, which was an infrequent event. It should be noted that the data link antenna at the bridge end was placed at an arbitrary height for this experiment. If placed sufficiently high, signal loss problems of this type could be eliminated altogether. Figure 10.1 illustrates the equipment set-up on the Humber Bridge deck during the first field test.

The wind during the trial on the 7 March 1996 was fairly low and in a generally North Easterly direction, along the length of the bridge, which may have contributed to the results. Figures 10.2, 10.3 and 10.4 show the results obtained from a selective period of time lasting for 15 minutes, when the wind speed was relatively low and did not appear to affect the flexible pole which attached the antenna to the bridge. The figures correspond to the longitudinal, vertical and lateral movement of the bridge respectively. It can be seen in the later results, in §10.2.3, that the vibration of this pole can contribute significantly to the errors, and hence the technique's apparent performance during that day.

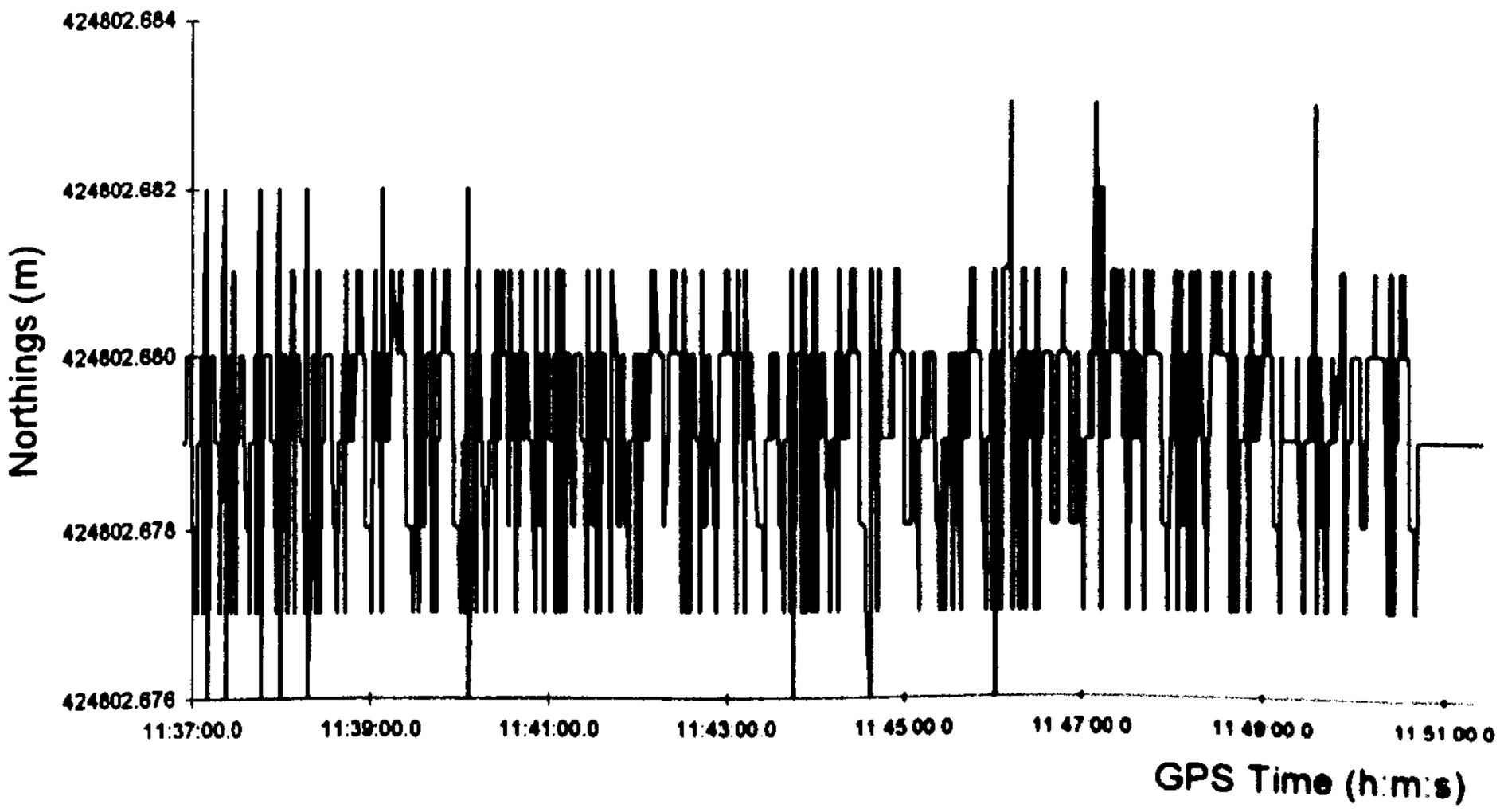

Figure 10.2

Longitudinal Movement of the Bridge Deck During Trial 1.

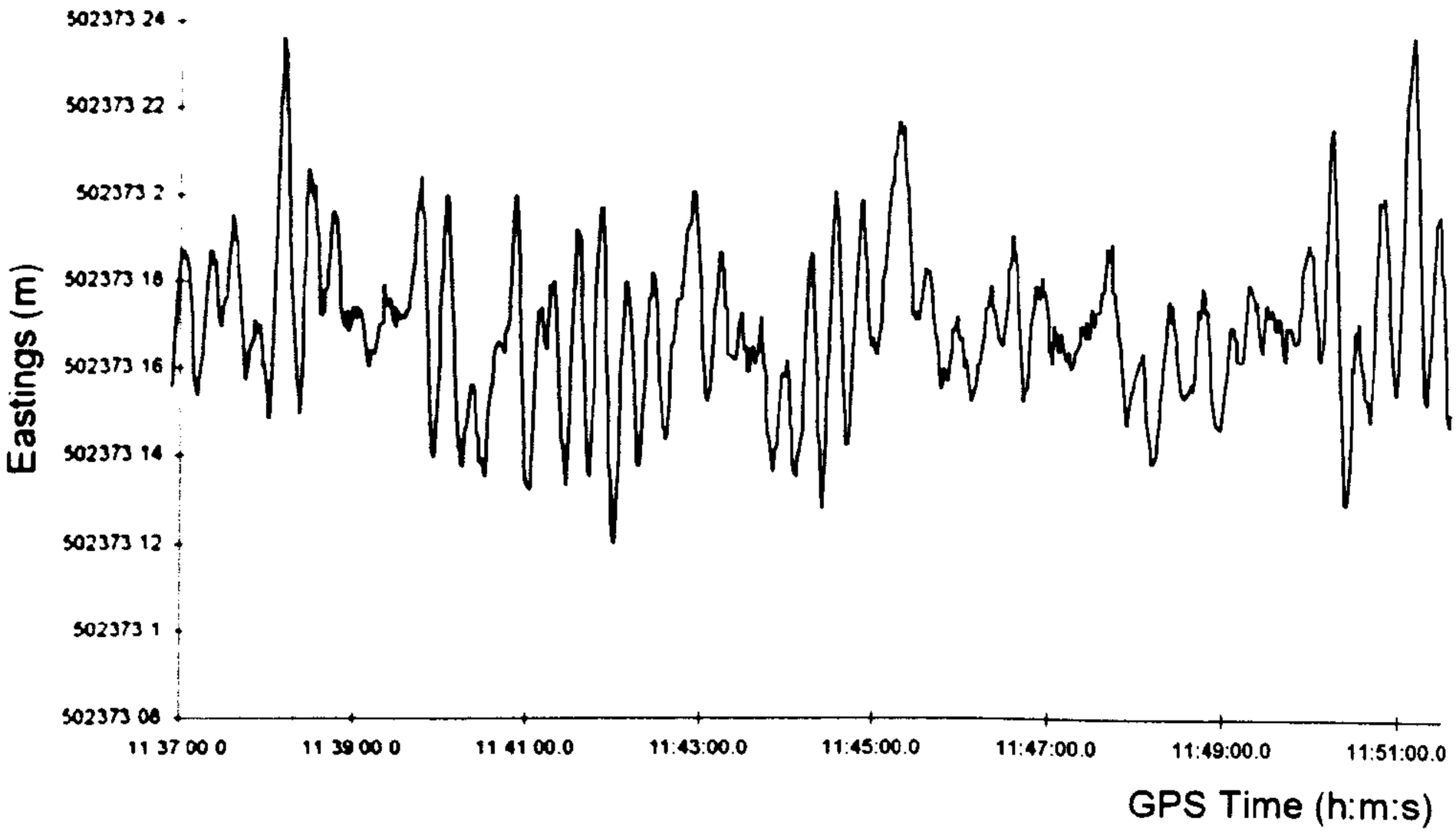

Figure 10.4

Lateral Movement of the Bridge Deck During Trial 1.

Figure 10.3 illustrates the vertical displacement, showing that the bridge moved by up to 40 cm at one point. This could be a result of the traffic loading or any other high frequency abnormal load in the vertical direction. Most of the vertical movements are of the order of 15 cm.

Figure 10.4 illustrates the East-West or lateral displacements of the bridge, covering a 14 cm range. From figure 10.4 it can be seen that the overall movement is constructed from both high and low frequency components.

10.2.2 Bridge Deck Real Time Deformation Results - Trial 2

Figures 10.5, 10.6 and 10.7 present deformation graphs corresponding to a longer series of tests, lasting for approximately 75 minutes. These tests were carried out on 7 May 1996, when the wind appeared to be more blustery and blowing in a North-to-South direction, i.e. approximately along the length of the bridge. The GPS antenna on the bridge was placed at a different location.

The data processing was, once again, carried out in real time using the Pentium 90 laptop PC and the Racal Deltalink II telemetry links, with the RTPNAV software. The GPS antenna was located on top of the bipole as in trial 1, which in turn was attached to the bridge's pedestrian rail.

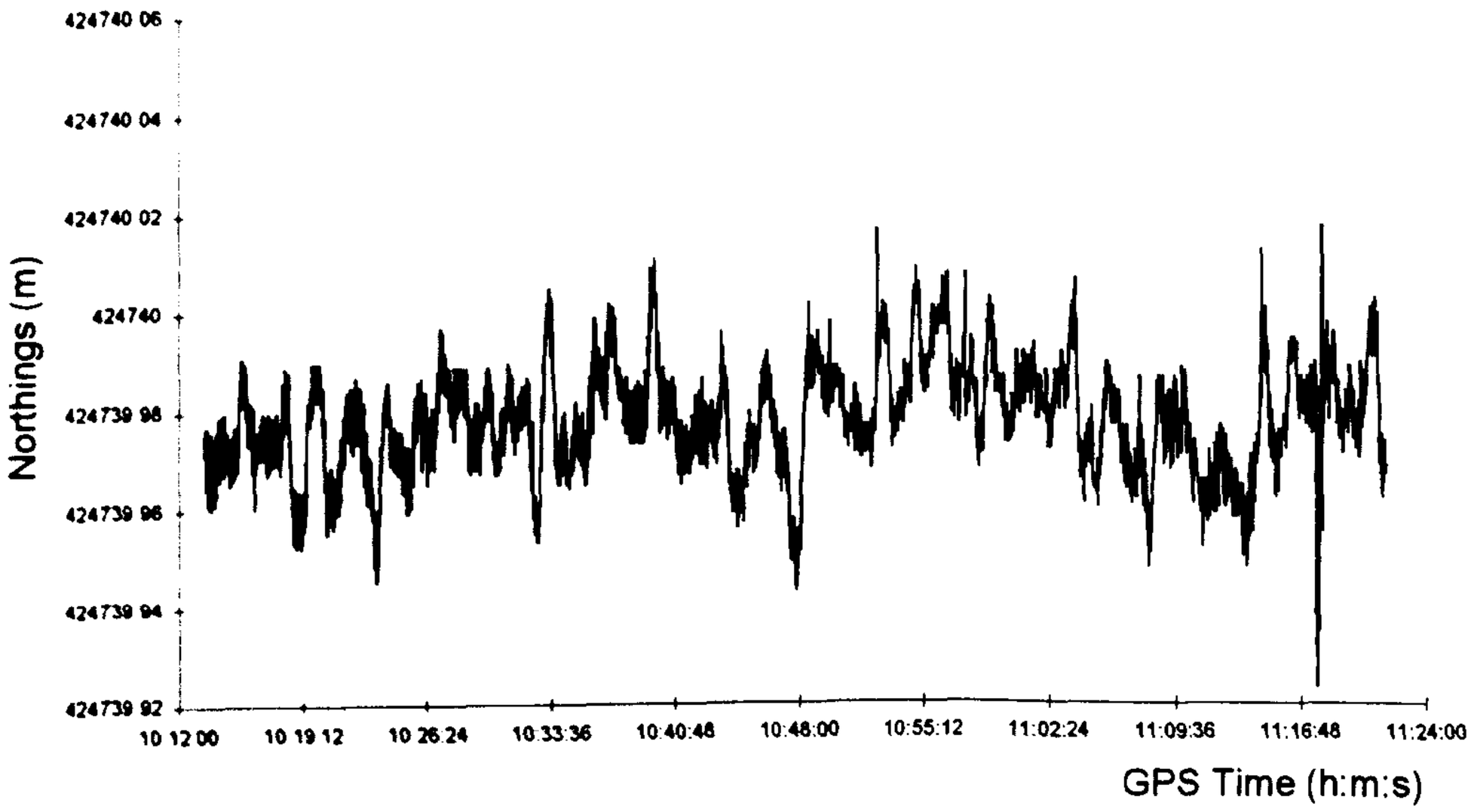

Figure 10.5

Longitudinal Movement of the Humber Bridge During the Second Trial.

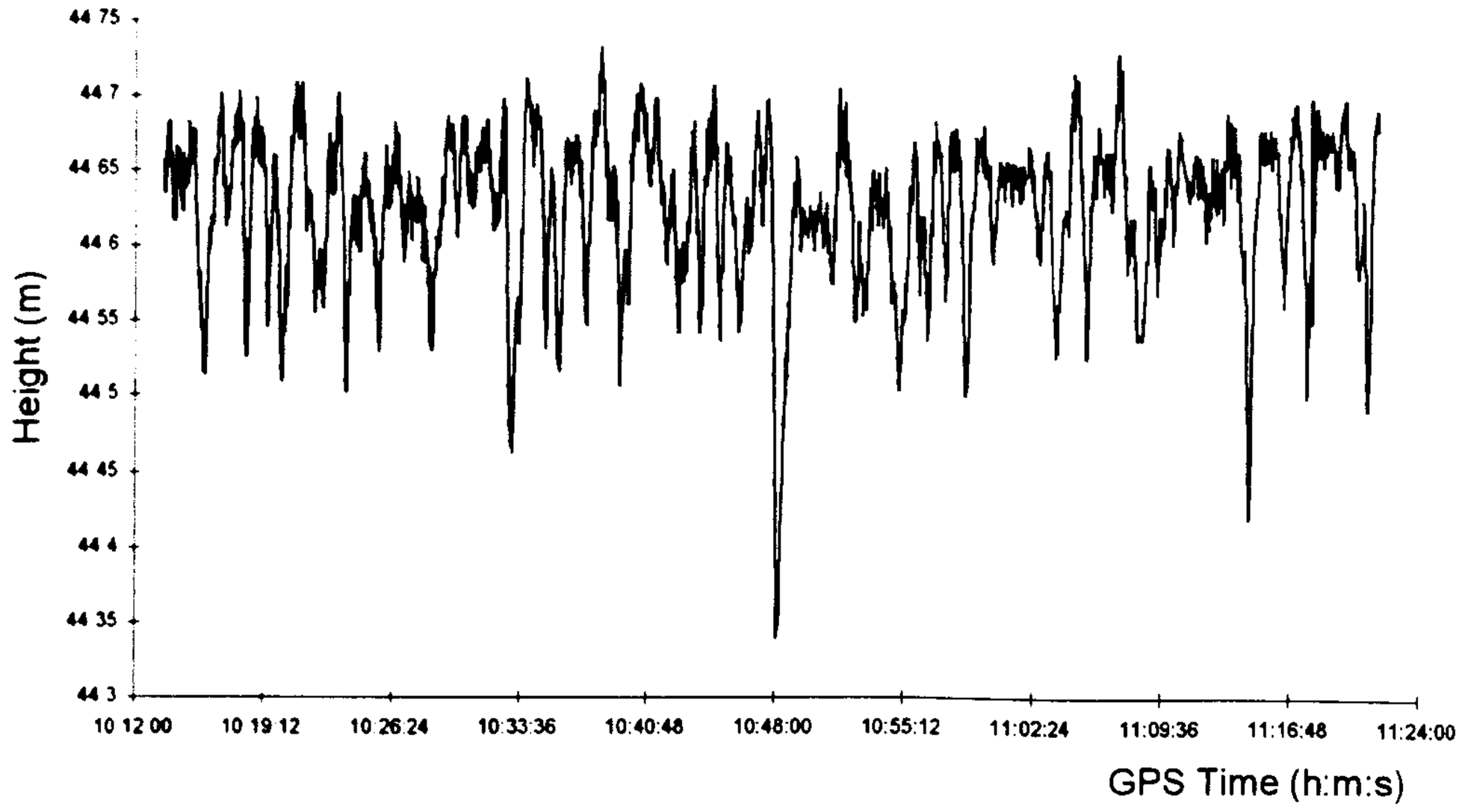

Figure 10.6

Height Deflection of the Humber Bridge During the Second Trial.

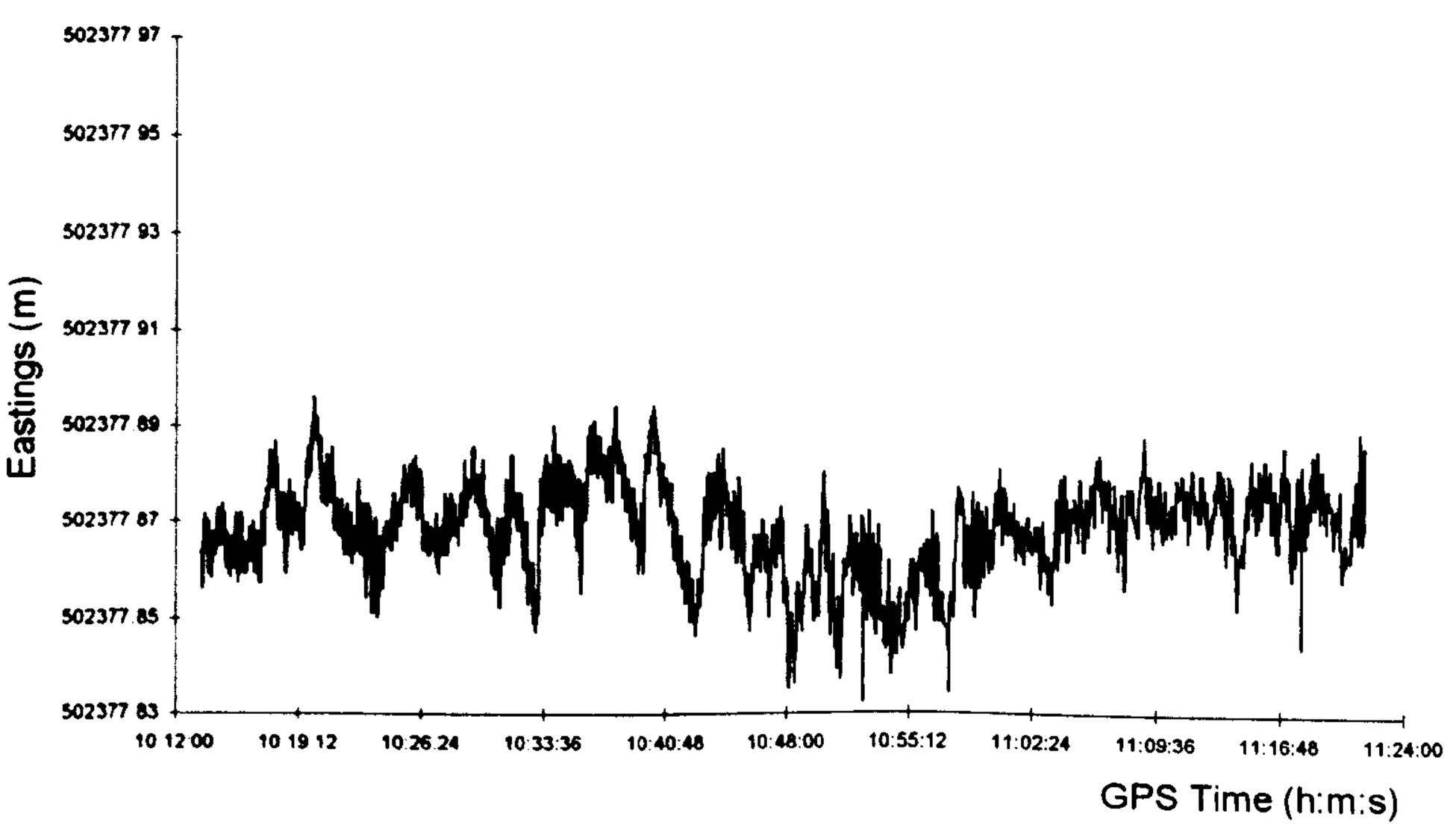

Figure 10.7

Lateral movement of the Humber Bridge During the Second Trial.

From the three graphs, it appears that the blustery winds has caused a vibration of the bipole holding the antenna to the bridge. This is particularly evident in Figure 10.5, where the longitudinal movements of the bridge over the 75 minute observation period are of the order of a few centimetres rather than millimetres

as in the previous test (Figure 10.2). Nevertheless, there is a close agreement between the expected movements of the bridge and the GPS measurements in the same direction. Other contributors to the measured movements include the bridge's actual motion, and also the effects of multipath. Indeed, the results of trial 3 also indicate the presence of multipath and also indicate that movement of the bridge in the longitudinal direction, over a short period of time, can occur.

The movements shown in Figures 10.6 and 10.7 are in "broad" agreement with those shown in Figures 10.3 and 10.4 respectively. The vertical movements average about 15 cm, with occasional spikes apparently corresponding to heavy vertical loading (e.g. vehicles). The lateral movements are of the order of around 5 cm as a result of transverse loading (e.g. wind). The vibration of the pole caused by the wind, however, would mainly affect the horizontal position and not the height. The height values in Figure 10.6 are therefore thought to be true.

10.2.3 Bridge Support Tower Real Time Deformation Results - Trial 1

Tests were carried out during the first trial whereby a GPS antenna was situated upon the top of the northern support tower. Fifteen minutes of data was collected and processed relative to the reference receiver located on top of the control tower. Figure 10.8 illustrates the GPS antenna located upon the top of the support tower.

Figure 10.8

The GPS antenna located on the top of the bridge's northern tower.

Figures 10.9, 10.10 and 10.11 present the 3-D movements of the Northern Support Tower of the bridge in a North-to-South direction, East-to-West direction and Vertical direction respectively. In a real monitoring scenario, a series of several GPS antennas located at strategic locations on the bridge deck and towers could be operating simultaneously.

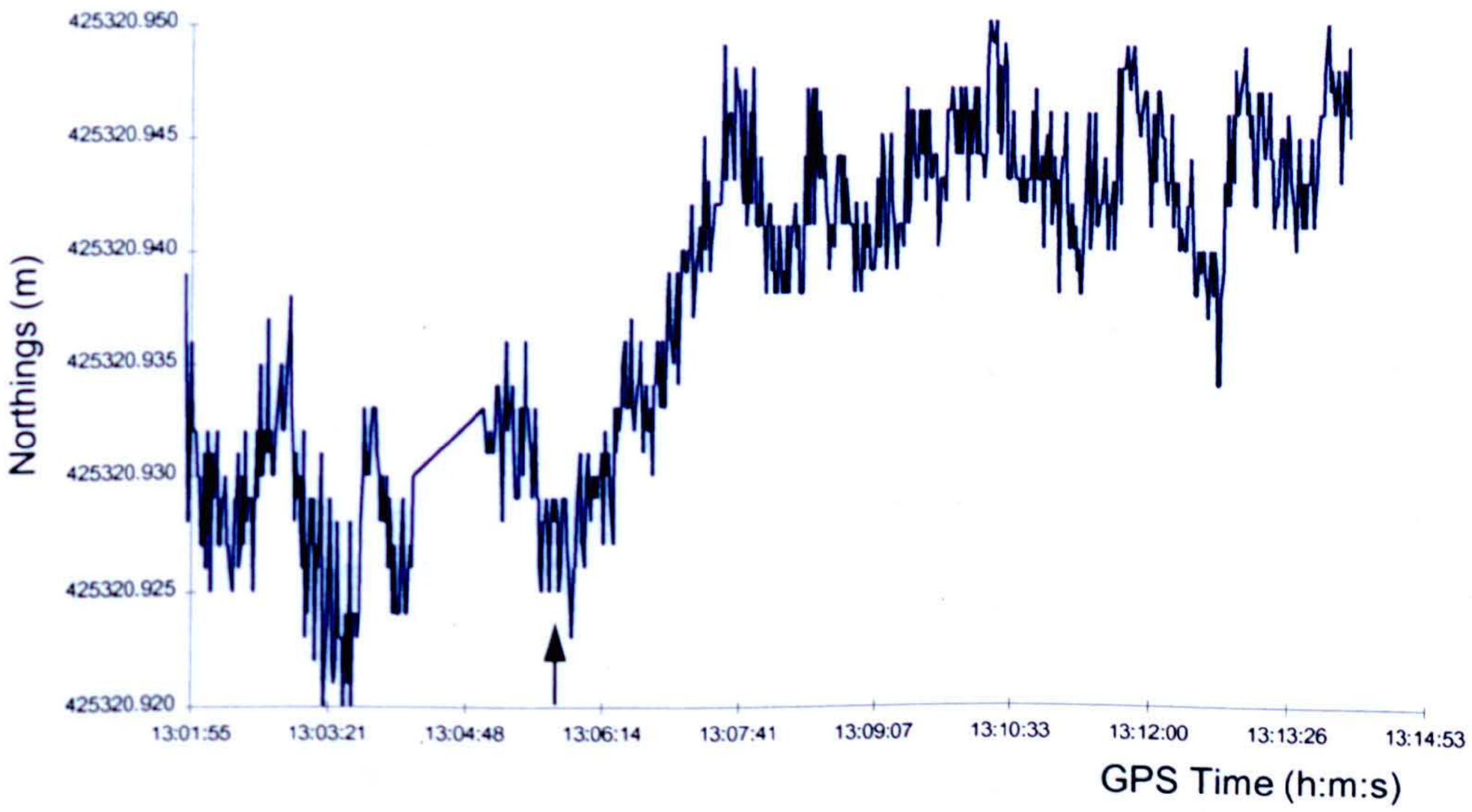

Figure 10.9

North-South Movement of the Northern Support Tower.

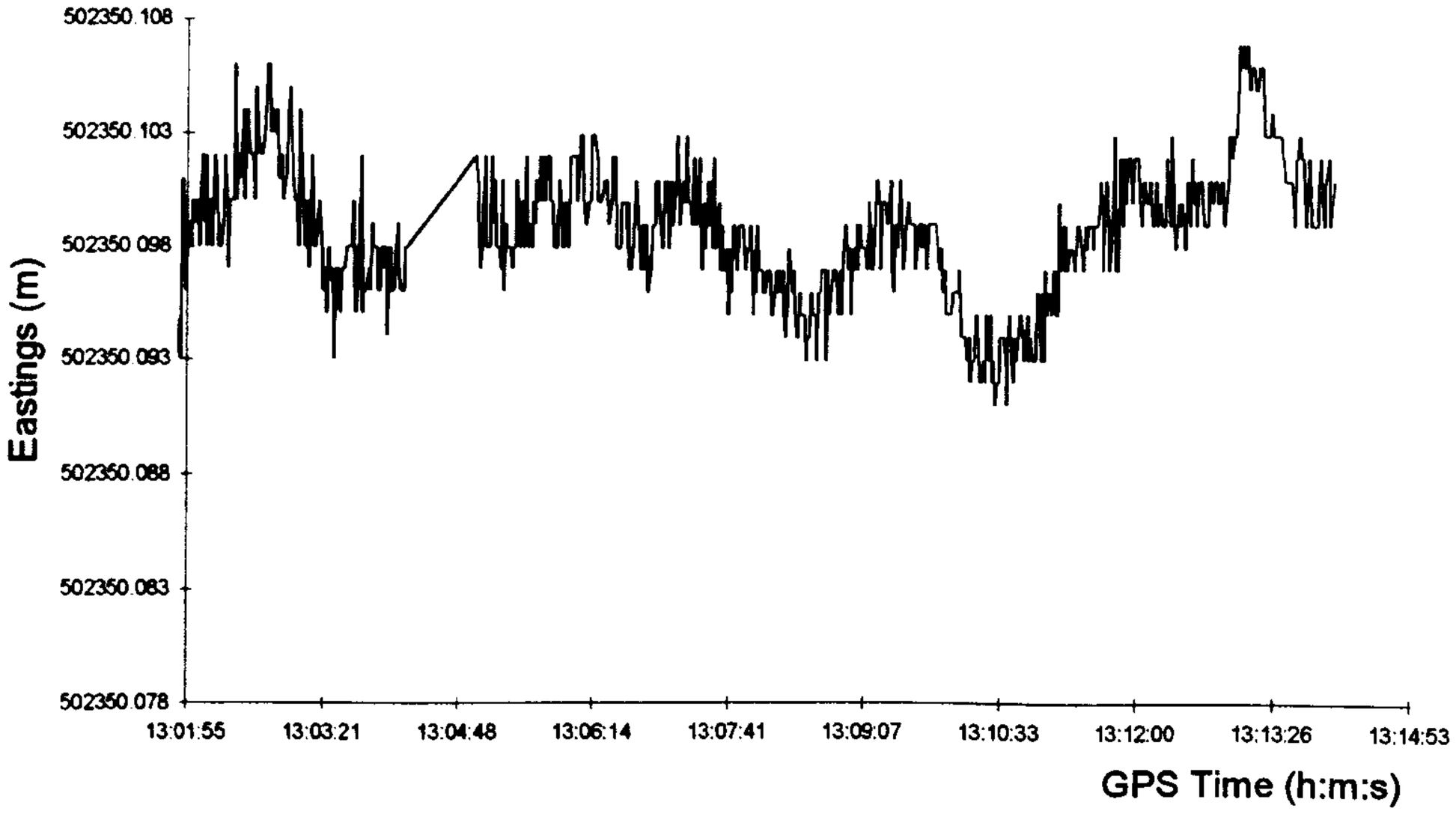

Figure 10.10

East-West Movement of the Northern Support Tower.

The North-South (along the bridge) movements of the order of 1 to 2 cm shown in Figure 10.9, and the East-West (across the bridge) movements, of 0.5 to 1 cm shown in Figure 10.10, are plausible. Some of this may be due to the noise of the GPS technique, some to actual structural movement and some due to multipath noise. The tower may be flexed through the bridge deck movements pulling on the support towers through the cables. This would cause a greater movement in the support tower in the North-South direction, as seen in the figures. However, the vertical movement of nearly 4 cm, over a period of 15 minutes, cannot be explained in terms of GPS noise alone, and requires further investigation. There is correlation between figures 10.9 and 10.11. At approximately 10:06:00, marked with an arrow on the graphs, sharp changes in the Northings and height are seen. However, in order to result in a height change of 3 cm, the tower would have to slant by over 3 m. It is possible that this apparent change in position is due to multipath, as in §10.2.6.

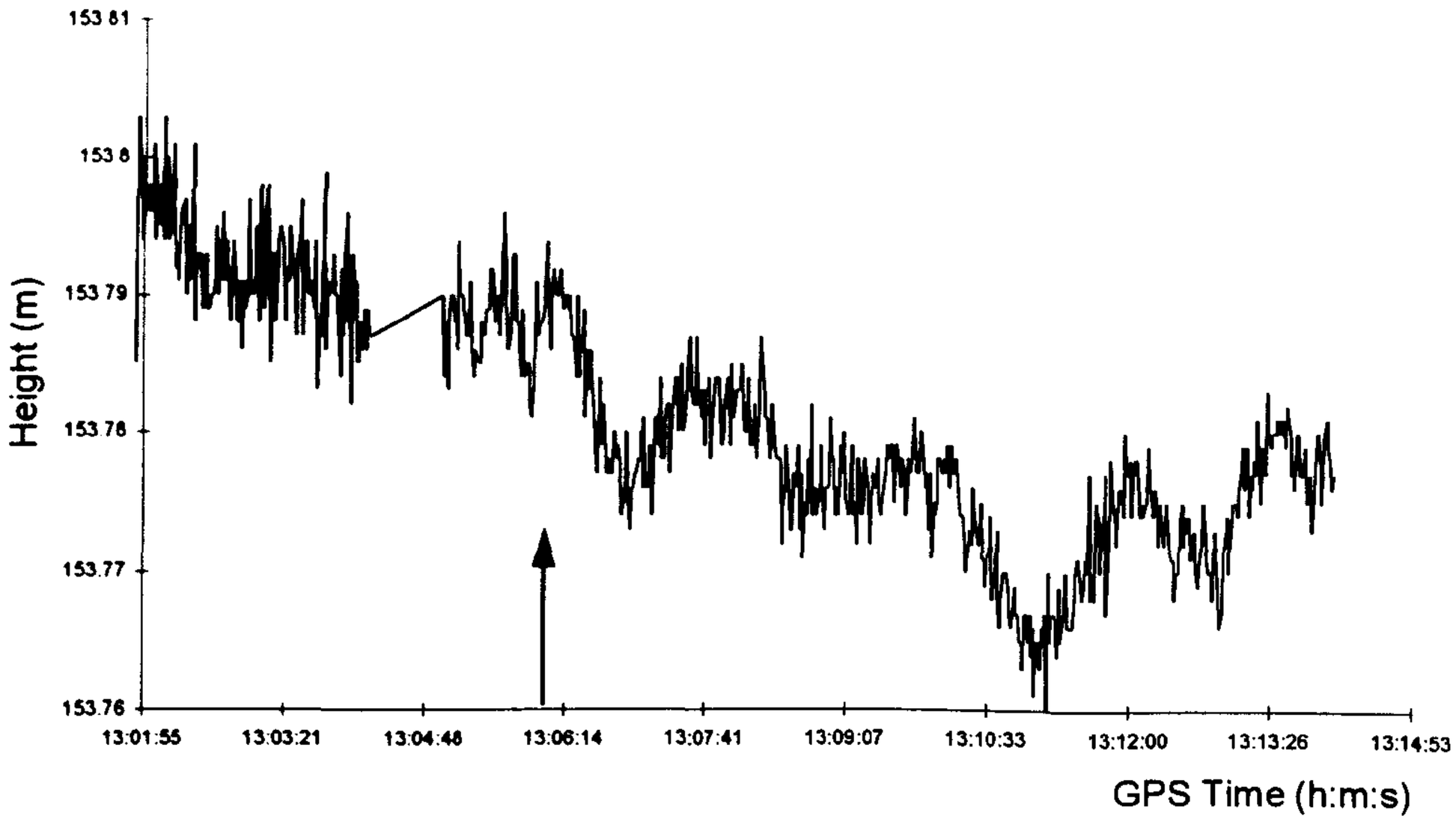

Figure 10.11

Vertical Movement of the Northern Support Tower.

10.2.4 Bridge Deck Real Time Deformation Results - Test 3

Due to the evident vibration of the pole connecting the GPS antenna to the bridge deck, further tests were carried out. During this third trial, two GPS antennas were situated upon the bridge deck. They were both situated near the mid-span, approximately 2.5 m apart. The antennas were clamped during this test onto the hand rail on the side of the deck. Figure 10.12 shows the two GPS antennas clamped onto the Humber Bridge rail, a similar set-up was used on the Clifton Bridge, §10.4. Using the clamps ensured the effects of vibration were minimised. Two antennas were used during the trial in order to determine the precision of the GPS results. The data from the two GPS receivers located on the bridge were processed relative to the reference receiver situated on top of the control tower. The resulting vector between the integer fixed OTF coordinates of the two bridge receivers was analysed at every epoch. Again, the analysed results were those of the fixed integer ambiguity values. This

provides the most precise solution. Gaps seen in the data are due to cycle slips or loss of lock in either of the two bridge receivers.

Figure 10.12

Two GPS Antennas Clamped onto the Side Rail of the Humber Bridge.

The trial was carried out over two sessions, each lasting approximately 1¼ hours. During both sessions, the GPS data was recorded at ½ second epoch intervals. Post processing was carried out on the data as the software and hardware was not capable of performing ½ second real time OTF processing at the time of the trial. Choke ring antennas were used the trial, enabling multipath to be reduced.

The GPS data was post processed using the Ashtech PRISM/PNAV software [ASHTECH (i), 1994] using forward processing only to emulate real time processing. The resulting datafile contained WGS84 Latitude, Longitude and ellipsoidal height at every epoch. An example of this data file can be seen in Appendix F. To provide an understandable representation of the movements of the bridge, the WGS84 coordinates were converted into movements along the bridge's length, across the bridge and it's height. In order to do this, the

WGS84 coodrinates were transformed into OSGB36 and then projected onto OSGB National Grid using the IESSG WinCODA software. The OSGB National Grid coordinates were then changed into movements along and across the bridge's length in a similar manner as discussed in §9.6, through using the average azimuth between the two bridge antennas as being that of the bridge. An example of a typical OSGB National Grid data file can be found in Appendix F.

Figures 10.13, 10.14 and 10.15 illustrate the along bridge (longitudinal), across bridge (lateral) and height movements respectively for the first half of trial three for one of the two GPS antennas.

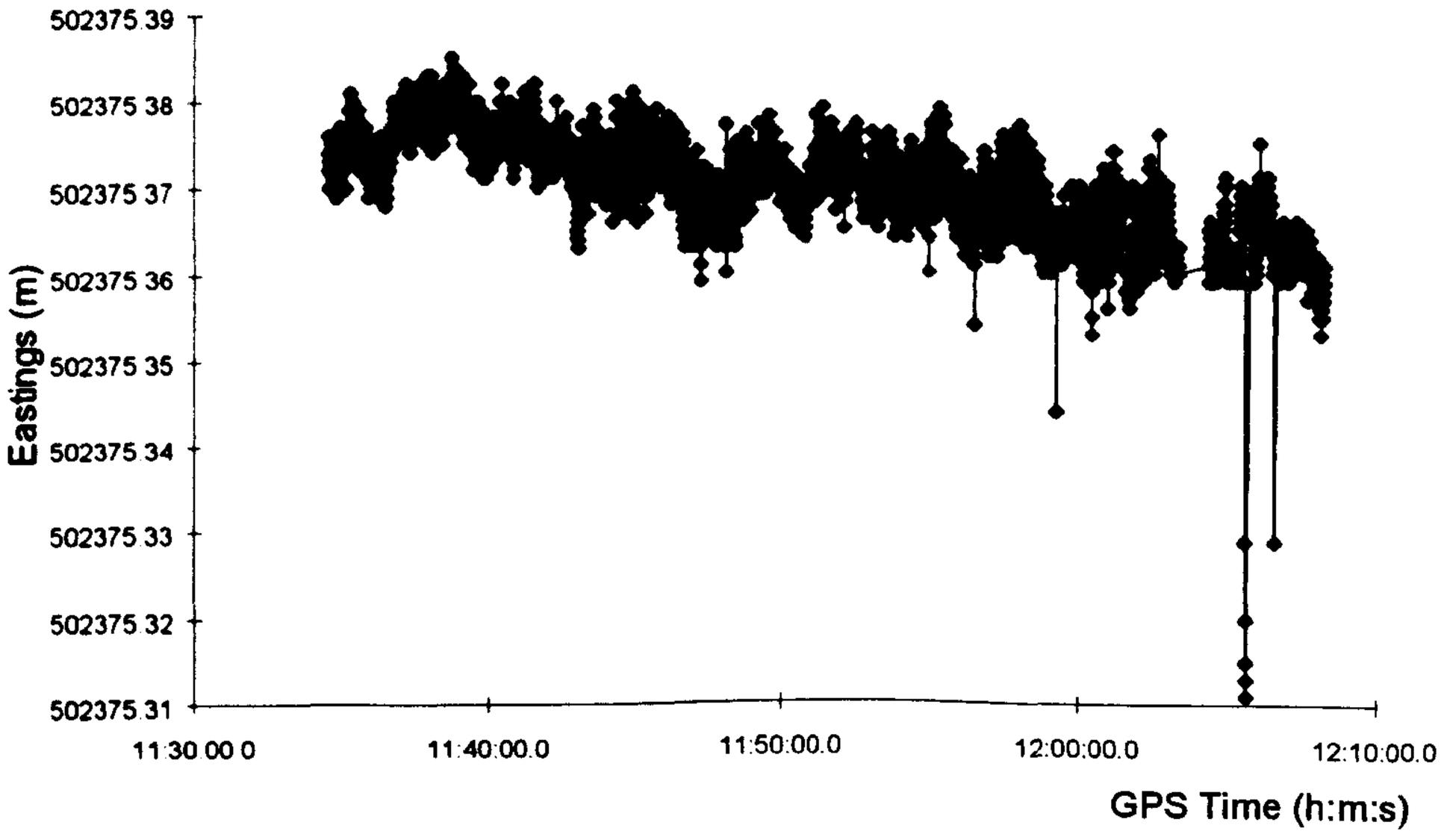

Figure 10.13

Lateral movement of the Humber Bridge During the Third Trial.

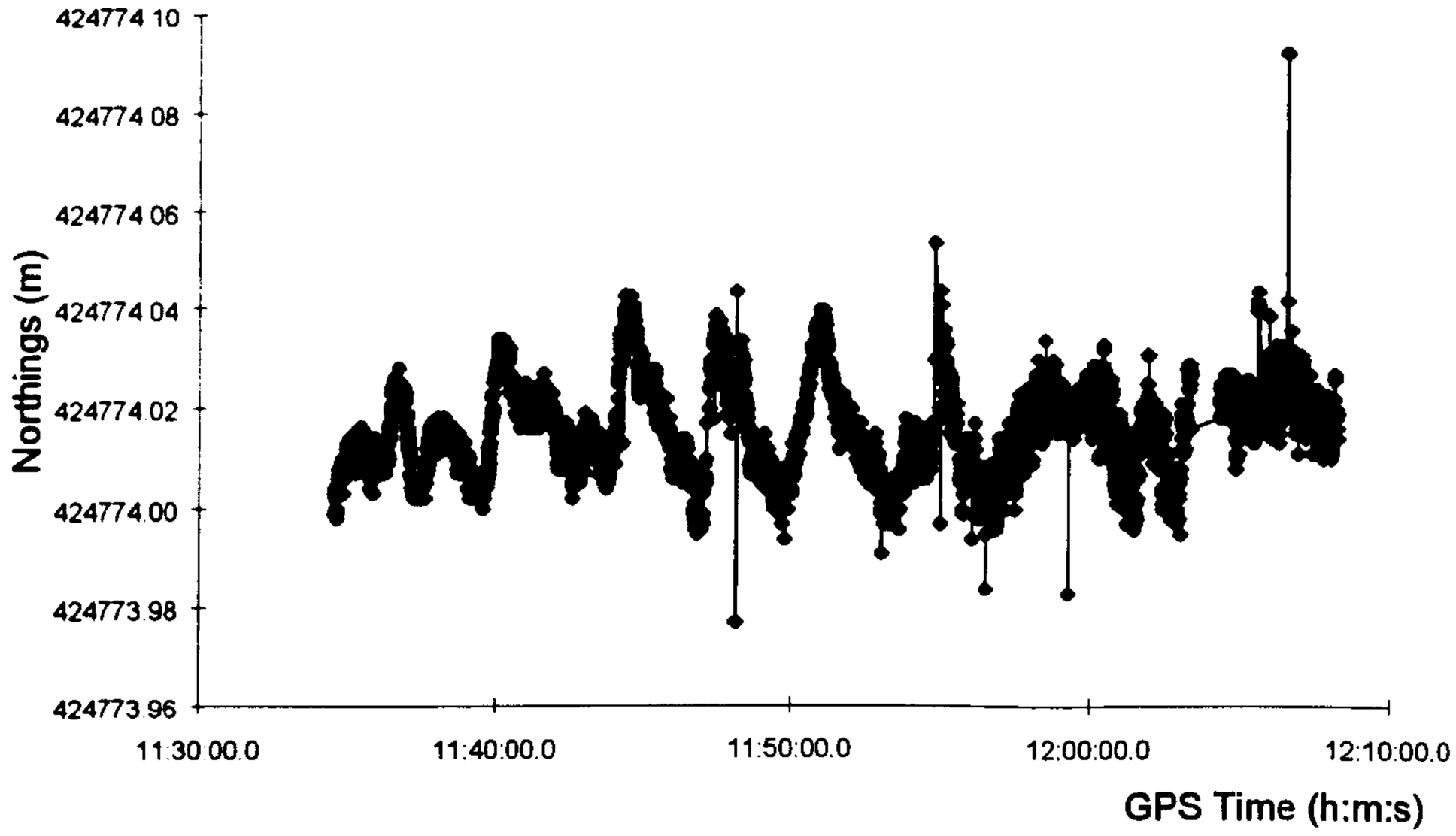

Figure 10.14

Longitudinal movement of the Humber Bridge During the third Trial.

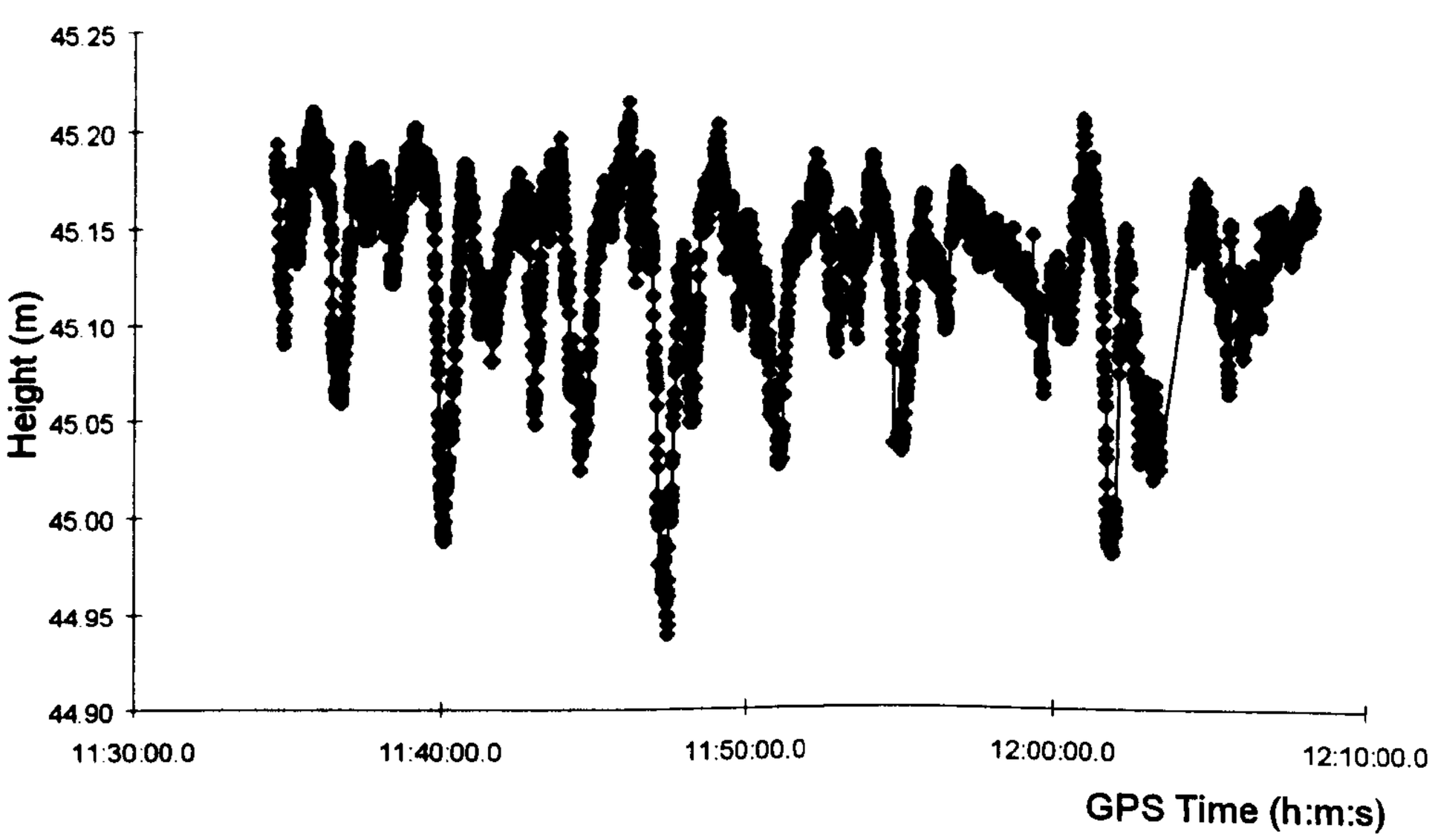

Figure 10.15

Vertical movement of the Humber Bridge During the Third Trial.

The figures show that the Eastings (lateral) movement of the bridge is in the order of 30 mm, whilst that of the Northings (longitudinal) component is if the order of 50 mm. The type of movements seen in these two figures are both different. Figure 10.13 shows a lateral movement which gradually changes by

around 30 mm over a period of 30 minutes. Within this gradual change, there is a constant scatter of ± 5 mm. Figure 10.14 shows the longitudinal movement of the bridge, which is seen to fluctuate by up to 50 mm. The movement could be due to the expansion joints on the bridge expanding along the direction of the bridge.

Figure 10.15 illustrates the vertical movement of the bridge deck during the period. Here, it can be seen that the GPS results suggest that the bridge has a fluctuating movement, of up to 270 mm. These figures, however, are simply the resulting OTF GPS coordinates, which may be influenced by many types of noise. The noise and truth of the figures can be determined through the following Figures, 10.16, 10.17 and 10.18.

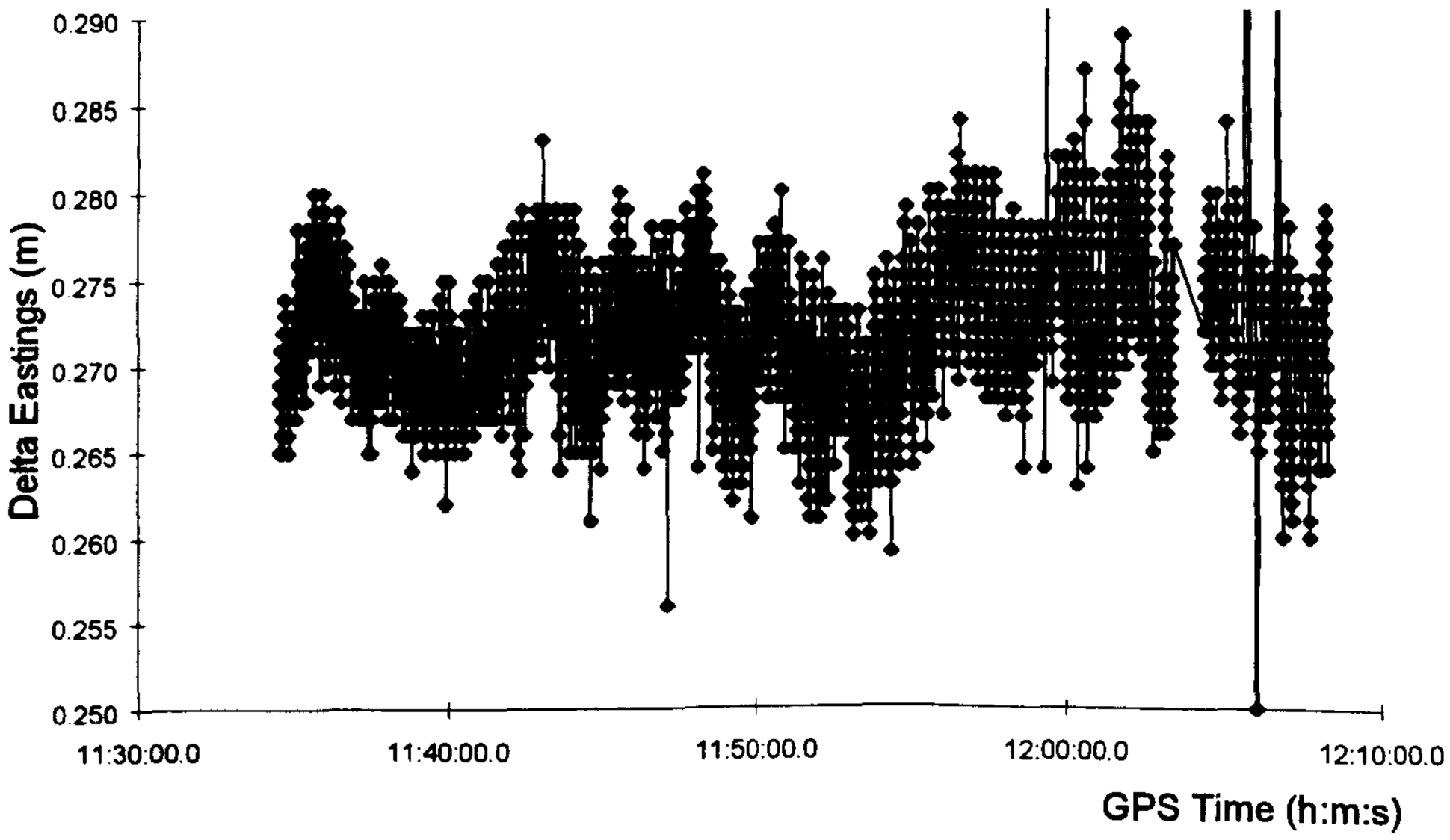

Figure 10.16

Lateral Vector Between the Two GPS Antennas Situated Upon the Humber Bridge During the Third Trial.

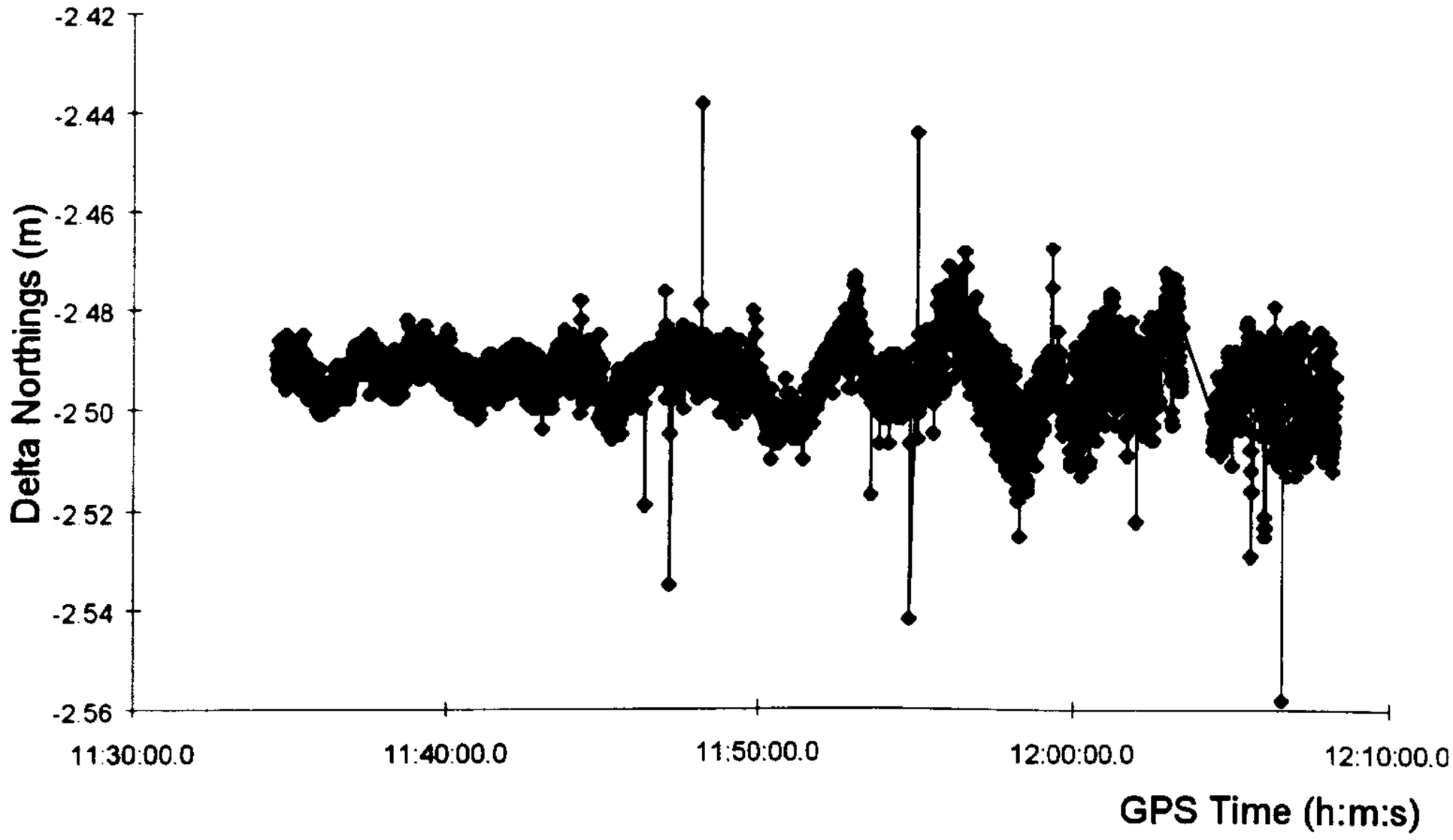

Figure 10.17

Longitudinal Vector Between the Two GPS Antennas Situated Upon the Humber Bridge During the Third Trial.

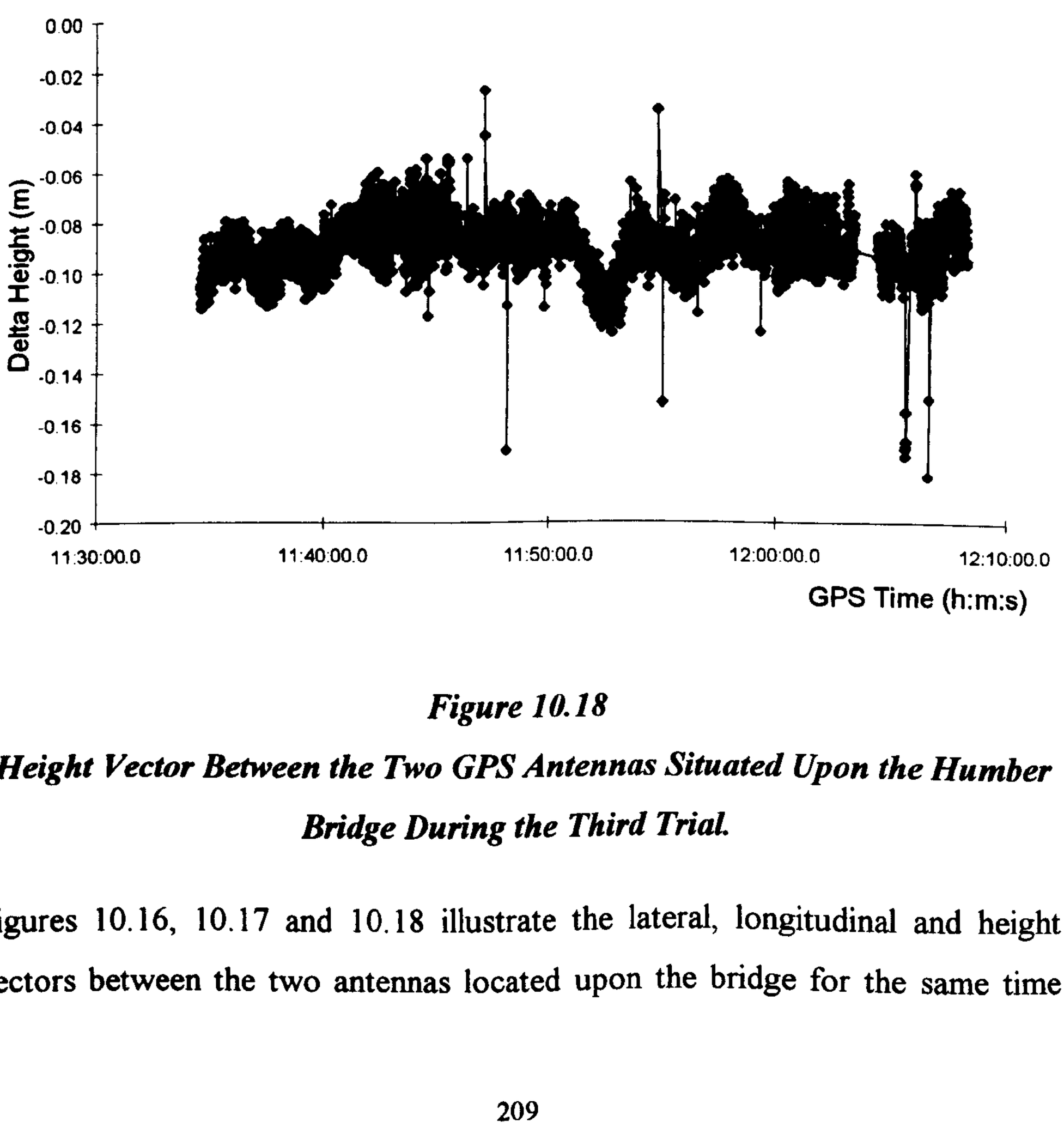

Figure 10.18

Height Vector Between the Two GPS Antennas Situated Upon the Humber Bridge During the Third Trial.

Figures 10.16, 10.17 and 10.18 illustrate the lateral, longitudinal and height vectors between the two antennas located upon the bridge for the same time

period as 10.13, 10.14 and 10.15. It can be seen from these figures that the plan vector has a scatter of ± 10 mm, and the height vector a scatter of ± 15 mm. These three graphs illustrate the possible precision achieved during the trial. The scatter is due to the measurement and processing noise expected to be a couple of millimetres, §8.4, and the remainder is thought to be due to multipath noise on one or both the antennas. Similar results are seen from the data taken from the second session during trial 3. These figures are presented in Appendix F.

10.3 Real Time Positioning of the Dee Estuary Bridge Deck During its Construction

A bridge crossing is currently being constructed over the River Dee, near Chester. The Dee Estuary Bridge is a single tower, cable stay suspension bridge, Figure 10.19 illustrates the bridge during construction. The construction is being carried out by Gifford Graham and Partners for Flintshire County Council, who own the bridge.

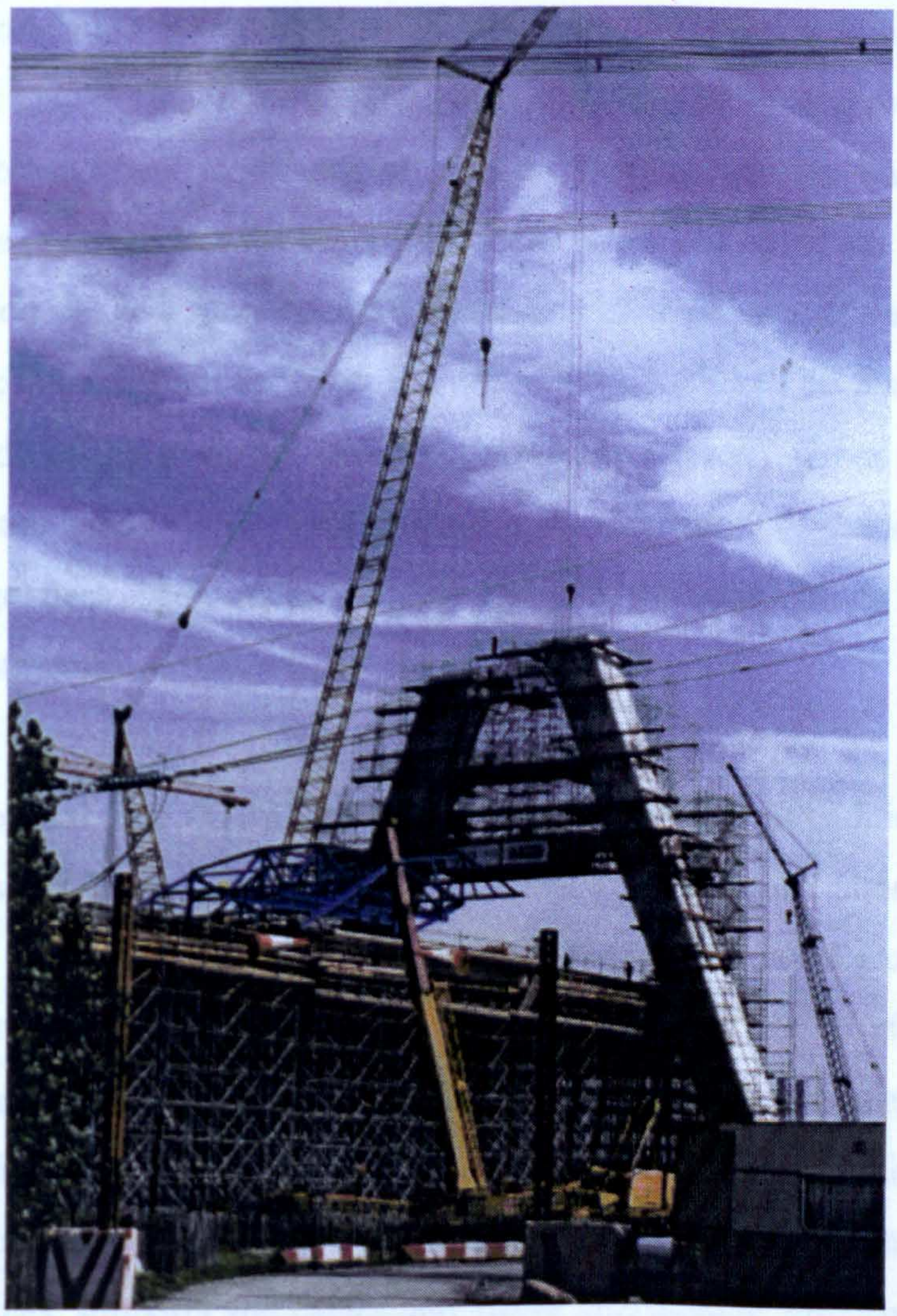

Figure 10.19

The Dee Estuary Bridge under Construction.

During construction, the tower is firstly erected, then the bridge deck is built out over the river, a section at a time. Once a section is built, the cable stays for that section are put in place, and are tensioned. The next section is then put in place and the procedure continues. This operation has been carefully planned, knowing the weight of each section, hence its moment force and the tension required in each cable stay to result in the bridge deck being accurately positioned as planned. Terrestrial survey techniques, such as levelling, angle measuring and distance measuring, are all used to check whether the sections

have been located correctly. This can be a lengthy and costly procedure, and the result may not necessarily determine which section is incorrectly placed or which cable has been incorrectly tensioned. This procedure is carried out until the bridge deck reaches the other side of the river, and hopefully agreeing with the position of the structure on the other side of the river. If the bridge deck was not continuously monitored, the end result could well be that the deck on the far side of the river would not be in the right place. Other consequences could be the need to over tension or under tension some of the stays to "pull" the bridge deck back to its correct location, resulting in an un-uniformly stressed structure.

The use of real time OTF GPS has been investigated as an additional check to the terrestrial survey techniques, and perhaps as a future alternative. The reference station used for the GPS could be placed upon solid ground a couple of kilometres from the construction site, which would not be affected by the local construction process, and located away from any land movements caused by the soft ground situated near the river. Tests were carried out by the author, establishing whether real time OTF GPS could be used in such an environment where cranes, supports and cables may cause interference with the satellite and telemetry link signals. Furthermore, the Dee Bridge is being constructed near to a power station, from which high voltage power lines pass over the bridge, as seen in Figure 10.19 and maybe a possible cause of signal interference.

The tests had two prime objectives. Firstly to demonstrate the potential of GPS for real-time setting out and guidance of large construction projects and secondly to assess the precision of the technique in such environments.

The coordinates of a reference point were established by the author by processing 3 hours of GPS data relative to an ETRF89 coordinate at the IESSG building, using the IESSG's GAS package [STEWART *et al*, 1995] and a precise ephemeris [IGS].

Two sets of tests were carried out by the author. The first consisted of mounting a single GPS antenna onto a tripod upon the bridge deck. The second consisted of placing two GPS antennas mounted on tripods upon the bridge deck, as well as the reference receiver placed near the bridge. This allowed the vector between the OTF coordinates of the two bridge receivers to be established, in turn providing an indication of the precision of the technique in a typical construction environment.

10.3.1 Dee Bridge - Trial 1

The first test consisted of placing a GPS receiver upon the bridge deck and positioning it through OTF processing relative to the reference receiver. Post processing was carried out, as the data was gathered on the same day as that used to coordinate the reference station. Forward processing was used to simulate a real time system.

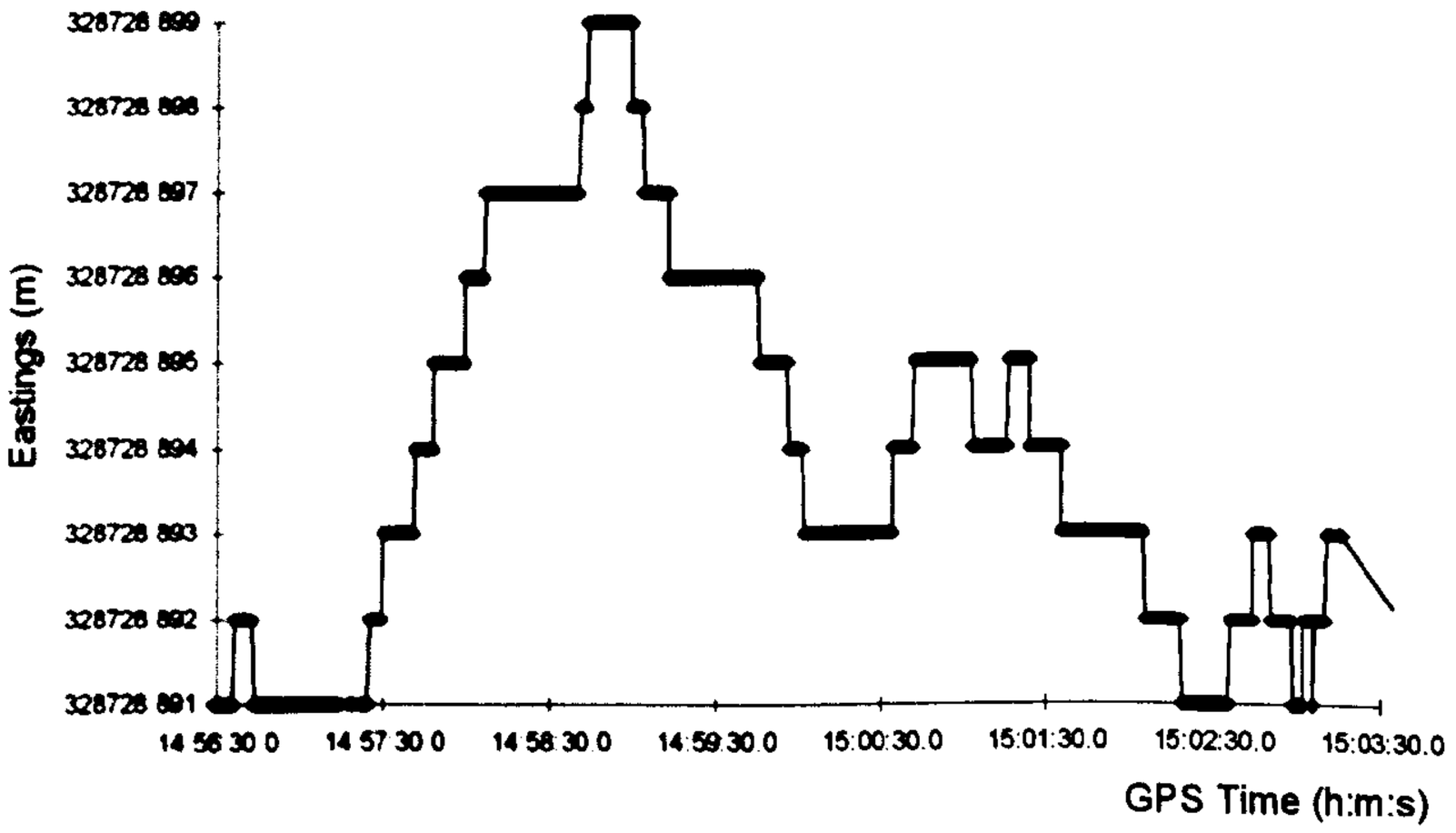

Figure 10.20

Dee Bridge Eastings During Trial 1.

The resulting fixed integer OTF coordinates are seen in Figures 10.20, 10.21 and 10.22, showing the bridge's Northings, Eastings and ellipsoidal height respectively.

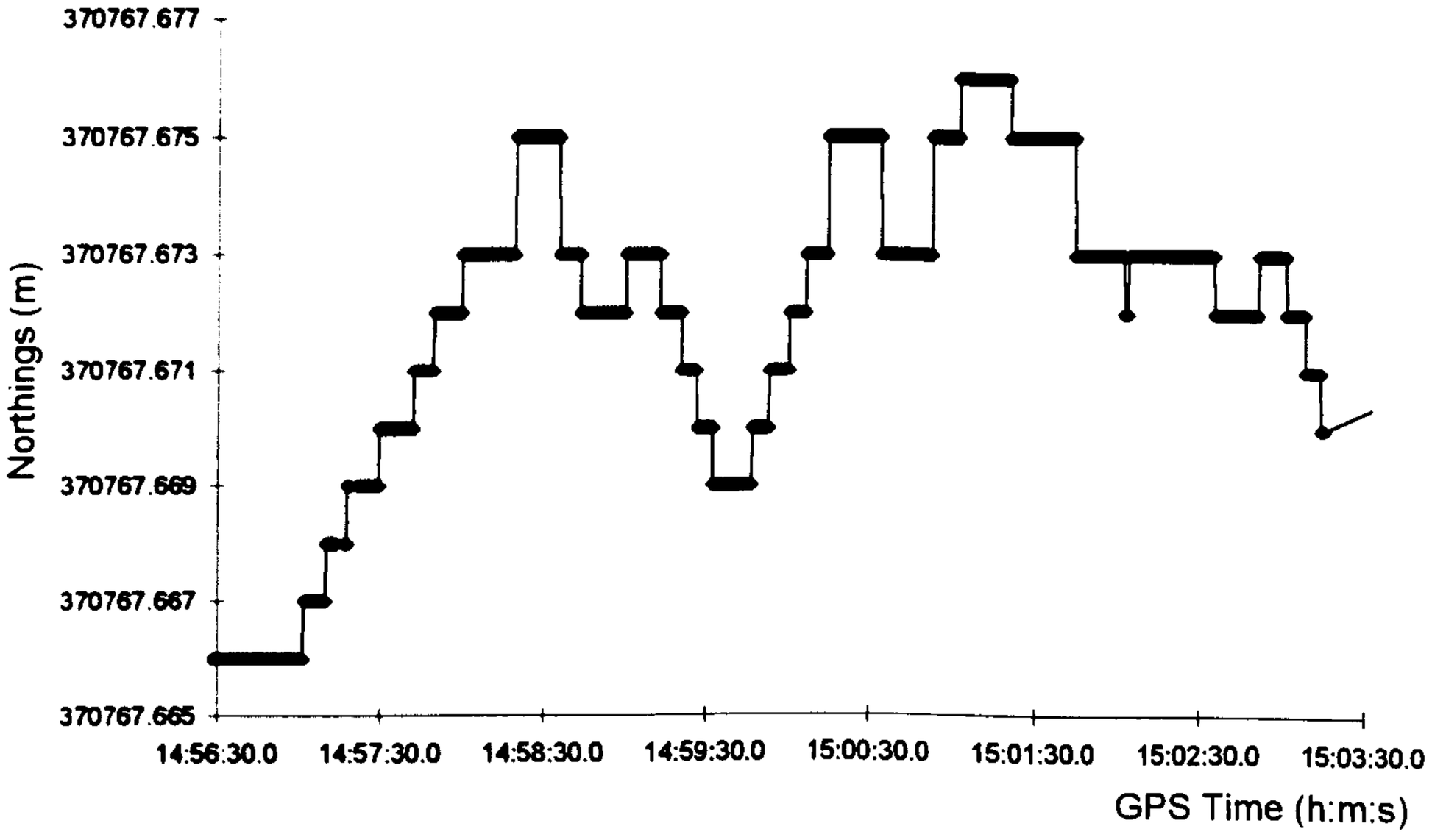

Figure 10.21

Dee Bridge Northings During Trial 1.

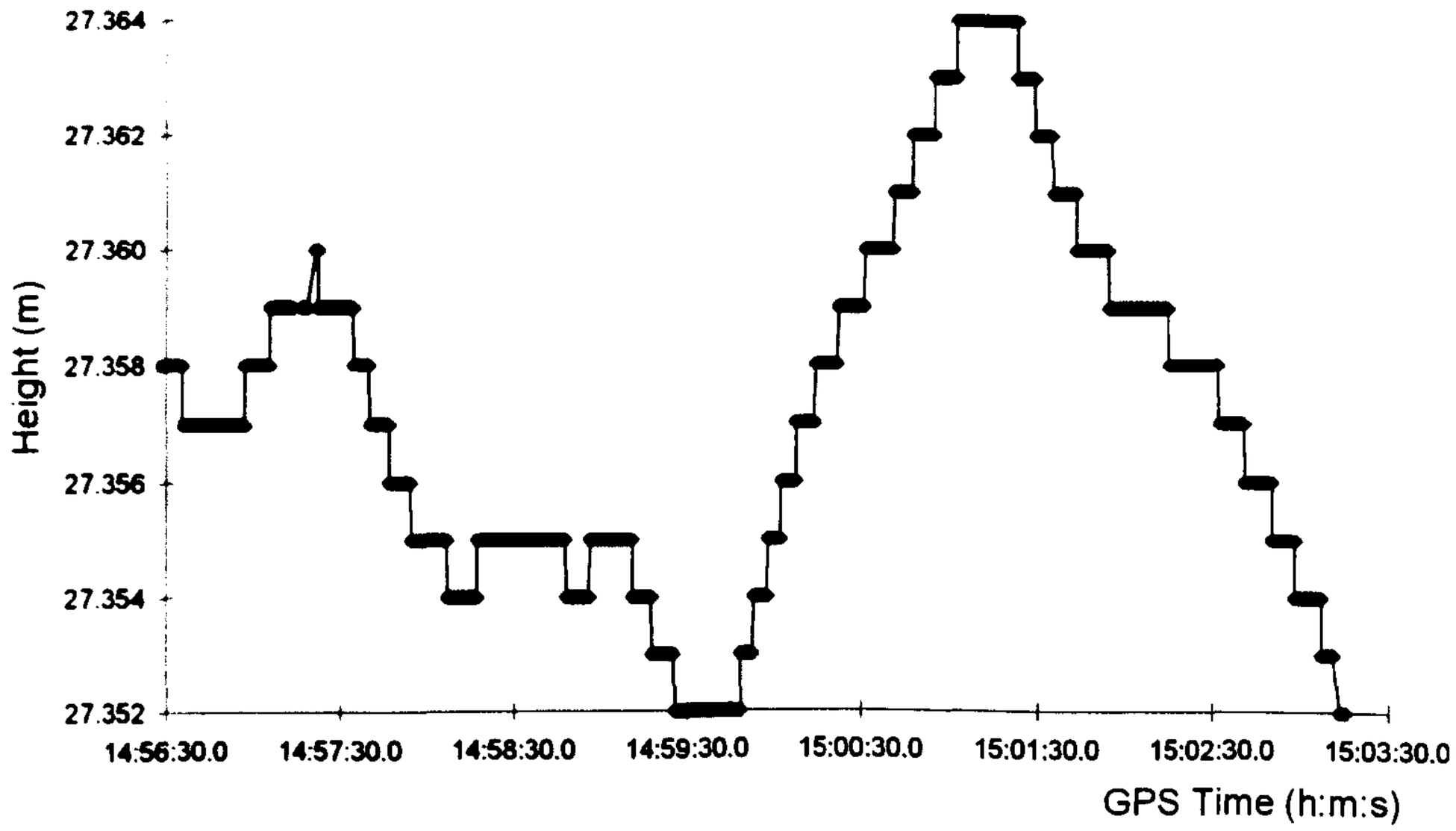

Figure 10.22

Dee Bridge Heights During Trial 1.

The bridge at this location was not expected to move, as it was a rigid structure, and there was no flow of traffic over it. Construction plant, however, was moving around at the time of the trial. These figures suggest that the resulting precision of the OTF coordinates are in the region of ± 5 mm at the start of the trial for both Eastings and Northings (Figures 10.20 and 10.21 respectively). At around 15:00:00, both the Eastings and Northings become more precise, at around ± 2 mm. The height component of the resulting coordinates vary by ± 4 mm during the first half of the trial, then again at 15:00:00, the precision changes, this time it becomes worse, at around ± 6 mm.

Whether or not this apparent movement is entirely due to GPS noise or in fact due to actual movement is difficult to say. The introduction of multipath from the overhead cables or other obstructions may be a cause of this noise. However, the bridge deck was saturated with workmen and plant, which may well have deformed the bridge by this amount at this location. Further tests should be carried out at this location on the bridge, taking data on consecutive

days at instances of the same GPS satellite constellation. Any multipath would be seen as a similar trend in the residual plots on a daily basis [SHARDLOW, 1990], [JACK, 1994]. The trend would be offset by 4 minutes every day, as the GPS constellation has an orbit period of 11 hours 58 minutes, and repeats itself every 23 hours and 56 minutes.

10.3.2 Dee Bridge - Trial 2

The second trial consisted of placing two Ashtech Z-XII GPS receivers upon the bridge deck, mounting their respective antennas upon tripods. The two receivers collected data at 0.5 second epoch intervals, and were positioned through post processing OTF techniques. Again, the processing was carried out to simulate a real-time scenario, which was not possible at this time due to hardware limitations. The receivers recorded approximately 40 minutes of data, which was processed using Ashtech's PNAV package [ASHTECH, 1994 (i)]. Figure 10.23 illustrates one of the two GPS antennas located upon the Bridge deck during Trial 2. It is evident from this photograph that obstructions are present, and could prove to introduce multipath noise. The photograph shows the presence of large obstacles which may be the cause of multipath errors.

Figure 10.23

An Ashtech Z12 GPS Receiver and Geodetic Choke Ring Antenna Situated upon the Dee Estuary Bridge During Construction.

Figures 10.24, 10.25 and 10.26 illustrate the results for Eastings, Northings and Height respectively, indicating that the bridge moved by up to 25 mm northwards, 10 mm eastwards and 30 mm in height. The bridge lies in a generally East-West direction, therefore the bridge moved across its length more than along it.

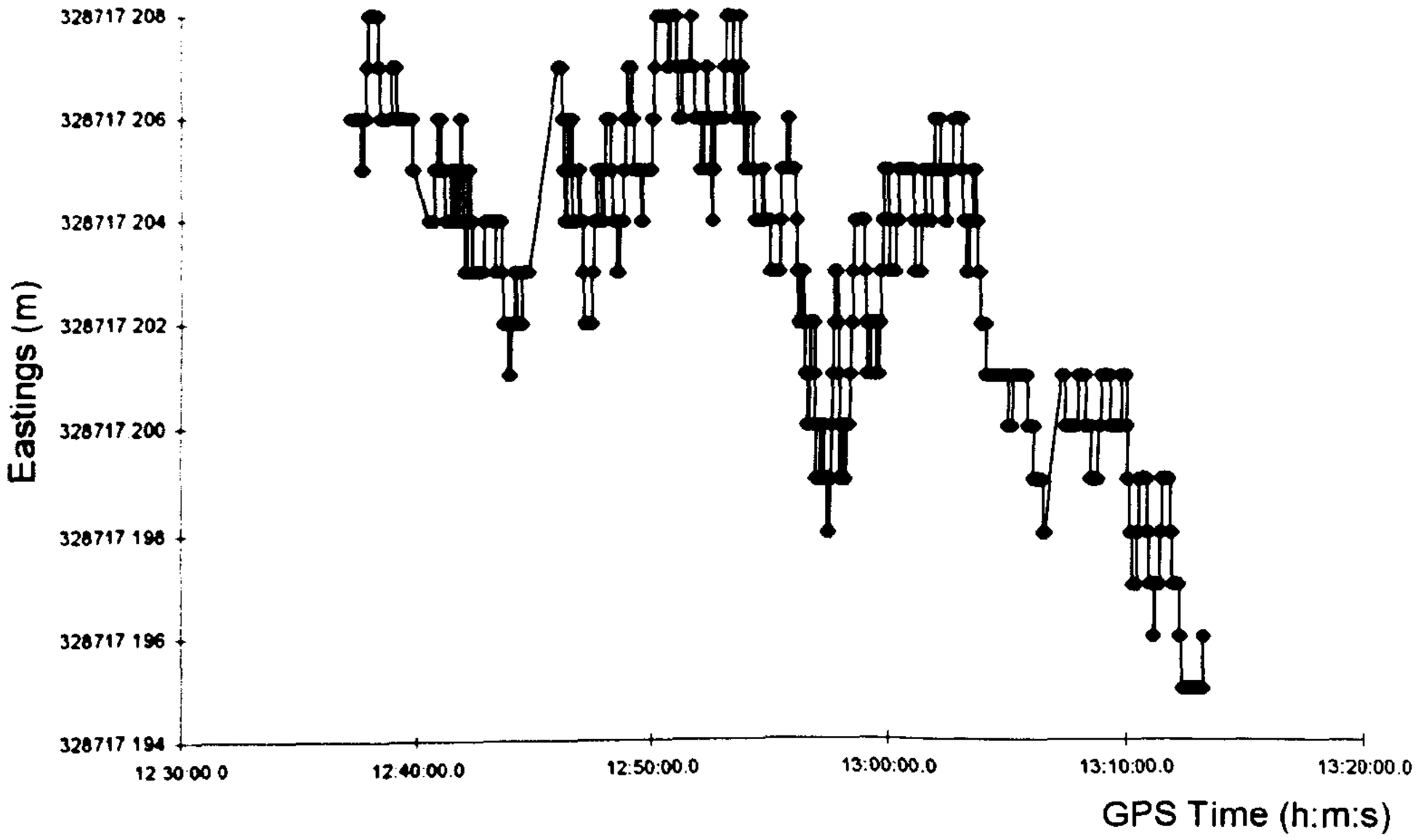

Figure 10.24

Movement of the Dee Bridge in the Eastings (longitudinal) Direction.

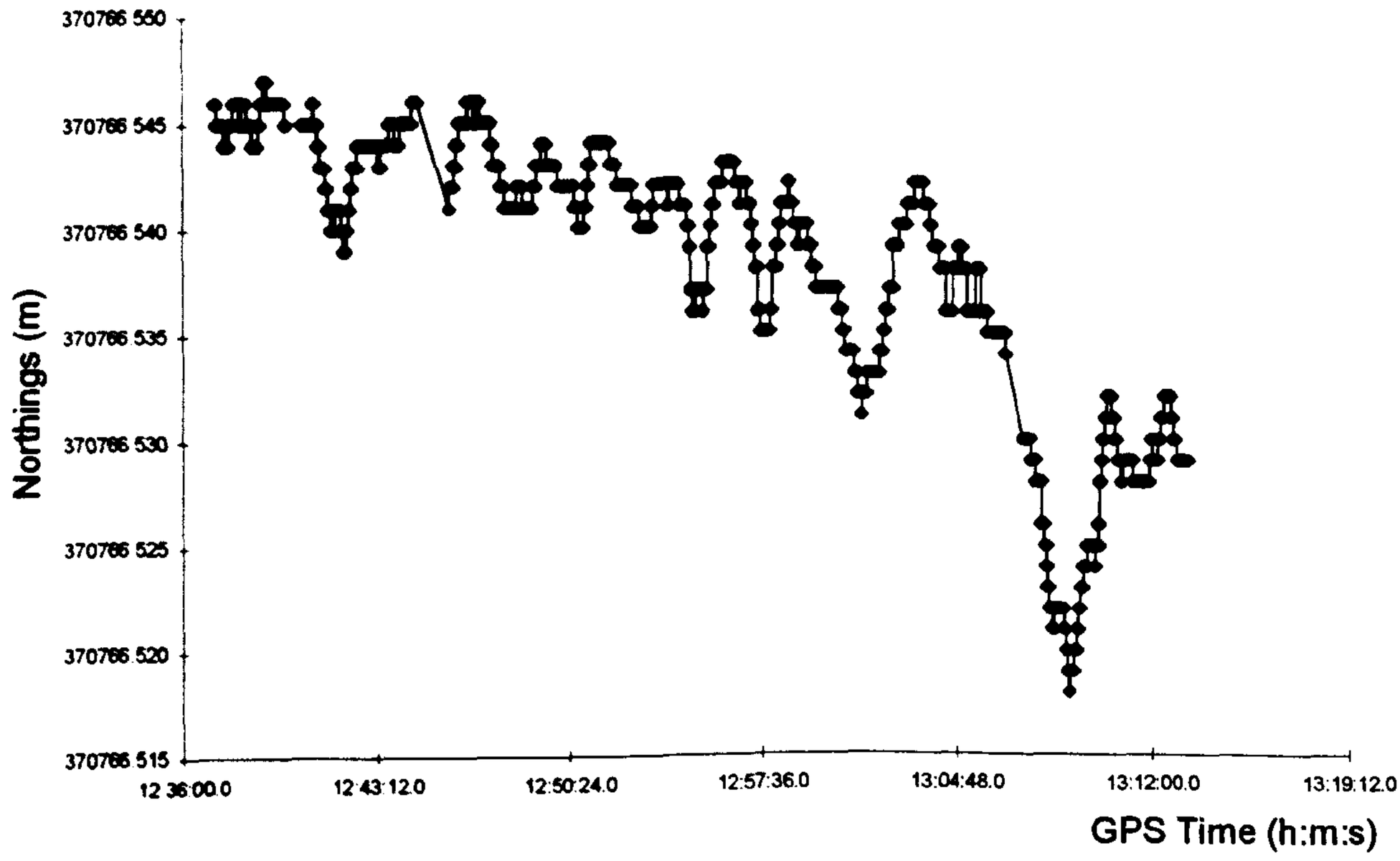

Figure 10.25

Movement of the Dee Bridge in the Northings (lateral) Direction.

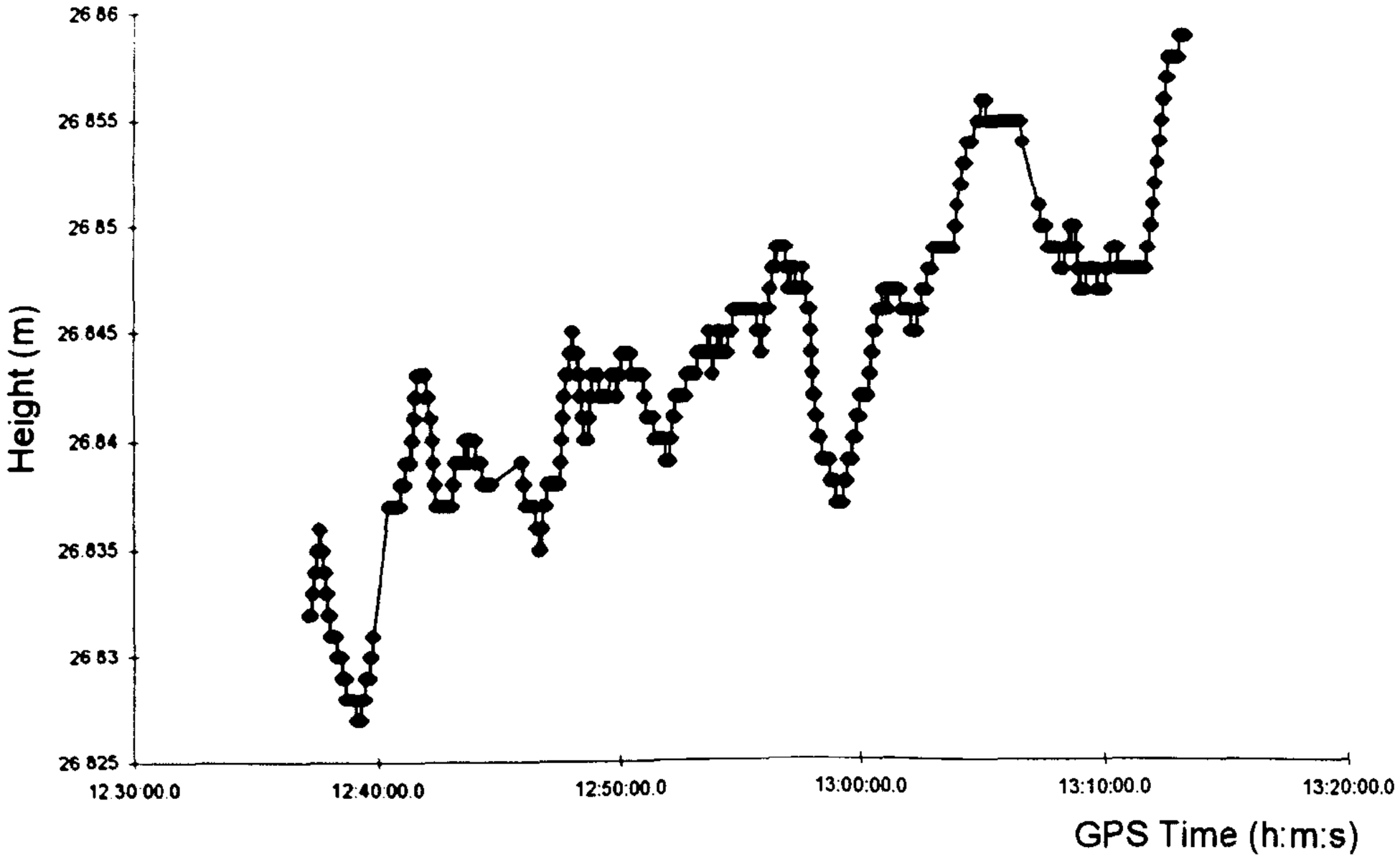

Figure 10.26

Movement of the Dee Bridge in the Vertical Direction.

Figures 10.27, 10.28 and 10.29 illustrate the corresponding vectors between the two bridge receiver's integer fixed OTF coordinates for Eastings, Northings and height respectively. The precision of the results obtained in Figures 10.24, 10.25 and 10.26 can be determined from these Figures.

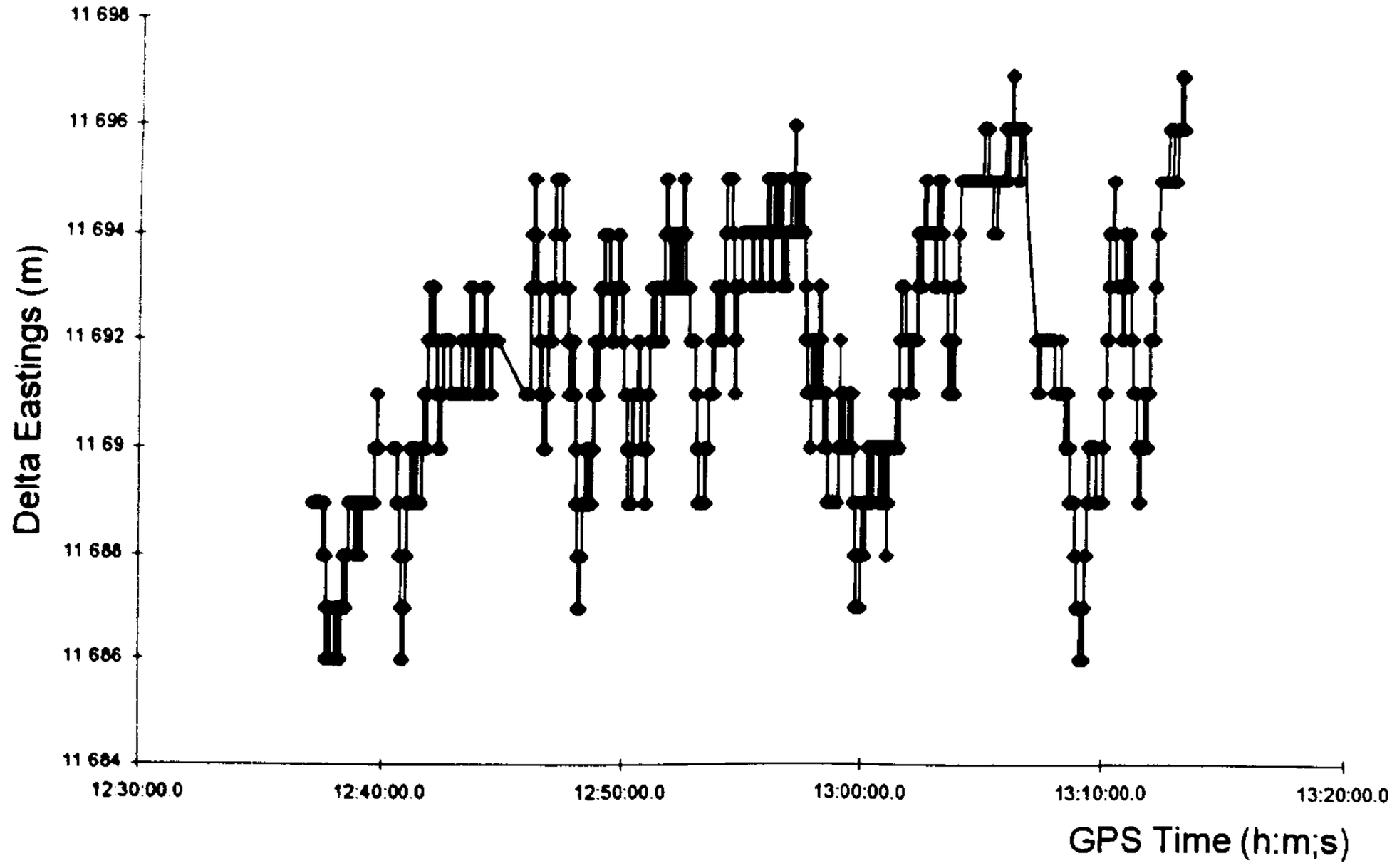

Figure 10.27

Vector between the two Antennas Situated upon the Dee Bridge in the Eastings Component.

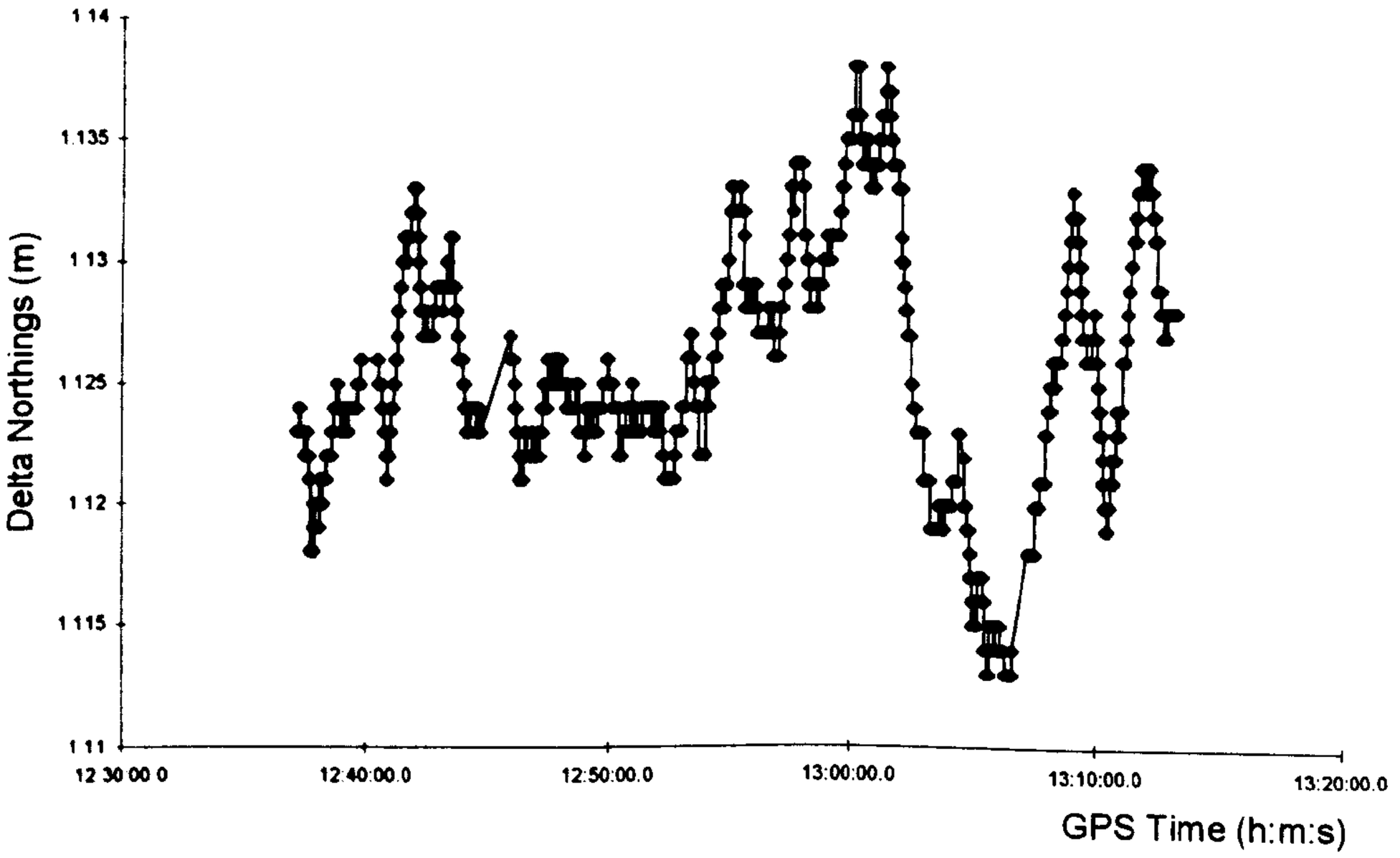

Figure 10.28

Vector between the two Antennas Situated upon the Dee Bridge in the Northings Component.

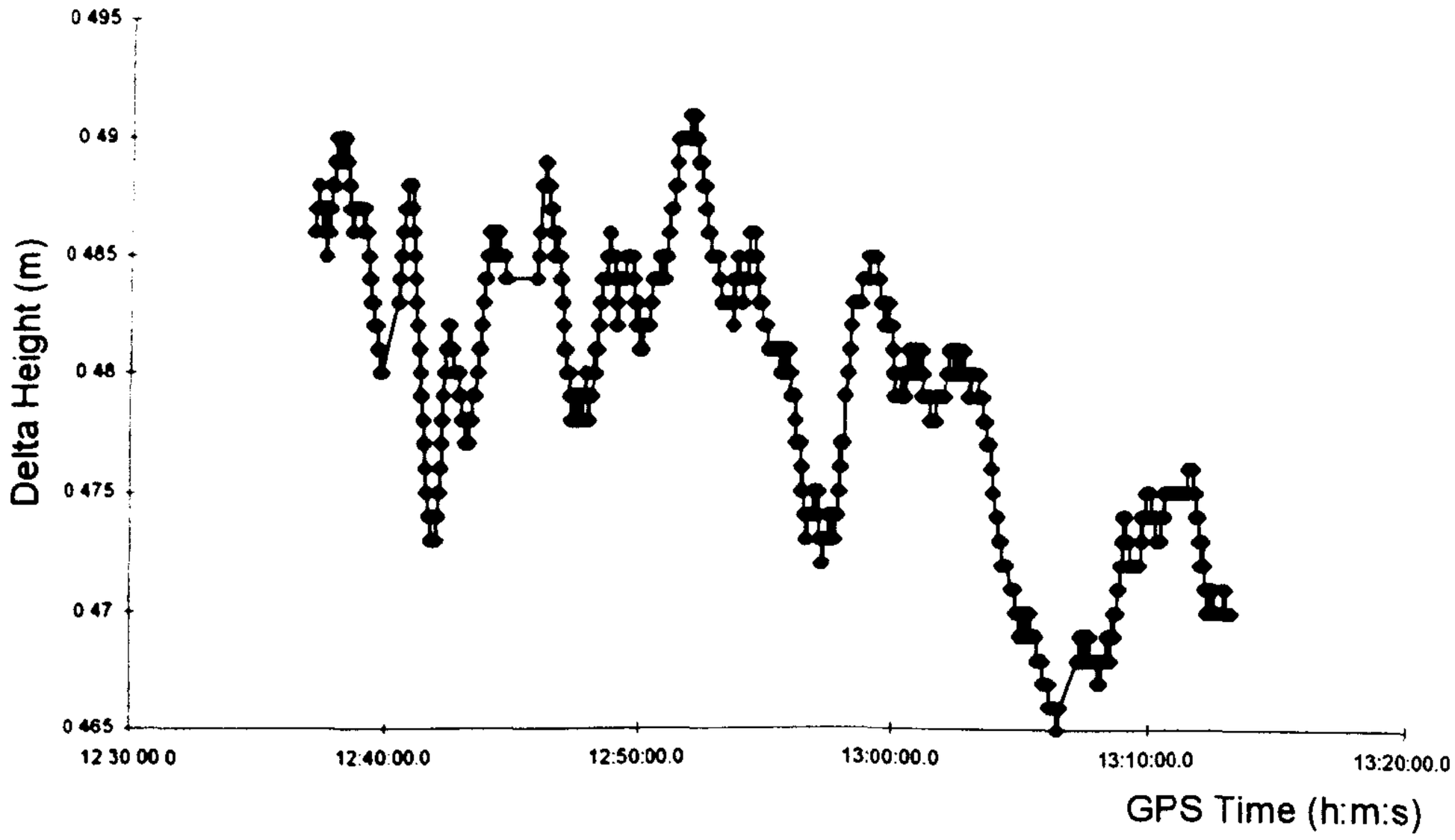

Figure 10.29

Vector between the two Antennas Situated upon the Dee Bridge in the Height Component.

Figure 10.27 shows that the vector between the two antennas on the bridge have a scatter of ± 5 mm. This value is an indication of the precision of the resulting OTF positions of the two antennas. Figure 10.28, however, indicates a precision of ± 10 mm at worst, but from approximately 12:47:00 to 12:55:00 a precision of ± 3 mm is evident. It is thought that this increase in precision is due to decreased multipath activity. The height precision, Figure 10.29, is seen to be worse than that of plan, at about ± 10 mm.

By comparison, Figures 10.27, 10.28 and 10.29 do in fact suggest that Figures 10.24, 10.25 and 10.26 show true movement, and not only multipath and receiver noise.

10.4 Real Time Monitoring of the Clifton Bridge

Tests were carried out through placing two GPS receivers upon the Clifton Bridge in Nottingham. A reference GPS receiver was situated over a position whose coordinates were accurately known, approximately 1 km away from the bridge. This being situated upon the IESSG building at the University of Nottingham. Two Ashtech choke ring GPS antennas were clamped onto the bridge handrail in order to determine the precision of the system. This was carried out in a similar manner to the third trial carried out on the Humber Bridge, §10.2.6. The precision was determined by analysing the change in the vector between the coordinates of the two antennas at every epoch. Theoretically, the vector should remain constant, as the antennas were placed some 2 metres apart, and did not move relative to each other. Any discrepancy from this continuity would be due to noise of the survey technique.

Figures 10.30, 10.31 and 10.32 illustrate the resulting OTF Eastings, Northings and height components of one of the receivers. It can be seen that over a period of 40 minutes, the bridge's height deflects by up to 50 mm, due to traffic loading. The Clifton Bridge is a short span bridge, and larger deflections were not expected. It is seen from Figure 10.31 that the Eastings component (lateral) movement of the bridge is of the order of ± 2 mm. This is undoubtedly the GPS receiver noise. Figure 10.32 illustrates the Northings (longitudinal) movement of the bridge. Here it is seen that the bridge moves in this direction by up to 16 mm, which is due to the expansion joints on the bridge.

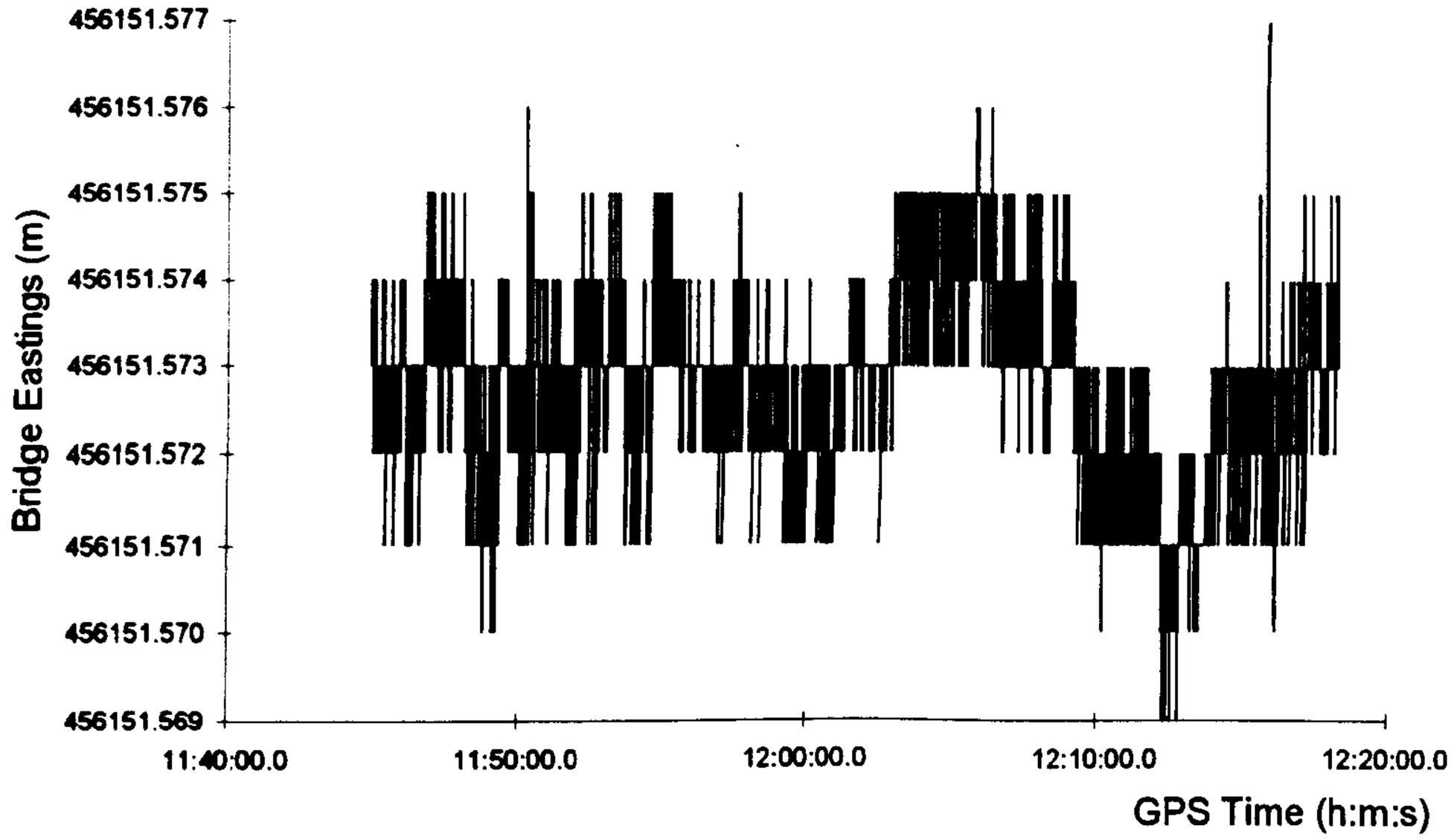

Figure 10.30

Movement of the Clifton Bridge in the Eastings Component (lateral).

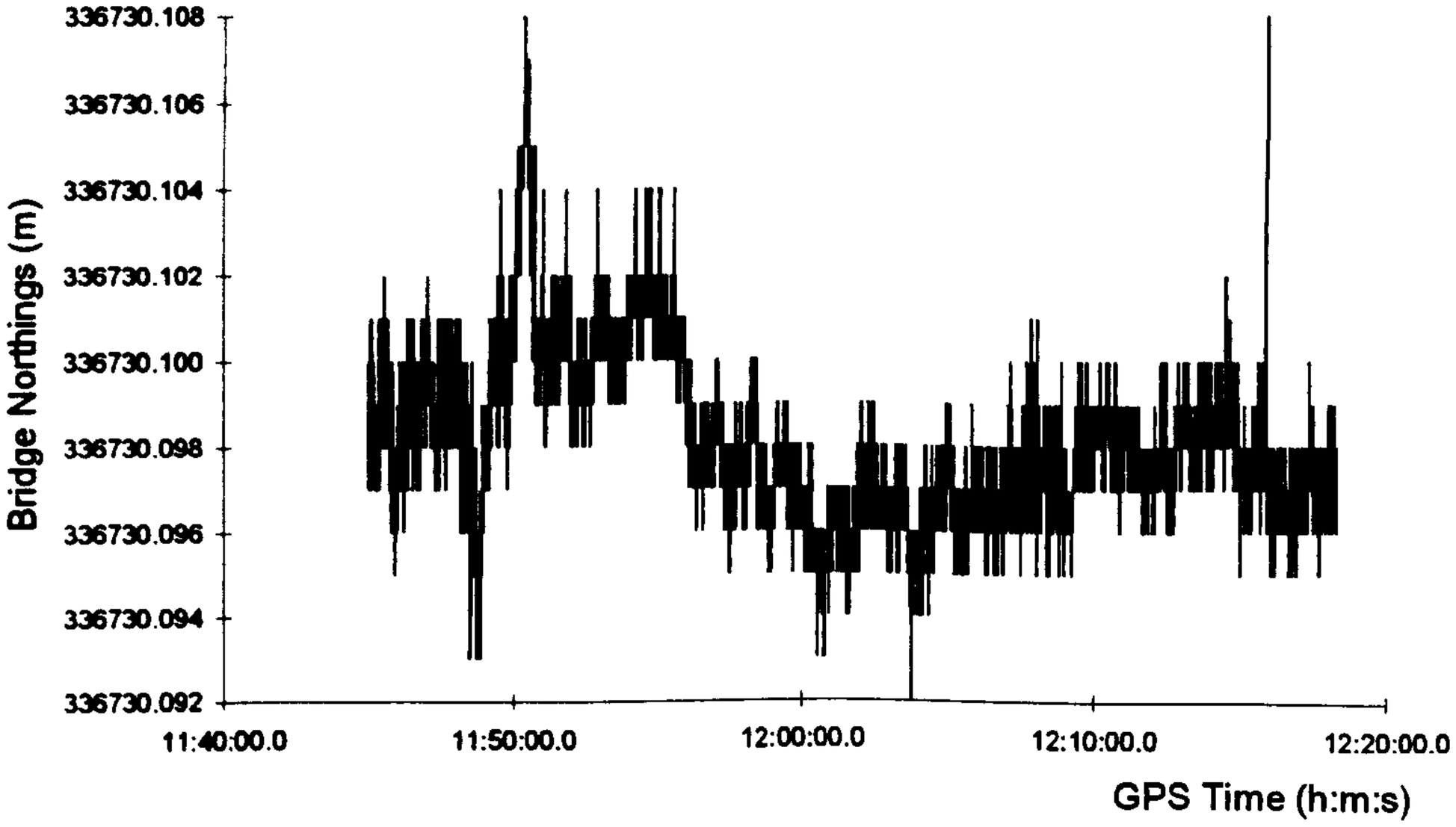

Figure 10.31

Movement of the Clifton Bridge in the Northings Component (longitudinal).

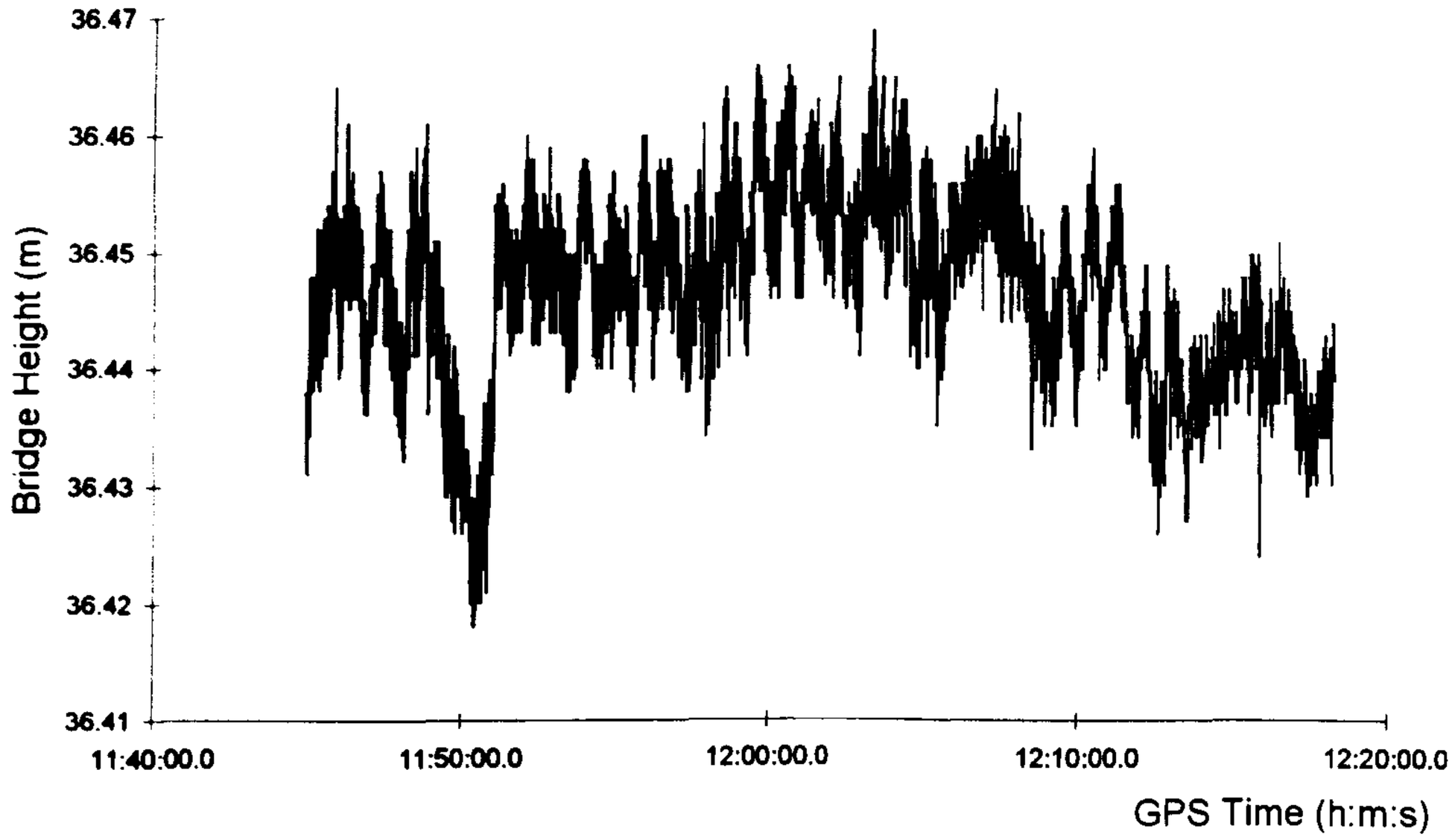

Figure 10.32

Movement of the Clifton Bridge in the Height Component.

The precision of these figures are illustrated through the vectors between the two antennas. The vectors shown in Figures 10.33, 10.34 and 10.35 are in the Eastings, Northings and height components. Figures 10.33 and 10.34, however, show the Eastings and Northings vectors (Delta East and Delta North) respectively, to be ±2 mm. Figure 10.35 shows that the vector between the two antennas in the height component (Delta Height) has a scatter of ± 20 mm. Delta east (lateral movement) seen in Figure 10.33 is seen to maintain this precision throughout the period. Delta north (longitudinal movement) seen in Figure 10.34 is seen to vary its precision from ± 5 mm for the first third of the test to ± 2 mm for the remainder. The increased noise level at the start of this trial is thought to be due to multipath noise. Again, the precision seen in the figures have a combination of two GPS receivers' noise values, therefore the true precision would be better than that shown in the figures.

Very large errors due to multipath are not evident during these trials. This is thought to be because the Clifton Bridge does not have any over hanging

supporting structures. The only problem with this trial was the traffic as the GPS antennas were placed approximately 3 m from the road.

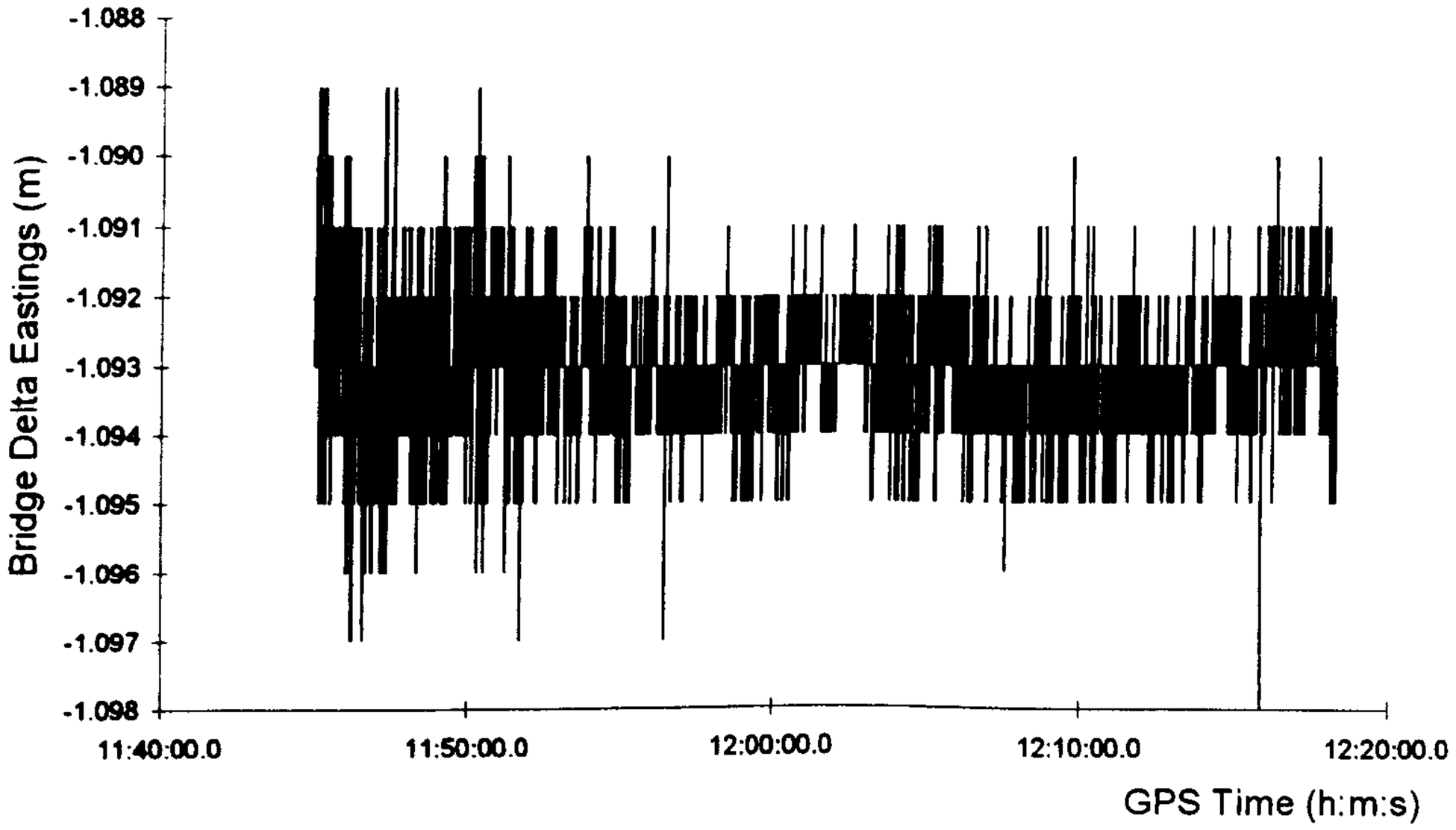

Figure 10.33

Vector between the two Antennas Situated upon the Clifton Bridge in the Eastings Component.

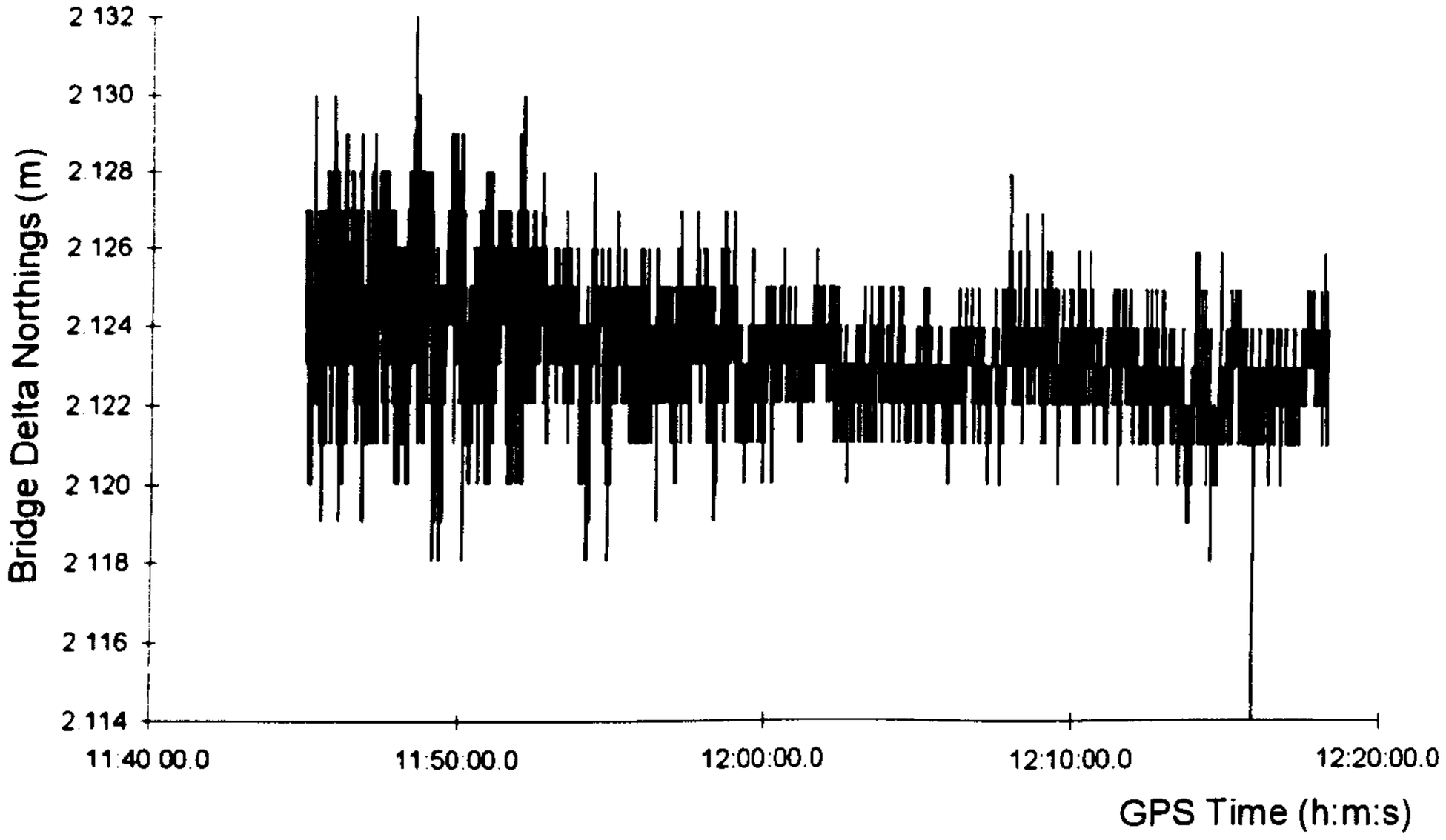

Figure 10.34

Vector between the two Antennas Situated upon the Clifton Bridge in the Northings Component.

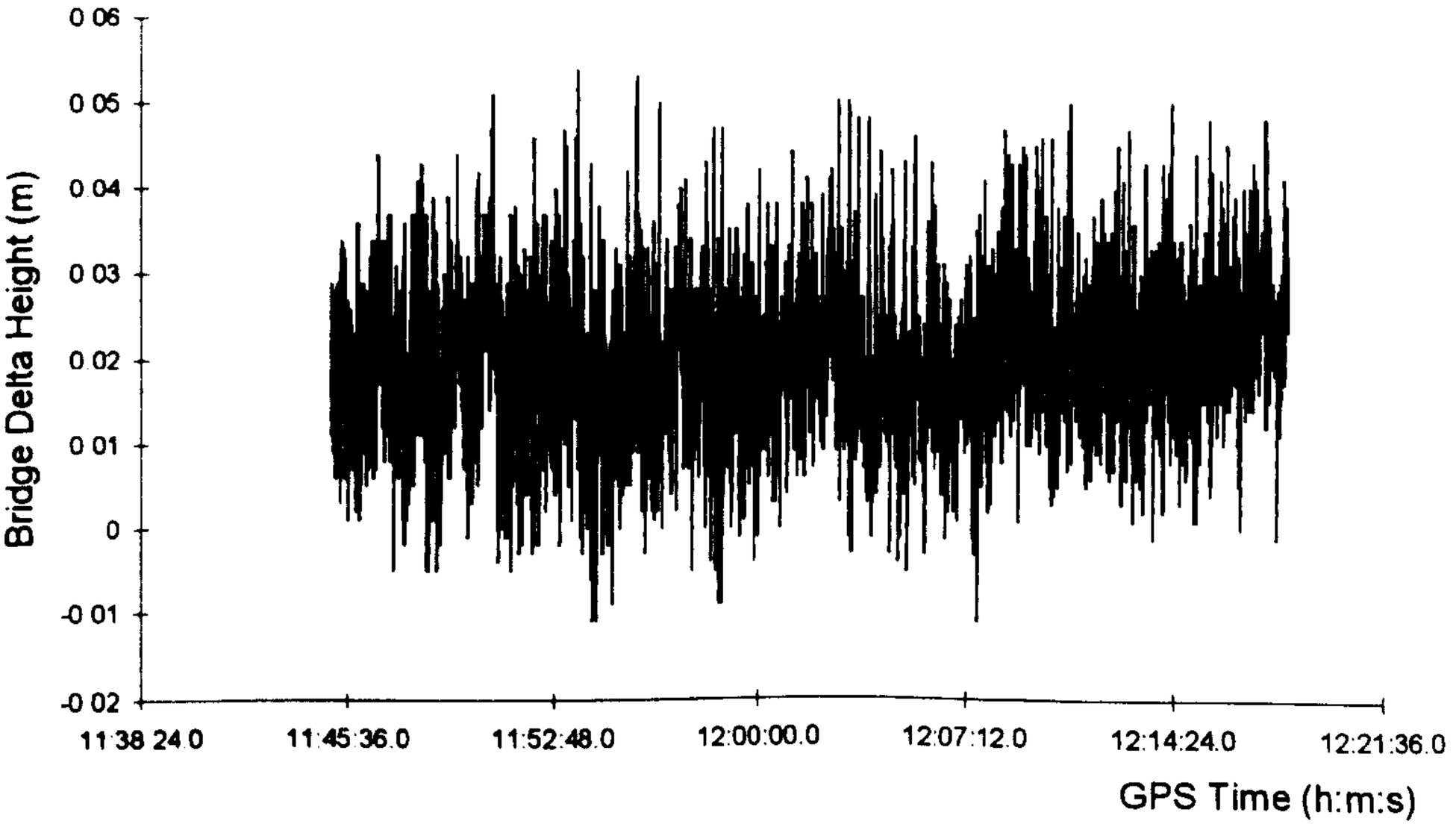

Figure 10.35

Vector between the two Antennas Situated upon the Clifton Bridge in the Height Component.

10.5 Conclusions and Recommendations

The tests and results have shown the potential of using real time OTF GPS on large structures for deformation analysis. Such systems could be used to analyse dangerous movements such as large wind speeds or heavy traffic loads as seen on the Humber Bridge. The result would be a failure alarm, bringing down emergency barriers to prevent traffic travelling into dangerous situations.

The real time OTF technique has been shown to be an aid for the construction of large structures such as the Dee Bridge. The monitoring of the Dee Bridge should continue throughout its construction, thus allowing any deformations in the structure during construction to be detected. One such deformation is the cantilever effect on the shore structure whilst the bridge deck is built over the river. The support tower movements of this bridge could also be analysed.

Geodetic antennas were used for al the trials detailed in this chapter. These were either ground plane antennas or choke ring antennas, which are large and bulky. To enable this technique to become viable in an everyday situation, the GPS antennas used should be smaller and lighter, such as small patch antennas. Further tests are required to enable the characteristics of patch antennas to be determined for such monitoring techniques.

Multipath is a major problem with successful positioning to millimetre level using real time OTF GPS. The use of small patch antennas could result in more multipath noise than the choke ring antennas as the patch antennas don't have any physical characteristics, such as ground planes or choke rings, to reduce the multipath signal. The planning of such a monitoring exercise, especially long term, includes the need to position the GPS antennas onto the structure in a low multipath location. This would require pre-surveying of the bridge to determine the locations of low and high multipath, or the introduction of new processing software or GPS receiver firmware which could detect and correct

the multipath. Such firmware [TRIMBLE, 1996] and software [AXELRAD *et al*, 1995], [COMP and AXELRAD, 1996] is currently under research.

The use of a combined GPS and GLONASS system would allow more satellites to be viewed and a quality control of each of the two systems by the other. At the time of writing this thesis (January 1997) commercial GPS/GLONASS receivers are becoming available [ASHTECH, 1996], [VAN DIGGLEN, 1996], [ASHTECH, 1997]. Although such receivers are currently only available in L1 only frequency, and processing packages are limited, the future holds a great deal of potential for such systems, where the optimum goal would be a dual frequency real time OTF GPS/GLONASS system. The problem may arise, however, in the fact that an integer fixed double differenced solution is not possible with GLONASS due to the satellites broadcasting on different frequencies.

Future research should be aimed at using the deformation results determined though OTF GPS to determine the characteristics of the bridge itself. The simultaneous positioning of many GPS antennas along the bridge deck length and on top of the support towers could provide a deformation analysis of the whole bridge at any one time. Future tests could also be carried out by driving a large mass of a known weight over the bridge, and analysing the vertical deformation.

Tests need to be carried out over long periods of time, preferably during peak traffic and off peak to correlate traffic flow with the vertical deformations. Tests also need to be carried out on the Humber Bridge during high wind speeds, especially during winds which travel across the bridge. During such instances, the OTF GPS results should show large horizontal deformations.

Any future trials carried out on any of the bridges should be carried out in conjunction with a video camera. Any large vertical displacements could then

be correlated to the traffic flow at any instant. Future tests should also be carried out in conjunction with accurate anemometers so that the wind speeds and horizontal displacements could be correlated.

Further research should be carried out into the application of real time OTF GPS for the monitoring of other large structures. Such could include tall slender buildings, stock piles and reservoirs, all of which could be monitored allowing an instantaneous indication to their failure, and useful information for future designs.

10.6 References

ASHTECH, 1994 (i), *Ashtech Prism Precision Survey Software, Vol I.* Publication date 17 march 1994, Document Number 600116, Revision B. . Ashtech Inc, 1170 Kifer Road, Sunnyvale, CA 94086

ASHTECH, 1996, *GG24™ Receiver, GPS+GLONASS all-in-view Positioning on the Board*, Ashtech specifications pamphlet, June 1996, gg24696. Ashtech Inc, 1170 Kifer Road, Sunnyvale, CA 94086.

ASHTECH, 1997, *Ashtech's World Wide Web Page*, http://www.ashtech.com.

AXELRAD. A., COMP. C., MACDORAN. P., 1995, *Use of Signal-To-Noise Ratio for Multipath Correction in GPS Differential Phase Measurements: Methodology and Experimental Results.* Proceedings of Institute of Navigation, ION95 GPS Conference.

COMP. C, and AXELRAD. P., 1996, *An Adaptive SNR Based Carrier Phase Multipath Mitigation Technique*. Paper presented at of Institute of Navigation, ION96 GPS Conference.

IGS, *The International GPS Service for Geodynamics World Wide Web Page.* http://igscb.jpl.nasa.gov/.

JACK, O. T. J, 1994, *Multipath Effects on GPS Observations*, MSc Thesis, University of Nottingham.

RACAL, 1995, *Deltalink II Operating Manual,* ref no STM1320, Racal Survey Ltd, Burlington House, 118 Burlington Road, New Malden, Surrey. KT3 4NR.

SHARDLOW, P.J. 1990. *Multipath: An Investigation.* MSc Thesis, University of Nottingham.

STEWART, M. P., FFOULKES-JONES G. H., OCHIENG, W. Y. and SHARDLOW, P.J., 1995, *GAS: GPS Analysis Software User manual. Version 2.3.* IESSG Publication, University of Nottingham.

THE HUMBER BRIDGE BOARD (i), *Engineering, The Humber Bridge.* Information Pamphlet. Printed in England by The Hillingdon Press, Uxbridge, Middlesex.

THE HUMBER BRIDGE BOARD (ii), *The Humber Bridge Information Pack.* Information Pamphlet.

TRIMBLE, 1996, *Improvements in Real-time GPS Surveying performance Using EVEREST™ Multipath Rejection Technology.* Trimble Navigation, Surveying and Mapping Division, 645 North Mary Avenue, Sunnyvale, CA. Product Bulletin. TID 1602 (4/96)

VAN DIGGLEN, F., 1996, *GG24 GPS+GLONASS Receiver,* paper prepared by Dr Frank van Digglen. Ashtech Inc, 1170 Kifer Road, Sunnyvale, CA 94086

Chapter 11

Conclusions and Recommendations

The following conclusions and recommendations have already been discussed in the context of this thesis and are summarised below.

11.1 Conclusions

The cycle slip detection techniques have been shown to operate, but all have their disadvantages. These disadvantages have been overcome somewhat by utilising all the techniques into a single cycle slip detection and correction package.

The detection of cycle slips is an important process. Even if the cycle slips cannot be quantified, it allows an OTF integer ambiguity search to be carried out. The detection of cycle slips is an important process for the use of OTF processing to be successful, especially in a real time manner.

Ideally, the cycle slips should be calculated within the GPS receiver. Also, if the user were to record data at a 30 second epoch interval, for instance, then cycle slips would be difficult to detect even in a post processed sense. The GPS receiver, however, would be sampling data at a far higher rate, allowing easier cycle slip detection. Any cycle slip detected should, however, be flagged,

allowing post processing to take this into account, and be cautious during such instances.

The future use of combined GPS and GLONASS receivers may make cycle slip detection and correction less of a problem, as the two systems may check one another. The combination of the two systems may also decrease the integer ambiguity search time, due to the increased number of satellites. The increase in satellite numbers may also mean that single frequency GPS/GLONASS receivers may be able to resolve the integer ambiguities in as short a time as a dual frequency GPS receiver.

The results for the 134 km trial in Chapter 7 have shown that the MRS technique can be used over long ranges to fix the integer ambiguities quickly and reliably, resulting in coordinates with a precision of 12 cm. The resulting L1 solution, however, is affected by the ionosphere and troposphere, and these need to be modelled in NOTF.

The polar flight showed that NOTF could be used over long distances, but no means of comparison was available. Future trials should include more than one roving GPS receiver on the plane, which could be positioned, and the resulting vector between them analysed.

The real time aspect of such a system needs further investigation. Current telemetry links available are low powered UHF radios, and have a very short range of about 10 km. Alternative links should be looked at, which could include cellular telephones, which could increase the range. Other alternatives include satellite communications for the telemetry links.

It has been shown in chapter 9 that real time OTF GPS can be precise to a few millimetres once the integer ambiguities have been resolved.

The reference GPS coordinates should be as accurate as possible, thus allowing quick and accurate integer ambiguity resolution. Initial trials detailed in this chapter have suggested that using reference GPS receiver as inaccurate as a

stand alone GPS positioning (~100 m) can impede the OTF search. This may only be true for baseline lengths of ~ 10 km or greater; shorter baseline lengths, < 1 km, may work with inaccurate reference receiver coordinates. Further work should be carried out in this region, comparing satellite numbers, satellite geometry, baseline lengths and coordinate accuracies with the success of the resulting OTF search. This would then allow a user to be able to decide the order of accuracy of the reference receiver's coordinates required for successful OTF initialisation.

The real time aspect of such a system may cause problems when using a 0.5 Watt UHF data link. The signal transmitted from such low powered telemetry links may not be powerful enough, and signals are easily lost due to obstructions or interference. Other forms of data links should be researched, such as the use of cellular telephone links.

The experiments and results discussed in chapter 10 have indicated that real time OTF GPS has potential positional precision to an order of a few millimetres. This means that it could be used for plant control and monitoring to a high order of precision.

The vibration due to the engine and plant movement is clearly evident in the results. The noise is amplified in these experiments due to the flexible poles used to attach the GPS antennas to the blade. These noise sources and other possible methods of attaching the antennas to the bulldozer should be examined, as well as the use of filtering algorithms to smooth out the data.

A working real time system which incorporates the OTF GPS data could be set up in a similar manner as that currently being used with the laser level system. Here, the real time OTF GPS coordinates would be used to control the blades height, according to its position, via the hydraulics of the bulldozer.

Multipath was not evident during the trials. This is thought to be because the antennas were located above the body of the bulldozer. This error source, however, is shown to be a problem with kinematic OTF GPS positioning in chapter 10. The positioning of the antennas is an important aspect of being able to successfully monitor and control construction plant by GPS.

The antennas used during these trials were geodetic and choke ring antennas. These proved adequate for the trials, but due to their weight may have caused a lot of the vibration. The use of smaller antennas would make this type of application more practical, however, these types of antennas can suffer more from multipath. Further research is necessary in this field.

Further work should also be carried out to investigate the use of tilt sensors and compasses to aid the GPS positioning of the blade. Such systems could help a single antenna on a blade to determine the direction of travel of the plant as well as the tilt of the mast.

The use of GPS/GLONASS receivers should be investigated in future trials. Currently, commercial GPS/GLONASS receivers are limited to single frequency. Dual frequency receivers are required for quick OTF GPS integer ambiguity resolution. When future dual frequency GPS/GLONASS receivers are made available, these would be very useful in environments where large buildings and foliage mask satellite signals. The use of a combined system would also give a quality control, as the two systems are separate, allowing possible positioning from both.

The tests and results have shown the potential of using real time OTF GPS on large structures for deformation analysis. Such systems could be used to analyse dangerous movements such as large wind speeds or heavy traffic loads as seen on the Humber Bridge. The result would be a failure alarm, bringing down emergency barriers to prevent traffic travelling into dangerous situations.

The real time OTF technique has been shown to be an aid for the construction of large structures such as the Dee Bridge. The monitoring of the Dee Bridge should continue throughout its construction, thus allowing any deformations in the structure during construction to be detected. One such deformation is the cantilever effect on the shore structure whilst the bridge deck is built over the river. The support tower movements of this bridge could also be analysed.

Geodetic antennas were used for al the trials detailed in this chapter. These were either ground plane antennas or choke ring antennas, which are large and bulky. To enable this technique to become viable in an everyday situation, the GPS antennas used should be smaller and lighter, such as small patch antennas. Further tests are required to enable the characteristics of patch antennas to be determined for such monitoring techniques.

Multipath is a major problem with successful positioning to millimetre level using real time OTF GPS. The use of small patch antennas could result in more multipath noise than the choke ring antennas as the patch antennas don't have any physical characteristics, such as ground planes or choke rings, to reduce the multipath signal. The planning of such a monitoring exercise, especially long term, includes the need to position the GPS antennas onto the structure in a low multipath location. This would require pre-surveying of the bridge to determine the locations of low and high multipath, or the introduction of new processing software or GPS receiver firmware which could detect and correct the multipath. Such firmware and software is currently under research.

The use of a combines GPS and GLONASS system would allow more satellites to be viewed, and a quality control of each of the two systems by the other. At the time of writing this thesis (January 1997) commercial GPS/GLONASS receivers are becoming available. Although such receivers are currently only available in L1 only frequency, and processing packages are limited, the future holds a great deal of potential for such systems, where the optimum goal would be a dual frequency real time OTF GPS/GLONASS system.

11.2 Recommendations for Future Work

Further work needs to be carried out into the detection and possible quantification of multipath. This would be useful for both the techniques which rely on the pseudorange data to detect cycle slips as well as multipath detection in general.

NOTF should be implemented into a real time package, allowing the use of MRS and long range real time OTF to be researched.

The use of alternative telemetry links such as cellular telephone links should be investigated, as this would increase the possible applications for real time OTF GPS.

Any future trials carried out on any of the bridges should be carried out in conjunction with a video camera. Any large vertical displacements could then be correlated to the traffic flow at any instant. Future tests should also be carried out in conjunction with accurate anemometers so that the wind speeds and horizontal displacements could be correlated.

Further research should be carried out into the application of real time OTF GPS for the monitoring of other large structures. Such could include tall slender buildings, stock piles and reservoirs, all of which could be monitored allowing an instantaneous indication to their failure, and useful information for future designs.

Future research should be aimed at using the deformation results determined though OTF GPS to determine the characteristics of the bridge itself. The simultaneous positioning of many GPS antennas along the bridge deck length and on top of the support towers could provide a deformation analysis of the whole bridge at any one time. Future tests could also be carried out by driving

a large mass of a known weight over the bridge, and analysing the vertical deformation.

Tests need to be carried out over long periods of time, preferably during peak traffic and off peak to correlate traffic flow with the vertical deformations. Tests also need to be carried out on the Humber Bridge during high wind speeds, especially during winds which travel across the bridge. During such instances, the OTF GPS results should show large horizontal deformations.

APPENDIX A

NAVSTAR #	SVN, PRN	LAUNCH	SLOT	OPERATIONAL	NAV LOST	REASON FOR FAILURE	MONTHS OPERATIONAL
I-1	1 / 4	22 FEB 78	**	29 MAR 78	25 JAN 80	CLOCK	21.9
I-2	2 / 7	13 MAY 78	**	14 JUL 78	30 JUL 80	CLOCK	25.5
I-3	3 / 6	06 OCT 78	**	09 NOV 78	19 APR 92	CLOCK	161.3
I-4	4 / 8	11 DEC 78	**	08 JAN 79	27 OCT 86	CLOCK	93.6
I-5	5 / 5	09 FEB 80	**	27 FEB 80	28 NOV 83	WHEEL	45
I-6	6 / 9	26 APR 80	**	16 MAY 80	10 DEC 90	WHEEL	126.8
I-7	7 /	18 DEC 81	**			BOOSTER	0
I-8	8 / 11	14 JUL 83	C3	10 AUG 83	04 MAY 93	EPS DEGR	116.3
I-9	9 / 13	14 JUN 84	C1	19 JUL 84	28 FEB 94	CLOCK	115.2
I-10	10 / 12	08 SEP 84	A1	03 OCT 84	18 NOV 95	CLOCK	146.8
I-11	11 / 3	09 OCT 85	C4	30 OCT 85	27 FEB 94	TT & C	99.9
	TOTAL BLOCK I SATELLITE YEARS ON ORBIT				=	79.4 YEARS	
	AVERAGE OPERATING LIFE TO DATE (INCLUDING BOOSTER FAILURE)				=	7.22 YEARS	
II-1	14 / 14	14 FEB 89	E1	14 APR 89	OPERATING		92.4
II-2	13 / 2	10 JUN 89	B3	12 JUL 89	OPERATING		89.5
II-3	16 / 16	17 AUG 89	E5	13 SEPT 89	OPERATING		87.5
II-4	19 / 19	21 OCT 89	A4	14 NOV 89	OPERATING		85.4
II-5	17 / 17	11 DEC 89	D3	11 JAN 90	OPERATING		83.5
II-6	18 / 18	24 JAN 90	F3	14 FEB 90	OPERATING		82.4
II-7	20 / 20	25 MAR 90	B5	19 APR 90	10 MAY 96		80.3
II-8	21 / 21	02 AUG 90	E2	31 AUG 90	OPERATING		75.9
II-9	15 / 15	01 OCT 90	D2	20 OCT 90	OPERATING		74.2
IIA-10	23 / 23	26 NOV 90	E4	10 DEC 90	OPERATING		72.6
IIA-11	24 / 24	03 JUL 91	D1	30 AUG 91	OPERATING		63.9
IIA-12	25 / 25	23 FEB 92	A2	24 MAR 92	OPERATING		57.1
IIA-13	28 / 28	10 APR 92	C5	25 APR 92	OPERATING		56.1
IIA-14	26 / 26	07 JUL 92	F2	23 JUL 92	OPERATING		53.1
IIA-15	27 / 27	09 SEP 92	A3	30 SEP 92	OPERATING		50.0
IIA-16	32 / (32) 1[1]	22 NOV 92	F1	11 DEC 92	OPERATING		48.5
IIA-17	29 / 29	18 DEC 92	F4	05 JAN 93	OPERATING		47.7
IIA-18	22 / 22	03 FEB 93	B1	04 APR 93	OPERATING		44.8
IIA-19	31 / 31	30 MAR 93	C3	13 APR 93	OPERATING		44.5
IIA-20	37 / 7	13 MAY 93	C4	12 JUN 93	OPERATING		42.5
IIA-21	39 / 9	26 JUN 93	A1	21 JUL 93	OPERATING		41.2
IIA-22	35 / 5	30 AUG 93	B4	20 SEP 93	OPERATING		39.2
IIA-23	34 / 4	26 OCT 93	D4	01 DEC 93	OPERATING		36.9
IIA-24	36 / 6	10 MAR 94	C1	28 MAR 94	OPERATING		33.0
IIA-25	33 / 3	29 MAR 96	C2	09 APR 96	OPERATING		7.7
IIA-26	40 / 10	16 JUL 96	E3	15 AUG 96	OPERATING		3.5
IIA-27	30 / 30	12 SEP 6	B2	01 OCT 96	OPERATING		2.0
	TOTAL BLOCK II/IIA SATELLITE YEARS ON ORBIT				=	123.59 YEARS	
	AVERAGE OPERATING LIFE TO DATE				=	5.15 YEARS	

A1: GPS Constellation History and Status (as of 01 Jan 97)

APPENDIX B

```
2                    OBSERVATION DATA    G (GPS)                 RINEX VERSION / TYPE
ASRINEXO V2.6.1 LH  AIUB                 26-SEP-96 11:04         PGM / RUN BY / DATE
P-CODE  ASHTECH                                                  COMMENT
AR96                                                             MARKER NAME
                                                                 OBSERVER / AGENCY
                     ASHTECH Z-XII3      1G00                    REC # / TYPE / VERS
                     GEODETIC L1/L2 P                            ANT # / TYPE
   541418.2800 -1388140.5400  6180890.4900                       APPROX POSITION XYZ
        0.0000        0.0000        0.0000                       ANTENNA: DELTA
H/E/N
     1     1                                                     WAVELENGTH FACT
L1/2
     9    C1    L1    L2    P1    P2    D1    D2    S1    S2# / TYPES OF OBSERV
     1                                                           INTERVAL
  1996     5    14    19    48   50.000000                      TIME OF FIRST OBS
                                                                 END OF HEADER

96  5 14 19 48 50.0000000  0  3 15 02 07
  23221846.911      119456.493 9
     -3353.578       -2613.178         202.000          84.000
  25213641.209      321506.358 9
     -3691.282       -2876.324         193.000         110.000
  20955809.767       76587.06549     56930.08849  20955809.2064   20955813.7144
      -685.799        -534.389         149.000         153.000
 96  5 14 19 48 55.0000000  0  3 15 02 07
  23225039.663      136226.728 9
     -3354.438       -2613.848         199.000          95.000
  25217157.788      339961.760 9
     -3690.995       -2876.100         196.000         107.000
  20956463.394       80021.89649     59606.59149  20956461.9004   20956466.9514
      -688.143        -536.215         149.000         152.000



96  5 14 19 53  5.0000000  0  6 15 04 05 01 14 07
  23386395.020      984158.127 9
     -3428.053       -2671.210         204.000          74.000
  23197432.432     -925044.656 9
      3470.433        2704.234         199.000         109.000
  22836888.249     -566694.23649   -242268.76649  22836884.4994   22836890.5684
      2452.187        1910.795         125.000         135.000
  23370243.010      338522.81449    172535.83249  23370241.8654   23370248.4144
     -1288.400       -1003.948         126.000         133.000
  21985608.404     -421437.21349   -318540.88149  21985606.7744   21985613.2824
      1290.165        1005.323         137.000         144.000
  20992643.273      270154.20949    207761.46449  20992642.8684   20992648.5434
      -832.975        -649.071         147.000         150.000
```

B1: An Example of a RINEX data file

```
 300165 Satellite 25 just risen
 300165 Satellite 22 just risen
 300165 Satellite 20 just risen
 300165 Satellite  6 just risen
 300165 Satellite 18 just risen
 300165 Satellite 29 just risen
 300165 Satellite 28 just risen
 300165 Satellite 16 just risen
 300165 Satellite 17 just risen
300255.000 16           100.000             0.000
300270.000 16             0.000           100.000
300280.000 16             1.000             0.000
300290.000 16             0.000             1.000
300300.000 16             1.000             1.000
300310.000 16            10.000             0.000
300320.000 16          1000.000             0.000
300330.000 16            -1.000             0.000
300340.000 16            -1.000            -1.000
300350.000 16             9.000             7.000
300360.000 16            -9.000            -7.000
```

B2: The Output file from the filter slip program

```
FILES
  INPUT                                                          ! input file names
    STYLE  ***.95o
    DATA zb191652
  END
  OUTPUT                                                          ! Output filnames
    STYLE  ***.NOT    ! Output filename style, NOT format
  END
END

OPTIONS
! UNHEALTHY  8  24  26
! INTERVAL  60
!  START  GPS  826 470400 ! ymdhms  1993 08 13  07 45 00
!  STOP   GPS  826 470500 ! ymdhms  1993 08 13  17 45 00
 Slip_opt 3
! SLIP_TOL  500                              ! Gross cycle slip detection tolerance
 RRTOL 500
 DRTOL 1
 WLTOL 3
 IRTOL 0.3
 PSEUDO  no                                 ! Compute pseudorange point positon
END
```

B3: An Example of the Filter Slip Program's Control File

Examples of Doppler Shift data

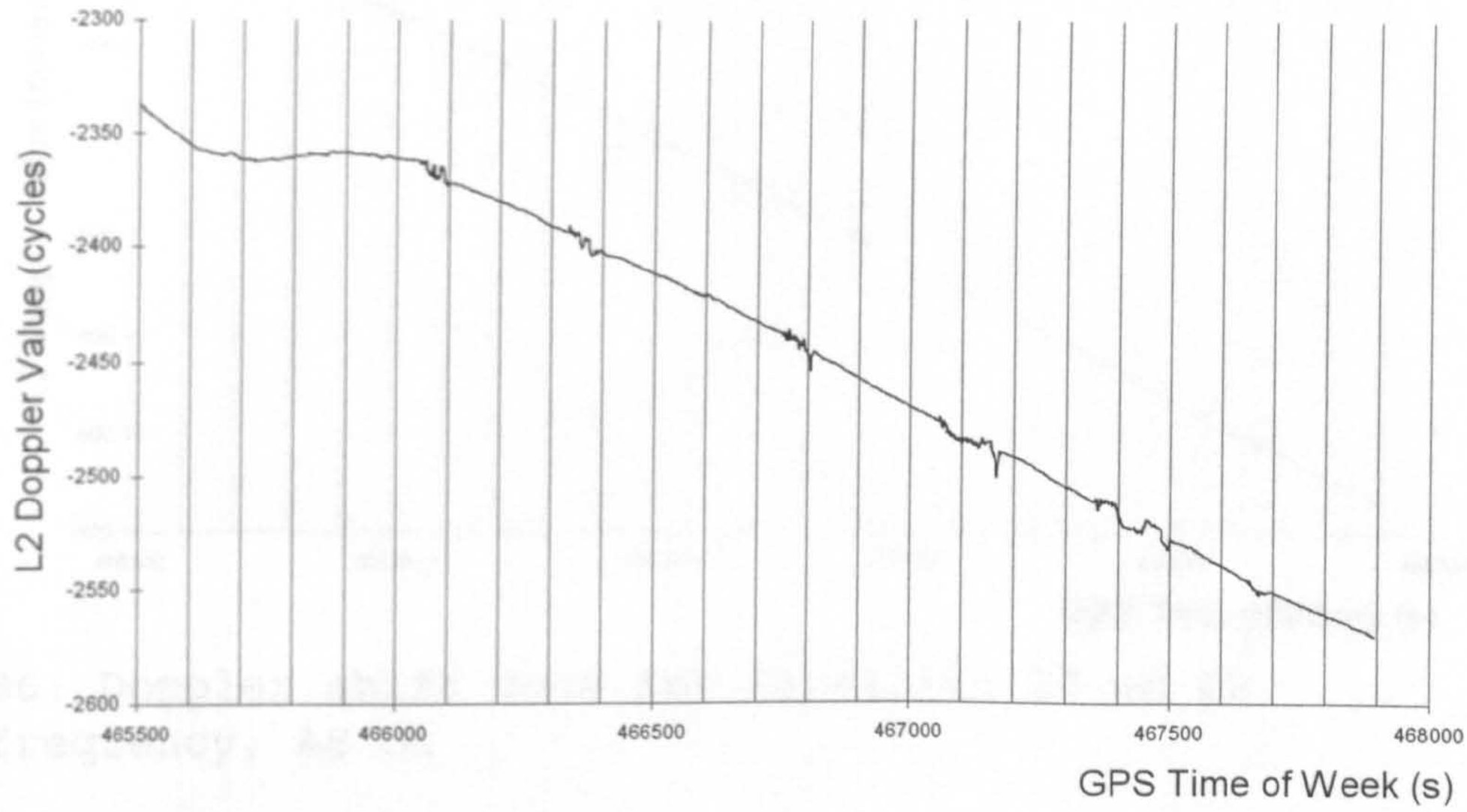

B4: Doppler shift data for Satellite 02 on L2 frequency, AS on

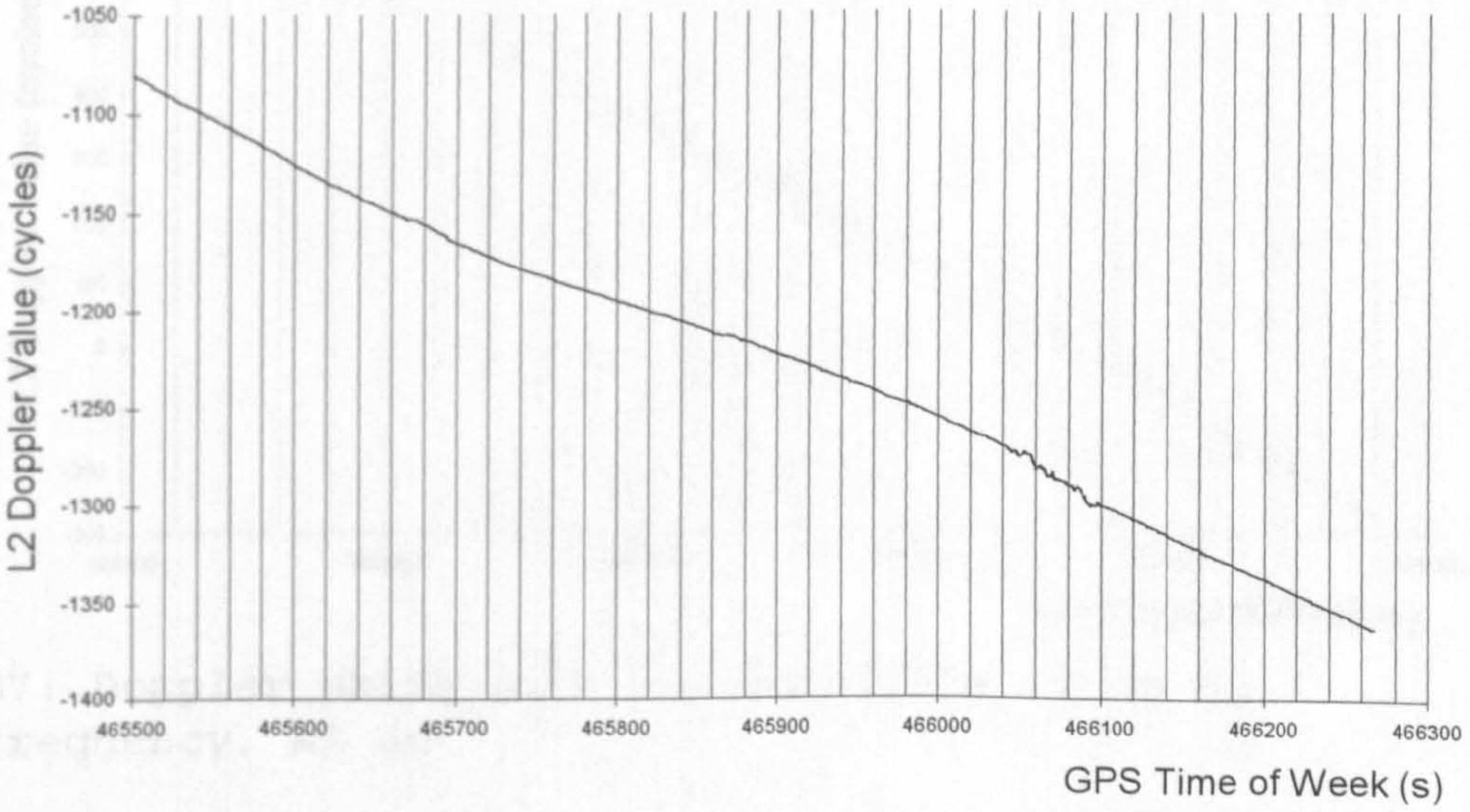

B5: Doppler shift data for Satellite 16 on L2 frequency, AS on

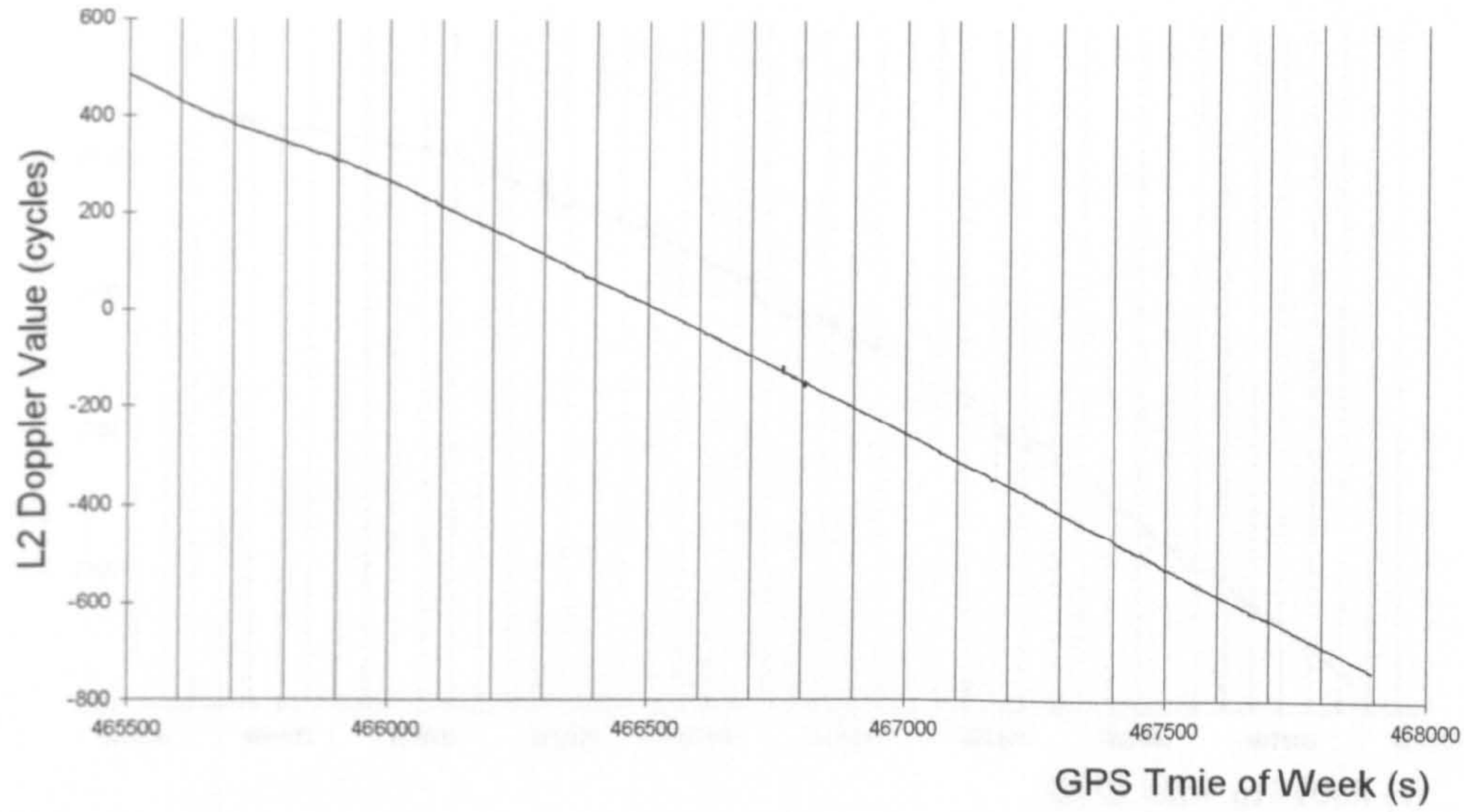

B6: Doppler shift data for Satellite 17 on L2 frequency, AS on

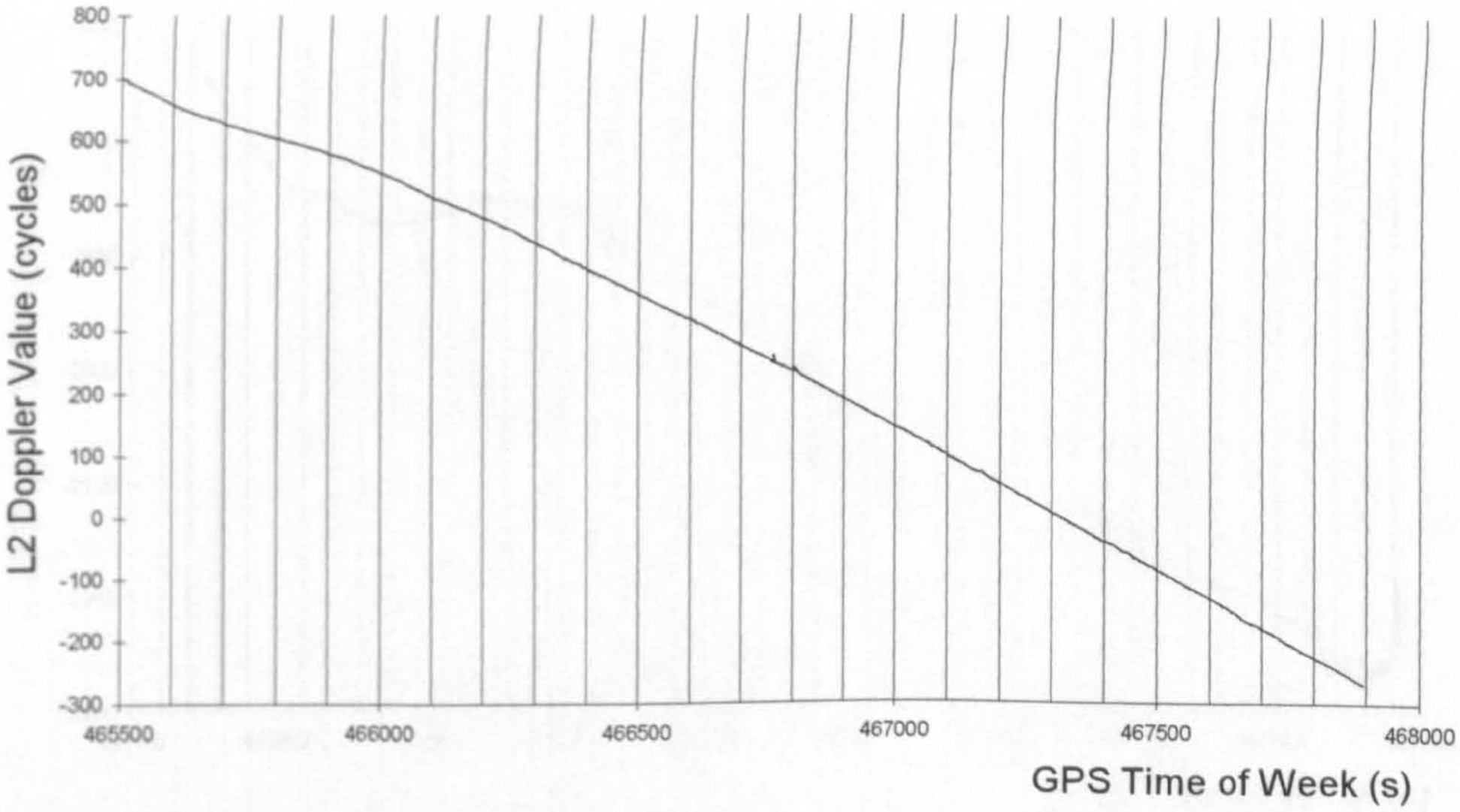

B7: Doppler shift data for Satellite 22 on L2 frequency, AS on

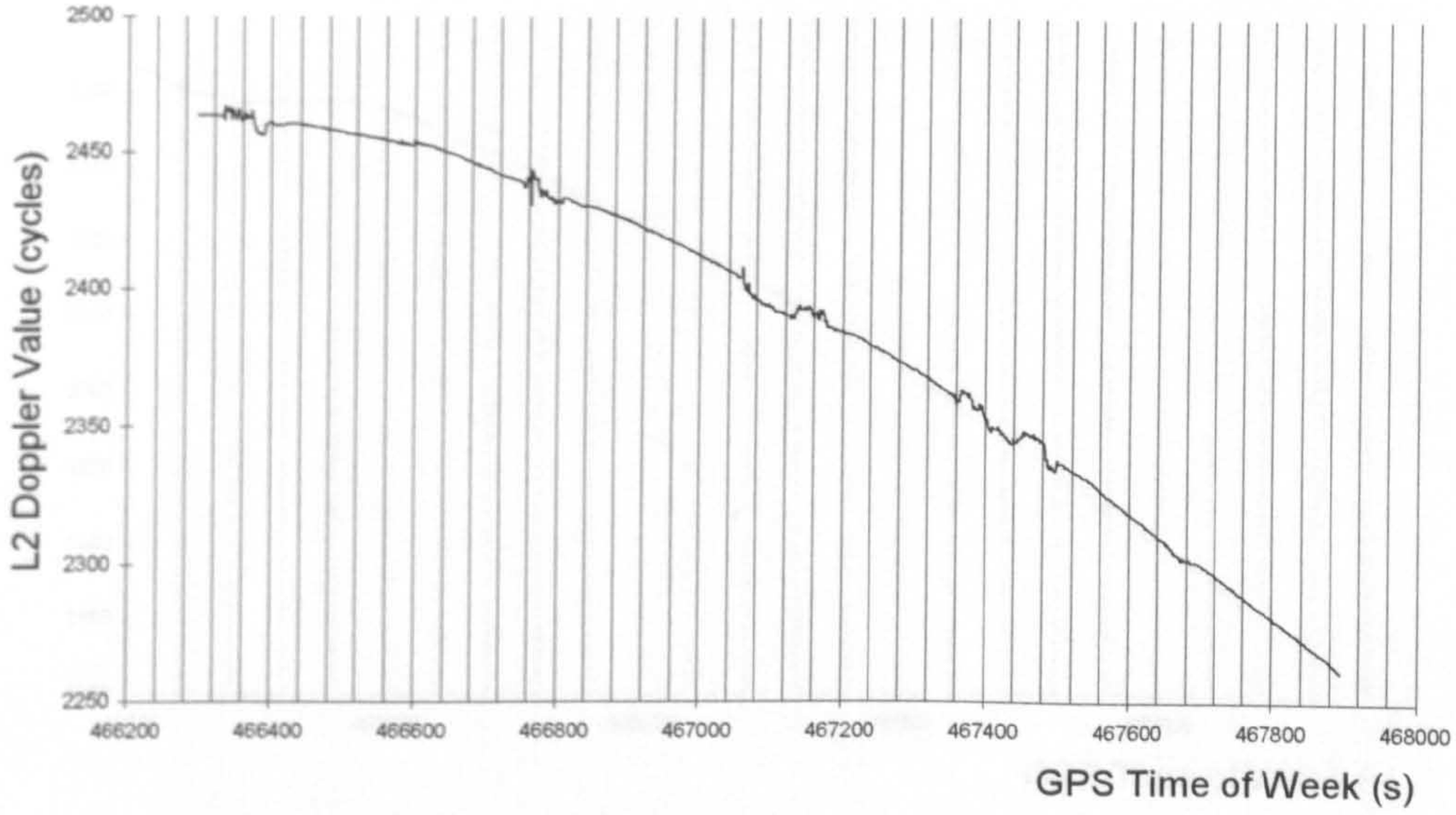

B8: Doppler shift data for Satellite 23 on L2 frequency, AS on

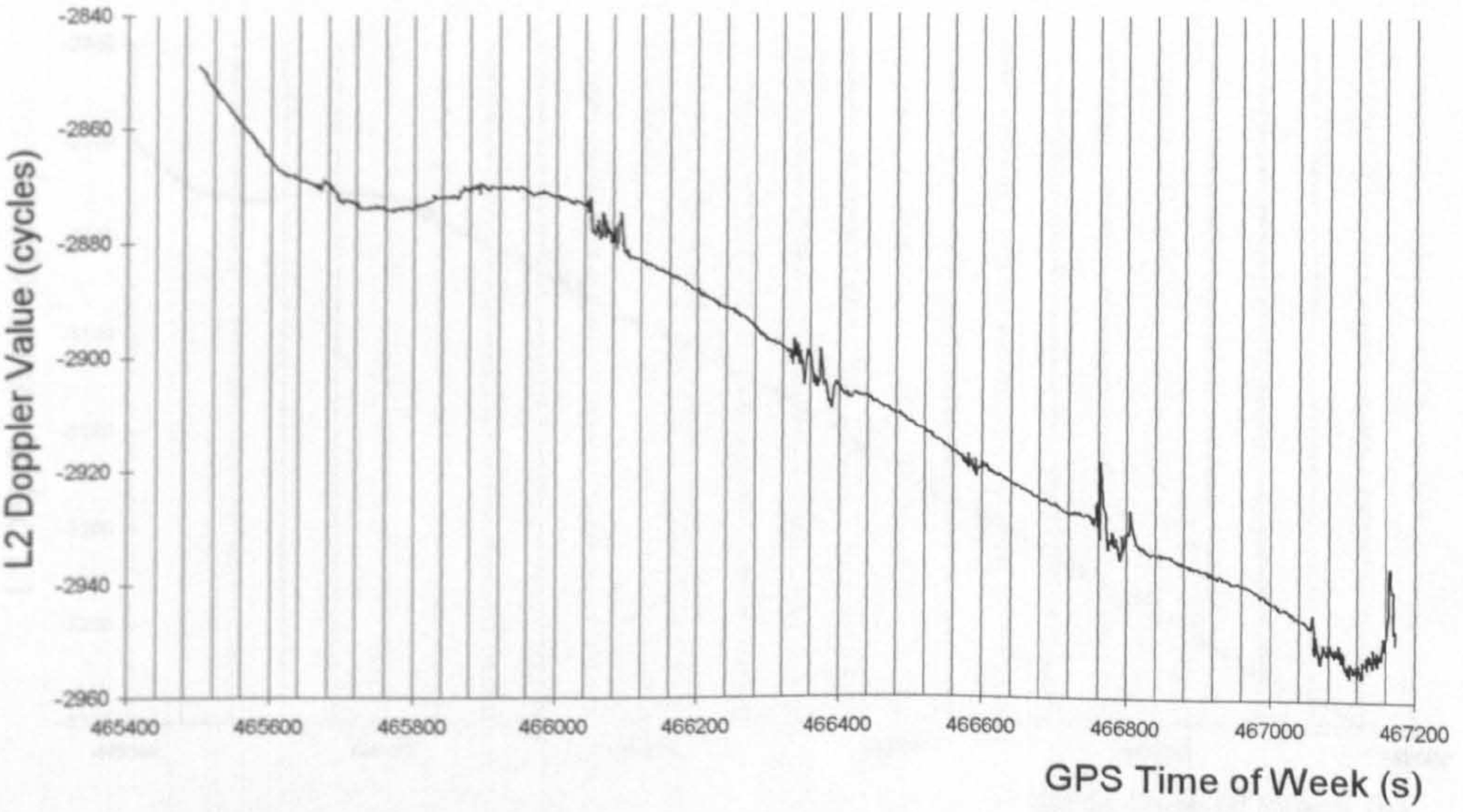

B9: Doppler shift data for Satellite 25 on L2 frequency, AS on

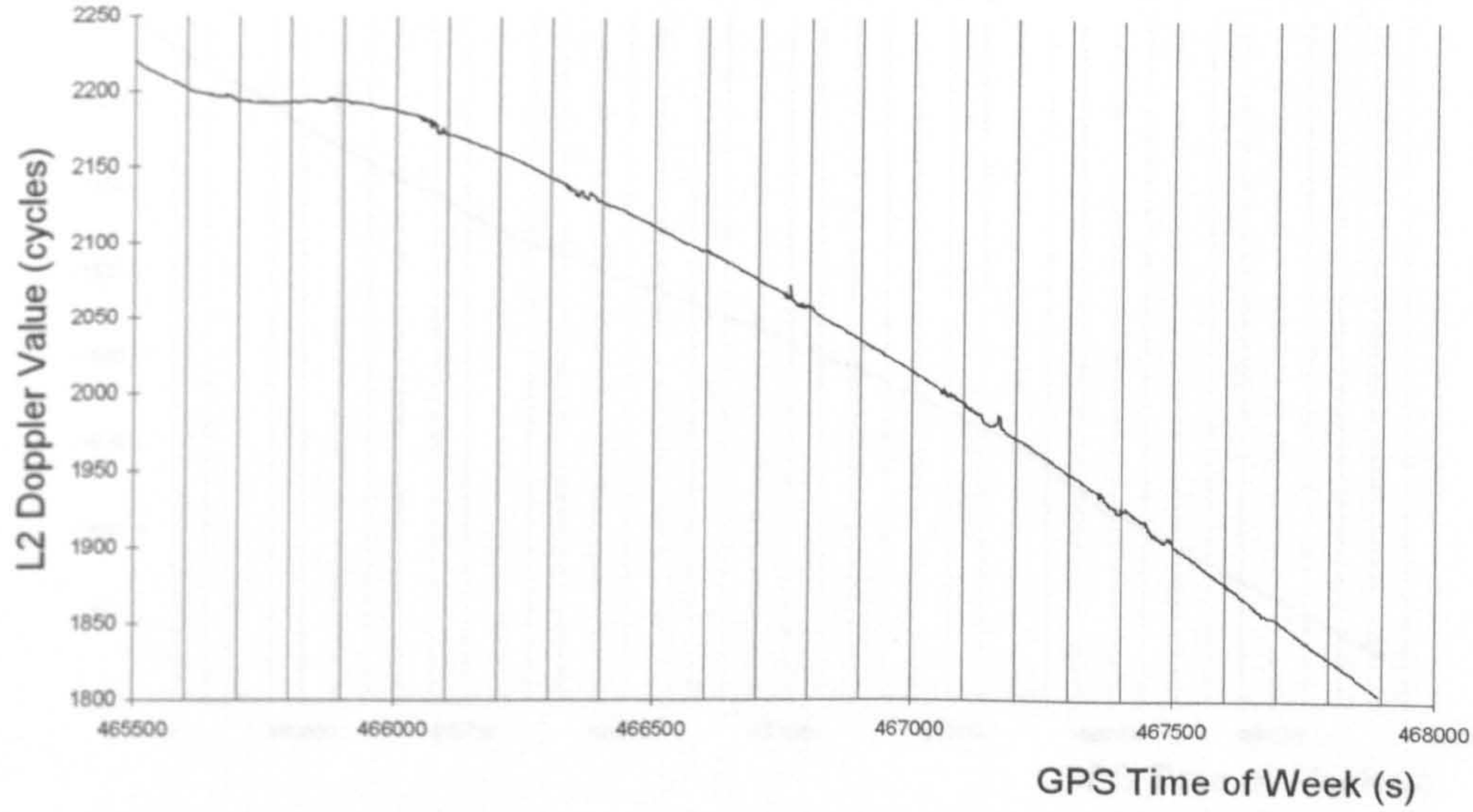

B10: Doppler shift data for Satellite 28 on L2 frequency, AS on

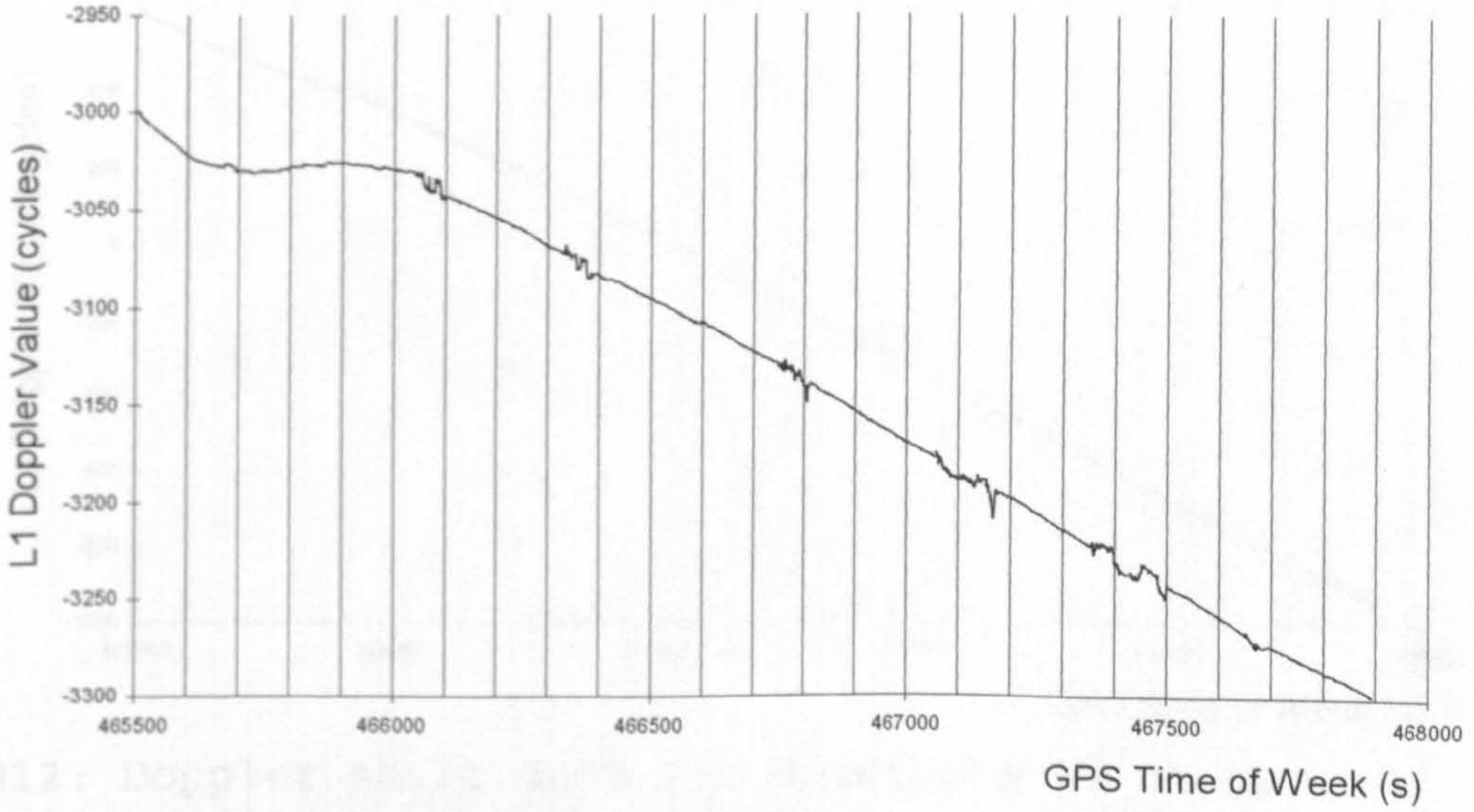

B11: Doppler shift data for Satellite 06 on L1 frequency, AS on

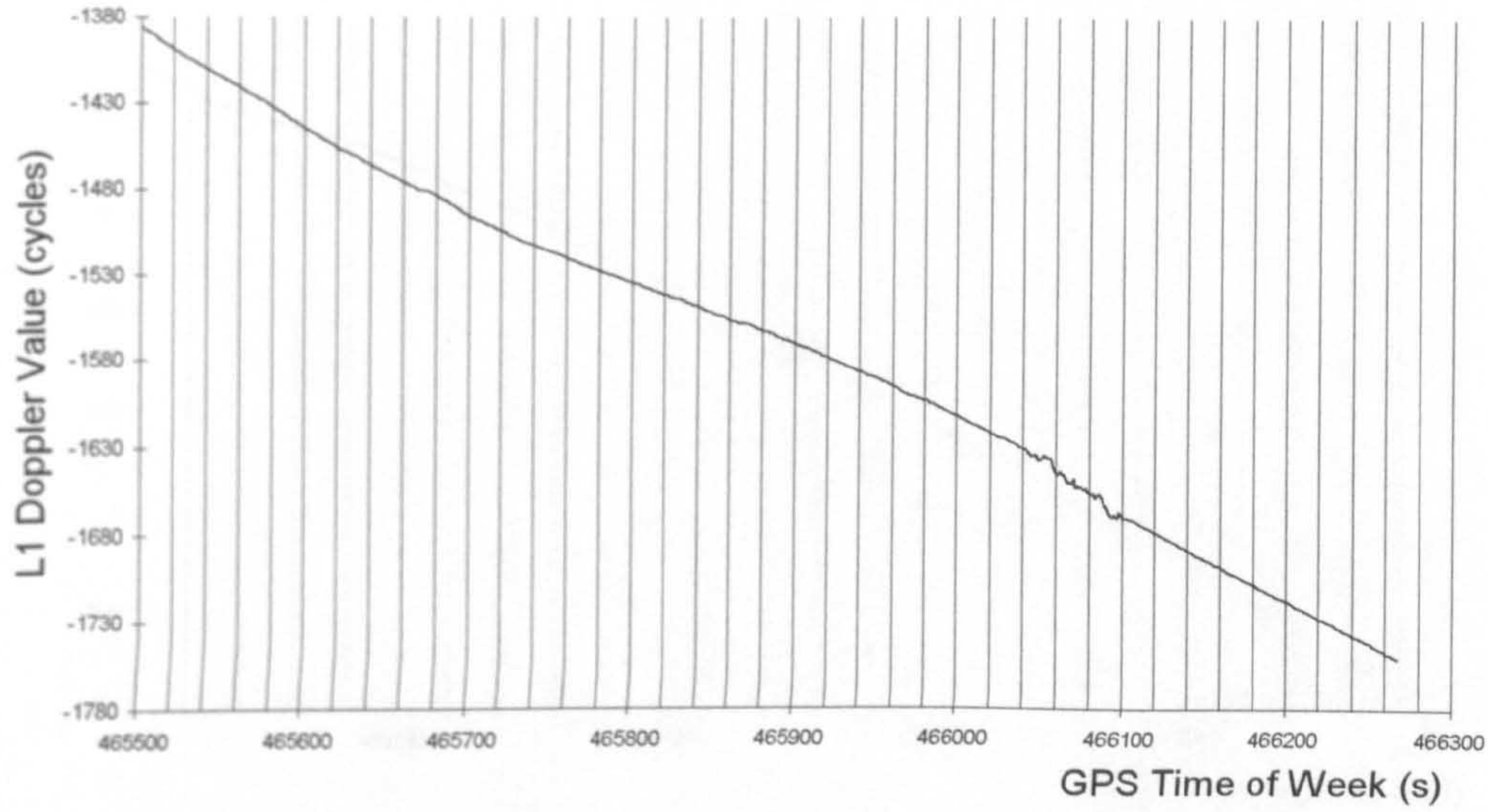

B12: Doppler shift data for Satellite 16 on L1 frequency, AS on

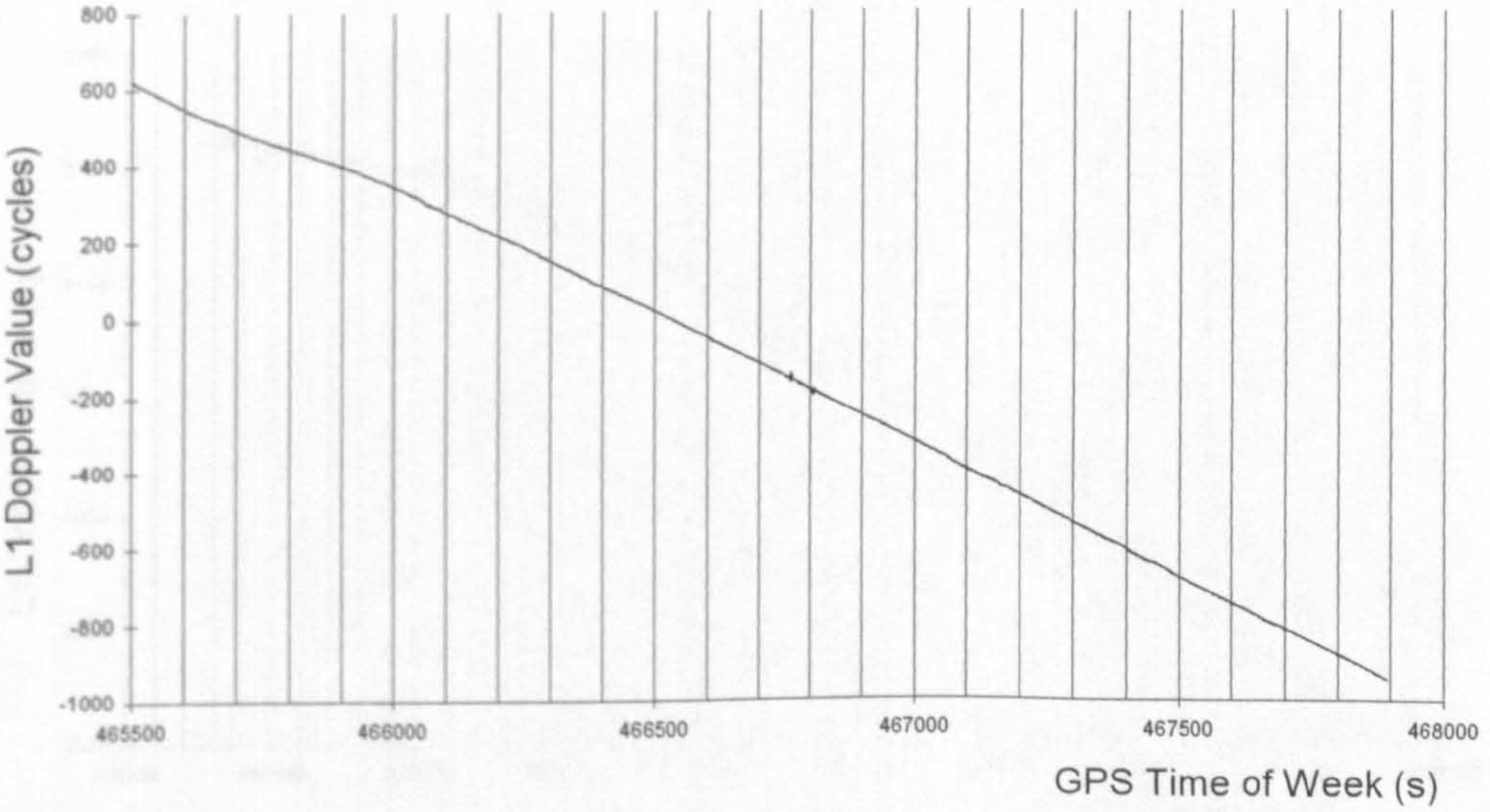

B12: Doppler shift data for Satellite 17 on L1 frequency, AS on

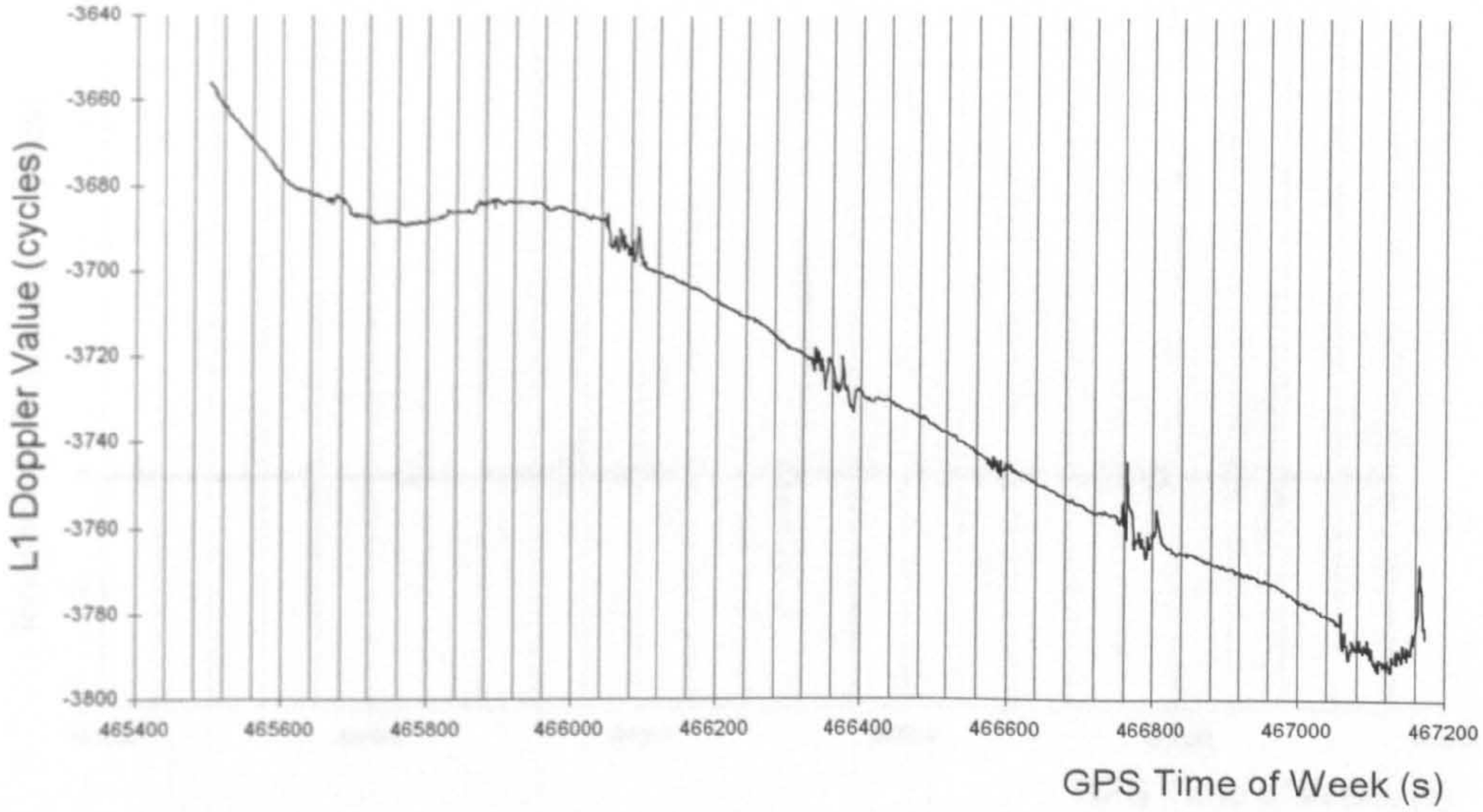

B15: Doppler shift data for Satellite 25 on L1 frequency, AS on

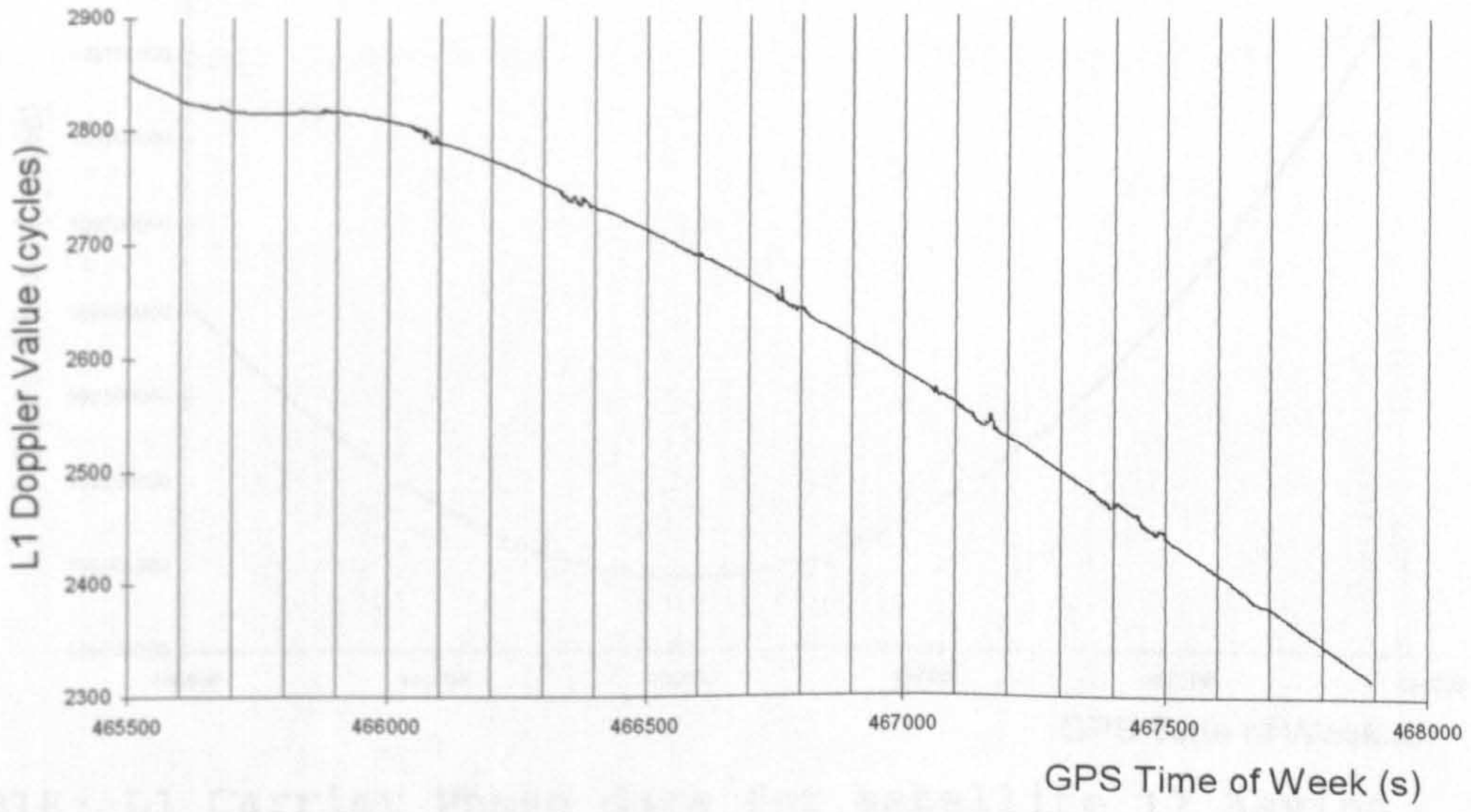

B16: Doppler shift data for Satellite 28 on L1 frequency, AS on

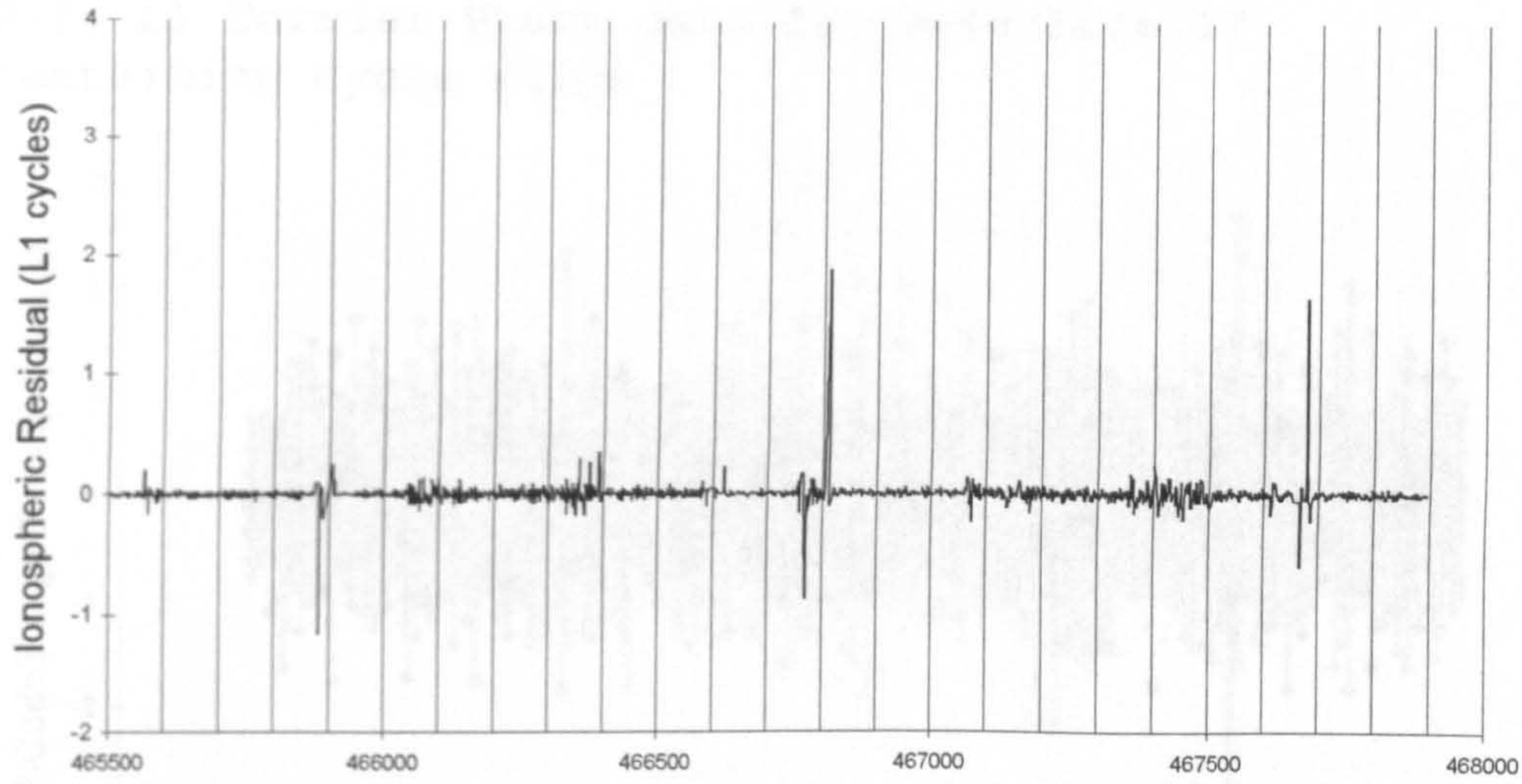

B17: Ionospheric Residual data for Satellite, AS on

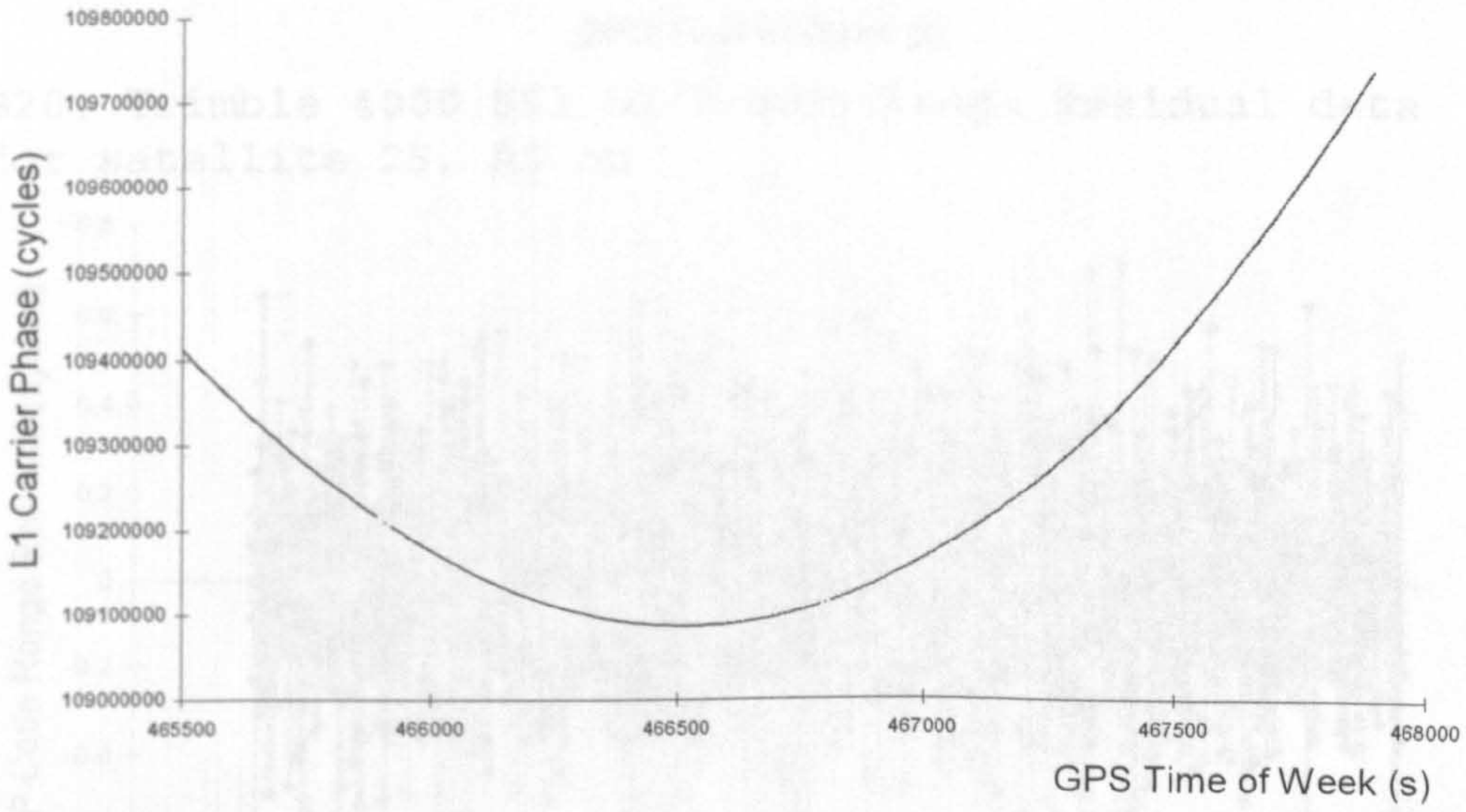

B18: L1 Carrier Phase data for satellite 17 having been corrected for cycle slips

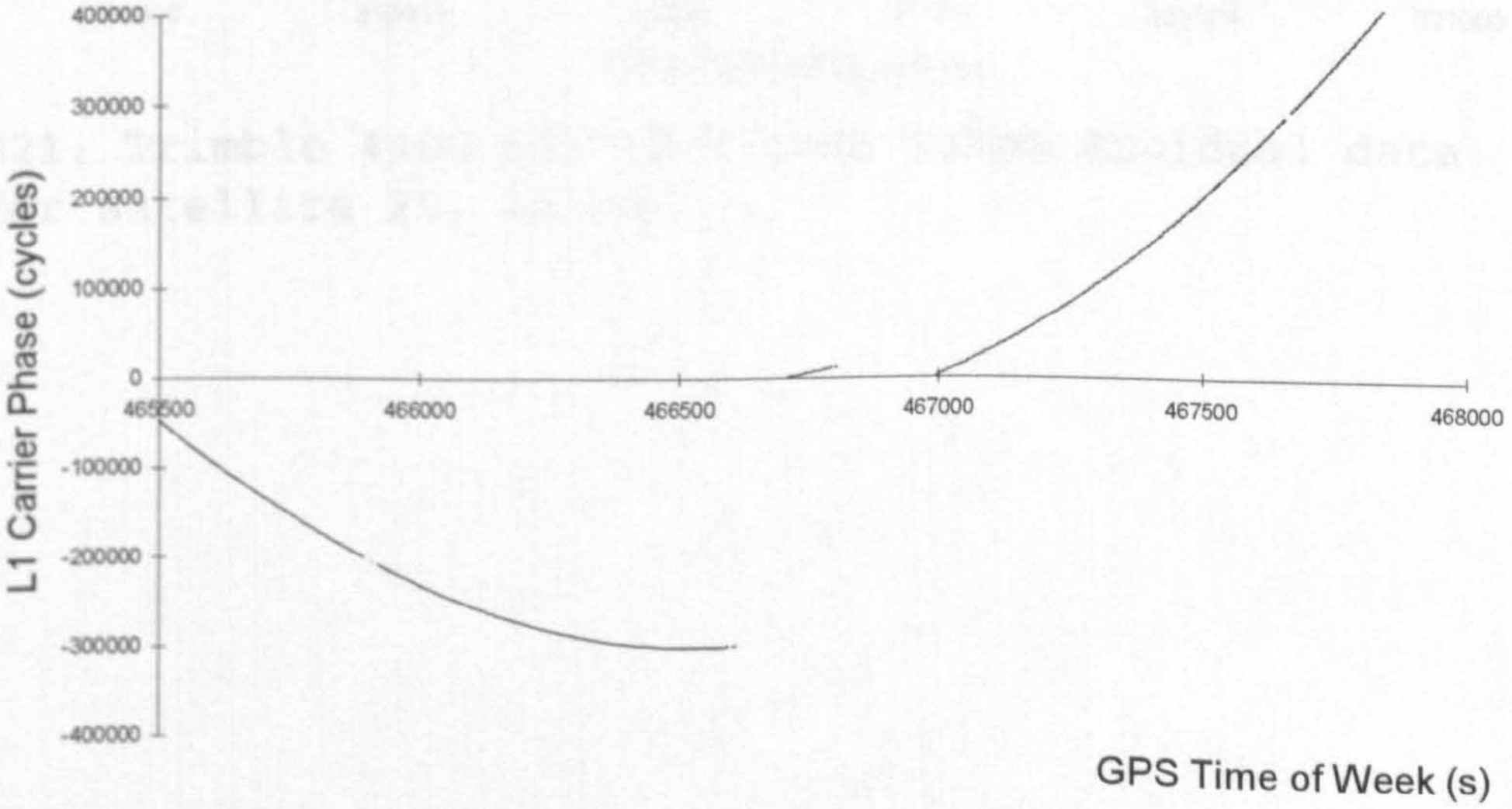

B19: L1 Carrier Phase data for satellite 17 containing cycle slips

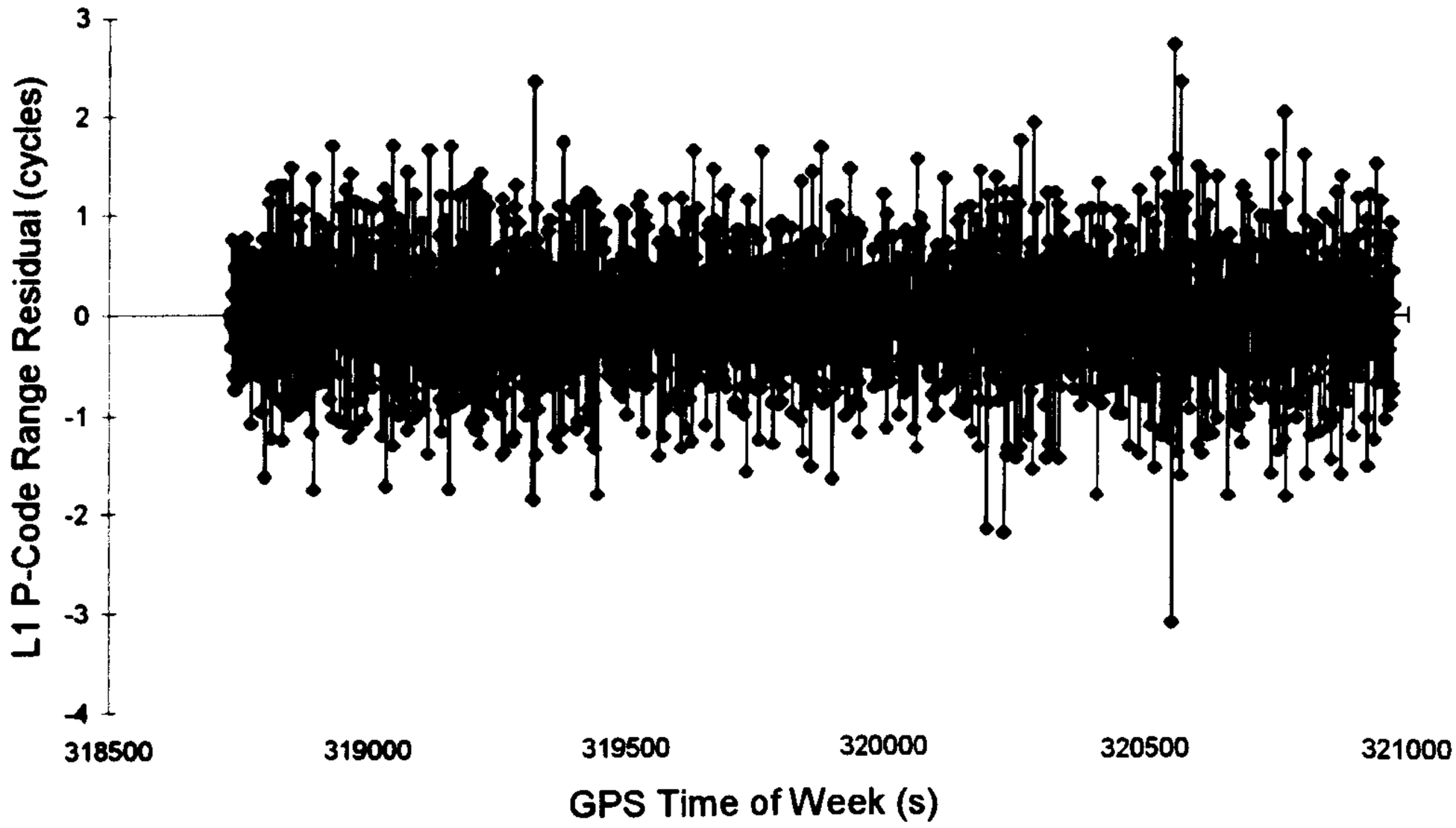

B20: Trimble 4000 SSI L1 Y-code Range Residual data for satellite 25, AS on

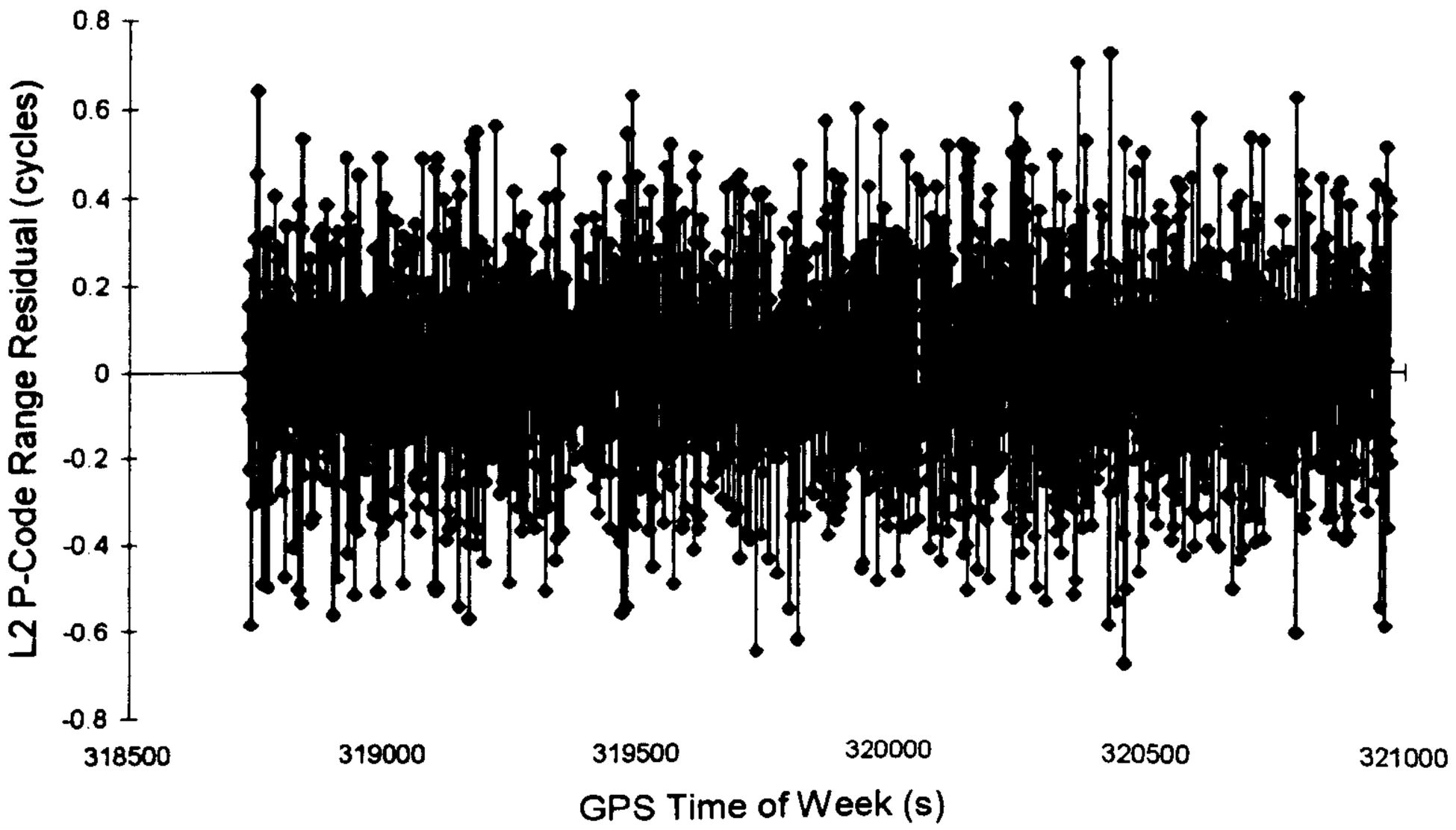

B21: Trimble 4000 SSI L2 Y-code Range Residual data for satellite 25, AS on

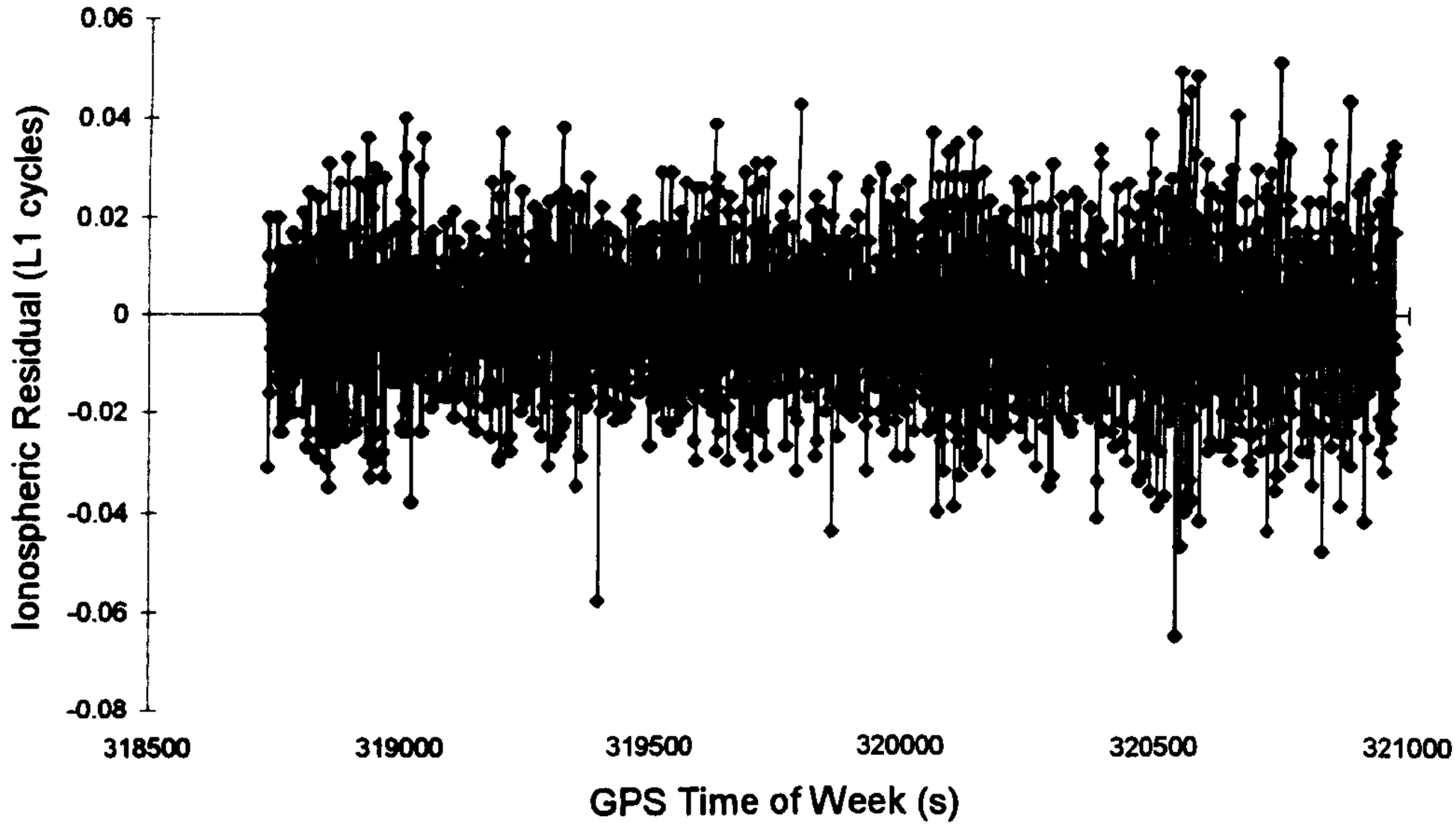

B22: Trimble 4000 SSI Ionospheric Residual data for satellite 25, AS on

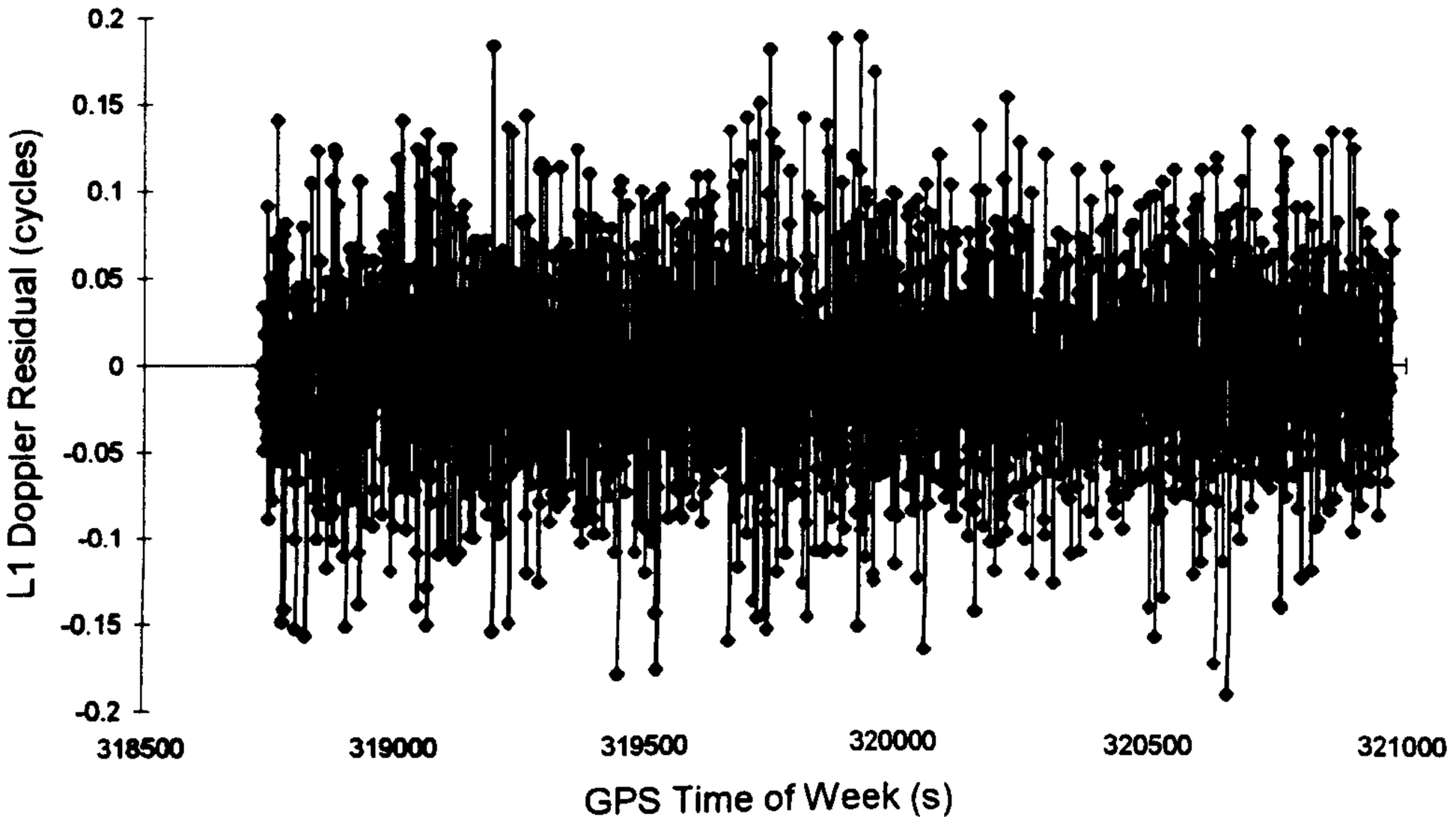

B23: Trimble 4000 SSI L1 Doppler Residual data for satellite 25, AS on

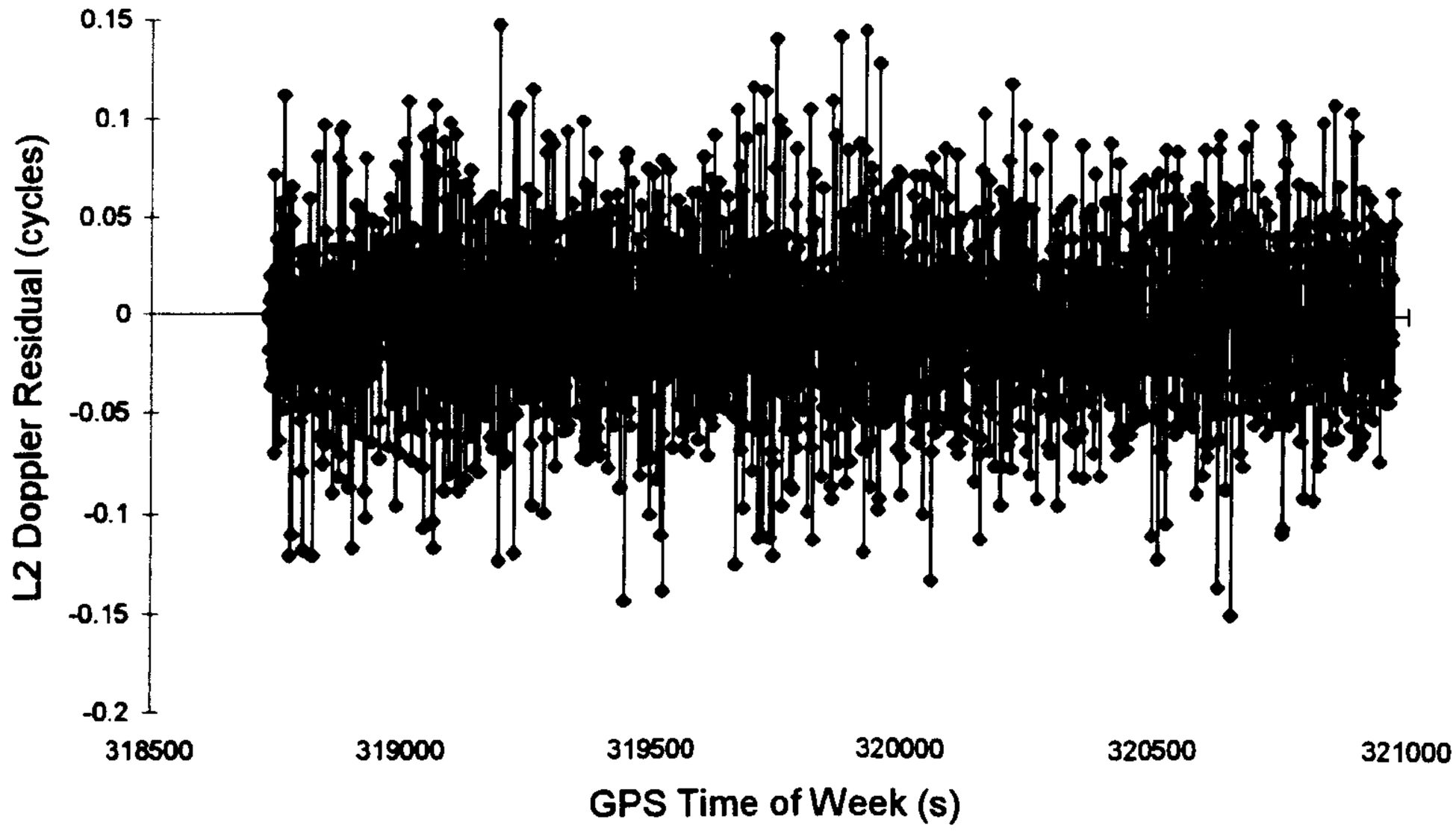

B24: Trimble 4000 SSI L2 Doppler Residual data for satellite 25, AS on

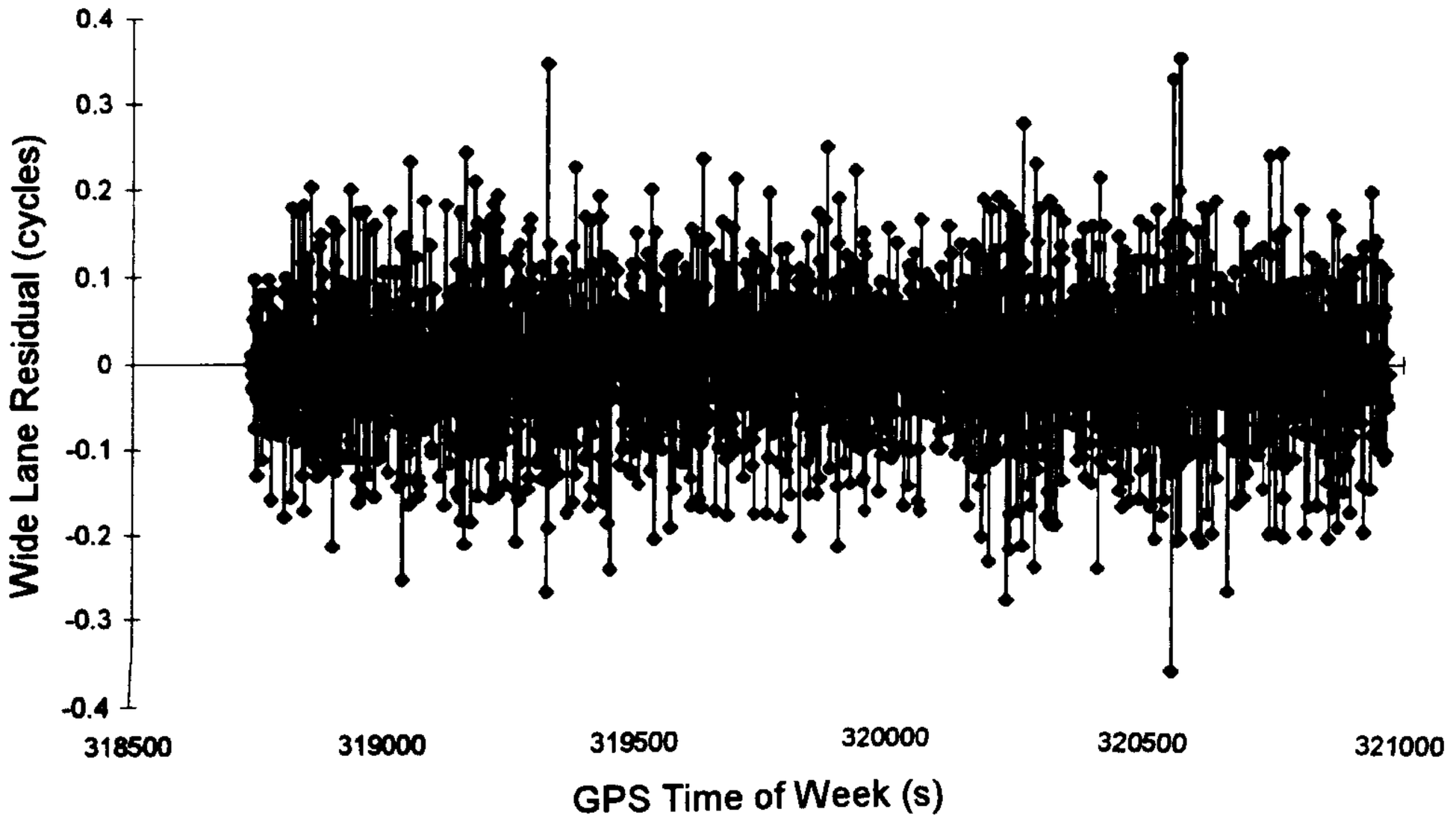

B25: Trimble 4000 SSI Wide Lane Residual data for satellite 25, AS on

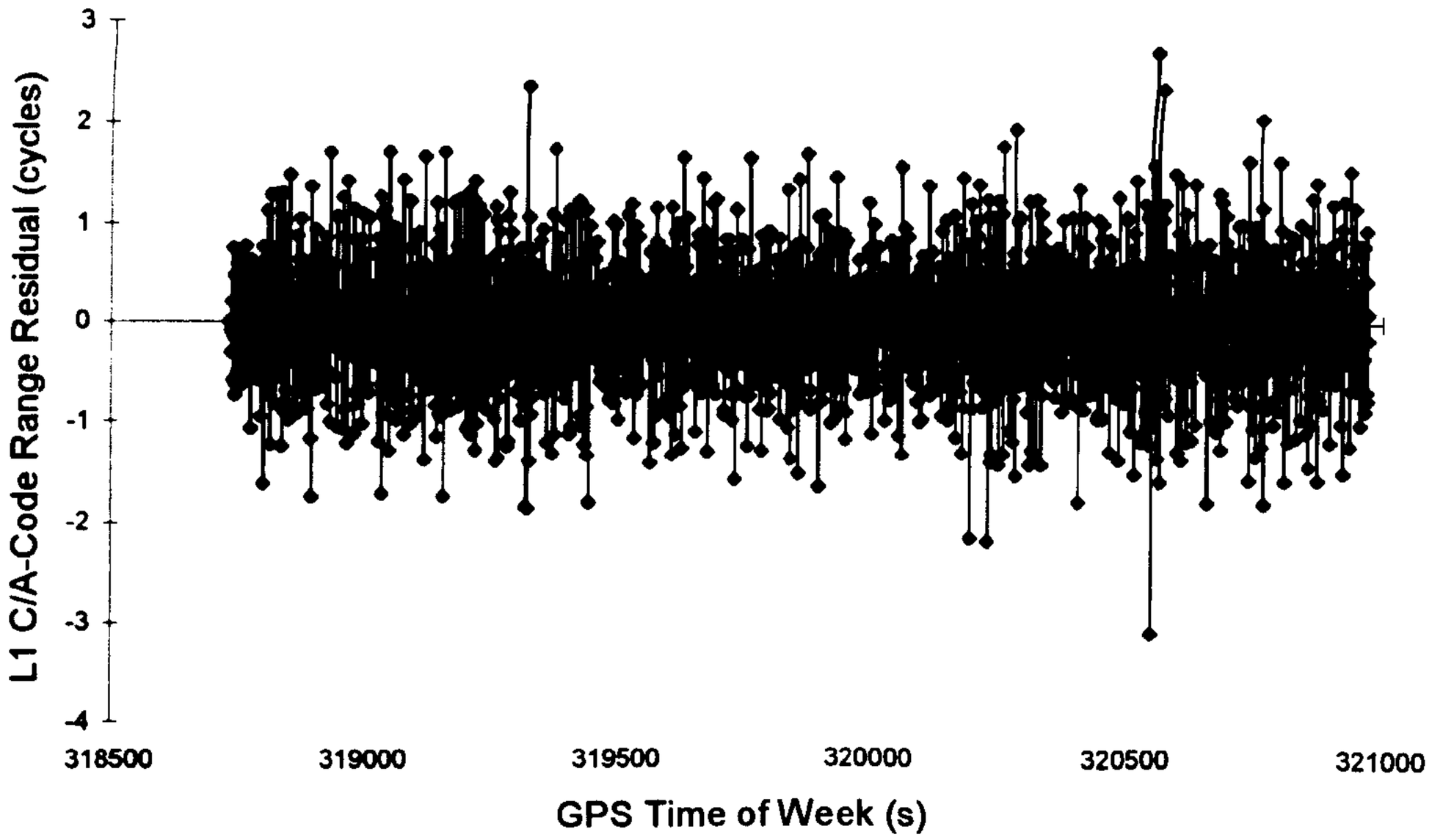

B26: Trimble 4000 SSI L1 C/A-code Range Residual data for satellite 25, AS on

APPENDIX C

Air Warfare Centre
Royal Air Force Cranwell

POLAR CERTIFICATE

This is to certify that

on Aries Flight 96/1
13-15 May 1996

Mr G Roberts

reached the 'Top of the World' and circumnavigated the North Geographic Pole.

Group Captain
Operational Doctrine & Training

APPENDIX D

Short Baseline results ENH, and Delta ENH

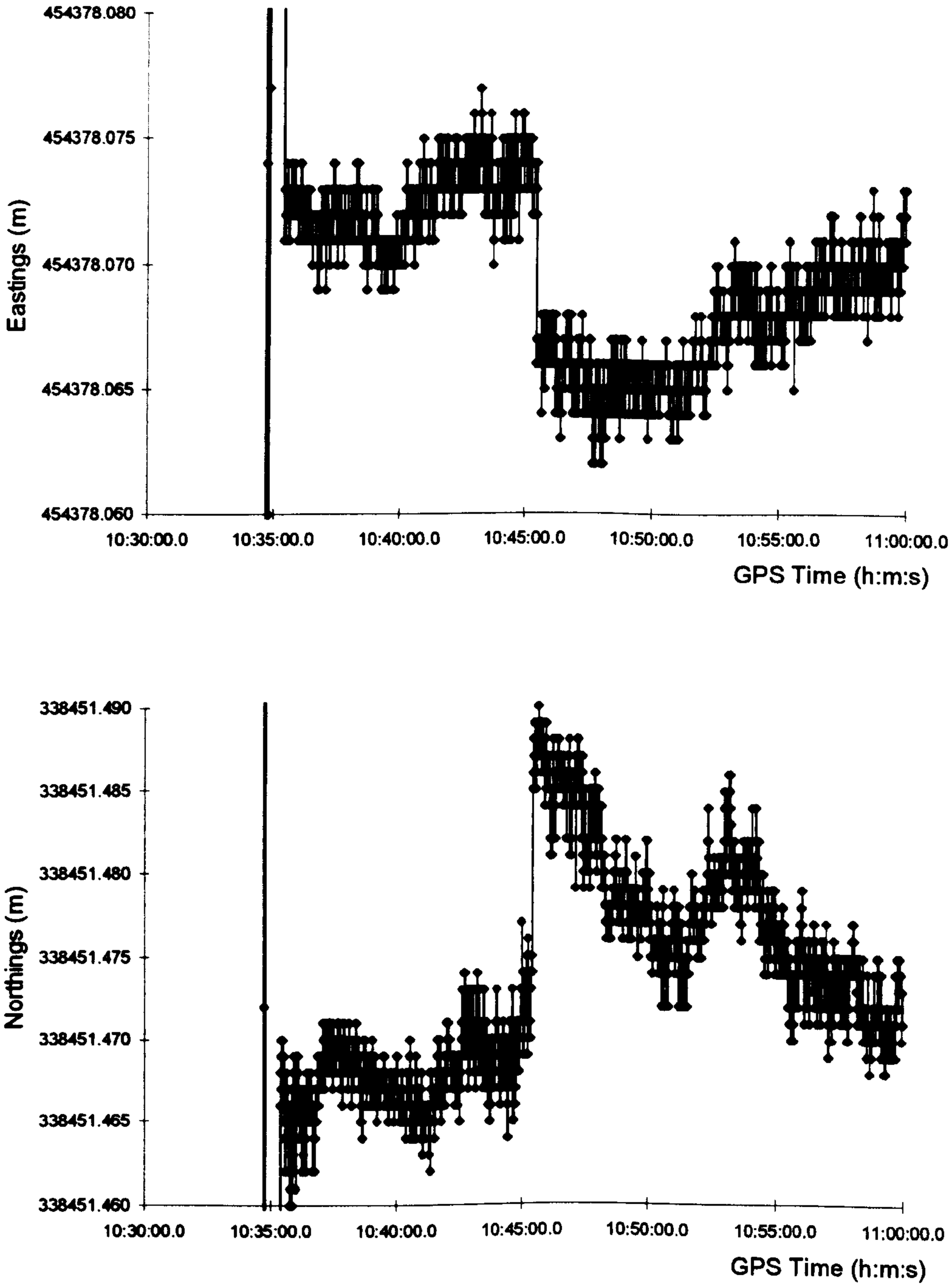

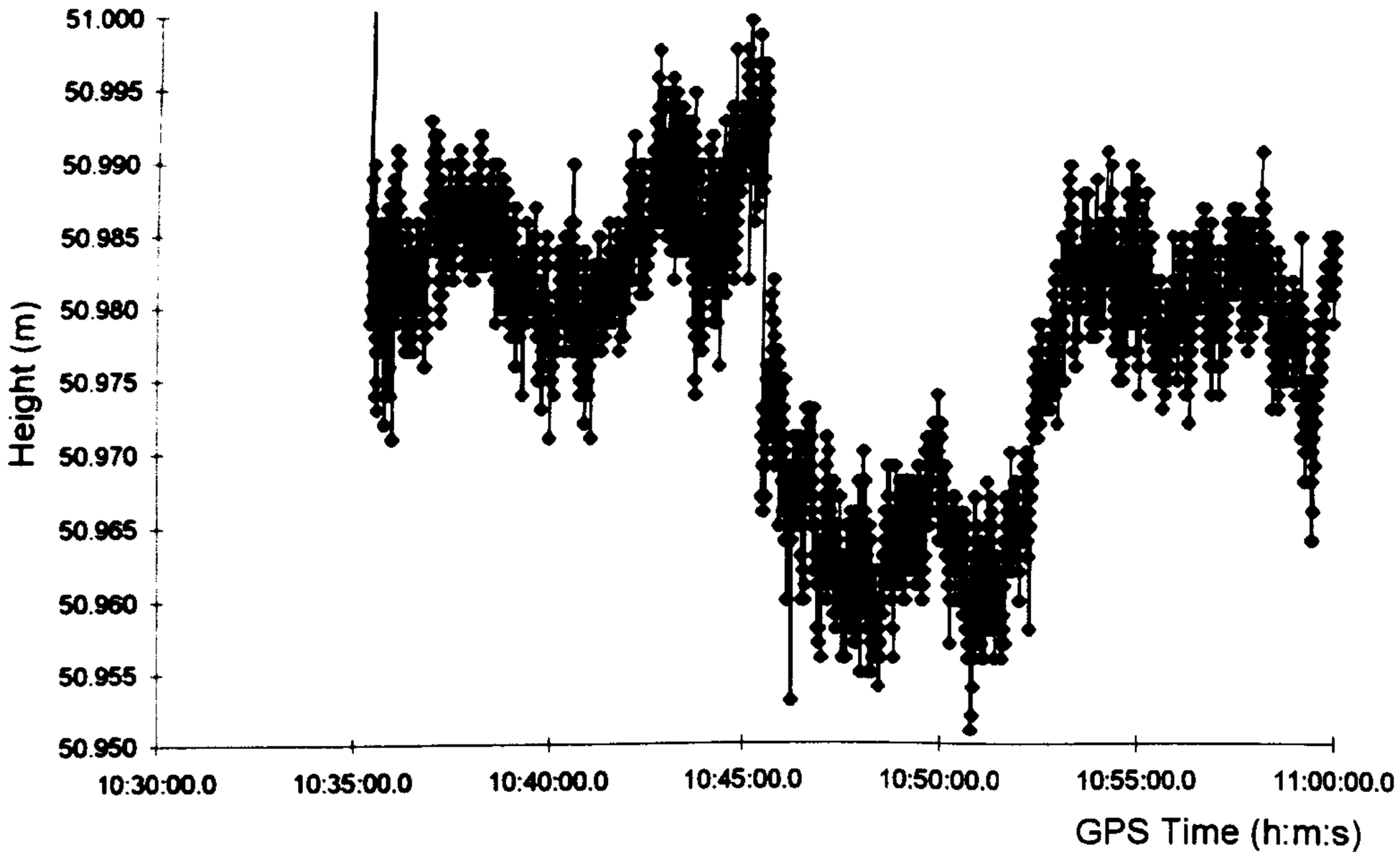
Height (m)
51.000
50.995
50.990
50.985
50.980
50.975
50.970
50.965
50.960
50.955
50.950
10:30:00.0
10:35:00.0
10:40:00.0
10:45:00.0
10:50:00.0
10:55:00.0
11:00:00.0
GPS Time (h:m:s)

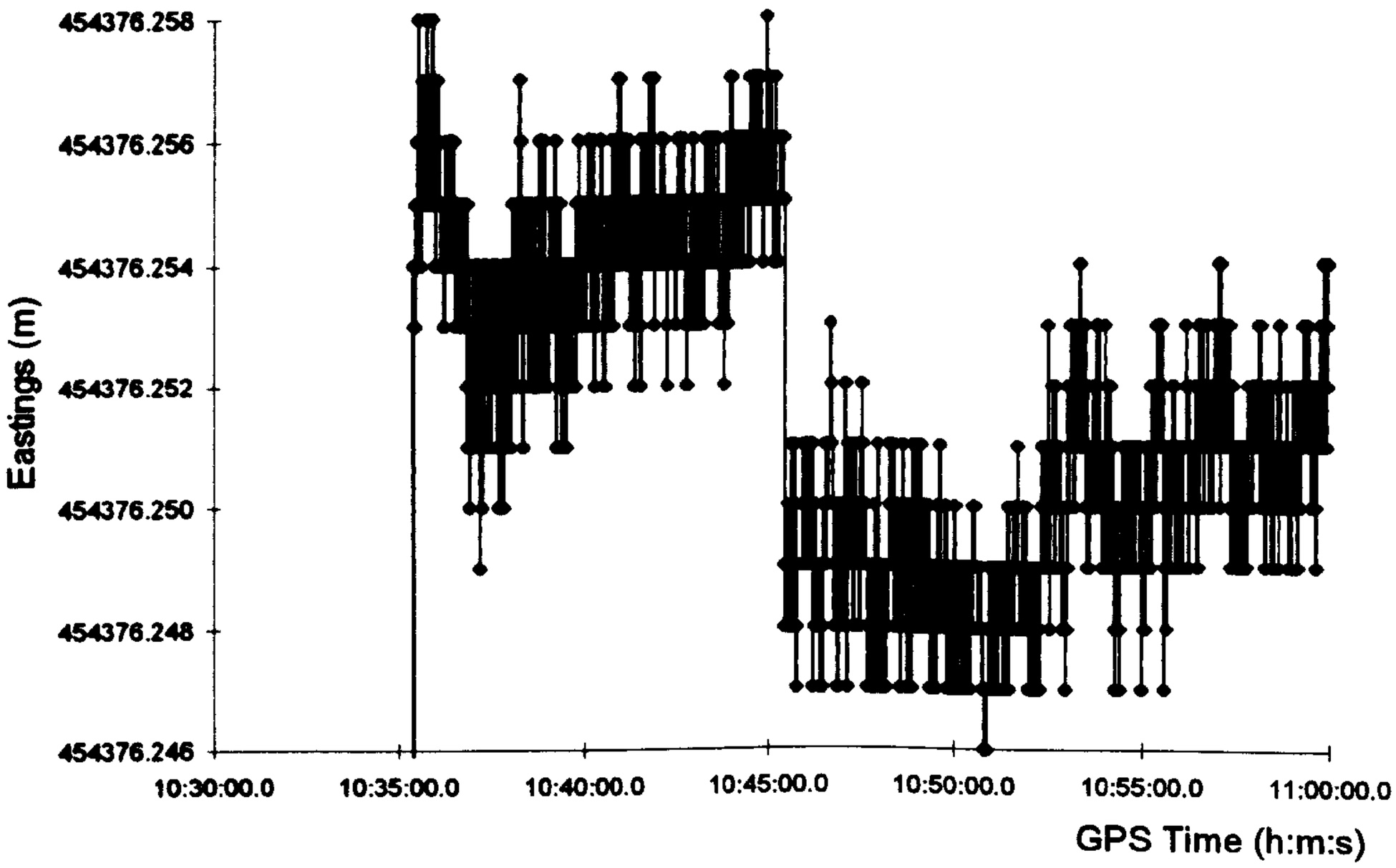
Eastings (m)
454376.258
454376.256
454376.254
454376.252
454376.250
454376.248
454376.246
10:30:00.0
10:35:00.0
10:40:00.0
10:45:00.0
10:50:00.0
10:55:00.0
11:00:00.0
GPS Time (h:m:s)

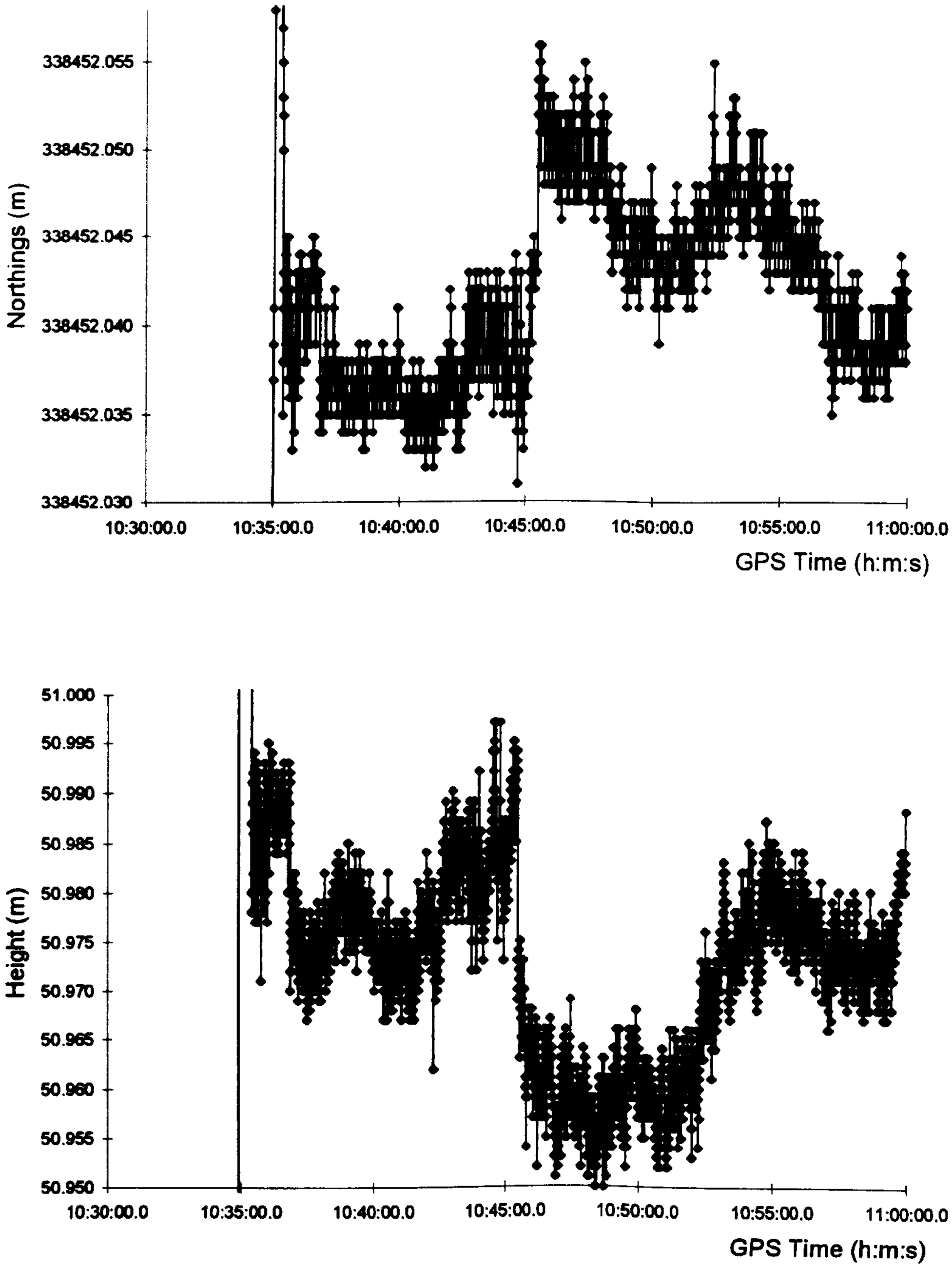
Northings (m)
338452.055
338452.050
338452.045
338452.040
338452.035
338452.030
10:30:00.0
10:35:00.0
10:40:00.0
10:45:00.0
10:50:00.0
10:55:00.0
11:00:00.0
GPS Time (h:m:s)
Height (m)
51.000
50.995
50.990
50.985
50.980
50.975
50.970
50.965
50.960
50.955
50.950
10:30:00.0
10:35:00.0
10:40:00.0
10:45:00.0
10:50:00.0
10:55:00.0
11:00:00.0
GPS Time (h:m:s)

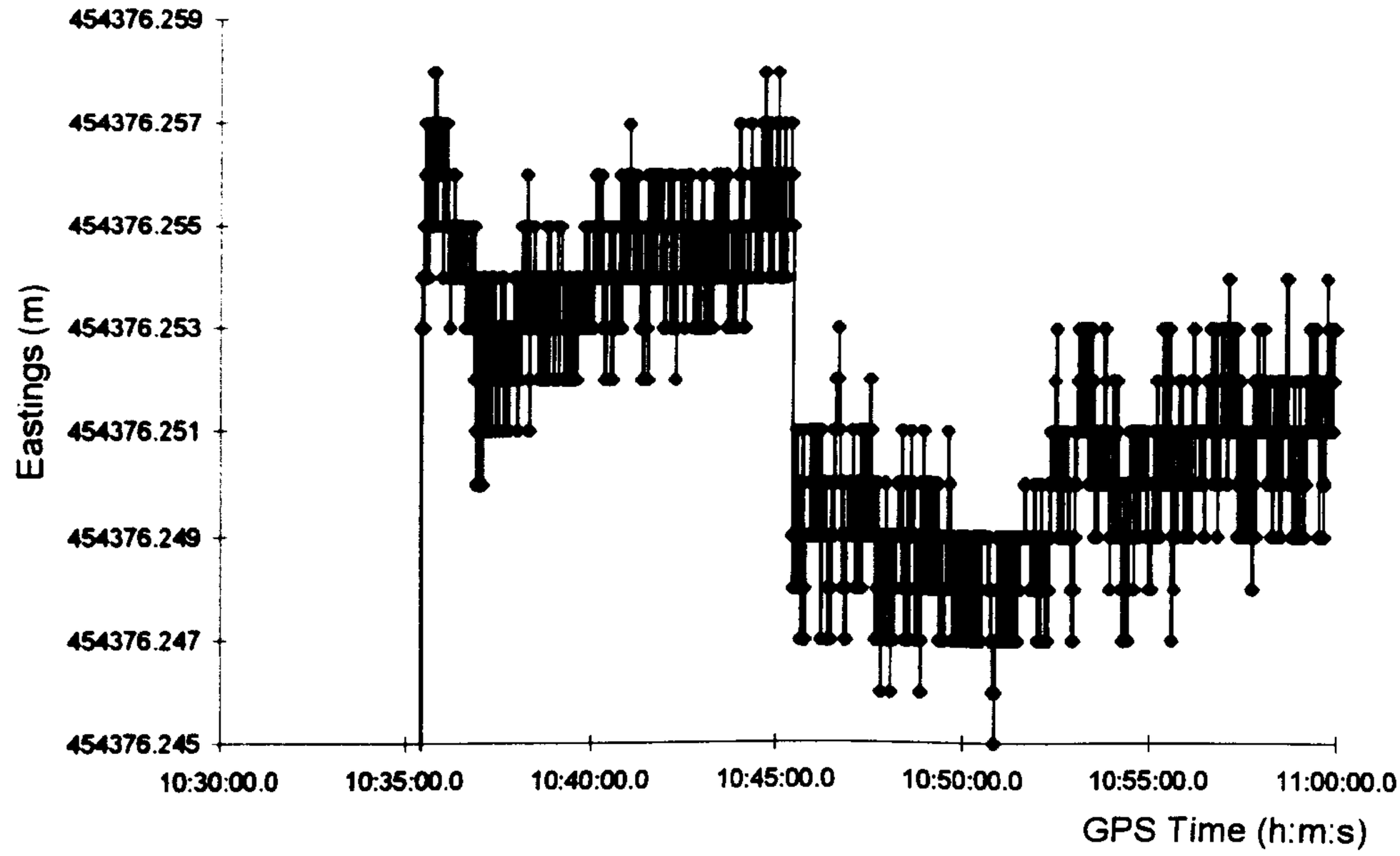
454376.259
454376.257
454376.255
454376.253
454376.251
454376.249
454376.247
454376.245
Eastings (m)
10:30:00.0
10:35:00.0
10:40:00.0
10:45:00.0
10:50:00.0
10:55:00.0
11:00:00.0
GPS Time (h:m:s)

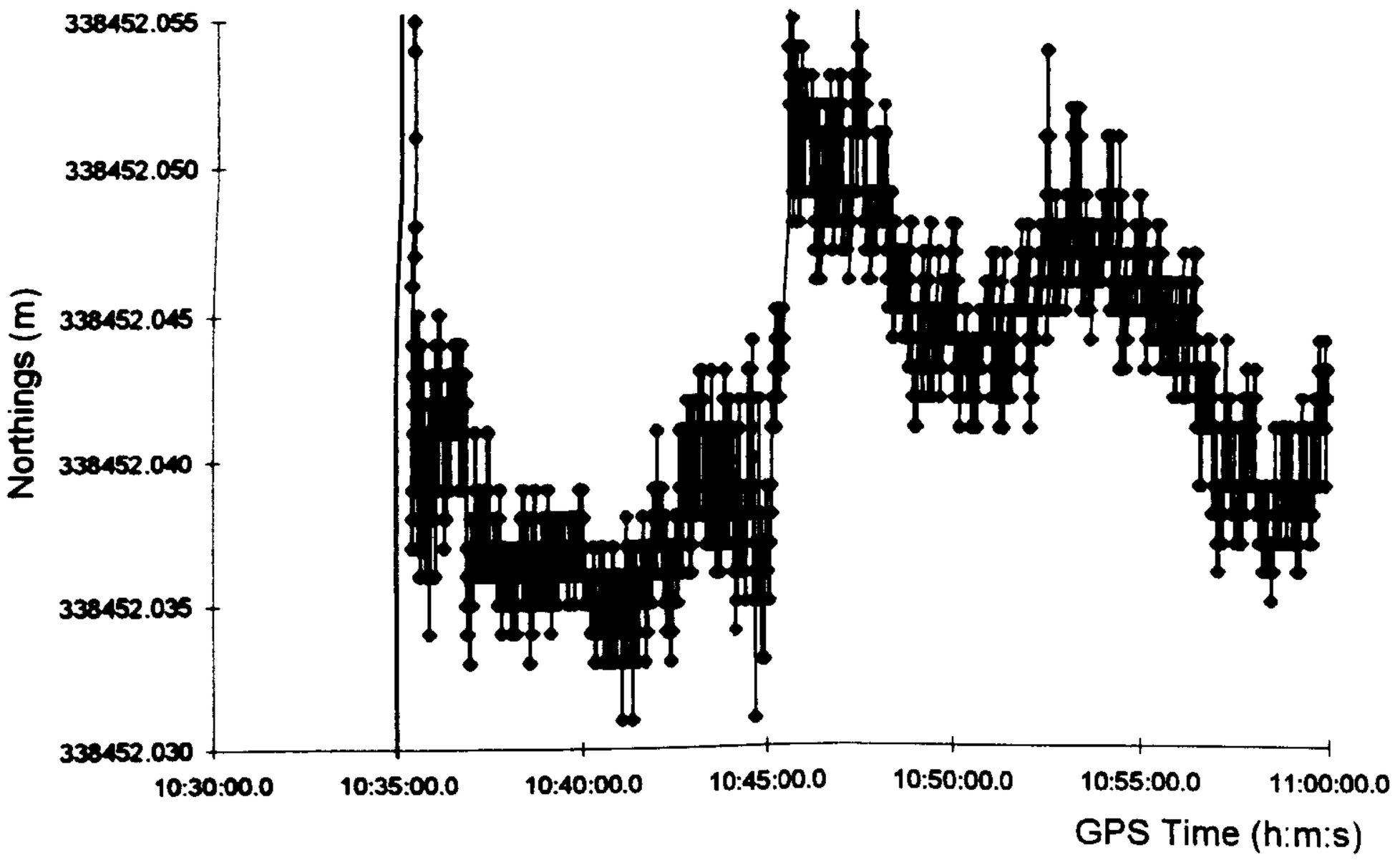
338452.055
338452.050
338452.045
338452.040
338452.035
338452.030
Northings (m)
10:30:00.0
10:35:00.0
10:40:00.0
10:45:00.0
10:50:00.0
10:55:00.0
11:00:00.0
GPS Time (h:m:s)

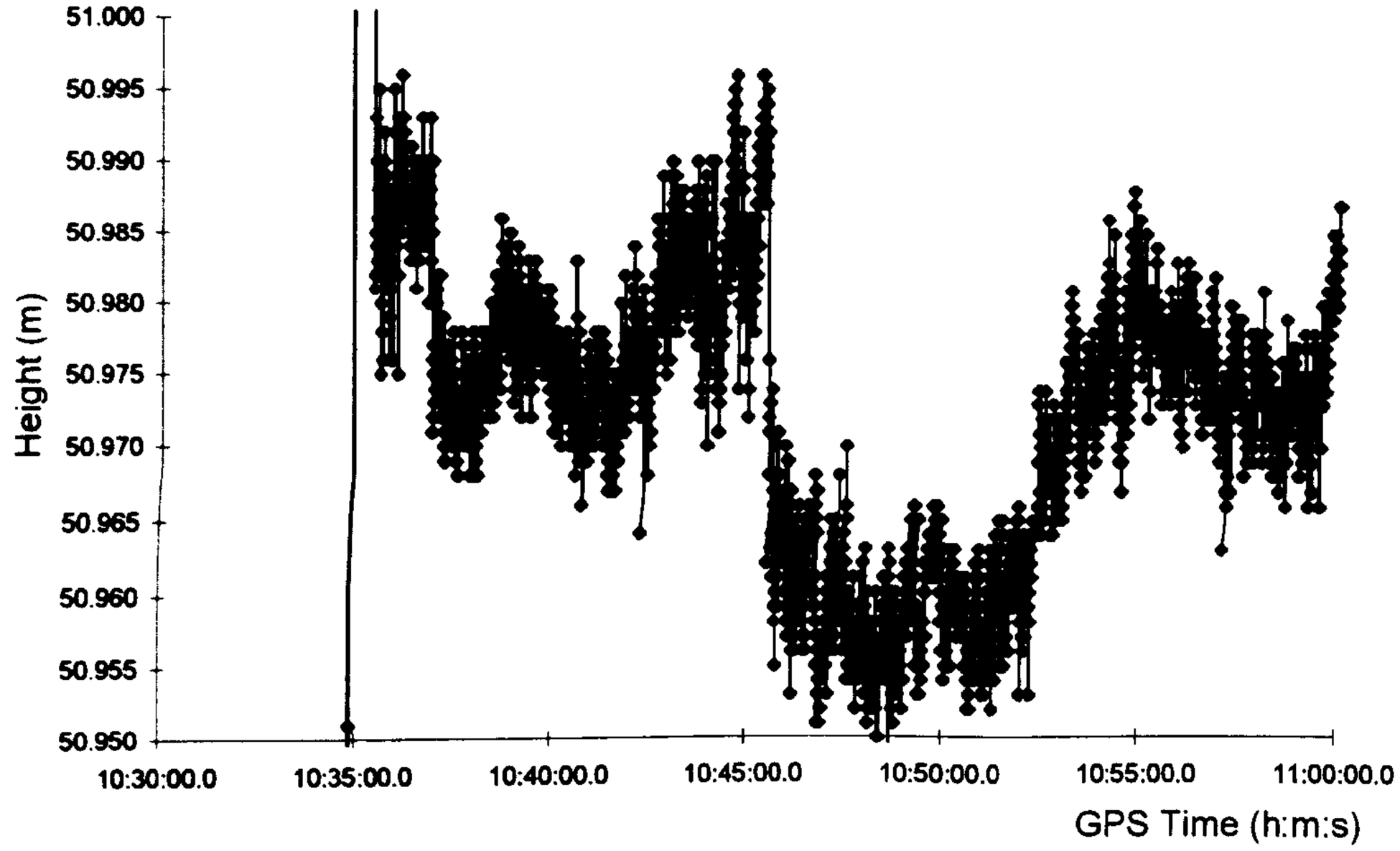
Height (m)
51.000
50.995
50.990
50.985
50.980
50.975
50.970
50.965
50.960
50.955
50.950
10:30:00.0
10:35:00.0
10:40:00.0
10:45:00.0
10:50:00.0
10:55:00.0
11:00:00.0
GPS Time (h:m:s)

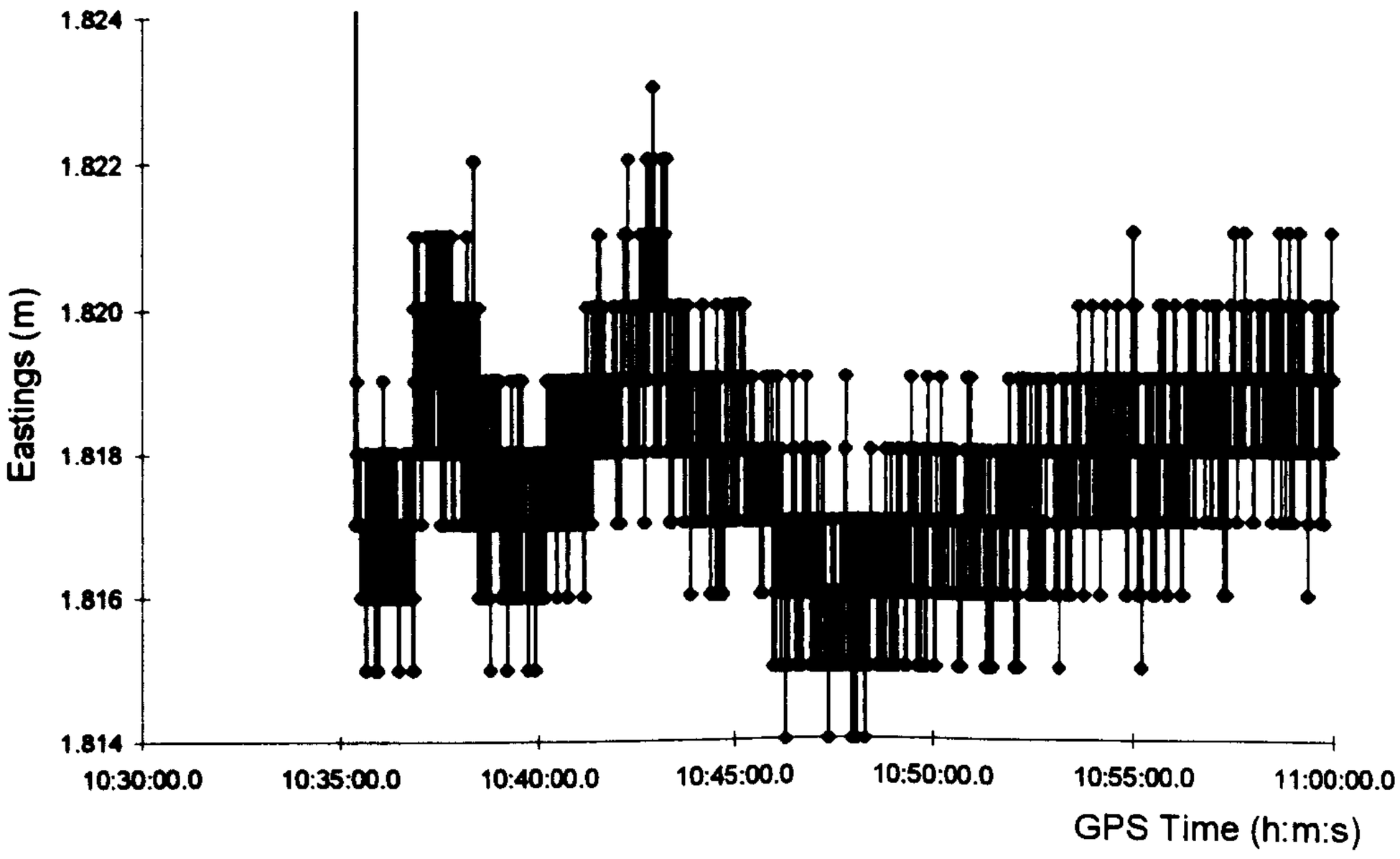
Eastings (m)
1.824
1.822
1.820
1.818
1.816
1.814
10:30:00.0
10:35:00.0
10:40:00.0
10:45:00.0
10:50:00.0
10:55:00.0
11:00:00.0
GPS Time (h:m:s)

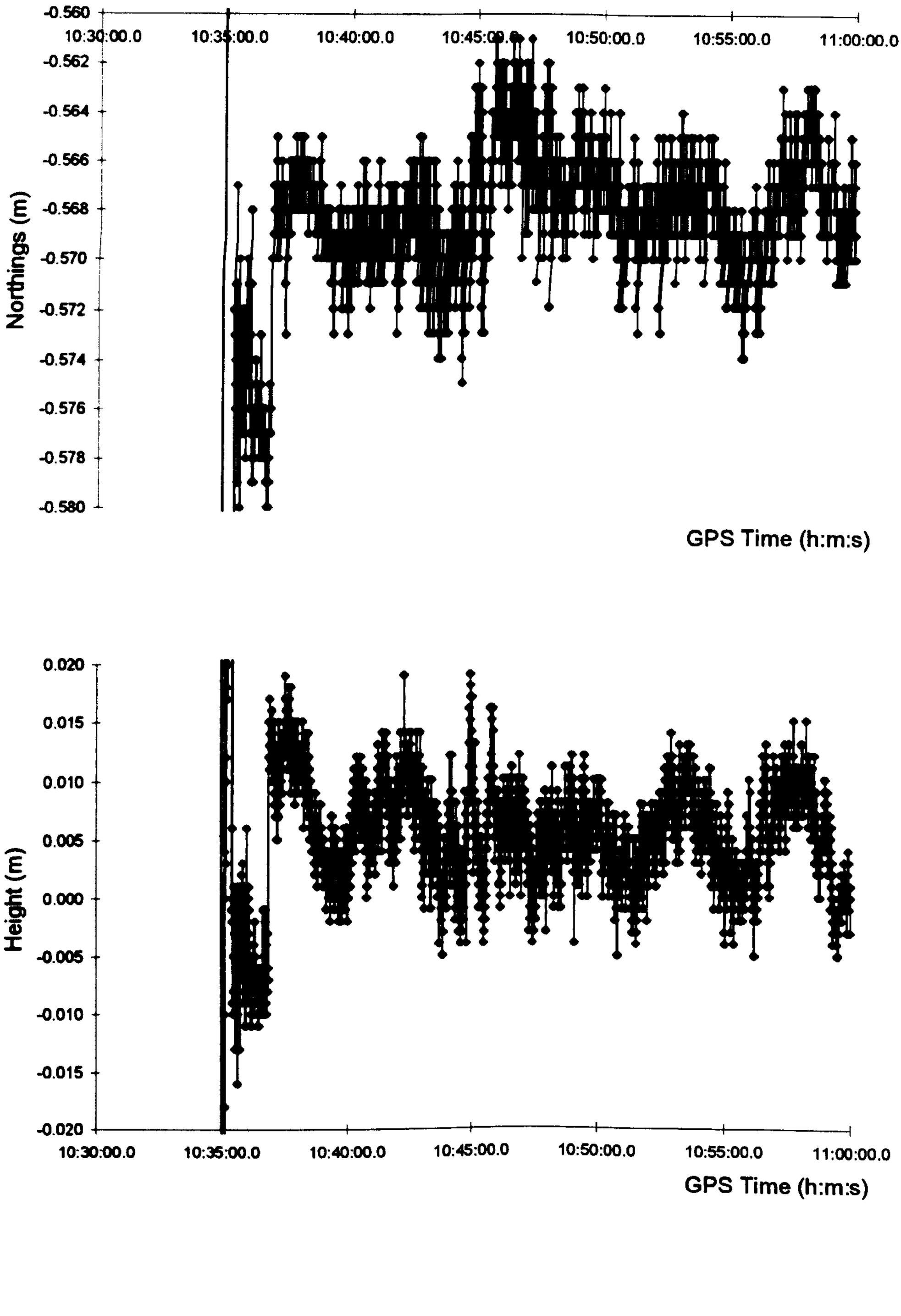
-0.560
-0.562
-0.564
-0.566
-0.568
-0.570
-0.572
-0.574
-0.576
-0.578
-0.580
Northings (m)
10:30:00.0
10:35:00.0
10:40:00.0
10:45:00.0
10:50:00.0
10:55:00.0
11:00:00.0
GPS Time (h:m:s)
0.020
0.015
0.010
0.005
0.000
-0.005
-0.010
-0.015
-0.020
Height (m)
10:30:00.0
10:35:00.0
10:40:00.0
10:45:00.0
10:50:00.0
10:55:00.0
11:00:00.0
GPS Time (h:m:s)

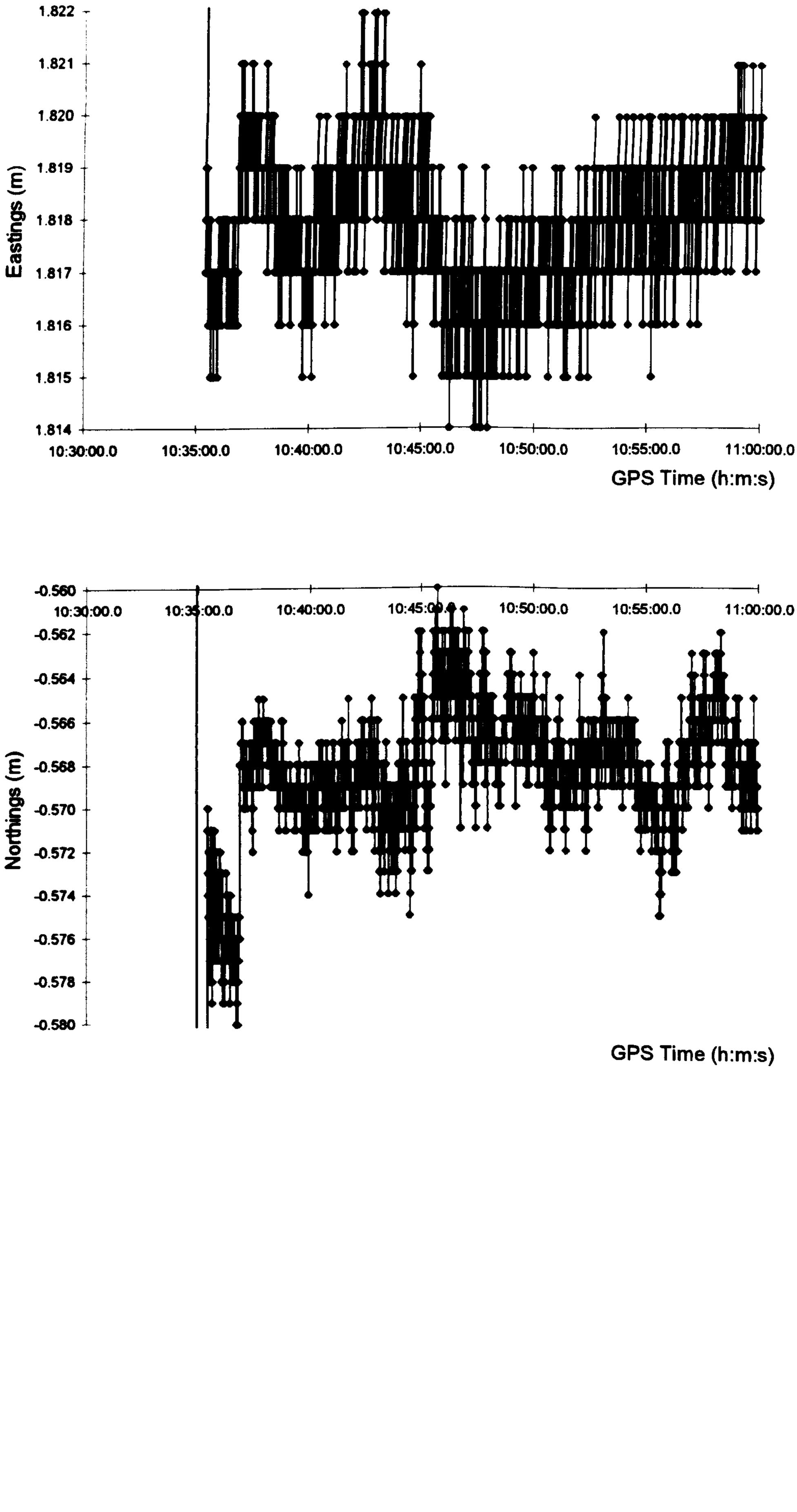
Eastings (m)
1.822
1.821
1.820
1.819
1.818
1.817
1.816
1.815
1.814
10:30:00.0
10:35:00.0
10:40:00.0
10:45:00.0
10:50:00.0
10:55:00.0
11:00:00.0
GPS Time (h:m:s)
Northings (m)
-0.560
-0.562
-0.564
-0.566
-0.568
-0.570
-0.572
-0.574
-0.576
-0.578
-0.580
10:30:00.0
10:35:00.0
10:40:00.0
10:45:00.0
10:50:00.0
10:55:00.0
11:00:00.0
GPS Time (h:m:s)

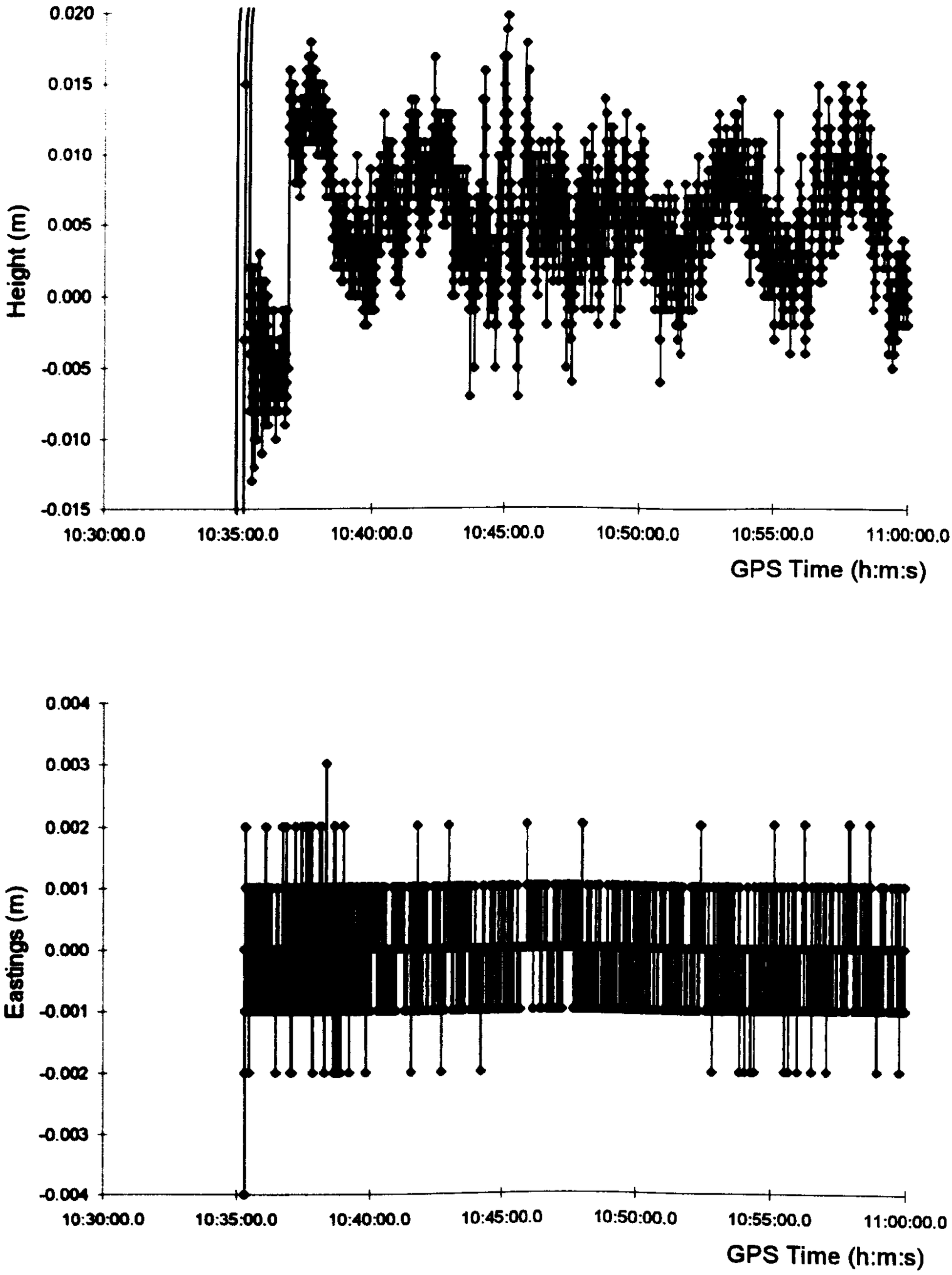
Height (m)
0.020
0.015
0.010
0.005
0.000
-0.005
-0.010
-0.015
10:30:00.0
10:35:00.0
10:40:00.0
10:45:00.0
10:50:00.0
10:55:00.0
11:00:00.0
GPS Time (h:m:s)
Eastings (m)
0.004
0.003
0.002
0.001
0.000
-0.001
-0.002
-0.003
-0.004
10:30:00.0
10:35:00.0
10:40:00.0
10:45:00.0
10:50:00.0
10:55:00.0
11:00:00.0
GPS Time (h:m:s)

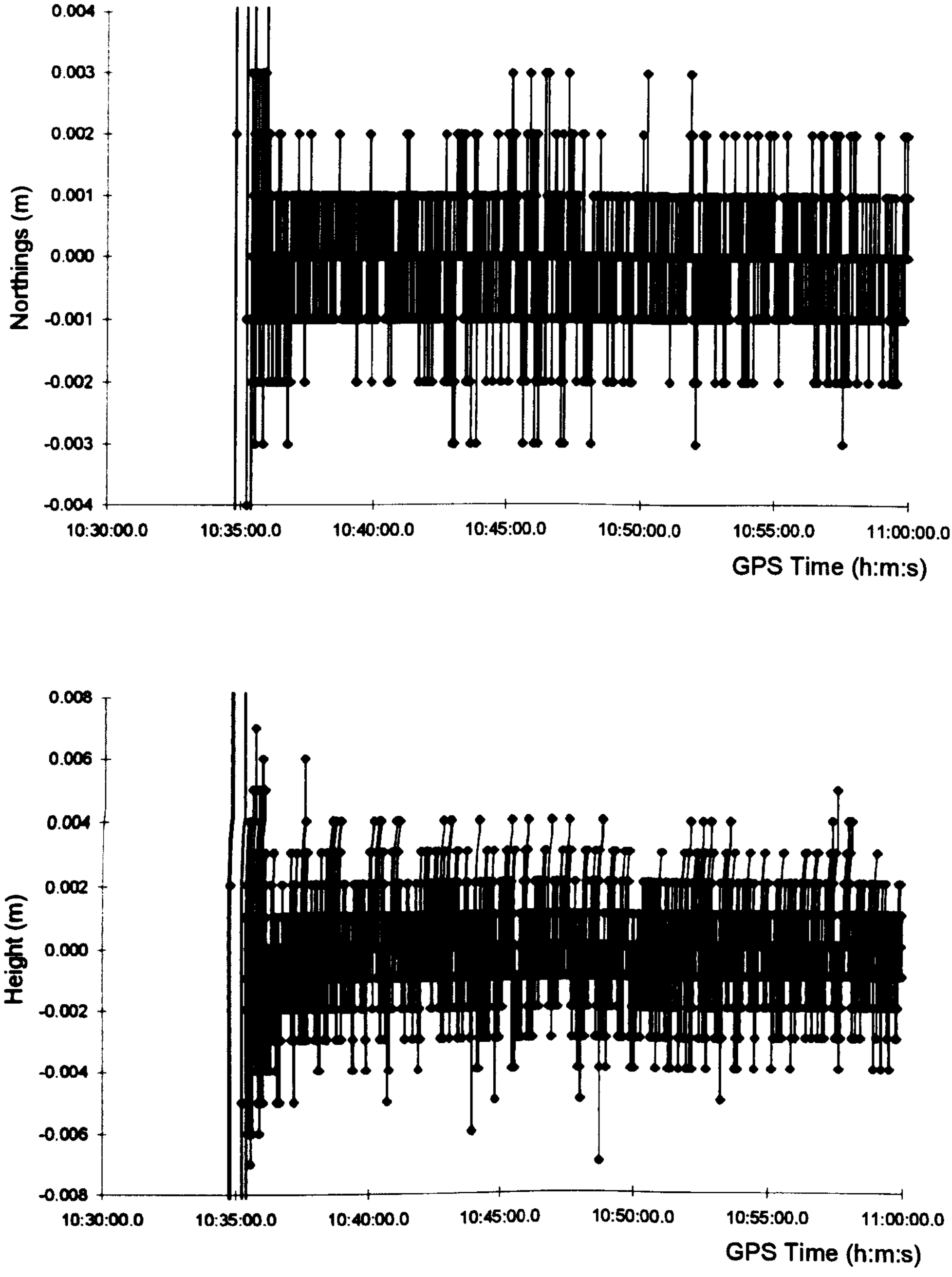
0.004
0.003
0.002
0.001
0.000
-0.001
-0.002
-0.003
-0.004
Northings (m)
10:30:00.0
10:35:00.0
10:40:00.0
10:45:00.0
10:50:00.0
10:55:00.0
11:00:00.0
GPS Time (h:m:s)
0.008
0.006
0.004
0.002
0.000
-0.002
-0.004
-0.006
-0.008
Height (m)
10:30:00.0
10:35:00.0
10:40:00.0
10:45:00.0
10:50:00.0
10:55:00.0
11:00:00.0
GPS Time (h:m:s)

APPENDIX E

OSGB NG	ENH	Coda 3	Server Version 951109.01 @ 17/08/96 13:34:17
14 21 46 5	449777.249	338322.650	56.127
14 21 47 0	449777.248	338322.651	56.123
14 21 47 5	449777.248	338322.650	56.128
14 21 48 0	449777.248	338322.649	56.129
14 21 48 5	449777.250	338322.651	56.126
14 21 49 0	449777.248	338322.651	56.126
14 21 49 5	449777.248	338322.648	56.124
14 21 50 0	449777.248	338322.650	56.129
14 21 50 5	449777.249	338322.648	56.127
14 21 51 0	449777.249	338322.651	56.123
14 21 51 5	449777.249	338322.649	56.125
14 21 52 0	449777.250	338322.651	56.125
14 21 52 5	449777.250	338322.651	56.128
14 21 53 0	449777.250	338322.651	56.128
14 21 53 5	449777.248	338322.650	56.128
14 21 54 0	449777.250	338322.650	56.129
14 21 54 5	449777.250	338322.652	56.125
14 21 55 0	449777.250	338322.651	56.126

E1: Eastings, Northings and Orthometric height output from WinCODA

Ashtech, Inc GPPS-2 Program: PPDIFF-PNAV Version: 2.1.04P
Sat Aug 17 09 15 37 1996 Differentially Corrected: Y

SITE	MM/DD/YY	HH:MM:SS	SVs	PDOP	LATITUDE	LONGITUDE	HI	RMS	FLAG	V_EAST	V_NORTH	V_UP
S196	08/16/96	14:17:36.500000	6	1.7	N 52.93999050	W 1.26080649	103.4175	8.872	2	0.000	0.000	0.000
S196	08/16/96	14:17:37.000000	6	1.7	N 52.93998933	W 1.26080670	103.6338	6.273	1	-0.005	-0.000	0.005
S196	08/16/96	14:17:37.500000	6	1.7	N 52.93998804	W 1.26080741	103.5481	5.121	1	0.007	0.003	0.005
S196	08/16/96	14:17:38.000000	6	1.7	N 52.93998744	W 1.26080763	103.4168	4.433	1	0.004	-0.003	-0.008
S196	08/16/96	14:17:38.500000	6	1.7	N 52.93998760	W 1.26080819	103.4414	3.964	1	-0.006	0.003	0.001
S196	08/16/96	14:17:39.000000	6	1.7	N 52.93998764	W 1.26080895	103.5234	3.617	1	-0.001	-0.010	-0.003
S196	08/16/96	14:17:39.500000	6	1.7	N 52.93998749	W 1.26080967	103.4874	3.347	1	0.004	0.013	-0.001
S196	08/16/96	14:17:40.000000	6	1.7	N 52.93998797	W 1.26080961	103.4539	3.128	1	-0.002	-0.002	0.005
S196	08/16/96	14:17:40.500000	6	1.7	N 52.93998792	W 1.26080973	103.4257	2.947	1	0.002	0.002	0.001
S196	08/16/96	14:17:41.000000	6	1.7	N 52.93998783	W 1.26080982	103.3605	2.794	1	-0.001	0.001	-0.009
S196	08/16/96	14:17:41.500000	6	1.7	N 52.93998828	W 1.26081010	103.3701	2.662	1	0.001	0.001	0.010
S196	08/16/96	14:17:42.000000	6	1.7	N 52.93998854	W 1.26081032	103.3664	2.546	1	0.002	-0.006	-0.010
S196	08/16/96	14:17:42.500000	6	1.7	N 52.93998881	W 1.26081040	103.3537	2.443	1	-0.000	0.004	0.002
S196	08/16/96	14:17:43.000000	6	1.7	N 52.93998896	W 1.26081046	103.3009	2.352	1	0.000	-0.004	0.001

E2: An Example of the Ashtech PRISM WGS84 File

APPENDIX F

Ashtech, Inc GPPS-2 Program: PPDIFF-PNAV Version: 2.1.04P
Wed Feb 12 13:52:25 1997 Differentially Corrected: Y

SITE	MM/DD/YY	HH:MM:SS	SVs	PDOP	LATITUDE		LONGITUDE		HI	RMS	FLAG	V_EAST	V_NORTH	V_UP
HUM3	11/26/96	11:00:00.500000	7	3.0	N 53.70932986	W	0.45042655	93.6137	14.834	2	0.000	0.000	0.000	
HUM3	11/26/96	11:00:01.000000	8	2.0	N 53.70933374	W	0.45042671	91.6411	5.739	1	-0.003	0.002	-0.002	
HUM3	11/26/96	11:00:01.500000	8	2.0	N 53.70933356	W	0.45042626	91.3090	4.409	1	0.002	0.004	-0.010	
HUM3	11/26/96	11:00:02.000000	8	2.0	N 53.70933370	W	0.45042673	91.2537	3.724	1	-0.001	0.001	0.023	
HUM3	11/26/96	11:00:02.500000	8	2.0	N 53.70933420	W	0.45042682	91.4357	3.284	1	0.002	-0.001	0.003	
HUM3	11/26/96	11:00:03.000000	8	2.0	N 53.70933450	W	0.45042614	91.4941	2.969	1	0.003	0.003	-0.024	
HUM3	11/26/96	11:00:03.500000	8	2.0	N 53.70933526	W	0.45042569	91.5854	2.730	1	0.000	0.001	-0.002	
HUM3	11/26/96	11:00:04.000000	8	2.0	N 53.70933584	W	0.45042567	91.8163	2.539	1	-0.003	-0.002	0.018	
HUM3	11/26/96	11:00:04.500000	8	2.0	N 53.70933606	W	0.45042585	91.9082	2.382	1	0.002	-0.001	-0.007	
HUM3	11/26/96	11:00:05.000000	8	2.0	N 53.70933642	W	0.45042559	91.9583	2.250	1	0.014	0.002	-0.020	
HUM3	11/26/96	11:00:05.500000	8	2.0	N 53.70933656	W	0.45042539	92.0462	2.137	1	-0.006	-0.001	0.041	
HUM3	11/26/96	11:00:06.000000	8	2.0	N 53.70933671	W	0.45042514	92.1160	2.038	1	0.004	0.000	-0.016	
HUM3	11/26/96	11:00:06.500000	8	2.0	N 53.70933669	W	0.45042515	92.1406	1.950	1	-0.006	0.001	-0.008	
HUM3	11/26/96	11:00:07.000000	8	2.0	N 53.70933676	W	0.45042513	92.2248	1.872	1	0.010	0.004	0.003	

F1: OTF Data file for Humber Bridge

OSGB NG	ENH	Coda 3 : Server Version 951109.01 @ 02/01/97 11:50:04	
11:10:00.0	502375.636	424771.515	45.035
11:10:00.5	502375.636	424771.516	45.034
11:10:01.0	502375.636	424771.516	45.034
11:10:01.5	502375.636	424771.516	45.034
11:10:02.0	502375.636	424771.516	45.034
11:10:02.5	502375.636	424771.516	45.034
11:10:03.0	502375.636	424771.516	45.034
11:10:03.5	502375.636	424771.516	45.034
11:10:04.0	502375.636	424771.516	45.034
11:10:04.5	502375.637	424771.516	45.034
11:10:05.0	502375.637	424771.516	45.034
11:10:05.5	502375.637	424771.516	45.034
11:10:06.0	502375.637	424771.516	45.034
11:10:06.5	502375.637	424771.516	45.033
11:10:07.0	502375.637	424771.516	45.033
11:10:07.5	502375.637	424771.516	45.033
11:10:08.0	502375.637	424771.516	45.033
11:10:08.5	502375.637	424771.516	45.033
11:10:09.0	502375.637	424771.518	45.033
11:10:09.5	502375.637	424771.518	45.033
11:10:10.0	502375.637	424771.518	45.033
11:10:10.5	502375.637	424771.518	45.033
11:10:11.0	502375.637	424771.518	45.033
11:10:11.5	502375.637	424771.518	45.033
11:10:12.0	502375.637	424771.518	45.033
11:10:12.5	502375.637	424771.518	45.033
11:10:13.0	502375.637	424771.518	45.033
11:10:13.5	502375.637	424771.518	45.033
11:10:14.0	502375.637	424771.519	45.033
11:10:14.5	502375.637	424771.518	45.032
11:10:15.0	502375.637	424771.519	45.032
11:10:15.5	502375.637	424771.519	45.032
11:10:16.0	502375.637	424771.519	45.032

F2: ENH data file for humber bridge

Further examples of movements on the Humber Bridge during Trial 3.

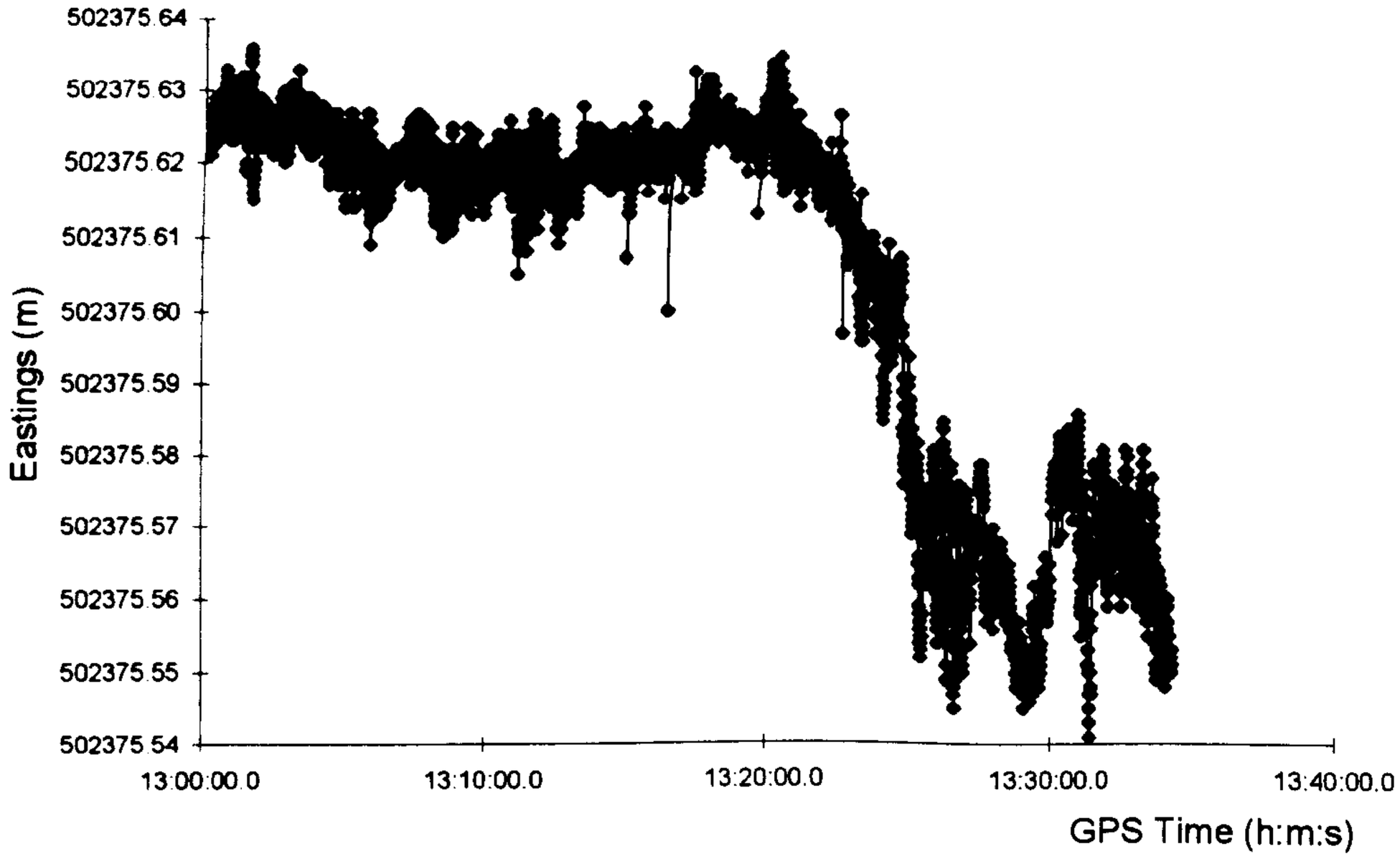

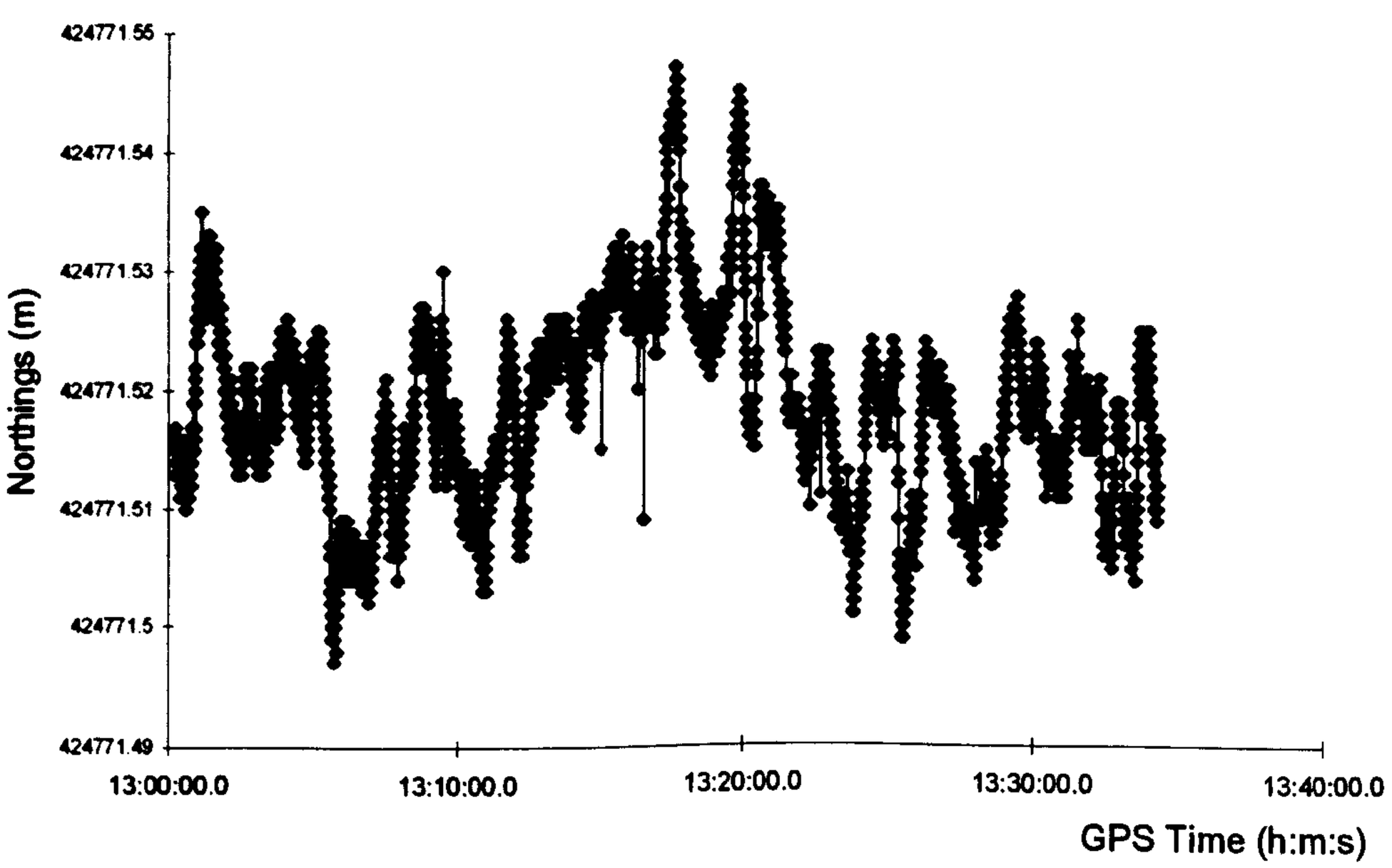

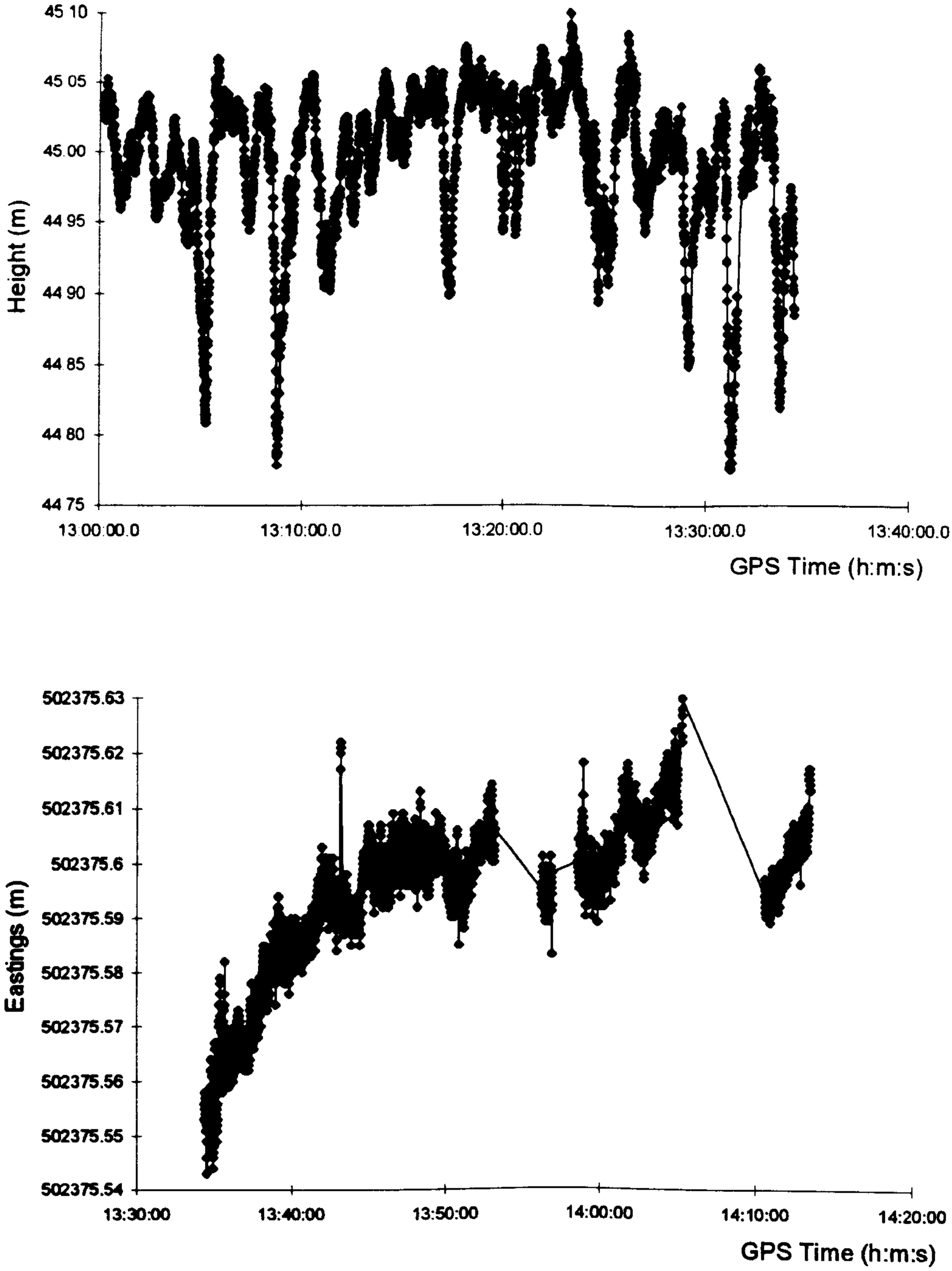
45 10
45 05
45.00
44 95
44 90
44 85
44 80
44 75
Height (m)
13:00:00.0
13:10:00.0
13:20:00.0
13:30:00.0
13:40:00.0
GPS Time (h:m:s)
502375.63
502375.62
502375.61
502375.6
502375.59
502375.58
502375.57
502375.56
502375.55
502375.54
Eastings (m)
13:30:00
13:40:00
13:50:00
14:00:00
14:10:00
14:20:00
GPS Time (h:m:s)

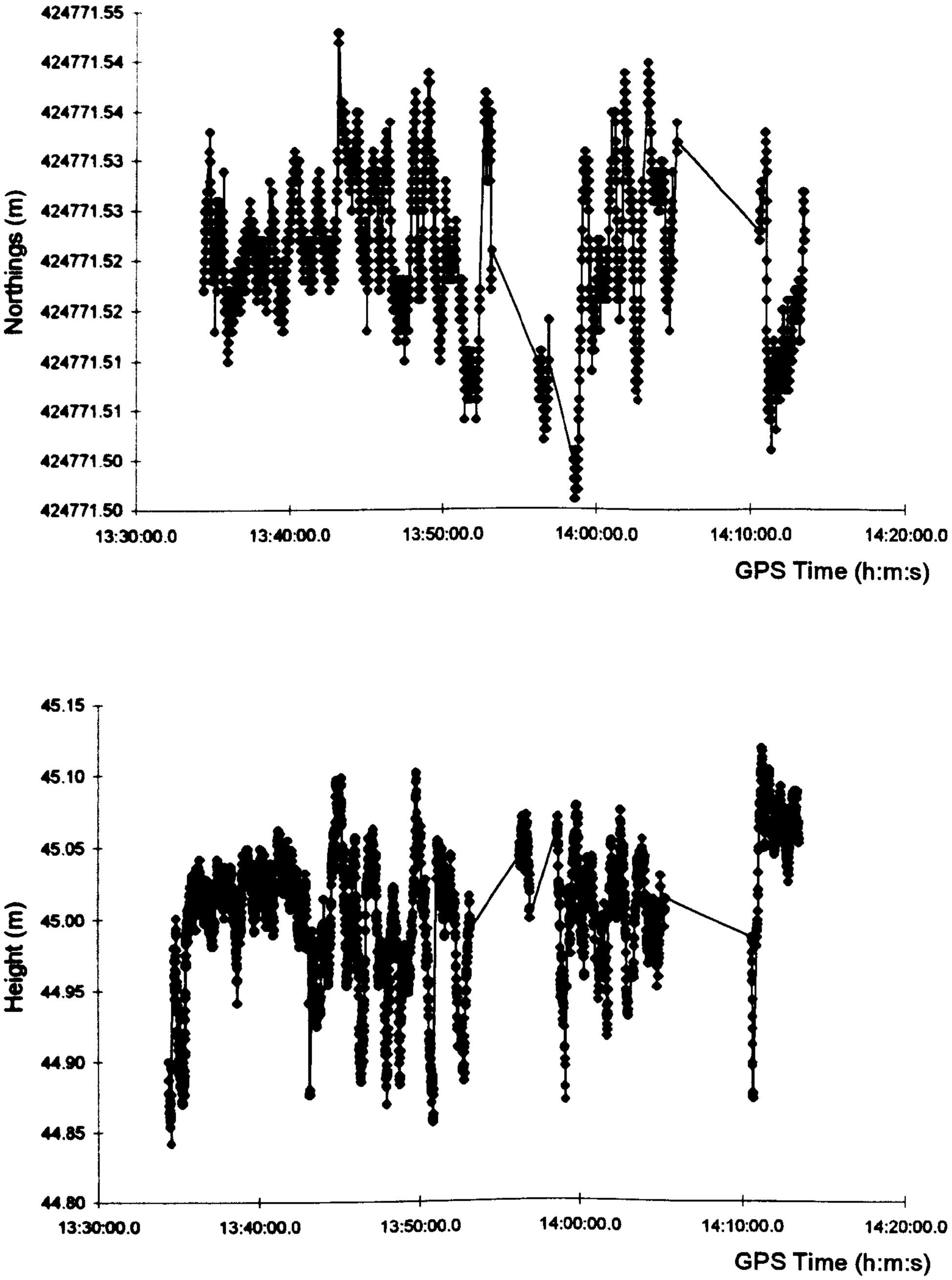
Northings (m)
424771.55
424771.54
424771.54
424771.53
424771.53
424771.52
424771.52
424771.51
424771.51
424771.50
424771.50
13:30:00.0
13:40:00.0
13:50:00.0
14:00:00.0
14:10:00.0
14:20:00.0
GPS Time (h:m:s)
Height (m)
45.15
45.10
45.05
45.00
44.95
44.90
44.85
44.80
13:30:00.0
13:40:00.0
13:50:00.0
14:00:00.0
14:10:00.0
14:20:00.0
GPS Time (h:m:s)

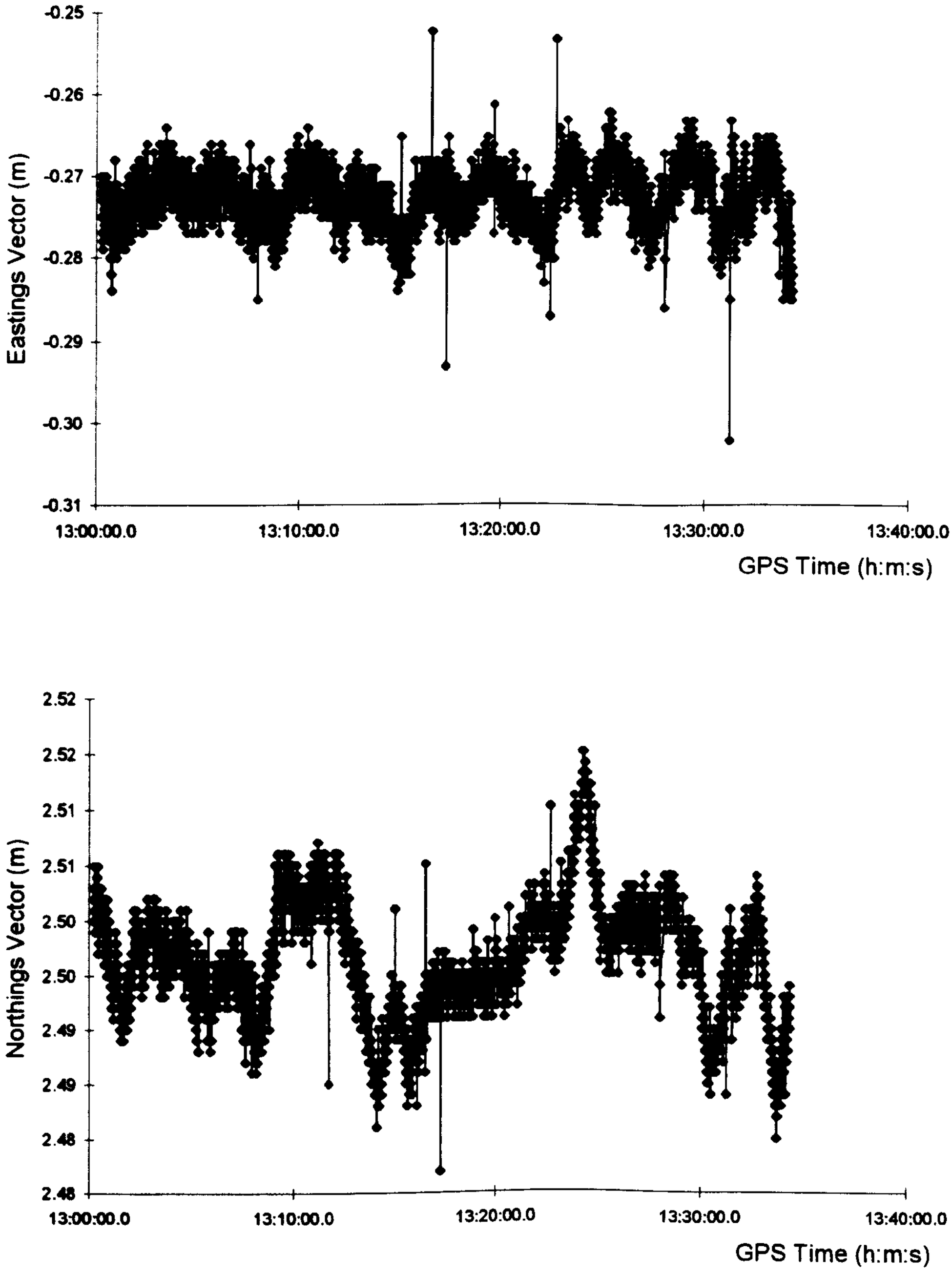
Eastings Vector (m)
-0.25
-0.26
-0.27
-0.28
-0.29
-0.30
-0.31
13:00:00.0
13:10:00.0
13:20:00.0
13:30:00.0
13:40:00.0
GPS Time (h:m:s)
Northings Vector (m)
2.52
2.52
2.51
2.51
2.50
2.50
2.49
2.49
2.48
2.48
13:00:00.0
13:10:00.0
13:20:00.0
13:30:00.0
13:40:00.0
GPS Time (h:m:s)

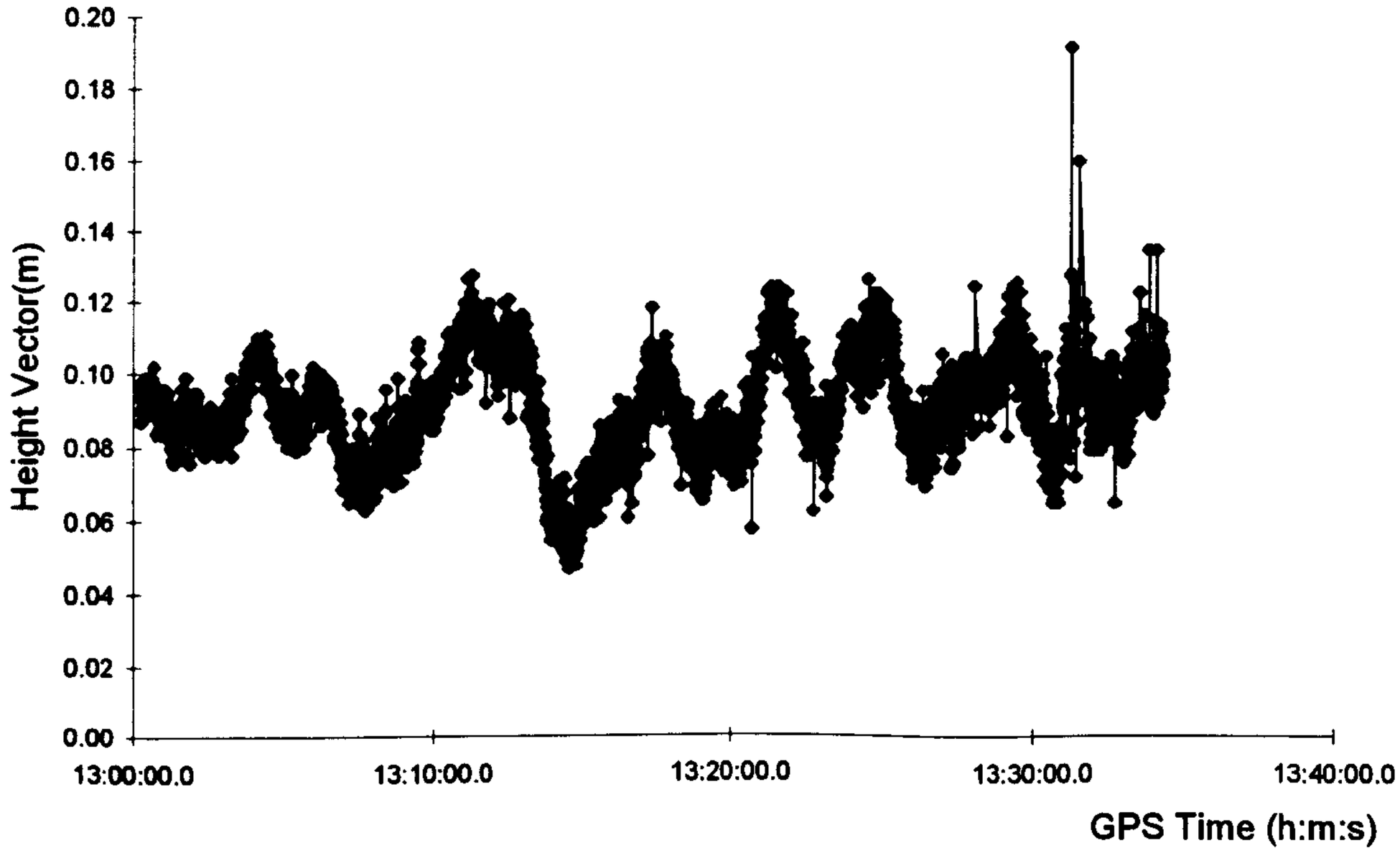
Height Vector(m)
0.20
0.18
0.16
0.14
0.12
0.10
0.08
0.06
0.04
0.02
0.00
13:00:00.0
13:10:00.0
13:20:00.0
13:30:00.0
13:40:00.0
GPS Time (h:m:s)

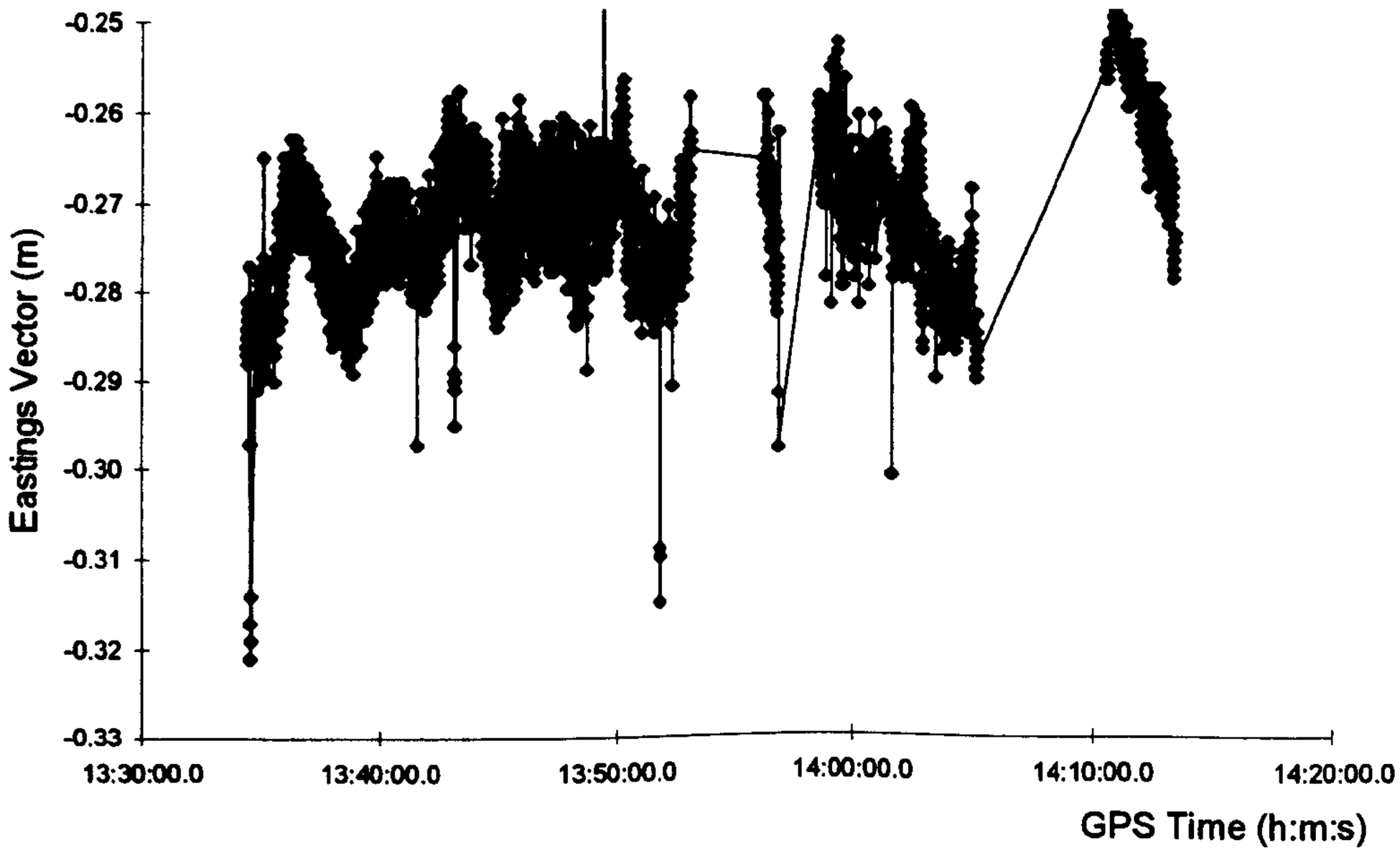
Eastings Vector (m)
-0.25
-0.26
-0.27
-0.28
-0.29
-0.30
-0.31
-0.32
-0.33
13:30:00.0
13:40:00.0
13:50:00.0
14:00:00.0
14:10:00.0
14:20:00.0
GPS Time (h:m:s)

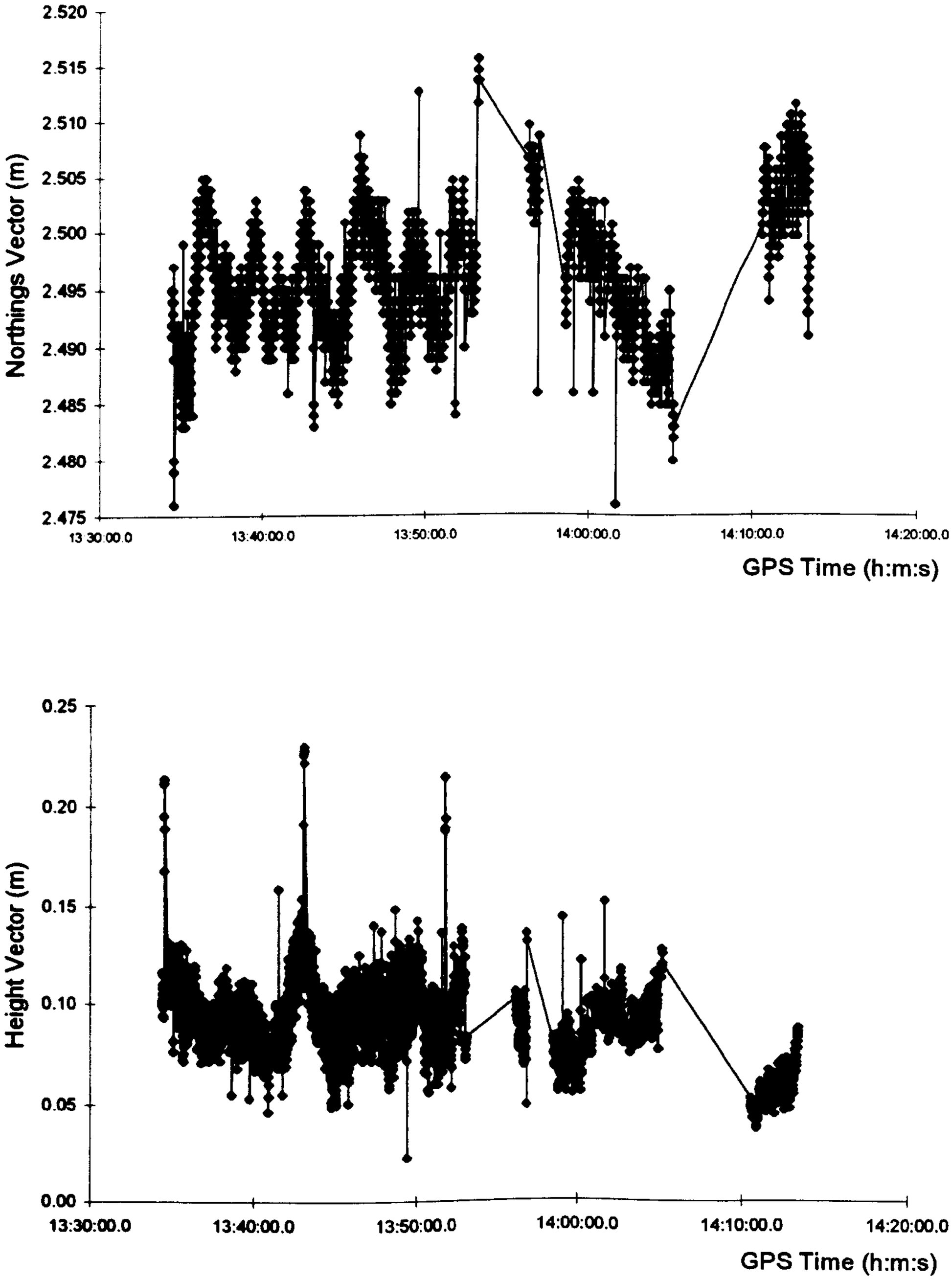
Northings Vector (m)
2.520
2.515
2.510
2.505
2.500
2.495
2.490
2.485
2.480
2.475
13:30:00.0
13:40:00.0
13:50:00.0
14:00:00.0
14:10:00.0
14:20:00.0
GPS Time (h:m:s)
Height Vector (m)
0.25
0.20
0.15
0.10
0.05
0.00
13:30:00.0
13:40:00.0
13:50:00.0
14:00:00.0
14:10:00.0
14:20:00.0
GPS Time (h:m:s)